GEOTECHNICAL INVESTIGATIONS OF VISHNUGAD-PIPALKOTI HYDEL PROJECT, GARHWAL, INDIA

Ph.D THESIS

by

K. LAKSHMANAN

DEPARTMENT OF EARTH SCIENCES
INDIAN INSTITUTE OF TECHNOLOGY ROORKEE
ROORKEE- 247667, INDIA

MAY, 2016

GEOTECHNICAL INVESTIGATIONS OF VISHNUGAD-PIPALKOTI HYDEL PROJECT, GARHWAL, INDIA

A THESIS

Submitted in partial fulfilment of the requirements for the award of the degree

of

DOCTOR OF PHILOSOPHY

in

EARTH SCIENCES

by

K. LAKSHMANAN

DEPARTMENT OF EARTH SCIENCES
INDIAN INSTITUTE OF TECHNOLOGY, ROORKEE
ROORKEE- 247667, INDIA
MAY, 2016

INDIAN INSTITUTE OF TECHNOLOGY ROORKEE
ROORKEE

CANDIDATE'S DECLARATION

I hereby certify that the work which is being presented in the thesis entitled "**GEOTECHNICAL INVESTIGATIONS OF VISHNUGAD-PIPALKOTI HYDEL PROJECT, GARHWAL, INDIA**", in partial fulfilment of the requirements for the award of the Degree of Doctor of Philosophy and submitted in the Department of Earth Sciences of the Indian Institute of Technology Roorkee, Roorkee is an authentic record of my own work carried out during a period from July, 2009 to May 2016, under the supervision of Dr. R. Anbalagan, Professor, Department of Earth Sciences, Indian Institute of Technology Roorkee, Roorkee.

The matter presented in the thesis has not been submitted by me for the award of any other degree of this or any other Institute.

(K. Lakshmanan)

This is to certify that the above statement made by the candidate is correct to the best of my knowledge.

Dated: ____________

(R. Anbalagan)
Supervisor

ABSTRACT

The demand for energy has increased many folds in the recent times in India due to tremendous industrial growth and rapid urbanization. India is endowed with enormous water potential, which is confined within the high altitude glacial peaks of Himalaya. It is one of the most important prospective potential source forming hydropower reserves of the country. However, a large part of water resource in Himalaya is yet to be harnessed fully. This slow pace of developments related to hydropower projects can be attributed mainly to the difficult terrain characteristics related to Geology and Engineering. The Engineering Geological challenges during construction and post construction of dams in Himalayan terrain are many due to complicated geology, high seismicity, rugged terrain and high relative relief in addition to excessive seepage problems.

The Vishnugad–Pipalkoti Hydroelectric Project, a run-of-the river (ROR) Scheme envisages construction of a 65m high diversion dam near village Helong (79°29’30” E and 30°30’50” N), a 13.4 km long Power tunnel (PT) and an underground power house to the south of village Hat (79°24’56” E and 30°25’31”N) to produce 444 MW of power (4 x 111 MW). The project is located on Alaknanda River, a major tributary of river Ganga, in Chamoli District in the state of Uttarakhand. A detailed Engineering Geological evaluation of the project has been carried out, to understand various Engineering Geological problems, which may arise during construction and to find suitable control measures.

Hydroelectric projects have many irreversible geo-environmental impacts due to blocking of the water course. During dam construction, stability of hill slopes in natural condition as well as after dam stripping is an important consideration in the geo-environmental appraisal of the dam. The vibrations induced during blasting due to use of explosives to achieve maximum pull may often cause instability of hill slopes above the tunnel in addition to causing damages to houses, and other civil structures. In view of greater importance of these aspects, they have been given suitable consideration in the present study so that a proper geo-environmental evaluation of the project as a whole could be achieved.

The present research includes Geological mapping and Engineering Geological evaluation of suitability of various project components on appropriate scales as well as identification of problems likely to be encountered during construction and immediately after construction. Geological 3D logging of exploratory drifts was carried out in addition to

logging of drill holes done at the site. Extensive water pressure tests were also done in the foundation area to understand the seepage pattern below the dam. Based on collection of extensive field data, the geomechanical rock mass classification for different rock types forming the project components were evaluated through Rock Quality Designation (RQD) of Deere et al, 1967, Rock Mass Rating (RMR) of Bieniawski, 1989, Q-system of Barton, 1974 and Geological Strength Index (GSI) of Hoek and Brown, 1980 were used to obtain the rock mass properties of rocks exposed within the project area. Joint strength parameters were obtained based on Joint Roughness Coefficient (JRC) of Barton and Choubey, 1977 and Joint wall compressive strength (JCS) of Deere and Miller, 1966.

Recent research in the field of Rock Mechanics shows some encouraging developments in stability analysis for surface and underground structures by providing graphical visualization programs. The facility of the programmes with enabled option to incorporate available field data and freedom in selection of method based on which the factor of safety (FOS) will be estimated. The extensive data collection from field and systematic laboratory studies help in better understanding of the graphical output generated from the softwares.

Slope stability analysis of left and right abutments was carried out. The collected data was used to interpret dam abutment conditions including designing of stripping limits of the foundation and other foundation treatments. The problems that were likely to arise in different segments during construction of power tunnel were identified in detail. Since uncontrolled blasting causes damages due to excessive vibrations, safe limits of charges per delay for blasting were assessed so that the blast impacts can be minimized. A detailed Engineering Geological study was done on stability of power house cavern.

On the basis of mapping of the power house area, the construction problems that are likely arise during and excavation and construction of underground powerhouse were identified. The pattern of unstable wedges, support pressures and support requirements for the powerhouse cavern were evaluated.

The construction of a dam and impounding water behind it causes a major environmental feature that is reservoir, which is a standing water body. The fluctuations of water levels due to drawdown conditions cause instability of the hill slopes. Important unstable locations were identified and over all stability assessment of hill slopes around the rim has been carried out.

ACKNOWLEDGEMENTS

Apart from my efforts, the success of this study depended on the encouragement and guidelines of many others. At this juncture, I would like to take this opportunity to thank all those who have directly or indirectly helped me in the completion of my research work.

First and foremost, I would like to express my profound gratitude to my supervisor, **Prof. R. Anbalagan** for giving me opportunity to work along with him. His precious guidance and constructive criticism during the tenure keeps the research inside me alive. Professional expertise, open discussions, endless advices and constant unflinching support rendered by **Prof. R. Anbalagan** have shaped this thesis to its present form. I'm immensely thankful to him for his patience, motivation, enthusiasm, and immense knowledge. His guidance helped me in all the time of research and writing of this thesis. To him, I remain, professionally and emotionally indebted. I could not have imagined having a better advisor and mentor for my Ph. D study.

I'm grateful to the Students Research Committee members **Prof. Mohd. Israil, Prof. M.N. Viladkar and Prof. G. J. Chakrapani,** for sparing their valuable time in monitoring the work progress and providing useful tips, critical comments and precious suggestions from time to time. **Prof. D. C. Srivastava** (Head, Department of Earth Sciences) is gratefully acknowledged for providing me the necessary research facilities to complete this work.

I'm thankful to Sh.RK Vishnoi GM **THDC Ltd.** (Rishikesh, Uttarakhand) and other officers of THDC for extending their support by providing accommodation and other facilities during my field work. I owe to thank Sh. Ashish Yadav, Dy.Manager the man who stood all the time 24x7 to clarify any doubts regarding the project components. I would like to thank Sh. Manikandan, Sr.Officer for his timely help, I would like extend my thanks to Sh. Nalinikanth Oja, Dy.Manager, Sh. KC Uniyal Sr.Manager and all other officers of THDC posted at Pipalkoti who consider me as one among them during my stay.

I am thankful to the Director General GSI for his kind permission and support to continue my research as part time by providing NOC.

I wish to express my deep gratitude to CH. Venugopal Rao, Dy.D.G., GSI, Chandigarh for his kind helps and fruitful discussions from which the thesis has been greatly benefited

Thanks are due to Dr. K. Jayabalan, Director, GSI, Sh. Manoj Kumar Suptg. Geologist, GSI for their timely helps and encouragements in pursuing this work

I wish to express my sincere appreciations to Smt Jina Lakshmanan, Sr.Geologist, Sh. DP. Dangwal Sr.Geologist Smt. Athira and Ramesh Geologist, GSI for extending their untiring assistance in the preparation of maps and other works

I feel lucky to be blessed by the company of wonderful friends who shared my failures and triumphs. I owe a special appreciation and gratitude to all those who helped me in final editing, map preparation and compilation of the thesis, particularly **Neethu** and others such as Bipin, Gaurav, Rohan, Anoop, and R K Tiwari

There's another person without whose help the journey to this thesis would have been very difficult. I specially thank **Nair Ji** for being always there and helping me with all the paper works and other formalities for completion of this thesis. I extend my thanks to all the staffs of Earth Science Department for their direct and indirect service render to me during this tenure

I would like to thank my wife, **JINA** for her understanding, patience, and unconditional support during my research work helped me keep going. I am deeply thankful to her for her love, support, and sacrifices. Without her help and co-operation I would have never reached this mile-stone.

I am indebt thankful to my **Appa (R Kalamegam)-Amma (Amirtham)**, my in-laws **Parimal** uncle, **Raki** aunty, Dadi, Rajbi Mama and Mami from Kolkata for their wishes and continuous support throughout the year. I specially thank my Sister and Brother **Kalai**-Ramesh, **Ram**-Vinothini, and the little ones Nakshatra, Aaradhana, Simithra and all my friends for their faith in me and encouraging me to be as ambitious as I wanted and shared their support, morally and physically.

Above all, I surrender myself to the **Great Almighty**, the author of knowledge and wisdom, for His countless love and strength that He bestowed upon me throughout this journey.

CONTENTS

ABSTRACT **i**

ACKNOWLEDGEMENTS **ii**

LIST OF FIGURES **ix**

LIST OF TABLES **xv**

CHAPTER I: INTRODUCTION **1**

1.1 HYDROPOWER PLANNING AND DEVELOPMENT IN INDIA **3**

1.2. HYDROPOWER PROSPECTS IN HIMALAYA **3**

1.3 GEOTECHNICAL PROBLEMS OF HYDROPOWER DEVELOPEMENT IN HIMALAYA **4**

1.4 LITERATURE REVIEW **4**

1.5 STUDY AREA-A BRIEF PROFILE **7**

1.5.1. Location and Accessibility 8

1.5.2. Geomorphology 9

1.5.3 Climate 10

1.5.4 Seismicity of the Area 11

1.6 RESEARCH GAP **12**

1.7 OBJECTIVES, METHODOLOGY AND ANALYTICAL TOOLS **13**

1.7.1 Research objectives 13

1.7.2. Methodology Overview 14

1.8 ANALYTICAL TOOLS **16**

1.9 OVERVIEW OF THESIS **16**

CHAPTER II: GEOLOGICAL SETTING **19**

2.1 REGIONAL GEOLOGY **21**

2.2 GEOLOGY OF PROJECT SITE **25**

2.3 THERMAL SPRINGS **32**

CHAPTER III: GEOTECHNICAL INVESTIGATIONS **35**

3.1 SUBSURFACE EXPLORATIONS **36**

3.1.1 Exploratory Drill Holes 36

3.1.2 Hot Water Springs 50

3.1.3 Subsurface Permeability 50
3.1.3.1 Interpretations 53
3.1.3.2 Rock Quality Designation (RQD) 55
3.2 SUBSURFACE EXPLORATORY DRIFTS 55
3.3 LABORATORY DETERMINATION OF ENGINEERING PROPERTIES OF ROCKS 68
3.3.1 Uniaxial Compression Tests (For determination of UCS) 69
3.3.2 Brazilian Tests for Determination of Tensile Strength 73
3.3.3 Triaxial Compression Tests 77
3.4 RESULTS AND INTERPRETATION OF TEST DATA 80
3.5 GROUND CHARACTERIZATION 89
3.5.1 Characterization of Rock Mass – RQD, RMR and Q 91
3.5.1.1 Rock Quality Designation (RQD) 91
3.5.1.2 Evaluation of Rock Mass Rating (RMR) 92
3.6 Q-SYSTEM 93
3.7 ROCK MASS STRENGTH 94
3.7.1 Geological Strength Index (GSI) 94
3.7.2 Hoek-Brown shear strength parameters 95
3.7.3 Rock Mass Deformability and Shear Strength 97
3.7.4 Empirical estimation of Rock Mass Modulus 98

CHAPTER IV: ENGINEERING GEOLOGICAL APPRAISAL OF PIPALKOTI DAM SITE 99
4.1 DETAILED GEOLOGICAL MAPPING OF DAM AREA 103
4.1.1 Lithology 104
4.1.2 Thin Section Description 104
4.1.3 Structure 104
4.2 SUBSURFACE INVESTIGATIONS 108
4.2.1 Drill Holes 108
4.2.2 Drifts 109
4.2.3 Geological Cross Sections 120
4.3 SLOPE STABILITY ANALYSIS OF ABUTMENTS 122
4.4 DISCUSSION 131

CHAPTER V: GEOTECHNICAL EVALUATION OF POWER TUNNEL **133**

5.1 VISHNUGAD-PIPALKOTI POWER TUNNEL (PT) **135**

5.2 GEOLOGICAL MAPPING **137**

5.3 CHARACTERIZATION OF ROCK MASS USING RQD, RMR, Q AND GSI **143**

5.4 STABILITY ANALYSIS OF POWER TUNNEL **145**

5.4.1 Segment A-B of Power Tunnel 146

5.4.2 Segment B-C of Power Tunnel 148

5.4.3 Segment C-D of Power Tunnel 150

5.4.4 Segment D-E of Power Tunnel 152

5.4.5 Segment E-F of Power Tunnel 153

5.5 ESTIMATION OF SUPPORT REQUIREMENT **159**

5.5.1 Determination of Maximum Unsupported Span 159

5.5.2 Length of Bolts and Anchors 159

5.5.3 Types of Support by Q-System 160

CHAPTER VI: EVALUATION OF IMPACTS OF BLASTING ON STABILITY OF GROUND AND CIVIL STRUCTURES ABOVE HRT & TRT **163**

6.1 GEOLOGY OF AREA 167

6.2 STABILITY ANALYSIS OF SLOPES 176

6.3 IMPACTS OF BLASTING IN AREA 177

6.4 CONCLUSIONS AND RECOMMENDATIONS 179

CHAPTER VII: STABILITY STUDIES OF UNDERGROUND POWERHOUSE **1**83

7.1 GEOLOGY OF POWERHOUSE AREA **1**85

7.2 SUBSURFACE EXPLORATIONS **188**

7.2.1 Drilling: 188

7.2.2 Drifting: 188

7.3 CHARACTERIZATION OF ROCK MASS - RMR, Q AND RQD **19**7

7.3.1 Field estimation of JRC and JCS 198

7.4 STABILITY ANALYSIS FOR UNSTABLE ROCK WEDGES AT ROOF & SIDEWALL **19**9

7.5 SUPPORT AND MEASURES **205**

CHAPTER VIII: STABILITY OF HILL SLOPES IN RESERVOIR RIM AREA 209
8.1 GEOLOGY OF RESERVOIR 212
8.2 SLOPES ON THE RIGHT BANK 214
8.3 SLOPES ON THE LEFT BANK 221
8.4 DISCUSSION 234

CHAPTER IX: SUMMARY AND CONCLUSIONS Error! Bookmark not defined.**235**

REFERENCES 241
ANNEXURES 253-284

LIST OF FIGURES

Figure No.	Title	Page No.
Figure 1.1	Location map of Vishnugad - Pipalkoti project	8
Figure 1.2	Geomorphology map of Vishnugad-Pipalkoti area.	10
Figure 2.1	Satellite image showing Himalayan range with DEM of Garhwal Himalaya	22
Figure 2.2	The Regional Geological map of Himalayan range (After Ganesser 1964)	22
Figure 2.3	Regional Geology of Garhwal Himalaya Valdiya (1980). A &B. Regional Geology of Pipalkoti Area. Abbreviations: MBT—Main Boundary Thrust; MCT—Main Central Thrust.	24
Figure 2.4	Geological map of the project area. (After Gaur et. al., 1977)	26
Figure 3.1	Graph showing percentage distribution of Lugeon value for different litho units	55
Figure 3.2	Geological section along VHEP Dam axis	56
Figure 3.3	Photo illustrating the observed glide crack on the left bank of the dam axis	57
Figure 3.4	Presence of slate just above the drift opening at Hat village	60
Figure 3.5	Geological cross section across powerhouse area showing the older and new PH proposed locations	61
Figure 3.6	3D–Drift log of DL-01 located on the left bank near dam axis	66
Figure 3.7	3D–Drift log of DL-01 located on the right bank near dam axis	67
Figure 3.8	Deere–Miller (1966) Classification of Rocks	81
Figure 3.9a	Mohr’s Envelope for Quartzites (Dry)-Desilting Chambers Area	83
Figure 3.9b	Mohr’s Envelope for Quartzites (Saturated)-Desilting Chambers Area	83
Figure 3.10a	Mohr’s Envelope for Dolomitic limestone (Dry)-Powerhouse	84
Figure 3.10b	Mohr’s Envelope for Dolomitic limestone (Saturated)-Powerhouse	84
Figure 3.11a	Mohr’s Envelope for Slates (Dry)-Powerhouse	85
Figure 3.11b	Mohr’s Envelope for Slates (Saturated)-Powerhouse	85
Figure 3.12	Hoek-Brown parameters for intact rock and jointed rock masses of Quartzites a) Dry Condition and b) Saturated Condition	86

Figure 3.13	Hoek-Brown parameters for intact rock and jointed rock masses of Dolomitic limestone a) Dry Condition and b) Saturated Condition	87
Figure 3.14	Hoek-Brown parameters for intact rock and jointed rock masses of Dolomitic limestone a) Dry Condition and b) Saturated Condition	88
Figure 3.15	General chart for GSI estimates from the geological observations (Hoek et al.1992)	94
Figure 4.1	Dam, Intake, Desilting chamber and Diversion tunnel plan laid over satellite imagery(ArcGIS10.2 Base map image)	102
Figure 4.2	Steep narrow gorge of VHEP dam area with massive Garhwal quartzites	102
Figure 4.3	Geological map of Dam area with major project structures	103
Figure 4.4	Garhwal Group Quartzites with bands of cholrite schist exposed on the left abutment	105
Figure 4.5	Quartzite Core samples from Dam area showing foilation traces	106
Figure 4.6a	Tightly packed angular quartz grains in quartzite. (Mgf. X 20 cross nicol)	106
Figure 4.6b	Mica defining the foliation in the rock. (Mgf. X 20 PPL)	106
Figure 4.7	Stereonet showing the pole concentration of major discontinuities in dam area (Dips version 5.1)	107
Figure 4.8	Geological cross section across dam axis	110
Figure 4.9	Geological section 100m D/s of Dam axis	110
Figure 4.10	Geological cross section 100m Up/s of dam axis	110
Figure 4.11	Planar analysis for left bank showing with friction cone and day light envelope	110
Figure 4.12	Planar analysis for right bank showing with friction cone and day light envelope	120
Figure 4.13	Analysis for Wedge for left bank	121
Figure 4.14	Analysis for Wedge for right bank	121
Figure 4.15	Topple Analysis result for left Bank	124
Figure 4.16	Topple Analysis result for right Bank	124
Figure 4.17	Geometric plane Geometries of plane slope failure: (a) tension crack in the upper slope; (b) tension crack in the face. (Hoek and	125

	Bray 1981)	
Figure 4.18	Analysis for Wedge for right bank	125
Figure 4.19	Topple Analysis result for left Bank	126
Figure 4.20	Topple Analysis result for right Bank	126
Figure 4.21	Geometric plane Geometries of plane slope failure: (a) tension crack in the upper slope; (b) tension crack in the face. (Hoek and Bray 1981)	128
Figure 5.1	Layout map of the Vishnugad–Pipalkoti HEP showing the power tunnel alignment along the right bank of Alaknanda river	138
Figure 5.2	Geological map along power tunnel (PT) alignment passing through various litho units.	139
Figure 5.3	Geological cross-section along the Power Tunnel alignment with stereonet kinematic analysis with respect to tunnel orientation and structural discontinuities	140
Figure 5.4	Kinematic analysis for PT segment A-B	146
Figure 5.5	Wedges formed between A–B Segment 1	147
Figure 5.6	The unstable wedges formed on the top right roof cornerand top left roof corner of the PT in segment A-B	147
Figure 5.7	Kinematic analysis along B-C segment	149
Figure 5.8	Figure Wedges formed along B–C Segment	149
Figure 5.9	Geological cross-section along PT crossing point at MainaRiver (Section Direction S25°W–N25°E)	150
Figure 5.10	Stereonet kinematic analysis along C-D segment	151
Figure 5.11	Wedges formed along C–D Segment 3	151
Figure 5.12	Stereonet kinematic analysis along D-E segment	152
Figure 5.13	Wedges formed along D–E Segment	153
Figure 5.14	Stereonet kinematic analysis along E-F segment	154
Figure 5.15	Wedges formed along E-F Segment	154
Figure 5.16	Correlation between support pressure and rock mass quality (Q) Q-system (Barton et al., 1974)	156
Figure 5.17	The stabilized wedge after providing the required support pressure (A-B Segment)	160
Figure 5.18	The stabilized wedge after providing the required support pressure (B-C Segment)	161

Figure 5.19	The stabilized wedge after providing the required support pressure (C-D Segment)	161
Figure 5.20	The stabilized wedge after providing the required support pressure (D-E Segment)	162
Figure 6.1	Location Map of the study area with section lines of villages	166
Figure 6.2	Geological section across slope in Jharetha village	167
Figure 6.3	Geological section across slope in Surenda village	168
Figure 6.4	Geological section across slope in Tirosi village	169
Figure 6.5	Geological section across slope in Hyuna village	169
Figure 6.6	Geological section across slope in Tapon village	170
Figure 6.7	Geological section across slope in Math Dadhera village	171
Figure 6.8	Geological section across slope in Pokhani village	172
Figure 6.9	Geological section across slope in Lanji village	172
Figure 6.10	Geological section across slope in Dwing village	173
Figure 6.11	Geological section across slope in Jaisal village	174
Figure 6.12	Geological section across slope in Dhari village	174
Figure 6.13	Attenuation relationships showing scatter	175
Figure 6.14	Frequency based blast vibration control to protect Residential structures	175
Figure 7.1	ArcGIS image of powerhouse area showing the layout of powerhouse	186
Figure 7.2	Geological map of powerhouse area	187
Figure 7.3	Stereoplot for left limb of syncline	189
Figure 7.4	Stereoplot for right limb of syncline	189
Figure 7.5a	3D Geological log of powerhouse drift for RD 200m to 254m	192
Figure 7.5b	3D Geological log of powerhouse drift for RD 275m to 334m	193
Figure 7.5c	3D Geological log of powerhouse drift for RD 325m to 374m	194
Figure 7.5d	3D Geological log of powerhouse drift for RD 353 m to 410m	195
Figure 7.6	Geological cross section across powerhouse location with drift location and structural data obtained from 3D drift log projected showing the synclinal fold axis	196
Figure 7.7	Stereoplot analysis showing the possible wedges along the PH alignment	190
Figure 7.8	The possible stable and unstable wedges formed along the PH	201

	alignment for RD 350-450m	
Figure 7.9	The Unstable wedges formed along the powerhouse alignment	203
Figure 7.10	Wedge analysis showing possible major wedge on top right roof and side wall	204
Figure 7.11	Power house orientation plot with respect to trend and plunge	204
Figure 8.1	Geological map of Vishnugad–Pipalkoti reservoir area with section lines and MRL	213
Figure 8.2	Geological cross section of R1 near dam axis	215
Figure 8.3	Stereonet analysis for Slope R1	215
Figure 8.4	Geological cross section of R2 near dam axis Near intake structure,40m	216
Figure 8.5	Stereonet kinematic analysis for Slope R2	216
Figure 8.6	Geological cross section of R3 U/S of Nall, 270 m	217
Figure 8.7	Stereonet kinematic analysis for Slope R3	217
Figure 8.8	Geological cross section of R4 opposite of LSH-2, 490 m	218
Figure 8.9	Stereonet and kinematic analysis for Slope R4	218
Figure 8.10	Geological cross section of R5 along Urgam bridge, 1330m	219
Figure 8.11	Stereonet and kinematic analysis for Slope R5	219
Figure 8.12	Geological cross section of R6 near Kalpaganga, 2860m	220
Figure 8.13	Stereonet and kinematic analysis for Slope R6	221
Figure 8.14	Geological cross section of L1. Near dam, axis opposite to L1	222
Figure 8.15	Stereonet and kinematic analysis for Slope L1	222
Figure 8.16	Geological cross-section of L2. Along intake of diversion tunnel, 110m	223
Figure 8.17	Stereonet and kinematic analysis for Slope L2	223
Figure 8.18	Geological cross section of L3 near intake of diversion tunnel, 180m	224
Figure 8.19	Stereonet and kinematic analysis for Slope L3	224
Figure 8.21	Stereonet and kinematic analysis for Slope L4	225
Figure 8.20	Geological cross section of L4. Near LSH-2, 450m	225
Figure 8.22	Geological cross section of L5 downstream of Urgam bridge, 1120m	226
Figure 8.23	Stereonet and kinematic analysis for Slope L5	227
Figure 8.24	Geological cross section of L6, 1610m from dam axis	228

Figure 8.25	Stereonet and kinematic analysis for Slope L6	228
Figure.8.26	Foliated stained granitic gneissic rocks exposed near Urgam bridge	230
Figure. 8.27	Debris and RBM material present upstream of Urgam bridge on Left bank	230
Figure 8.28	Contact of Granitic gneiss and Quartzites of Gulakoti in Reservoir area (NH-58)	231
Figure 8.29	Debris and RBM material present along section L6	231

LIST OF TABLES

Table No	Title	Page No
Table 2.1	Litho-Tectonic Setup of the Vishnugad-Pipalkoti H-E Project (After THDC 2010, DPR)	27
Table 2.2	Details of thermal springs encounter in dam site area	32
Table 3.1	Summary of exploratory drill holes and drifts	37
Table 3.2	Summary of Drill Holes at Dam Site	38
Table 3.3	Summary of Drill Holes at Desilting Chamber	41
Table 3.4	Summary of Drill Holes at Diversion Tunnel	42
Table 3.5	Summary of Drill Holes at Power Tunnel (Pt) Alignments	44
Table 3.6	Summary of Drill Holes at Surge Shaft	46
Table 3.7	Summary of Drill Holes at Powerhouse	47
Table 3.8	Details of Lugeon test and their interpretation with respect to specific depth at dam site area	51
Table 3.9	Detail of permeability tests in drill holes at specific depths	53
Table 3.10	Condition of rock mass discontinuity associated with different Lugeon values.	54
Table 3.11	Frequency distributions of Lugeon values by rock type (After Heuer, 1995)	54
Table 3.12	Prominent joint sets for slates and dolomitic limestone in powerhouse area	59
Table 3.13	Details of Drift at Dam site	62
Table 3.14	Details of Drift at Powerhouse	65
Table 3.15	Number of samples tested for dam and powerhouse area	69
Table 3.16a	Results of UC tests on dry samples of Quartzites - Desilting chambers area	70
Table 3.16b	Results of UC tests on saturated samples of Quartzites - Desilting chambers area	71
Table 3.16c	. UC tests on dry samples of Dolomitic limestones	72
Table 3.16d	UC tests on saturated samples of Dolomitic limestones	72
Table 3.16e	UC tests on dry samples of Slates	73
Table 3.17a	Summary of results of Brazilian tests conducted on dry Quartzite samples	74

Table 3.17b	Summary of results of Brazilian tests conducted on dry samples of Dolomitic limestone	76
Table 3.17c	Summary of results of Brazilian tests conducted on dry samples of Slates	76
Table3.18a	Shear strength parameters from triaxial strength tests on dry rock samples of Quartzites	77
Table 3.18b	Shear strength parameters from triaxial strength tests on saturated rock samples of Quartzites	78
Table 3.18c	Shear strength parameters from triaxial strength tests on dry rock samples of Dolomitic limestone	78
Table 3.18d	. Shear strength parameters from triaxial strength tests on saturated rock samples of Dolomitic limestone	78
Table 3.18e	Shear strength parameters from triaxial strength tests on dry samples of slates	79
Table 3.18f	Shear strength parameters from triaxial strength tests on saturated rock samples of slates	79
Table 3.19	Averaged results of laboratory tests for different rock types	80
Table. 3.20	Summary of mechanical properties for major rock type in the project area	81
Table 3.21	Structural details Recorded at Dam site	90
Table 3.22	Structural details Recorded at powerhouse site	90
Table 3.23	Water inflows in exploratory drifts	91
Table 3.24	Rock Quality Designation (RQD) values obtained for different rock types	91
Table 3.25	Estimation of RMR for different rock type (Bineiawski, 1984)	92
Table 3.26	Summary of Q values calculated for quartzites, slate and dolomitic limestones	93
Table 3.27	Rock mass strength parameters as per Hoek and Brown (1997) criterion obtained from Triaxial tests	96
Table 3.28	Results of in situ tests on deformability and shear strength	97
Table 3.29	Summary of rock mass modulii values using GSI: Hoek and Diederichs (2006)	98
Table 4.1	Structural discontinuities (Dam site) obtained from field and stereographic analysis	107

Table 4.2	Summary of Drill Holes At Dam Site	111
Table 4.3	Frequency distributions of Lugeon values by rock type (after Heuer, 1995)	115
Table 4.4	Details Geomechanical properties and rock mass properties	115
Table 4.5	Rock mass strength parameters as per Hoek and Brown (1997) criterion obtained from Triaxial tests	115
Table 4.6	Details of Drift at Dam site	116
Table 4.7	Estimation of RMR (Bineiawski, 1984)	119
Table 4.8	Results of in situ tests on deformability and shear strength	119
Table 4.9	Attitude of foliation and joints of the Dam site obtained from contour plot	122
Table 5.1	Structural details observed in Quartzite	136
Table 5.2	Summary of Drill Holes at Dwing Pt Crossing Point	141
Table 5.3	Summary of Drill Holes at Maina Pt Crossing Point	142
Table 5.4	Rock Quality Designation (RQD) values obtained for different rock types	143
Table 5.5	Estimation of RMR for different rock type (Bineiawski, 1984)	143
Table 5.6	Summary of Q values calculated for quartzites, slate and dolomitic limestone	143
Table. 5.7	Summary of mechanical properties for major rock type in the project area	144
Table 5.6	Shear strength parameters as per Hoek and Brown (1997) criterion	144
Table 5.9	The representative values of JRC and JCS for Quartzites Slates and Dolomitic limestone (Barton and Choubey, 1977) and ISRM (1978)	145
Table 5.10	Correction factor for overburden f and tunnel closure f’ by using approach of Singh et al. (1992)	158
Table 5.11	Support pressure using equation of Singh et al.(1992)	158
Table 5.12	Estimation of support by Q-System	160
Table 6.1	Results of Stability Analysis of Village Slopes Close to Power Tunnel	176
Table 6.2	Analysis of blasting impact for calculating safe charge weight per delay	178
Table 7.1	The structural discontinuities obtained for PH	187

Table 7.2	Structural details of synclinal fold limbs obtained from 3D drift log	191
Table 7.3	Calculated RMR, GSI & Q between RD 200–410 in hat powerhouse drift	197
Table 7.4	The representative values of JRC and JCS for slates and dolomitic limestone (Barton)	198
Table 7.5	The average (φ r) obtained for various discontinuities	199
Table 7.6	Data set used in for wedge analysis recorded between Rd 350-450m	200
Table 7.7	Support in Power House and Transformer Hall	205
Table 8.1	General discontinuity attitude (Right Bank)	212
Table 8.2	General discontinuity attitude (Left Bank)	212
Table 8.3	Summary of slope sections on right bank	214
Table 8.4	Summary of slope sections on left bank	214
Table 8.5	Geological cross-section details for Right and Left Bank.	229
Table 8.6	Kinematically possible failure modes in rocks: Right bank	229
Table 8.7	Kinematically possible failure modes in rocks: Left bank	232
Table 8.8	Concluding remarks on stability and corrective measures required (Right Bank)	232
Table 8.9	Concluding remarks on stability and corrective measures required (Left Bank)	233

CHAPTER I

INTRODUCTION

Energy is an important input for the socio-economic development of a country. It is important to harness the energy from all available sources in order to provide an accelerated momentum for the overall development. The consumption of power has drastically increased in the past few decades and has been closely tied to rising levels of prosperity and economic opportunity around the world (Ahuja and Tatsutani, 2009). The sustained economic growth of the country depends on access to cleaner and environmental friendly energy sources.

Among the renewable resources, the cleanest and cheapest is the hydropower, from which 95% electricity energy output can be often achieved with 5% of loss if water supply is assured. The cost effectiveness and environmental benefits of hydroelectric power make it an important contributor to the future world energy source. The hydropower energy generation in the past few decades shows a commendable growth in energy sector due to positive contributions from Engineering Geological studies. The requirement to enhance the hydropower generation is important especially for the developing nations like India where the fossil fuel energy is getting scarcer (CEA, 2014) and the human population has been increasing at alarming rate. Moreover, the harnessing of hydropower energy involves least environmental pollution as well as extremely cheap and cost effectiveness in production.

1.1 HYDROPOWER PLANNING AND DEVELOPMENT IN INDIA

India's geographical location, geomorphic features and river system provide several advantages for the extensive use of hydropower energy resources. The Himalayan Rivers are perennial with a dominant contribution derived from the precipitation of Indian summer monsoon (June-Sep) and melting of glaciers. India is gifted with enormous amount of hydroelectric potential and ranks 5th in terms of exploitable hydro-potential on global scenario. As per the assessment made by Central Electricity Authority of India, the country is blessed with economically exploitable hydropower potential to the tune of 1, 48,700 MW of installed capacity (*CEA Report, 2014*).

1.2. HYDROPOWER PROSPECTS IN HIMALAYA

About 15% of our land area is covered in Himalayan ecosystem and consists of a comparatively dynamic young section of the geo-sphere of our nation. The high altitude glacial peak in Himalaya holds an enormous water potential, which help to augment hydroelectric resources of our country. The Himalaya accounts for the highest unused hydroelectric potential in India. The high elevations with snow covered peaks act as a source for numerous perennial streams that offer excellent opportunity to tap energy. A number of major hydroelectric projects constructed during post-independence period are considered as Engineering marvels of the past century. However, a large part of water resources in Himalaya are yet to be harnessed. The slow pace of developments related to hydropower projects can be attributed to difficult terrain characteristics, Geology and Engineering aspects.

1.3 GEOTECHNICAL PROBLEMS OF HYDROPOWER DEVELOPEMENT IN HIMALAYA

The Himalayan mountain range encompasses an area with highest topographic reliefs and has a wide range of topographical variation ranging from plains, piedmonts to steep rocky hill slopes with low to very high relief causing sudden and erratic difference in slope gradient. This region is characterized by a variety of lithological changes comprising rock types ranging from sedimentary, meta-sedimentary, metamorphic rocks of high to low grade and igneous rocks (Valdiya, 1980). Additionally, the ongoing tectonic activity in the Himalaya results in changes of terrain morphology with highly dissected hills, steep, rugged, narrow valleys and escarpments. These geological and topographical complexities make the water-resource development projects in Himalaya to face a number of constraints during planning, investigation, construction and post construction. Various geological complexities during underground excavations experienced on different project sites in Himalaya includes presence of thrust zones, shear zones, folded rock sequence, in-situ stresses, rock cover, ingress of water, geothermal gradient, gases and high level of seismicity (Sharma et al, 2015).

1.4 LITERATURE REVIEW

The Engineering Geological challenges are many and vary from terrain to terrain, both during construction and post construction of dams particularly in Himalaya. The damages caused due to huge excavation leave irreversible impact in and around the project area. A better way to understand the geomechanical behaviour of rock mass is by quantifying it (Singh and Goel, 1999). Different rock mass classification systems have evolved based on empirical approaches over the past six decades.

Many rock mass classifications were developed during this time based on a combination of factors, ever since Terzaghi (1946) proposed rock load theory classification for engineering purpose. Deere et al. (1967) developed a quantitative method called Rock Quality Designation (RQD) to estimate rock mass character from drill core logs. Palmström (1982) supplemented the RQD for estimation from surface volumetric joint count in cases of non-availability of drill core log, from visual estimation of discontinuity traces that are noticeable in surface exposures or from exploratory drifts.

Rock Quality Designation (RQD) Deere et al (1967), Rock Mass Rating (RMR) Bieniawski (1989), Q-system of Barton, 1974 are the some of the well-known, widely followed classification systems developed during past few decades. Rock Mass Rating (RMR) system was first developed by Bieniawski in 1973. Noteworthy modifications have been made over the years with corrections in 1974, 1976, 1979 and 1989. In the study, the discussion is based on Bieniawski's (1989) classification system. Though RMR and Q are very famous, they are dependent on RQD.

Hoek and Brown (1980) proposed a method for obtaining estimates of strength of jointed rock masses, based upon an assessment of the interlocking of rock blocks and their nature of joint surface condition. This was further upgraded by Hoek, Wood and Shah in 1992, which presented a modified form of failure criteria applied to jointed rock mass. Over the years, this technique was modified and upgraded (Hoek 1983, Hoek and Brown 1988) and a new classification called the Geological Strength Index (Hoek, Kaiser and Bawden 1995, Hoek 1995, Hoek and Brown 1997) was developed.

Geological mapping along with subsurface investigations, gives an overall picture about the terrain characters. The subsurface permeability test in terms of Lugeon developed by Maurice Lugeon (1933) is widely used to estimate the subsurface ground conductivity. Goodman (1980) elucidated that the values obtained from Lugeon test, directly reflects the subsurface ground conductivity of rock masses, their nature of aperture, interconnectivity, spacing and infilling material characteristics present in the weak discontinuous plane/zone. Houlsby (1976) made a significant modification by introducing the representative hydraulic conductivity values computed for different pressure stages. Grouting requirements slowly started to hold Houlsby's (1976) method as base for establishing grouting standard. Many encouraging researchers like Behrestaghi, Seshagiri Rao and Ramamurthy (1996) emphasised that the evaluation of mechanical and physical characteristics of the intact rocks is necessary to assess the rock mass quality. The overall subsurface behaviour of rock mass is dominantly controlled by the nature of discontinuities (Ghosh & Daemen, 1993).

With the increased development activities such as dams, tunnels, roads, underground powerhouses and petroleum as well as nuclear repositories, it is essential to have a more comprehensive and updated understanding of rock mass (Ramamurthy, 2010). The stability problems associated with slope and underground structures due to excavation and blasting are more pronounced in Hydro projects. The slope stability problems associated with dam abutments and reservoir area are of greater importance from environmental point of view. Computer programs with 3D graphical visualization to determine the FOS has been developed and improved in the recent years. Some famous packages like Unwedge, slide, Dip by Rocsscience (Hoek, 2006) offers quite interactive results.

The stability analysis for the slope was carried out using software package developed by Singh and Goel (2002) based on joints shear strength theory of Barton and Bandis (1990). The softwares are meant for the stability analysis of rocks, debris and talus materials. It has an inbuilt arrangement for the design of rock anchor system. The software SASW (Singh and Goel, 2002) is based on computation of the factor of safety (Hoek and Bray, 1981) of translational slip of a tetrahedral wedge formed in a rock slope by two intersecting discontinuities, the slope face and the upper ground surface.

Evaluation of slope stability by probabilistic approach can be significant contribution over deterministic approach (Chowdhury and Flentje, 2003). Heuristic methods based on landslide hazard zonation were extensive applied in Gharwal Himalaya (Anbalagan, 1992; Gupta et al. 1999; Sarkar and Kanungo 2004). Deterministic model for slope stability assessment have been carried out by Anbalagan et al (2008) and Singh et al, (2008). Computation of FOS for individual slope was detailed by Vanmarcke (1980), Kainthola (2013) and Dahal et al, (2008). Earthquake induced landslides were discussed by Dahal et al, (2013). Study by Hasegawa et al (2009) deals with slope failure during monsoon in Lesser Himalaya of Nepal. Kinematic analysis, examines the slope geometry with respect to structural discontinuities and shear strength parameters help to identify the potential mode of failure. (Markland, 1972; Goodman, 1976, Hoek and Bray 1981).

The slope instability caused due blasting for underground excavations is one of the serious issues. Though some eminent work and guidelines are present on mine blast monitoring like response of structures and damages produced from mine blast (Siskind, 1983). Measurement of ground vibration from closely controlled production blast in quarry and resultant damages were monitored (Silitonga, 1986, Indian Standard code IS 14881:2001) Effect of blast vibration on slope stability (Djordjevic et al, 2014), Impact of blasting vibration on soil slope stability (Yue Yan et al, 2014) were studied. A new predictor for ground vibration by Rai et al (2004) and few inserting research works based on numerical approach to estimate vibration (Jommi, 2008) provide some recent advances in ground monitoring. Almost in all these methods, the workers focused on the attenuation of waves and peak particle velocity for numerical modelling of the dynamic stability.

A vast study and extensive research has been seen in the field of underground space technology. Some of the pioneered workers like Barton et al, (1974), Bhasin et al, (1996), Bieniawski (1973), Goel (1994), Goel et al (1995), Jethwa et al (1980), Jethwa et al., (1996), Singh et al (1992, 1995, 1997) have developed realistic rock mass classification systems.

1.5 STUDY AREA-A BRIEF PROFILE

The Vishnugad-Pipalkoti Hydroelectric project is under construction and envisages construction of a 65m high concrete gravity dam across River Alaknanda about a kilometer downstream of the confluence of Vishnugad near village Helong (N 30º30’50”: E 79º29’30”). The impounded water shall be conveyed to an 8.8m diameter Power Tunnel (PT) of 13.4km length and finally carried to an underground power house to be located on the right bank to generate 444 MW of power near Hat village (N30º25’31” : E79º24’56”).

The geological investigations indicate that the region comprises of Garhwal Group of rocks belonging to the Proterozoic age (GSI, 2012). These rocks were separated in the north from Central Crystalline group of rocks by the Main Central Thrust. The project area lies within the Zone V of the Seismic Zoning map of India (IS1893 Part I, 2002). Hard and fairly fresh quartzite rocks are exposed with some interbanded schist in the dam site and the initial reaches of PT. The dark grey colored, dense and puckered slates are exposed further south close to Maina River area. The dolomitic limestones with slate bands are exposed on the right bank close to the powerhouse area. The option for a surface powerhouse is abandoned in favor of an underground structure as it would not only have a lesser impact on the local environment but would also be more secure.

KEY PROJECT FEATURES

VPHEP comprises a 4x111 MW (444 MW) run of the river hydro development with associated power house and related facilities. The key project features to be constructed include:

- 65m high concrete diversion dam with spillway section having 4 no. 7.2m x 15m openings.
- Intake structure with 3 no. modified horse shoe shaped intake tunnels of 6m dia.
- Desilting Complex with 3 no. underground sedimentation chambers 390m long x 20.6m wide x 17.5m deep
- Silt flushing tunnel of size 3.6m x 4.0m

- 13.40km long Power Tunnel (PT) of 8.8m finished dia.
- 140m high restricted orifice type Upstream Surge Shaft of 15m dia from El. 1165 to 1240m, 22m dia from El.1240-1305.
- 2 no. penstocks consisting of about 90m upper horizontal length, with about 130m deep vertical shafts of 5.2m diameter followed by lower horizontal penstocks of about 60m each further bifurcating into two Hig Pressure Tunnels of size 3.65m dia of about 30m length.
- Underground Power House 146m long x 20.30m wide x 50m high
- Underground Transformer Hall 142m long x 16m wide x 24.50m high

1.5.1. Location and Accessibility

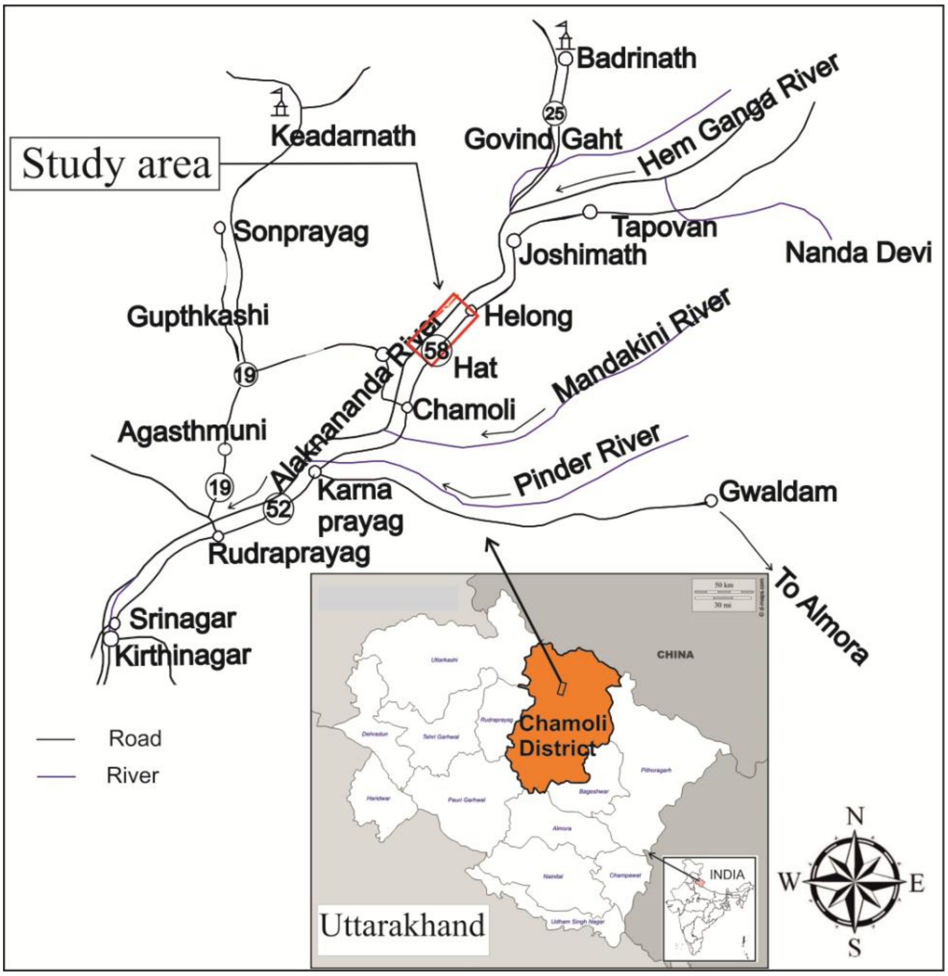

Fig 1.1 Location map of Vishnugad-Pipalkoti project.

The nearest railway station is at Rishikesh about 225km from project site. The National Highway NH-58 (Ghaziabad–Rishikesh–Pipalkoti-Joshimath) is located on the left bank of the Alaknanda river and all the project components are located on right bank of the River Alaknanda. The location map of the study area is given in Fig 1.1

1.5.2. Geomorphology

The Alaknanda River flowing southwest from Helong towards Birhi has an overall catchment of approximately 4672 sq km till the dam site. The river originates from the Satopanth-Bhagat Kharak group of glaciers (Negi et al, 1990) and has been fed by countless numbers of perennial and ephemeral tributaries–the prominent ones being Dhauli Ganga, Nandakini, Pinder and Mandakini rivers. The streams and minor watercourses have developed a trellis type of drainage pattern in the area indicating structural controls on the development of drainage pattern. The River Alaknanda in the project area runs between two high ridges running roughly NNE–SSW (Fig 1.2). The dam site is located within a narrow gorge till the height of the dam. Further above the valley on the left bank opens out. The valley in the immediate upstream of the dam fairly opens out and that will help to increase the storage capacity of the dam. The outcrops are continuously exposed on the right bank, whereas the left bank slope is mainly occupied by debris due to past slope failures. From dam site to tailrace tunnel outfall, the Alaknanda River is joined by three important tributaries namely Maina river on the right bank and Patal Ganga and Garur Ganga on the left bank. Further downstream of the dam site, the Alaknanada River flowing towards SW to SSW directions has a fairly narrow to steep valley up to power site. The left bank valley slope further downstream opens out to form a fairly wide valley. The right bank slope is generally steep with more rock exposures. Pockets of debris overburden materials could be seen at the right bank at higher levels, where agricultural terraces and human habitations are located. The left bank has a thick cover of fluvial and colluvial debris materials in the middle slope extending for considerable heights. Human habitations are more concentrated on the colluvial debris on the left bank. Since the major geological discontinuity, namely foliation, dips upstream and slightly towards the right bank, the toe erosion and the resultant failures were possibly responsible for the thick debris cover on the left bank.

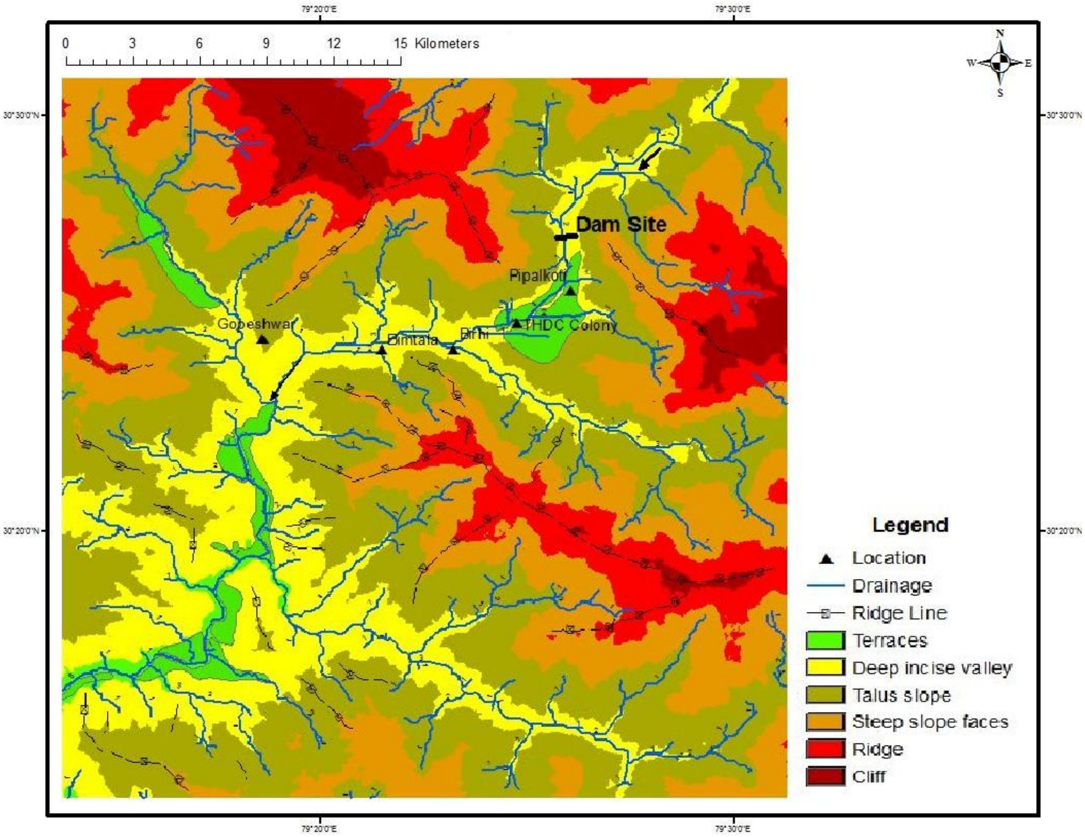

Fig 1.2 Geomorphology map of Vishnugad-Pipalkoti area.

The project units are located at lower levels on the right bank of River Alaknanda. The hill slopes on the right bank are steeper (>50º) from river bed upwards except for some patches of agricultural terraces located close to river bed. However, the left bank generally has many terraces, constituted of debris, where human habitations as well as agricultural lands are located. These terraces are located above and below the road (NH58). Out of the two rivers on left bank, the river Patal Ganga has a wider river valley with a generally higher discharge. The Garur Ganga has a narrow course with limited water discharge. In the down reaches, the river widens in the vicinity of Patal Ganga River. The Maina River on the right bank has a tight and deeper valley with vertical escarpments.

The Power tunnel traverses through a rugged mountainous terrain on the right bank of River Alaknanda in a general NE–SW direction. The ridge line also trends nearly in the same direction.

1.5.3 Climate

The total catchment area of Alaknanda River above the proposed project is 4672 sq km with approximately 2896 sq km covered with snow. The area has a mean annual rainfall ranging from 1000mm to 1500mm with maximum contribution (80%) occurs between mid June and mid-September (DPR,THDCL, 2010). The mean daily temperature fluctuates from 2° to 14° during December-January and 17° to 25° during May-June. The January (non-monsoon) period mean flow in the Alaknanda River is about 40 cumecs increasing to about 450 cumecs in the monsoon months. Peak monsoon flows are about 1300 cumecs (EA Report THDCL, 2009). The dam has been designed for a Standard Project Flood of 6700 cumecs with the appurtenant structures being designed to pass a Probable Maximum Flood (PMF) of 10840 cumecs without affecting the stability of the dam. The formation of glacial and landslide dams in the upper catchments and breaching of such structures may flush out debris along with the glacial lake outburst flow (GLOF) and may influence the project functioning.

1.5.4 Seismicity of the Area

The earthquakes in Uttarakhand during the past 200 years have been associated with loss of life accounting to thousands of people and damage of property worth crores of rupees. The Chamoli district comes under Seismic Zones V of Seismic Zoning Map of India (NIDM, 2014), which corresponds to zone factors of 0.36 (effective peak ground acceleration in terms of ‘g’) (IS 1893 part I, 2002).

The earthquake record reveals that several seismic events have ravaged different parts of the State in the last 200 years. Oldham (1869) mentions of a strong earthquake occurring in the upper valley of Ganga on September 1, 1803 at 1.35 hrs. The Oldham catalogue mentions of another major earthquake near Gangotri onMay 25, 1816 that caused numerous landslides. On August 28, 1916 an earthquake of magnitude 7.5 on Richter’s Scale having its epicenter in west Nepal had a considerable influence in Kumaon region and caused heavy damage at Dharchula. In the Kapkot earthquake of December 28, 1958 over a dozen houses collapsed. The July 29, 1980 Dharchula-Bajang earthquake of M 6.1 with epicentral intensity of VIII on MM scale caused extensive damage of land and buildings. The most destructive earthquake documented so far in Uttarakhand was that of Uttarkashi of October 20, 1991 which took a toll of 768 human lives, caused injuries to 5000 people and damaged 45,765 houses, besides inducing numerous rock slides, ground fissures and changes in hot spring chemistry (GSI, 1992). The epicentral tract occupying an area of 20 sq km around Maneri in Bhagirathi valley recorded an intensity of IX on MSK-64 scale. The main shock was followed by a series of over 2000 aftershocks in a period of two months (Valdiya, 2014).

On March 29, 1999 another major earthquake shook the entire State and inflicted moderate to heavy damage in the central part of Uttarakhand. The event, referred to as Chamoli earthquake, registered a magnitude of 6.8 at Richter's scale and an epicenter intensity of VIII. Its effects, most severe in the Alaknanda valley, were noticeable as far as up to Delhi. The strong motions damaged a total of 1,87,619 houses in Chamoli, Rudraprayag, Tehri and Pauri districts causing death of 106 persons and injuries to 453. Numerous landslides were induced by the tremors apart from development of tension fissures.

The project area forms a part of the seismic zone V, which corresponds to a zone factor of 0.36 (Effective Peak Ground Acceleration in terms of 'g' as per IS 1893: Part 2002). The north dipping Main Central Thrust (MCT) lies about 2 km northeast of the proposed dam site and the seismic status of this thrust is not properly known. The Alaknanda fault, and Srinagar thrust (NAT) are located about 32 km and 45 km southwest respectively of the proposed dam site.(Kumar, 2005) A number of other less prominent structural dislocations are also present in the area. All the project components of this project lie downstream of the Main Central Thrust.

1.6 RESEARCH GAP

Literature review has reflected a few research gaps which are summarized below. Hydroelectric Projects have serious irreversible geo-environmental impacts due to excavation during construction of mega structures blocking the water course. Though lot of environmental policies and assessment reports are found, very few research oriented works are focused to minimize the impact on geo-environmental degradation due to reservoir formation and the consequent slope instabilities due to draw down condition.

During dam construction, stability of hill slopes in natural condition as well as after dam stripping is an important consideration in geo-environmental appraisal. The stability of portal areas is also an important consideration for long term function of the tunnel. The vibrations induced due to excess use of explosives to achieve maximum pull may often lead to destabilization of hill slopes above the tunnel. This in turn may cause damages and subsidence to agricultural lands, houses, and other civil structures. These aspects though require adequate studies are some of the major research gaps, which have been successfully handled in the present research program.

Numerical modelling usually refer to homogeneous continua, they may not be adequate as a predictive tool for complex geological sites. They do not give realistic values for heterogeneous material with inclination of different layers. Though a good number of works are published on blast induced vibrations, most of them are models and numerical approaches. The few experimental studies focus mainly on the propagation peak partial velocity (PPV) and the mean square distance between the source and damage area. Overall there are as such no significant studies in particular to a site specific, with reference to its geological complexities. More over the sort of studies, Impact of blasting due to underground excavation for tunnels and effects of blasting induced vibration on the ground and civil structure on the surface with reference to geological setting of the area.

General slope stability analysis of individual hill slopes above the blasting source point with respect to aspect and morphometric and geology on fair suitable scale are almost nil. There is a gap between attenuation law and geology. In the present study an attempt was made to first delineate the area above blast source, category them material wise such, rock slopes, debris slopes and talus slope. Slope stability analysis were carried out to determine their factor of safety under natural dry static, dry dynamic, saturated static and saturated dynamic conditions. These values indicate the factors that govern the stability of a particular slope before blasting.

The studies on the relation of PPV as a function of distance R divided by the square root of charge per delay given by IS Code-14881:2001 were related to the slope stability studies. This heuristic method of estimation of charge weight per delay and the robust values are quit significant. This can be considered as a significant contribution in the field of damage assessment related to blast vibrations.

1.7 OBJECTIVES, METHODOLOGY AND ANALYTICAL TOOLS

The following are the research objectives envisaged under the research program.

1.7.1 Research objectives

1. Engineering Geological evaluation of project components of Vishnugad-Pipalkoti HEP
2. Geo-Environmental Impact assessment of the project.
3. Appropriate corrective measures and recommendations

1.7.2. Methodology Overview

The following methodology has been adopted to achieve the above mentioned objectives

A) ENGINEERING GEOLOGICAL APPRAISAL OF PIPALKOTI DAM SITE

1. Mapping of the Dam site on 1:1000 scale and preparation of Geological cross sections across the dam
2. Subsurface explorations and interpretations using drilling and drifting
3. Analysis & interpretation of water pressure tests
4. Slope stability analysis of abutments
5. Remedial / control measures.

B) GEOTECHNICAL EVALUATION OF POWER TUNNEL

1. Preparation of Geological map along PT on 1: 15,000 scale
2. Preparation of a geological cross section along PT
3. Characterization of Rock Mass-RMR, Q and RQD
4. Prediction of tunnelling condition along PT Alignment
5. Evaluation of rock pressure on roof and walls of PT
6. Evaluation of stability & support requirements

C) EVALUATION OF IMPACTS OF BLASTING ON STABILITY OF GROUND AND CIVIL STRUCTURES ABOVE PT & TRT

1. Identification of vulnerable slopes and villages likely to be affected by blasting for tunnelling
2. Preparation of geological sections across unstable slopes
3. Stability analysis of potential unstable slopes
4. Analysis of blasting impacts for calculating safe charge weight per delay

D) STABILITY STUDIES OF UNDERGROUND POWERHOUSE

1. Geological Mapping of Powerhouse area
2. 3D logging of exploratory drift
3. Geological cross section across powerhouse cavity
4. Characterization of Rock Mass-RMR, Q and RQD
5. Stability analysis for unstable rock wedges at roof & sidewall

E. STABILITY OF HILL SLOPES IN RESERVOIR RIM AREA
1. Geological Mapping of Reservoir area on 1:10,000 Scale
2. Identification of landslide prone slopes
3. Preparation of geological sections across potentially unstable slopes
4. Stability analysis of identified slopes
5. Control Measures wherever required

During field investigation, the data related to lithology and structure was collected. The rock samples were also collected for laboratory testing. The input parameters for Rock Mass Rating (RMR) were also collected at the dam area, PT alignment, powerhouse area and reservoir area.

The ground motion created due to blasting decrease with increasing distance. The impacts of blasting have been studied taking both the cases into consideration. Based on a large number of vibration studies, the typical examples of decay the maximum particle velocity is plotted as a function of scaled distance from the blast divided by the square root of the charge weight per delay.

$$PPV = f\ (R/W^{1/2})$$

Where PPV = peak particle velocity (mm/sec), R = scaled distance (m) and W = Charge weight per delay (I.S Code–14881:2001)

Estimation of shear strength parameters for different rock types encounter in project site from field and laboratory studies

- Rock Mass Rating system (RMR) by Bieniawski (1976, 1989)
- Rock Quality Designation index (*RQD*) was developed by Deere (1967)
- Q–System by Barton (1974)
- GSI by Hoek and Bray (2002)

Analysis:

<u>*Slope stability:*</u> Kinematic analysis based on Markland's test (Hoek and Bray, 1981) to determine the feasibility of slope failure due to formation of daylighting of wedge or planar discontinuities has been carried out at dam abutments, slopes above PT alignment and reservoir area.

Simplified Bishop Method was used to estimate calculate the factor of safety for potential unstable debris/ soil slopes.

Tunnel and Power house cavern: The Markland's test has been carried out to determine the formation of wedges at roof and side wall.

1.8 ANALYTICAL TOOLS

<u>Softwares Used</u> **<u>Type of Analysis</u>**

<u>In Analysis</u>

- Dips – Kinematic Analysis
- Unwedge – Tunnel wedge Analysis
- ASP – Optimum angle of cut slope with planar failure
- ASW – Optimum angle of cut slope with wedge failure
- SARC – Reservoir slope with Circular failure
- SASP – Slope with planar failure

1.9 OVERVIEW OF THESIS

CHAPTER I: This chapter discusses about an overview of the hydropower planning, development prospects in Himalaya and geotechnical problems associated with hydro power development in India. Various approaches have been indicated which deal with the minimizing of these problems. A brief introduction and background information about the study area has also been provided. The objectives, methodology and the analytical tools have also been discussed.

CHAPTER II: This chapter provides general information related to regional geology and geology of the study area.

CHAPTER III: This chapter deals with Geotechnical investigations carried at the project site. This includes surface and subsurface investigations, their results and interpretations as well as determination of geomechanical properties using rock mass classification systems.

CHAPTER IV: This chapter mainly focuses on the detailed site investigation of dam area. The stripping has been estimated based on subsurface investigations. The foundation problems and cut slope design for the foundation have also been discussed. Slope Stability analysis in terms of factor of safety (FOS) for natural slope condition and after stripping has also been carried out.

CHAPTER V: This chapter deals with the general Engineering Geological problems of the power tunnel (PT). The lithological and structural setting vis-a-vis the stability of the tunnel in different reaches has been discussed. The ultimate support pressures for roof and wall as well as support requirements have also been discussed.

CHAPTER VI: This chapter essentially deals with the impacts of blasting on the stability of terrain and other civil structures in and around the villages located close the alignment of power tunnel and tail race tunnel. Stability analysis of the hill slope located above the blast source point were analysed and appropriate corrective measures were identified.

CHAPTER VII: This chapter deals with the geotechnical evaluation of power powerhouse cavern including surface and subsurface investigations. An Engineering geological appraisal of powerhouse location indicates the problems of overbreak and water seepage that are likely to be encountered during construction. The rock mass characterization in terms of RQD, RMR, Q and GSI has also been done. The ultimate support pressures for roof and wall as well as support requirements have also been discussed

CHAPTER VIII: This chapter deals with stability of slopes in the rim of the reservoir area due to draw down conditions of water level in different seasons. The locations of vulnerable slopes have been identified and the impacts due to instability were discussed.

CHAPTER IX: This chapter provides the summary of the work carried out related to different units of the project. Based on that, significant conclusions have also been derived.

CHAPTER II

GEOLOGICAL SETTING

The Himalaya is the youngest, highest and dynamic mountain peak in the world. The Himalayan orogenic belt is the result of convergence between formerly separated continental masses namely the Eurasian plate on north and Indian plate on south, which form compressive plate boundary zone (Windley, 1995). The Himalayan arc has a general strike of WNW-ESE (Gansser, 1939). It is bounded by the Nanga Parbat syntaxis in the northwest and the Namche Barwa syntaxis in the northeast over a length of about 2400km and an average width of about 270km (Sorkhabi, 1999).

2.1 REGIONAL GEOLOGY

The Garhwal and Kumaon Himalaya (Fig 2.1), forming the central part of the Himalayan folded belt, exposes rock types of varying age from Proterozoic to Late tertiary period and are disposed in four major tectonic belts, designated as Foothill Siwalik belt, Lesser Himalayan belt, Central Crystalline and Tethyan belt. The geology of this area had been studied by many pioneering researchers since nineteenth century (Middlemiss, 1885; Holland, 1908; Burrard and Hayden, 1934; Auden, 1935; Heim and Gansser, 1939; Misra and Sharma, 1967; Jain, 1971; Rupke, 1974; G Fuchs and Anush K. Sinha 1978; Valdiya, 1980; Valdiya, 1995; Srivastava and Mitra, 1994; Richards et al., 2005). Further based on the collective field evidences and studies Himalaya mountain range have been categorised into six tectonic sheets extending in series of parallel belts (Gansser, 1964; Le Fort, 1975; Windley, 1983; Thakur, 1992) (Fig 2.2). From north to south, they are as follows: (i) the Trans-Himalayan batholith; (ii) the Indus-Tsangpo suture zone; (iii) the Tethyan (Tibetan) Himalaya; (iv) the Higher (Greater) Himalaya; (v) the Lesser (Lower) Himalaya; and (vi) the Outer (Sub) Himalaya.

The Trans-Himalaya is mainly constituted of a linear, large plutonic complex (Trans-Himalayan batholith) partially covered by continental molasse and fore-arc sedimentary rocks derived from the uplift and erosion of magmatic rocks.

The tectonic boundary between India and Asia along was first defined as `Indus Suture Line’ by Gansser (1964). The Collision between Indian plate and the Kohistan–Ladakh arc is demarcated by Indus–Tsangpo Suture Zone (ITZS) in the western Himalaya (Windley, 1995). In the upper valley of the Indus and Tsangpo (Brahmaputra) rivers, the Indus-Tsangpo suture zone extrude and exhumed outcrops composed of deep-sea and flysch sedimentary rocks (Gansser, 1964).

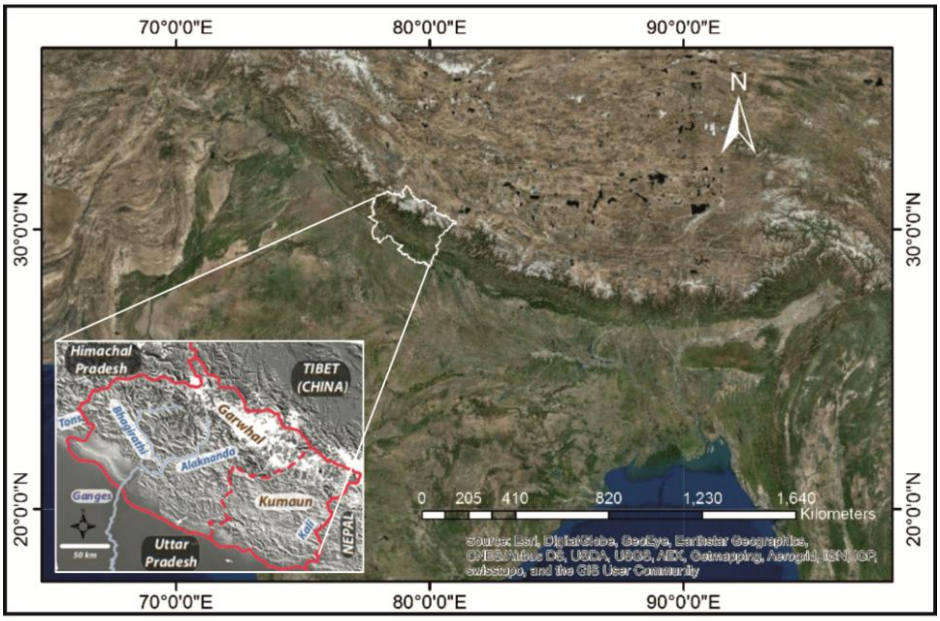

Fig 2.1 Satellite image showing Himalayan range with DEM of Garhwal Himalaya

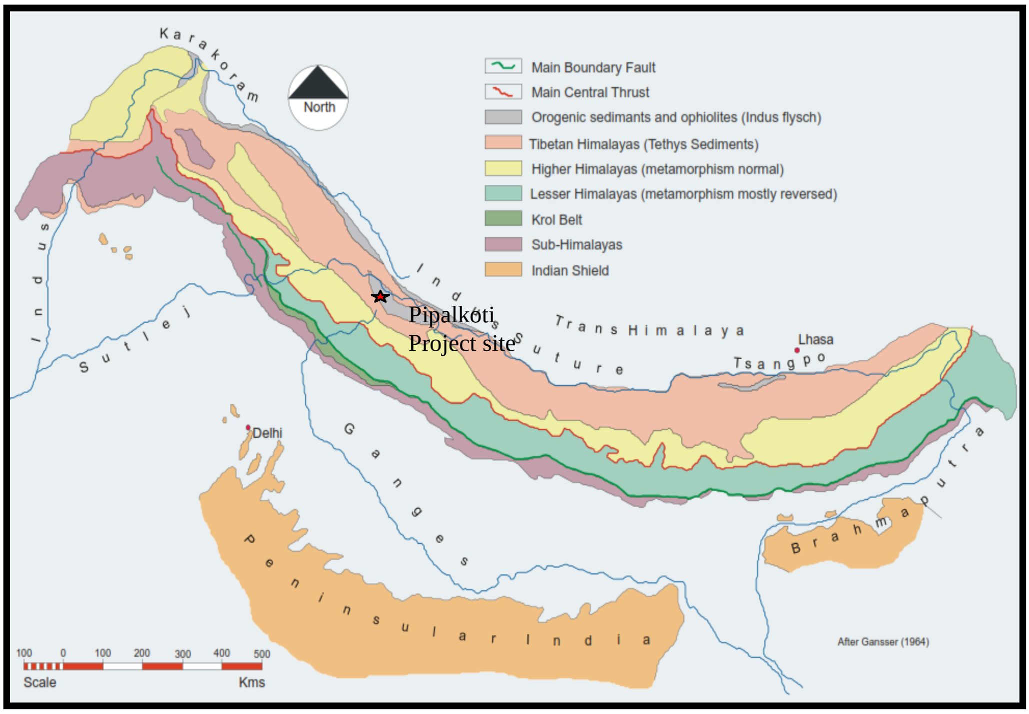

Fig 2.2 The Regional Geological map of Himalayan range (After Ganesser 1964)
http://www.geol-amu.org/himalaya

The Tethyan Himalaya (Tibetan) rocks are largely unmetamorphosed, exposed to the south of (ITSZ) with a thickness of about 10–17km marine rocks deposited on the Indian continental shelf comprised of highly fossiliferous Formations with no sharp geological discontinuity. The Tethys Himalaya occupies approximately a 40 km wide zone north of Higher Himalaya, (Verma, 1997).

The Higher (Greater) Himalaya is bounded on the south by the Main Central Thrust (MCT), which is a longitudinal thrusted low angle reverse fault as mapped by Heim and Gansser (1939) in Garhwal Himalaya. According to some workers, the real boundary lies to the south of Precambrian granite, which was designated as Munsiari Thrust by Valdiya, (1980). Most of the Himalayan geologists club these two units constitute to build the Central Crystalline Zone of the Higher Himalaya, which has been described as the Vaikrita Thrust Valdiya (1978), that demarcated as the base of the Vaikrita Group. The Main Central Crystalline belt consist of a complex of mylonite gneisses, phyllite, garnetiferous schist and kyanite bearing schist, calc silicate rock, quartzite and granites of different types (Heim and Gansser, 1939). The long belt of Central Crystalline is marked at many places by mica schist and gneisses with sills of the gabbroid to dioritic composition. In Garhwal Himalaya enormous thickness of quartzite is developed with linear intrusion of tourmaline granite at many places towards the upper most part of Garhwal Himalaya.

The Lesser Himalaya is been bounded by Main Central Thrust in the north and the Main Boundary Fault in the south. The major geological structural discontinuities in the Lesser Himalayan sequence include the Tons Thrust, the Ramgarh Thrust, and the Berinag Thrust (Fig 2.3 B). The Lesser Himalayan belt consists of a vast stretch of unfossiliferous zone in Garhwal and Kumaun regions. This could be demarcated into several important tectonic units by faults and thrusts. On the southern side, the Lesser Himalayan belt comprises of the Krol belt, a group of argillaceous, calcareous, arenaceous sedimentary rocks of Precambrian to Tertiary age. Doubly plunging synforms namely Mussorie Synform, Garhwal Synform and Nainital Synform form a part of this belt (Fuchs G and Sinha A. K, 1978). The Lesser Himalayan belt also includes rocks designated as Mandhalis, Chandpurs, Nagthat overlain by Blaini, Infra Krol, Krol, Tal and Paleogene Nummulitics in ascending order. The other belt is Almora-Dudatoli crystalline belt in Kumaon, consisting of pelitic, psemitic and semipelitic schists and quartzites intercalated with bands of migmatites, granitic gneisses and non-foliated granites rocks occurring in asymmetric synform. A vast northern sedimentary belt of unfossilferous rocks referred, as Garhwal group, latterly stretches from Uttarkashi in the north-west to Kali River in the south east and extends in to Nepal (Fuchs G and Sinha A. K, 1978).

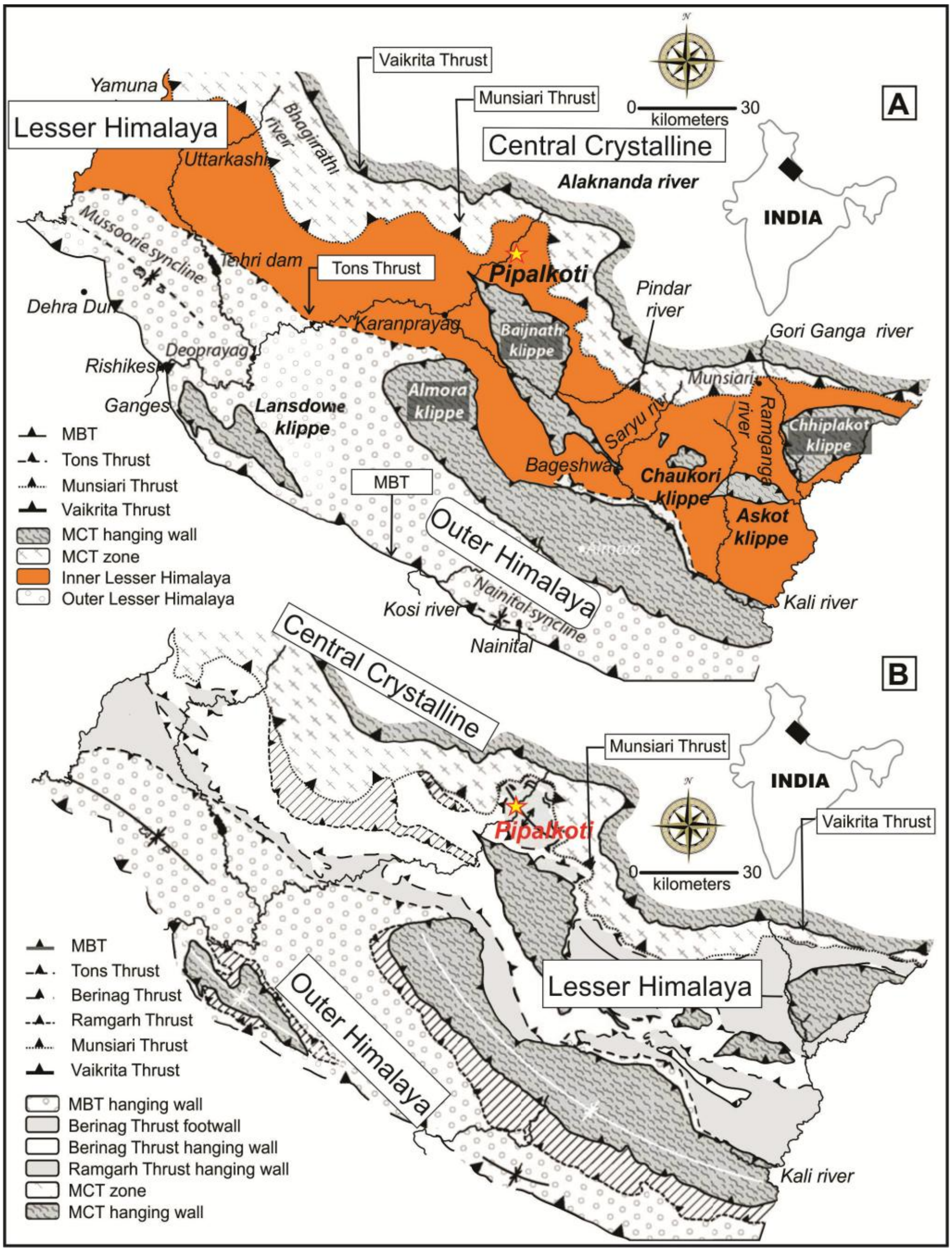

Fig 2.3 Regional Geology of Garhwal Himalaya Valdiya (1980). **A &B. Regional Geology of Pipalkoti Area. Abbreviations: MBT—Main Boundary Thrust; MCT—Main Central Thrust.**

The Sub/Outer Himalayan sequence, the Lesser Himalayan Sequence, the Greater Himalayan Crystallines and the Tethyan Himalayan Sequence are stacked from south to north by the north-dipping Main Frontal Thrust, Main Boundary Thrust and Main Central Thrust (Gansser, 1964). The Sub/Outer-Himalaya constitutes the foot-hill zone bounded by Ganges alluvial deposits on the south and by a clearly outlined tectonic feature called Main Boundary Fault on the north.

The Main Frontal Thrust (MFT) is the southernmost and neotectonically active thrust that brings the Siwaliks over the recent alluvium. The Outer Himalaya constitutes of Siwalik Hills with altitudes ranging from 250m to 800m and width between 25 and 100km characterized by flat floored structural valleys. The foothills consist entirely of a narrow belt of Lower Siwalik sediments consisting of sandstone, siltstone, shales and conglomerates. The contacts of Lower, Middle and Upper Siwalik Formations are gradational in general and at places marked by strike faults (Sorkhabi and Macfarlane, 1999).

2.2 GEOLOGY OF PROJECT SITE

The project area, forming a part of Alaknanda valley, is mainly constituted of rocks belonging to Garhwal Group in the Lesser Himalaya. Towards north and in the tail reaches of the reservoir, these rocks area truncated by MCT (Munisari Thrust) (Fig 2.4). A minor portion of Central Himalayan Crystalline rocks are exposed to the north of MCT. The rocks of ‘Carbonate Suite of Chamoli’ of ‘Garhwal Group’ occur between Chinka and Helong (Gaur et. al., 1977; Srivastava and Ahmad, 1979; Valdiya, 1980) and also contain the major magnesite bodies of this region.

Structure

Pipalkoti Anticline (doubly plunging anticline) is a regional fold between Birahi and Helong, representing the western continuation of anticlinorium of Tejam (Valdiya, 1980). The axis of this anticline trends WNW/NW-ESE/SE and passes about two kilometers south of Pipalkoti through Mayapur. In the east as well as west, the amount of plunge is low (about 20º). The northern limb of the anticline dips at low angle between 15 and 30° towards N, whereas the southern limb dips at 50 to 55 towards SW (Gaur et. al., 1977). The southern limb of this structure is cut short by a major fault. The northern limb of the fold extends from Mayapur upto Helong for a distance of nearly 23km, which itself has been folded repeatedly (VHEP, DPR 2010). At Helong, a tectonic break (MCT) is met with layers of basic rocks overthrusting of metamorphic schist and gneisses. Over the thrust plane immediately the Crystallines are represented by chlorite schist interbanded with quartzites. The Main Central Thrust dips at 45 towards northeasterly i.e. upstream direction.

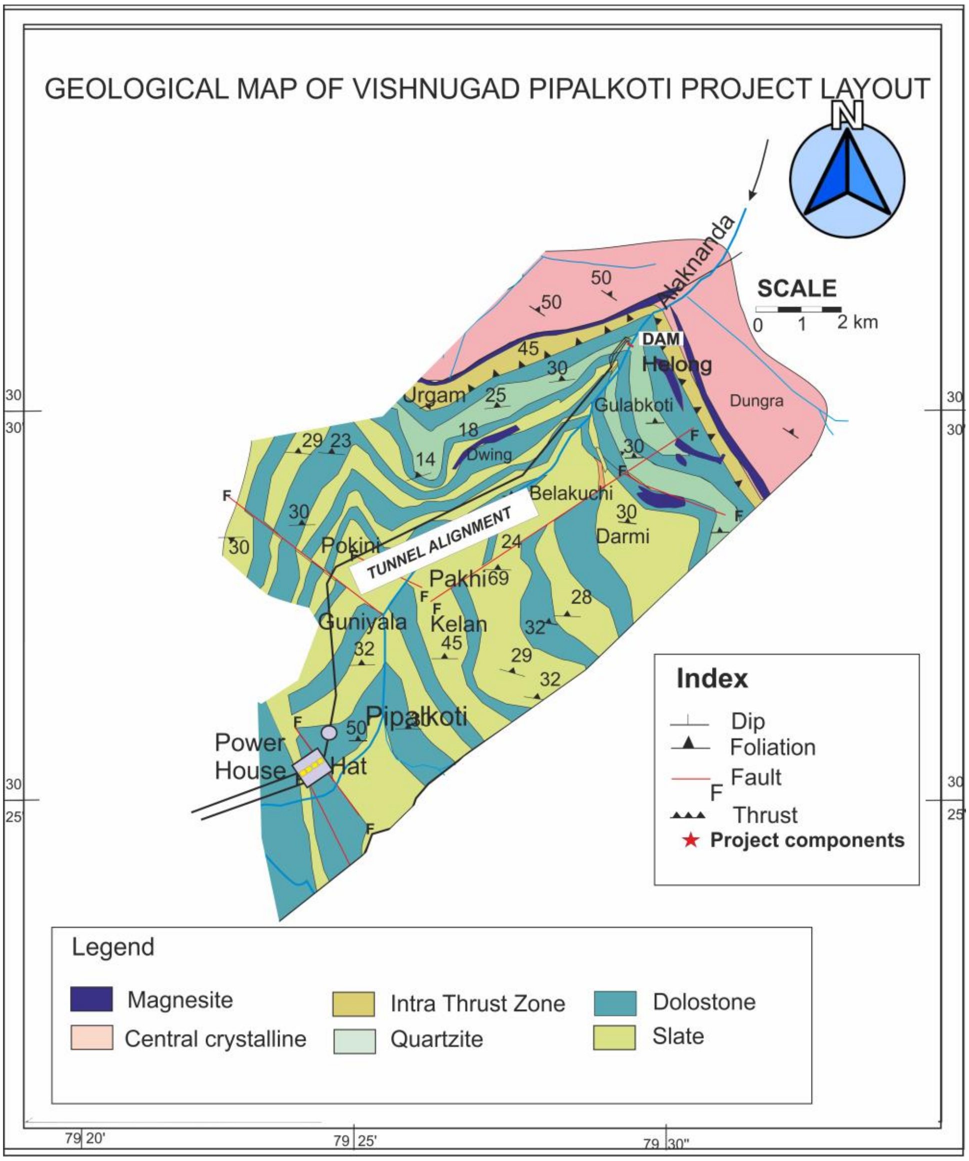

Fig 2.4 Geological map of the project area. (Modified after Gaur et. al., 1977)

All the project components are located between Birahi on south and Helong on north. The Geology of dam site, power tunnel and power house area were mapped on 1:1000, 1:15000 and 1:1000 scales respectively. In some of the inaccessible areas along power tunnel alignment on the right bank, the geological features have been projected from the left bank. The rocks occurring at the dam site are quartzites, which extends in the initial reaches of power tunnel also. In remaining parts of the tunnel alignment, alternating bands of grey slates and dolomitic limestones are exposed. The grey slates are interbedded with thin bands of dolomitic limestone and vice versa has also been observed.

Table 2.1 Litho-Tectonic Setup of the Vishnugad-Pipalkoti H-E Project (after THDC 2010, DPR)

	Litho-Units	Lithology
Central Crystalline	Joshimath Fm. (Inner Crystalline)	Kyanite gneiss, Banded augen gneiss, migmatite, garnetiferous-biotite-schit and amphibolite
	---------------Vaikrita Thrust / MCT-II---------------- (Jharkula-Bargaon-Saldhar)	
	Helong Fm. (Outer Crystalline)	Mylonitised augen gneisses and migmatites, mica-schist, amphibolites and crystalline marble Sericite quartzite and quartz mica schist Quartzite and chlorite schist.
	-----------------Munsiari Thrust / MCT-I / Floor Thrust----------------- (1.5 km South-west of Helong to south of Tapovan via Salur)	
Garhwal Group/ Lesser Himalaya	Chamoli/ Gulabkoti Formation	Grey fine-graineddolomitic limestone. Siliceous on the top and base. Numerous magnesite lenses. Medium grained, grey to greyish green quartzite along the contact. Subordinate schistose quartzites with a thin band of amphibolite.
		----------------------Gulabkoti Thrust (?)------------------------
	Pipalkoti Formation	Alternate slate anddolomitic limestone units. Slates are mainly graphitic and calcareous. Thinly intercalated limestone and slate unit. In the upper horizon of this unit limestone becomes massive and contains chip of bluish limestone. This is arenaceous phyllite and chloritoid slate. Numerous pockets of magnesite.
		------------------------**Birahi** Fault------------------------
	Chamoli/ Chinka Formation	Shear Zone: Mylonite quartzites, blasto mylonites, augen mylonites, augen schists. Thin amphibolites along **Birahi** fault.
		---------------------------Chinka Fault------------------------------

		Pure quartzites of greyish green colour. Orthoquartzites and subordinate schistose quartzites

However, the rocks occurring at powerhouse site include calcareous slates and dolomitic limestones, while dolomitic limestones, metabasics, augen gneisses and schists are exposed along tail race tunnel (TRT). The rocks on the whole are very complexly folded and sheared. The rocks of the area can be categorized into four Formations namely (Table 2.1): Pipalkoti Formation, Chinka Formation, Gulabkoti Formation and Helong Formation (Valdiya, 1980).

The Pipalkoti Formation forming core of the anticline consists of alternating sequence of slate and dolomitic limestone. In the north this Formation has been thrusted upon by the Gulabkoti Formation along Gulabkoti thrust whereas on the south, this has been separated from the Chinka Formaion by the **Birahi** fault (Gaur Girish et. al., 1977).

Pipalkoti Formation: It is made up of alternating sequence of slates and dolomitic limestone. The slates show variations in the physical appearance in difference location which can be summarised as follows - (i) Finely laminated greyish black slates intercalated with thin bands of bluish grey limestone, (ii) Black graphitic slates/phyllites, (iii) Dark coloured chloritic slates, (iv) Arenaceous phyllites with subordinate hematite schist, (v) Green and violate splintery slates and (vi) chloritoid slates with thin band of iron ore (Gaur Girish et. al., 1977). The greyish black slates are compact and massive with argillaceous bands and are well developed in the core of the Pipalkoti anticline. These slates contain thin bands (upto 10cm) of dark bluish grey, fine grained limestone. The black graphitic slates/phyllites are friable and ferruginous and show effects of pronounced iron leaching. The suite is best developed in the central part of the Pipalkoti Formation near the village Tangani, located on the northern limb and around Jaisal village on the southern limb. The dark coloured slates are encountered in the upper horizons near Gulabkoti and the finely laminated chloritic slates are marked by the smell of sulphuric acid and white encrustations of aluminum sulphate. On the southern limb of the anticline, arenaceous phyllites occur at the contact of slate unit and are exposed in nearly 15m thick zone along the Hat fault. Close to the fault, very thin bands (0.5 m) of hematite schist are also associated with these phyllites. Chloritoid slates are present near Jaisal village in a narrow zone between two dolomitic limestone bands close to southern limb along the Jaisal Fault (Gaur Girish et. al., 1977). The slates are greenish grey, hard compact and massive with well-developed chloritoid along the foliation planes. Geologically, Pipalkoti hamlet is situated on the apex of anticline structures composed of dolomitic limestone and slaty rock complex below quartzites. These dolomitic limestones are magnesite bearing due to hydrothermal alternations. The slaty rocks of greyish dark colour are exposed near Pakhi village, which are severely deformed at places with microfolds and cleavages. These slaty rocks are calcareous and the limestone bands can be often encountered as we go ahead upstream towards the dam site. These limestones are massive in nature and in turn they are overlain by thick white and greyish quartzites. Basic sills are seen emplaced in quartzites at places. They show well developed schistose structure in them. The quartzites grade to talc at many places.

Several units of dolomitic limestone constitute the Pipalkoti Formation. In the northern limb six dolomitic limestone units and in the southern limb only three units of the same have been established. Lithologically, these can be classified into 3 types - (i) Talcose dolomitic limestone and talc dolomitic limestone schist, (ii) Massive Dolomitic limestone with upper siliceous horizons and (iii) Well foliated dolomitic limestones. Of these, the talcose dolomitic limestones are extremely fine grained and show large scale development of talc along the fine laminae. At places, it grades into white, grey, buff and greenish grey coloured talc-dolomitic limestone schists due to intense shearing, as can be best seen in the Patalganga and Garurganga valleys and south of village Jaisal. Talc is found generally as thin films along the foliation palnes. The massive dolomitic limestone is mostly of grey to greyish-white colour and is intensely sheared at places. They grade upward into medium to fine friable siliceous dolomitic limestone of cream to greyish white colour. The limestones intercalated with slates are best exposed along the river **Birahi** Ganga. These rocks are fine grained and bluish grey in colour. A Well foliated, fine to medium grained cream coloured marble bearing thin bands or small pockets of flaky talc is present along the **Birahi** fault. In addition, the foliated dolomitic limestones can be commonly seen in many places, where the rocks are seen folded locally. Further the dolomitic limestone units contain numerous pockets and lenses of magnesite and talc.

Chinka Formation: South of the **Birahi**, the Chinka Formation consists mainly of greenish quartzite, orthoquartzite, schistose quartzite and subordinate mylonite. It makes a faulted contact with the rocks of the Pipalkoti Formation. The greenish grey quartzite is commonly hard, compact and occurs forming a syncline adjacent to the anticline of the carbonate suite. In the northern limb of the syncline, mylonitization is well observed along a shear zone bounded by the **Birahi** fault and the Chinka Fault (Gaur et. al., 1977). The mylonites are characterized by augen schists, augen mylonites, blastomylonites and mylonitic quartzites. The quartzite members of this Formation also exhibit cataclastic effects and mortar textures.

Gulabkoti Formation: The Gulabkoti Formation composed of quartzites, dolomitic limestones, magnesites and mylonites has been thrust upon by the rocks of 'Central Crystallines' along the low angle northerly dipping 'Main Central Thrust' close to tail reaches of reservoir near Helong village. At Gulabkoti, a thin concordant metabasic sill is observed in the quartzites (Mehdi et al., 1972). The quartzites, Dolomitic limestones and mylonites, are present in reservoir area close to Helong. The quartzite is somewhat friable and intercalated with a schistose type. The schistose quartzites bear mica flakes which lie oriented along the foliation planes and parallel to the original bedding and which can be marked by change in colour. The dolomitic limestones are fine grained, grey coloured and thinly bedded rocks, which are siliceous towards the top. The top of this dolomitic limestone unit is marked by the creamish pink marble in which the elongated calcite grains are prominently developed along the foliation planes. These rocks are characterized by augen schists, augen mylonites and mylonitic quartzites.

In the south of Birahi around Chinka area, the gneisses and schists with some phyllonite are exposed and these rocks are physical continuation of Nandprayag-Ghat section and therefore called the Baijnath Crystallines (Srivastava, and Ahmad, 1979; Valdiya, 1980). The Chamoli Formation occurs in a synformal core and the quartzite to the north of Pipalkoti occurs on the northern flank of Pipalkoti anticline, being stratigraphically younger to the Pipalkoti Formation. The quartzite rocks are fine grained and saccharoidal, often schistose and sericitic in nature. Magnesite bodies are mostly localized towards the margins of the Calc Zone (Gaur et. al., 1977).

The talc occurs as intergranular flakes, veins and pockets. The dolomitic limestone units of the southern limb of Pipalkoti anticline particularly show profuse recrystallization and intense development of talc. Shearing is more intense in this limb and numerous slip planes parallel to bedding are commonly developed. In brief, most of the dolomitic limestone units have discordant contacts with the overlying and the underlying units. In few localities (e.g.

near Patalganag) the Dolomitic limestones have been transformed into talc-dolomitic limestone schist.

Metabasics: Metabasics, mainly amphibolites and rarely hornblende-chlorite schist are found in the area. They are confined: (i) along the 'MCT', these separate the Central Crystallines from the sedimentaries of the Garhwal Group, (ii) along the **Birahi** fault, these separate the Pipalkoti Formation from the Chamoli Formation and (iii) near Gulabkoti, where, they are associated with the quartzites of the Chamoli Formation. Metabasics along the MCT appear to be syntectonic with the thrust movement, whereas along the **Birahi** fault, they are transgressive sills in the 'Shear Zone' and may be either syn-or post-tectonic (Ahmad and Tarney, 1991).

Helong Formation: The Outer Crystalline rocks of Helong Formation are exposed about half a kilometre from Helong village, towards north. These low grade metamorphic rocks belong to Green schist facies (Srivastava and Ahmad, 1979) which grade upwards up to almandine-amphibolite facies, comprised of chlorite-schist, quartzite, quartz mica-schist, amphibolites, calc-silicate marble, augen gneisses and migmatites (Bhattacharya et al., 1982).

Main Central Thrust: In the project area, close to the tail reaches of the reservoir, the 'MCT' has brought the Central Crystallines over the Garhwal Group and is not very well marked as in many other areas of the Himalaya. Earlier workers noted two thrusts in this locality, one passing from Helong and other passing through Gulabkoti (Valdiya, 1980). Above the dolomitic limestone of Gulabkoti Formation, a thin marble exhibiting cataclastic effects with elongated carbonate minerals in its upper parts is observed. This marble dips at 20° to 30° towards N20°, whereas the overlying mylonites of the 'Intra-Thrust Zone' dip at 30° to 50° towards N355°, showing discordance along the contact. Due to distinct mylonitic nature of the rocks of the 'Intra Thrust zone' and the cataclastic effects exhibited by the marble lying below it, a distinct plane of movement called Salur Thrust has been indicated (Mehdi et al., 1972). The foliation planes of central crystallines dip steeper than the rocks of 'Intra Thrust Zone'. A thin, impersistent amphibolite are encountered along the contact. Thus a major tectonic plane (MCT) is indicated between the rocks of the 'Intra Thrust Zone' and the 'Central Crystallines'. The "MCT' dips at low angles (15° to 20°) towards NE in the eastern region, whereas in the central parts it dips between 30^{o} and 40^{o} towards N. Further west, it dips between 45° and 55°, again towards north.

Maina nadi: A shear zone is postulated along of the Maina nadi based on surface evidences. The dolomitic limestone shows appreciable vertical upliftment of the northern block along the flow of the river close to its confluence with Alaknanda. The shear zone runs roughly N40^{o}W-S40^{o}E direction and can be traced for about 500m along the river course and dips at about 65° roughly towards S50°W. Though the scarp faces can be seen on the rock slopes of both the banks, the river bed is occupied by 10-15m thick alluvial deposits. The power tunnel is located about 20m from the surface of the river and as such the tunnel may have a top rock cover of about 10m.

2.3 THERMAL SPRINGS

In the Garhwal Himalaya, as many as 62 thermal springs are reported. As per the Geothermal Atlas of India (GSI Pub.) as many as 19 thermal springs have been recognized in Alaknanda valley from Kharbagar in the south (E 29°59’30”: N 79°55’56”) to Madhyamaheshwar (E 30°59’20”: N 79°12’30”) and the area includes the Tapovan (E 30°29’30”: N 79°33’30”) which is upstream of the dam site in the Dhauli Ganga valley. In addition to this site, one hot spring had been reported on the right bank of river Dhauli Ganga closer to river bank at Charmi Village (E 30°30’49.6’’: N 79°36’36.9’’). During mapping of the Dam site area, hot water springs have been recorded at three locations, two are closer to the right bank and one to the left bank. In the drill hole (DH-8) at El. 1229.07m (E 38°43’51.505”, N 75°42’81.48”) on the right bank, hot water was encountered in the overburden with a measured temperature of 68°C. In addition a number of cold water springs have also been seen in the area (Table 2.2).

Table 2.2 Details of thermal springs encountered in dam site area

Location	Lat/Long	Elevation	Geological Setting	Temperature (Centigrade)
Left Bank of Alaknanda	E3843547.416 N754365.372	1230.30m	On the left bank of river through the vertical joints in quartzites	50^{o}C
Right Bank of Alaknanda	E3843492.948 N754411.086	1231.84m	Through foliation joint of the quartzite on the right bank.	55^{o}C

Right Bank of Alaknanda	E3843500.135 N754407.922	1231.20m	Through oblique joint of the quartzite on the right bank.	60^{o}C

(Source: DPR 2010)

CHAPTER III

GEOTECHNICAL INVESTIGATIONS

The Geotechnical investigations constitute various site investigations carried out on surface and subsurface as well as laboratory studies. The understanding of quality of rock mass is the basic step required for a safer and rational design of engineering structures in or on rocks (Bhasin et al., 1995). The designers generally consider influential shear strength parameters and deformation behaviour of rock mass for the site selection (Singh and Rao, 2004), which can be achieved through evaluation of geo-mechanical properties such as Rock Mass Rating (Bieniawski, 1972), Q (Barton et al, 1974), Geological Strength Index (Marinos and Hoek, 2000) and other strength properties. The strength properties so obtained are used for carrying out further analysis related to stability and support system.

3.1 SUBSURFACE EXPLORATIONS

The overall subsurface behaviour of rock mass is dominantly controlled by the nature of discontinuities (Ghosh & Daemen, 1993). The detailed subsurface investigations in dam area, power tunnel and powerhouse facilitate to understand the rock mass condition and its nature of behaviour with respect to applied load. While carrying out borehole test like permeability to evaluate in-situ rock mass character, necessary caution was followed to avoid miscalculations. In-situ tests in the exploratory drifts give realistic results on shear strength properties of jointed rock masses, as large part of the deformability may depend upon the rock discontinuities (Bhasin, 1996).

In order to evaluate subsurface ground condition, geotechnical investigations were carried out in dam, power tunnel and powerhouse area of Vishnugad-Pipalkoti HEP. In total, borehole drilling of about 5500 m and exploratory drifting of 1700 m were done (Table 3.1). Exploratory drifts of 2.0 m x 1.8 m were driven at the dam site, surge shaft and powerhouse areas.

3.1.1 Exploratory Drill Holes

To understand the subsurface rock mass characteristics at specific depths, 17 bore holes were drilled along proposed dam axis with a spacing of 50 to 150 m and at different locations in powerhouse and surge shaft area. In addition this facilitated to establish the overburden and bed rock contact. The core log specimens obtained were used for determining physical and engineering properties of the rock by laboratory tests. In addition, cyclic percolation tests were carried out in the drill holes at dam site and the penne ability of the foundation material were studied. The results obtained are summarised in Table 3.2 to 3.7

Table 3.1 Summary of exploratory drill holes and drifts

Location	**No. of Drill holes**	**Total drilling (m)**	**No. of drifts**	**Total drifts (m)**
Pre-feasibility dam sites	2	61.35		
Dam sites	17	771.87	3	250
Power Tunnel (PT) & Maina	9	1107.95		
Diversion Tunnel	2	168.10		
Desilting Chamber	2	281.40	1 + 2 crosscuts	250
Upstream Surge Shaft	2	207.30		
Powerhouse	5	431.90	1 + crosscuts	960
Powerhouse drift	12	560.00		
Birahi drift	3	542.00	1	240
Downstream Surge Shaft	1	400.50		
Tail Race Tunnel	2	340.60		
Geothermal Studies	1	115.50		
Geophysical Tests	6	208.60		
Test Grouting (Dam)	7	293.00		
Totals	68	5490.07		1700

Table 3.2 Summary of Drill Holes at Dam Site

Drill Hole No	Collar Elevation El±(m)	Location	Over Burden Depth (m)	Nature of Over Burden	Total Depth Drilled El±(m)	Nature of Rocks	Remarks
DH-1	1231.85	On left bank 50m u/s of dam axis	7.40m	Pebble, cobble and boulders of quartzite and schist in sandy matrix.	30.20	Dirty white colour, fine grained sericite banded quartzite with thin interbands/ partings of sericite-chlorite schist.	Core recovery in the bed rock varies from 84% to 100% with RQD varying 56% to 100%
DH-2	1230.30	On left bank 50m u/s of dam axis	10.65m	Pebble, cobble and boulders of quartzite, gneiss and schist in sandy matrix.	50.30	Medium to fine grained recrystallized banded quartzite with thin interbands of sericite-chlorite schist along with quartz vein	At 28.50 m (El. 1201.8 m) depth hot water discharge of 25 litres/5 minutes with temperature of 54C has been observed. Core recovery in the bed rock varies from 69% to 100% with RQD varying 70% to 100%.
DH-3	1319.00	50m upstream on the left bank of the river,	12.0	Hill slope debris material compositing of quartzites	30	White to off-white banded, cross bedded, laminated, sericite	Core recovery in the weathered rock mass (below the debris) is 25% while below it varies from 52% to 100%

		from the dam axis				bearing quartzite	with RQD varying 11% to 74%.
DH-4	1291.0	50m upstream on the left bank of the river, from the dam axis	1.60	Scree and debris	61.10	Banded, off-white, recrystallized, sericite bearing quartzite with 2-5 cm thick quartz veins	The core shows the splitting along sub-vertical to vertical joints. Core recovery in the bed rock varies from 50% to 100% with RQD varying 10% to 99%.
DH-5	1230.45	Located in the main channel of the river towards the right bank 50m u/s of dam axis	13.20	River borne material composed of coarse sand, grit, gravel, pebble cobble and boulders of quartzite, gneiss and schist	36.80	Fresh, off-white, recrystallized, banded, sericite bearing quartzite with thin interbands of sericite-chlorite schist	Pot holes /cavities at 16.70m, 17.30m, 18.25m-18.80m and 20.20m–20.70m depth were observed. Core recovery in the bed rock varies from 75% to 98.88% with RQD varying 33% to 90%. The presence of hot water from 13.20 m depth under artesian conditions with temperature of 49°C while at 25.30 m the temperature of the hot water is 68°C
DH-6	1231.15	Located on the right bank of the river 50m u/s of	25.10	River borne material composed of coarse sand, grit, gravel,	38.20	Greenish to off-white, sericite bearing quartzite	Core recovery in the bed rock varies from 80% to 100% with RQD varying 9.09% to 98.66%. At 24.30 m depth

		the dam axis		pebble cobble and boulders of quartzite, gneiss and schist			discharge of hot water under artesian conditions with temperature of 55C has been reported. Further down discharge of hot water increased 5 litres to 20 litres / minute.
DH-7	1229.27	Located in the river channel near the right bank 25 m U/S of dam axis	21.50	River borne material composed of coarse sand, grit, gravel, pebble cobble and boulders of quartzite and schist	51.80	Fine grained greyish white quartzite with a quartz vein	Core recovery in the bed rock varies from 80% to 100% with RQD varying 24.00% to 97.00%. The hot water was recorded from 8.0 m depth under artesian conditions with temperature of 65°C
DH-8	1229.33	Located 30m D/S of dam axis at right bank of river bed	8.0	River borne material composed of coarse sand, grit, gravel, pebble cobble and boulders of quartzite	50.70	Fine grained greyish white quartzite	Core recovery in the bed rock varies from 50% to 100% with RQD varying nil to 92.00%
DH-9	1257.5	Located 105 m U/S of dam axis at the right bank of the river	Nil	Nil	50.40	Fine grained greyish white quartzite	Core recovery in the bed rock varies from 85% to 100% with RQD varying 24.00% to 98.00%.

DH-10	1303.73	Located 50m U/S of the dam axis on the left bank	1.0	Colluvial material	100.25	Fresh, off-white, recrystallized, banded quartzite with thin interbands of sericite-chlorite schist from 59-60 m	Minor shear zones were observed from 17.10-17.20m, 18.90-19.00m, 48.40-48.50m, 49.00-49.15 m, 74.60-75.00, 70.80-71.00 m, 86.00–86.50 m and 87.30–87.60 m. Core recovery in the bed rock varies from 80.00% to 100.00% with RQD varying nil to 100.00%

Table 3.3 Summary of Drill Holes at Desilting Chamber

Drill Hole No	Collar Elevation El±(m)	Location	Over Burden Depth (m)	Nature of Over Burden	Total Depth Drilled El±(m)	Nature of Rocks	Remarks
DCH 1	1319.30	20 U/S of dam axis in the desilting chamber area	9	Boulders and pebble of quartzite in a sandy matrix	110.30	Fine grained greyish white quartzite with a biotite chlorite schist band between 12.45-14.0 m has been met up to drilled depth of 110.3	Thin shear zone have been recorded from 49.50-49.70 m, 57.47-57.65 m, 78.50-78.70 and 91.70-92.40. The percentage core recovery ranges from 80 to 100 percent while the RQD varies from 10 to

						m (EL. 1208.73 m)	100 percent.
DCH 2	1379.13	100m D/S of dam axis in the desilting chamber area	4	Boulders and pebble of quartzite in a sandy matrix	171.30	Compact grained grayish white quartzite	The quartzite vein have been recorded 5to 10cm between 68.85-66.90, 99-99.10, 139.50-139.60.The rock is highly jointed & fractured. The percentage core recovery ranges from 80 to 100 % while the RQD varies from 0 to 100%.

Table 3.4 Summary of Drill Holes at Diversion Tunnel

Drill Hole No	Collar Elevation El±(m)	Location	Over Burden Depth (m)	Nature of Over Burden	Total Depth Drilled El±(m)	Nature of Rocks	Remarks
DTH-1	1289.30	Located on the left bank of the river, along the diversion tunnel,	10.50	Hill slope materials mainly chips and blocks of quartzites	60.20	Off-white to white, greenish, laminated, recrystallized, sericite bearing quartzite with thin partings of sericite-chlorite schist	Core recovery in the bed rock varies from 14.66% to 97% with RQD varying 0.0% to 63%.

		U/S of dam axis in the slope				is met from 10.50 m depths (EL. 1278.8 m) to 60.20 m depth (EL. 1229.1 m)	
DTH–2	1272.62	located on the left bank of the river, in the inlet of diversion tunnel, in the slope	38.50	Hill slope materials (Colluvial) mainly chips and blocks of quartzites, gneisses, schist, magnesite.	52.50	Greyish white quartzite, with a thin band of shear zone between 42.50 to 42.60 and 47.80 to 48.00 m depth. From 47.80 mainly chlorite schist has been proved down to 52.50 m with a thin band of quartzite between 48.50 to 48.70 m	Core recovery in the bed rock varies from 40% to 100% with RQD varying 12% to 50%.
DTH–3	1333.15	Located on the left bank of the river, in the out let of diversion tunnel.	7	Hill slope materials mainly chips and blocks of quartzites	115.55	Off-white to white, fine grained quartzite with thin partings of chlorite schist at places	Two minor shear zones between 103.67-103.83 and 105.23-105.83 have been encountered in the hole. Core recovery in the bed rock varies from 90% to 100% with RQD varying 20.0% to 100%.

Table 3.5 Summary of Drill Holes at Power Tunnel (Pt) Alignments

Drill Hole No	Collar Elevation El±(m)	Location	Over Burden Depth (m)	Nature of Over Burden	Total Depth Drilled El±(m)	Nature of Rocks	Remarks
PT-1	1240.21	Right bank of Maina Nadi bed	7.0	River borne gravels pebbles and boulders of gneiss, schist, shale/ slate and dolomitic limestone	50.10	Thinly foliated, greyish black, shale/slate with interbands of dolomitic limestone has been met up to a depth of 15.00 m, below this level splintery, grayish black shale/slate has been met upto drilled depth of 50.10m	The percentage core recovery varies from 50% to 100% while the RQD percentage varies from 10 % to 94%.
PT-2	1239.14	Located in the right bank of Maina river bed, at the PT crossing point	9.5	River borne material containing sand, grit, gravels pebbles and boulders of gneiss, schist, shale/ slate and dolomitic limestone	56	Bed rock consisting of thinly foliated, greyish black shale/slate with interbands of dolomitic limestone has been met up to a depth of 12.18 m, below this level splintery, grayish black shale/slate	The percentage core recovery varies from 80% to 100% while the RQD percentage varies from nil to 84%.
PT-3	1501.05	Located along	18.50	River borne material	285.05	Bed rock consisting of quartzite up	

		the Dwing nala, at the PT crossing point		containing sand, grit, gravels pebbles and boulders of gneiss, schist, shale/ slate and dolomitic limestone		to a depth of 22.50 m (EL. 1478.55 m), below this level a band of talc upto of 28.6m (EL. 1472.45 m) has encountered.	
Remarks on PT 3	In quartzite and talc the percentage of RQD is very low while the percentage core recovery in quartzite varies from 10 to 100% and in talc 60 to 80%. From 28.6 m to 71.5 (EL.1429.55 m) the quartzite with minor bands of talc and dolomitic limestone was observed with variation in percentage core recovery from 80 to 100%. With RQD ranging from 9 to 79%. From 71.5 m to 106.8 m (EL.1394.25 m) depth quartzite with bands of dolomitic limestone were recorded showing variation in core recovery from 80 to 100% with the RQD percentage ranges from 19 to 89%. From 106.8 m (EL. 1394.25 m) to 163.4 m (EL. 1394.25 m) depth dolomitic limestone with bands of magnesite was encountered and the percentage core recovery is 80 to 100% and the RQD percentage varies from 12 to 76%. From 163.4 m (EL.1394.25 m) to 178 m (EL. 1323.05 m) depth quartzite was observed and the percentage core recovery varies from 60.0 to 100% and the RQD percentage varies from 0.0 to 44%. From 178.0 m (EL. 1323.05 m) to 235.0 m (EL. 1266.05 m) depth dolomitic limestone with bands of magnesite was encountered and the percentage core recovery is 60 to 90%. The RQD percentage varies from 8 to 70%. From 235.0 m (EL. 1266.05 m) down to total depth i.e. 285.05 m (EL. 1216.45 m) slates were found and the percentage core recovery is 90 to 100% and the RQD percentage varies from 8 to 50%.						

Table 3.6 Summary of Drill Holes at Surge Shaft

Drill Hole No	Collar Elevation El±(m)	Location	Over Burden Depth (m)	Nature of Over Burden	Total Depth Drilled El±(m)	Nature of Rocks	Remarks
SSH-1	1346.30	Located at the surge shaft location	9	Clayey type matrix mixed with rock fragments of dolomitic limestone up to 9m.	166.53	White to grey banded, at places laminated, dolomitic limestone	The core recovery in this zone varies from 71 to 98%. The RQD varies in different rocks from Nil to 83% and all along the depth variations were recorded. Folding is observed in bed rocks. Minor shears (clay <2 cm) recorded at depth at El 1275.100-1274.100 m and El 1241.100-1240.100 m.

Table 3.7 Summary of Drill Holes at Powerhouse

Drill Hole No	Collar Elevation El±(m)	Location	Over Burden Depth (m)	Nature of Over Burden	Total Depth Drilled El±(m)	Nature of Rocks	Remarks
PHH 1	1157.62	Located on right bank in Hat village above urbanised area.	16.50 41.50	Clayey type matrix mixed with rock fragments of dolomitic limestone up to 4m. Further down river borne material consisting of medium to coarse grained sand, pebble and cobbles of gneiss, basic rock, quartzite and dolomitic lime stone are seen up to 16.5m. Below the overburden, weathered grayish black, thinly foliated splintery	115.30	Weathered and highly jointed slate with thin interbands of shale are encountered from depth of 16.5m up to 115.30m	Core recovery in dolomitic limestone varies from 20% to 100% with RQD varying 20% to 85%. In shale/slate zone it ranges from 16.50 to 41.50m while in calcareous shale/ slate zone the RQD percentage ranges from 0 to 85%.

				shale/slate is seen present up to 115.30m depth.			
PHH 2	1208.85	Located in powerhouse area, at Hat village below the cliff on the right bank upslope of Alaknanda	9	Reddish brown soil with rock fragments.	150.20	Weathered and jointed dolomitic limestone is present up to 19.00 m depth. The dolomitic lime stones continue till 67.00 m depth where after intercalated shale/slate and dolomitic limestone have been observed upto 91.00 m depth. From 91.00 m to 150.10 m dark gery calcareous shale/slate containing veins and specks of	Minor shears have been observed from 55.45 m-56.00 m, 58.00-59.00 m, 127.00-128.00 and 143.00 to 144.00 m. Core recovery in the bed rock varies from 38% to 99% with RQD varying from Nil to 66%. In dolomitic limestone zone (from 9.00 to 67.00 m) the RQD percentage ranges from Nil to 66% ; in shale/slate & dolomitic limestone zone (from 67 to 91 m) the RQD percentage ranges from Nil to 11% while in calcareous shale/ slate zone the RQD percentage

						pyrite have been reported. Minor folding, faulting and silicification have been observed in calcareous shale/slate.	ranges from Nil to 57%.
PHH 3	1261.58	Located along the nala in the powerhouse area	16	Pebble, cobble and boulders of colluvial material	40.50	Dolomitic limestone is met from 16.00 m depths (EL. 1245.35 m) to 40.50 m depth	Core recovery in the bed rock varies from 65% to 100% with RQD varying from Nil to 62%.
PHH 4	1130.00	Located in the powerhouse area near Hat village	17	Pebble, cobble and boulders of colluvial material	75.40	Dark grey, shale/slate	Core recovery 75% to 99% with RQD varying from 10 to 81%.

3.1.2 Hot Water Springs

The presence of hot water springs may cause drastic effect on the shear strength of any rock mass (Hasegawa et al, 2008). Especially this happens when it is found associated with sedimentary/metasedimentary rock masses like dolomitic limestone, limestone, slates and phyllites, as it contains sulphur and other acidic ingredients. The Geothermal Atlas of India' (1991) generated by Geological Survey of India (GSI), illustrates that about 340 hot water spring sites are present in the Indian Himalaya (Craig, 2013). As many as 62 thermal springs are known to be located in the Garhwal Himalaya with 19 of these being in the Alaknanda valley. Three hot water springs were recorded during investigations in the dam area in addition to hot spring indications in many drill holes. These hot springs, with temperatures ranging from 50° to 70°C, were located within quartzite in river bed area at EL± 1230 m just upstream of dam axis. Additionally, hot water springs with temperature ranging from 55° to 68°C were reported during drilling of drill holes DH-2, DH-6, DH-7 and DH-8 on the right bank with an average flow rate of 20 litres/minute (WAPCOS, 2010). Temperatures up to 40°C without water occurrence were observed and recorded in the cross cut of Drift DL-02 on the right bank near the dam site. Warm water inflows were also noted in the initial sections of the powerhouse exploratory drift along with the presence of hydrogen sulphide gases.

3.1.3 Subsurface Permeability

The subsurface permeability of litho units was determined through drill holes at number of locations in terms of Lugeon from water pressure tests. Originally the subsurface permeability in terms of Lugeon was defined by Maurice Lugeon (1933) as the loss of water in litre/min for 1 metre drill hole length at a pressure of 1 MPa. Goodman (1980) elucidated that the values obtained from Lugeon test, directly reflects the subsurface ground conductivity of rock masses, which depends on the nature of aperture, interconnectivity, spacing and infilling material characteristics present in the weak discontinuous plane/zone. The magnitude of Lugeon values helps to understand grout depth limit and their Lugeon value pattern illustrate the discontinuity characteristic to evaluate the grout type.

The following formula has been used for calculating the permeability

$$P = 10.33/ H * Q/L$$

Where,

Q = water loss in minutes

L = length of test section in m

H = pressure acting on test section

(Applied pressure in kg/cm2 + pressure due to water column in kg/cm2

- pressure loss due to friction in kg/cm2)

The water pressure tests were carried out in different segments of a drill hole covering many drill holes in the project area. The representative permeability in terms of Lugeon obtained from drill holes in dam site to evaluate the foundation condition are summarized in Table 3.8. The Lugeon interpretation is based on dominant flow pattern out of five permeability values obtained in every single stage (Houlsby, 1976).

Table 3.8 Details of Lugeon test and their interpretation with respect to specific depth at dam site area.

Drill Hole No:	Depth (m)	Permeability Representative Lugeon values	Remarks
DH–01	9–12	34. 7	The drill hole penetrates though well jointed quartzites. The water pressure test indicates that the rocks are more pervious with values ranging from 34.7-17 Lugeons. Since the permeability indicate a value of 17 Lu at a depth of 27m, the rocks are pervious (>1Lu) in nature. Hence it can be concluded that the depth of curtain grout shall extend beyond 27m.
	12–15	31.5	
	15–18	27	
	18–21	25.7	
	21–24	26.6	
	24–27	17	
DH-02	14.2-17.2	24.4	The total depth of the drill hole is 50 m, the water pressure test were carried from 14.2 m up to a depth of 50 m with 3 m interval. At the initial reaches of the drill depth from 14.2 to 26 m the Lu values considerably reduce indicating that the conductivity of the rock mass decreases
	17.2–20.2	19.6	
	20.2–23.2	13.3	
	23.2–26.2	10.9	
	26.2–29.2	9	
	29.2–32.2	7	

	32.2–35.2	9	with increase in depth at higher rate. However, after a depth of 26 m the rock mass shows negligible difference in Lugeon value up to 50 m. As the Lugeon values are > 1 the grout curtain should progress beyond the depth of 50 m.
	35.2–38.2	6.9	
	38.2–41.2	5.2	
	41.2–44.2	5.9	
	44.2–47.2	4.7	
	47.2–50.2	5.4	
DH-03	12–15	46.9	The Lugeon values ranging between 5–50 generally indicate that the material is moderately permeable with some wide opening. This indicates grout curtain should progress beyond the depth of 30 m.
	15–18	35.5	
	18–21	36.6	
	21–24	27.6	
	24–27	58.8	
	27-30	53.2	
DH-04	21-24	5.1	The Lugeon values show a gradual decrease up to a depth of about 50 m and then slowly increases. This indicated may be presence of joints along with fractures after a depth of 55 m. However as the Lugeon values are >1, the grout should be beyond the depth of 61 m.
	24-27	5.2	
	27-30	2.7	
	30-34	4	
	34-37	4.2	
	37-40	4.1	
	40-43	7.4	
	43-46	2.5	
	46–49	2.8	
	49–52	1.6	
	52-55	2.4	
	55-58	4.2	
	58-61	7.5	
DH-06	15–18	6.6	The Lugeon values indicate that the permeability decreases with depth up to
	18–21	6.5	

	21-24	4.3	25 m, thereafter the value shows slight increase. However the grout should progress beyond the depth of 37 m as the Lugeon value shows slightly increasing tendency.
	24-27	0.7	
	27–30	4.4	
	30–33	2.4	
	33-37	3.9	
DH-07	24-27	2.7	The Lugeon value remain constant with increase in depth up to 38 m. As the Lugeon values are >1, the grout should progress beyond the depth of 38 m. Preferred chemical grout.
	27-29	1.6	
	29–32	2.2	
	32-35	2.9	
	35-38	2.8	

3.1.3.1 Interpretations

The water pressure tests were carried out for different segments in a drill hole covering many drill holes in the project area. The details of the rock type encountered with respect to specific drill depths are summarized in Table 3.9. The results of the water pressure tests done in the project area are summarized in Table 3.10. Frequency distributions of Lugeon values (Heuer, 1995) for identified rock type are displayed in Table 3.11.

Table 3.9: Detail of permeability tests in drill holes at specific depths

Drill hole	Depth		Rock type
	From	To	
DH-2	30.0	50.3	Quartzite
DH-4	20.0	61.1	Quartzite
DTH-1	20.0	60.2	Quartzite
HRTH-3	20.0	56.0	Shale/slate
SSH-1	20.0	166.5	Dolomitic limestone
PHH-1	27.0	115.3	Shale/slate
PHH-2	20.0	67.0	Dolomitic limestone

	67.0	150.2	Shale/slate
PHH-3	20.0	40.5	Dolomitic limestone

The permeability analysis reveals that the quartzite, which forms foundation of the dam has maximum permeability value of 3 to 58 Lu. This indicated that the rocks are highly pervious in nature. Seven number of drill holes drilled at dam axis mostly range in depth from 30-61 m. The water pressure tests done in these drill holes indicate values more than 4 Lu even at a depth of 60 m (Fig 3.1). In view of this, it can be estimated that the depth of grout curtain should extent up to a minimum depth of 1H of dam (65m) at deepest foundation level.

Table 3.10 Condition of rock mass discontinuity associated with different Lugeon values.

Lugeon Range	Classification	Hydraulic Conductivity Range (cm/sec)	Condition of Rock Mass Discontinuities
<1	Very Low	$< 1x\ 10^{-5}$	Very tight
1-5	Low	1×10^{-5}- 6×10^{-5}	Tight
5-15	Moderate	6×10^{-5}- 2×10^{-4}	Few partly open
15-50	Medium	2×10^{-4}- 6×10^{-4}	Some open
50-100	High	6×10^{-4}- 1×10^{-3}	Many open
>100	Very High	$> 1 X 10^{-3}$	Open closely spaced or voids

Table 3.11 Frequency distributions of Lugeon values by rock type (After Heuer, 1995)

Rock type	Lugeon numbers					
	0 – 1	**1 – 3**	**3 – 10**	**10 - 30**	**30 – 100**	**> 100**
Quartzite	0%	15%	84%	1%	0%	0%
Shale/slate	3%	62%	32%	2%	0%	1%
Dolomitic limestone	17%	51%	32%	0%	0%	0%
Permeability cm/sec	$6x10^{-6}$	$2x10^{-5}$	$6x10^{-5}$	$2x10^{-4}$	$6x10^{-4}$	$2x10^{-3}$

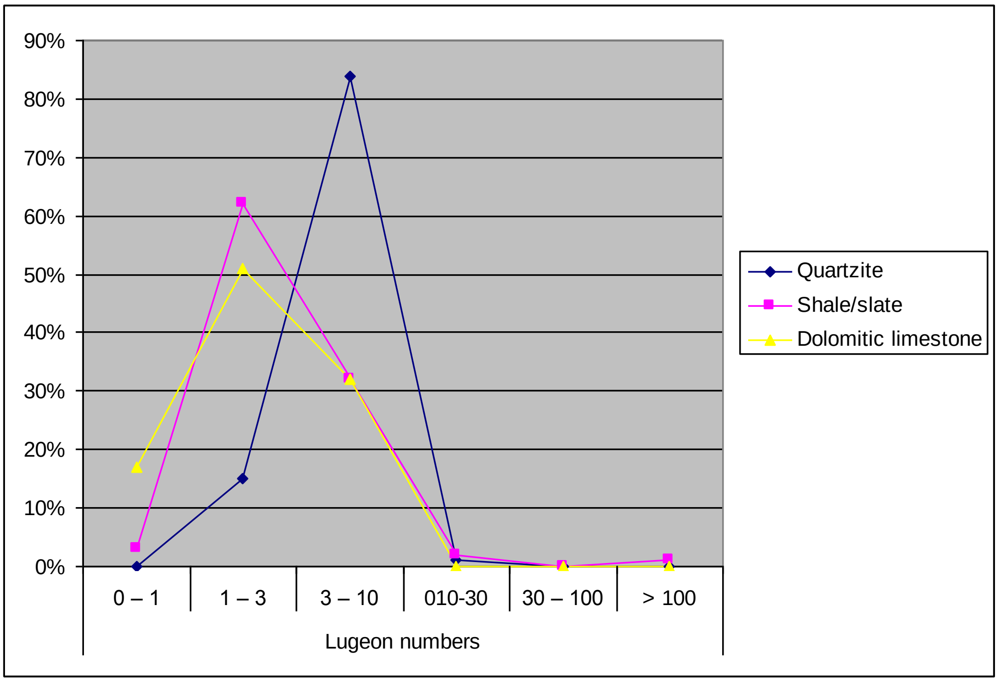

Fig 3.1 Graph showing percentage distribution of Lugeon value for different litho units

3.1.3.2 Rock Quality Designation (RQD)

The inspection of available drill cores at the project area reveals the RQD in terms of percentage that are summarized as follows:

- At dam area the RQD ranges from 75-80% indicates good to moderate core recovery.
- At surge shaft site the RQD varies in different rocks from 5 to 83% and all along the depth variations were recorded.
- The inspection of available drill cores at powerhouse site, obtained through a number of drill holes, generally indicates good to moderate core recovery (60–80%). However, values of RQD obtained from PHH-01 were found to be poor to very poor (< 20%) from drill depths 18 to 30m, 44 to 52m, 57 to 58m, 63 to 67m and 101 to 111m indicating that rocks are traversed by closely spaced joints.

3.2 SUBSURFACE EXPLORATORY DRIFTS

The exploratory drifts provide excellent information about the foundation condition for suitable design of the structure. According to Bhasin et al, (1995) major discontinuities and fracture zones should be delineated and characterised from subsurface investigations before the construction. The presence of water tends to increase pore pressure which may result in reducing effective frictional resistance on the rock mass affecting the stability of the structure (Pal et al, 2012).

Drifts at Dam site (DL-01 & 02)

DL–01

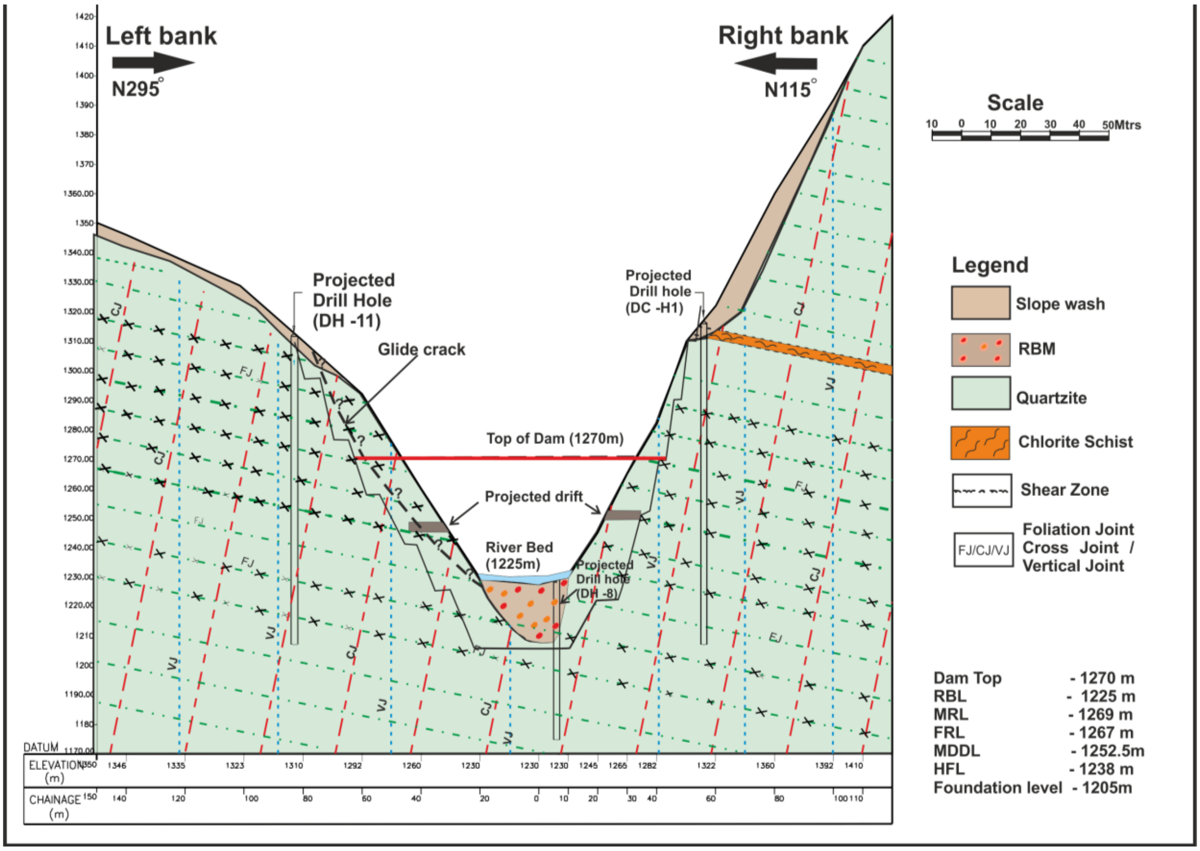

Fig 3.2 Geological section along VHEP Dam axis

Two number of exploratory drifts namely DL-01 and DL-02 of dimensions 2m x 1.8m were excavated at the dam site one on each bank. The drifts were used to infer the foundation condition of the rocks mainly to decide the depth of stripping limit. The drift DL-01 on the left bank has progressed to the length of 33m. It had a orientation towards N120^{o} for initially 7m and later took a turn towards N230^{o} (Fig 3.6). At RD 33m two cross cuts one in upstream direction with orientation N25^{o} and the other in the downstream direction oriented N220^{o} have been excavated for a length of 15m each to assess the rock condition. Quartzites are the major rock type exposed in the dam area. They appear as light grey to dark grey colour, fairly fresh, medium to coarse grained, laminated at places and jointed with foliation plane dipping 25^{o}–40^{o} in N5^{o}W to N10^{o}E direction with occasional iron stains.

Shear bands up to 10cm thick are present and they are generally seen within weathered rocks. In some shears ferruginous clay is present. Joints with 1-2cm opening have been recorded in early reaches of the drift. Shear zone up to 10cm thick are present with 2cm clay gauge and quartz veins of 1-3cm observed randomly in both the cross cuts. The 3D logging of exploratory drift indicates the presence of an adverse arcuate shaped glide crack at the end of the drift. The projection of this glide crack to the surface vertically indicates that it is seen on the surface at El±1320m (Fig 3.2). Its continuity is marked by thick vegetation cover since the glide crack having adequate separation has been subsequently filled with soil that supports vegetation (Fig 3.3). The slope material up to the glide crack has to be removed till sound rock level as part of stripping.

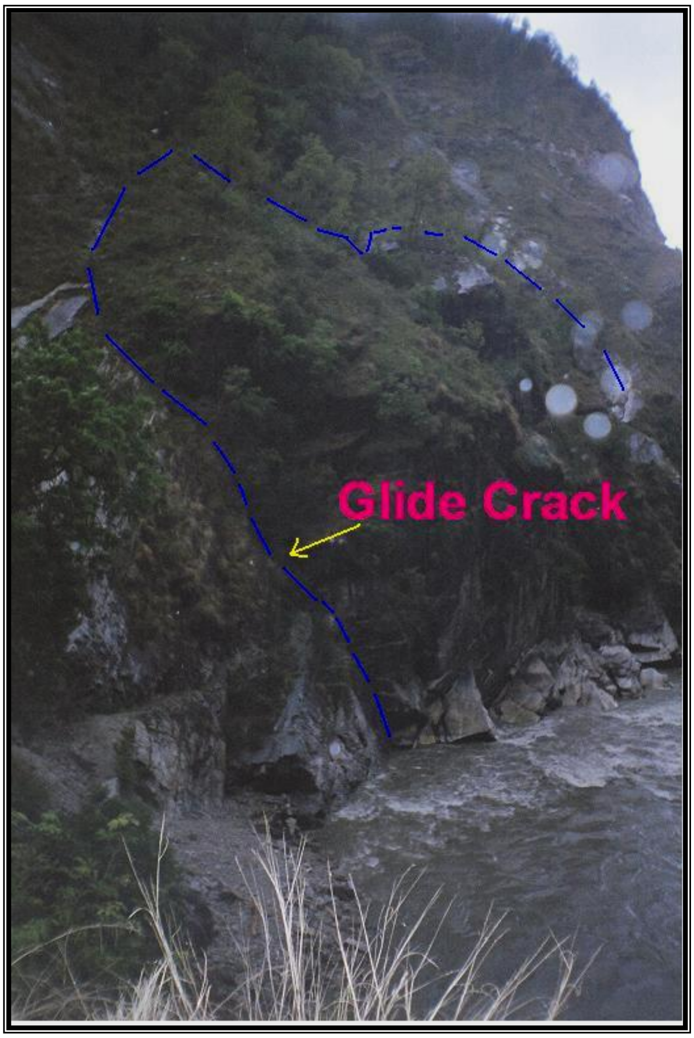

Fig 3.3 Photo illustrating the observed glide crack on the left bank of the dam axis

Drift DL–02

The drift DL-02 is located on the right bank of river Alaknanda. The drift has been excavated in N190° direction initially for about 27m (Fig 3.7). Thereafter two cross cuts have been excavated in N83°E and N260° direction respectively for 2m and 55m lengths. Quartzites seen within the drifts are dirty white, banded, and medium to coarse grained containing fine grained sericite. These are dipping at 32o-40o towards N40oE direction in upstream. Shear zones up to 10cm thick are present having clay gauge up to 2cm thick. Quartz veins of 1-3cm were observed randomly at many places. The drift lies in the geothermal zone. The temperature inside the drift was observed to be 35oC whereas it increases to 40oC in cross cut at RD 56.80m. Minor shears of 2-3cm thick have been observed at RD 19.70m, RD 50m of cross cut and shears 15-25cm thick were recorded at RD 50.50m. A minor fault with displacement of 20cm has been recorded at RD 34m of left wall. Quartz veins of 2.2cm thick have been observed from RD 30m of left wall to RD 25m on right wall. The drift appears to be moist along shear and some joints, rest of the reaches are dry. The rock mass condition has been estimated to be good rock (Class II) with the RMR value of 75. The stripping limit extends up to 15m depth in order to reach the sound rock. The details of drifts DL-01 and DL–02 are summarized in Table 3.13

<u>Powerhouse Drift</u>

The powerhouse drift is located on the right bank of Alaknanda River near Hat village at El±1057.63. The drift initially starts in N300° direction and progresses deeper with minor local variations. The drift has progressed to a length of 680m generally unsupported, few unstable stretches from RD 60 to 65.5m and RD 130 to 140m were found to be provided with supports. The drift has been started in intensely foliated slate with phyllitic sheen and the same lithology extends up to RD 439m (Fig 3.4). Thereafter interbedded slate and dolomitic limestone has been encountered up to RD 460m. Later dolomitic limestone with good water saturation could be observed along the entire drift. Shear zones up to 10 cm wide have been recorded inside the drift in many locations. Joints are generally tight in nature. Minor overbreaks are recorded between RD 210m and 220m and RD 290 and 300m. The drift is moist and dripping between crown and spring level from RD 42 to 64 m. The characteristics of prominent joint sets in slate and dolomitic limestone in the powerhouse drift are presented in Table 3.12.

Table 3.12 Prominent joint sets for slates and dolomitic limestone in powerhouse area

Slates				
Sl. No	**Strike**	**Direction**	**Dip Amount**	**Spacing (in cm)**
1	N10°E-S10°W	N80°W	25°-30°	15-30
2.	N70°W-S70°E	N20°E	55°-70°	2-30
3.	N70°W-S70°E	-	Vertical	5-10
4.	N50°W-S50°E	N40°E	30-45	5-10
Dolomitic limestones:				
	N25°W-S25°E	N65°E	60°	N25°W-S25°E
	N65°W-S65°E	S25°W	60°-65°	N65°W-S65°E
	N35°W-S35°E	-	Vertical	N35°W-S35°E
	N25°W-S25°E	N65°E	60°	N25°W-S25°E

Flow of water from the roof has been observed at many places from RD 550m onwards, which was initially planned for locating the powerhouse. Foliations developed due to metamorphism are more prominent. The beddings traces and foliations in rocks seem to be parallel. The rocks shows small scale folds at many places within the drift. In addition, two sets of joints with close spacing are distinctly visible. The contact between dolomitic limestone and slates appears to be gradational in nature. Originally the powerhouse was located in the closer area of the broad syncline (Fig 3.5). In view of large seepage observed in this area due to synclinal closer, the powerhouse has been shifted further towards the valley between RD 350m and 550m. Here mainly slates are exposed in the powerhouse with only a part of dolomitic limestone seen in the roof area of powerhouse.

Based on the study of exploratory drift, the following can be concluded:

i) The dense to moderately foliated slates with phyllitic sheen are present in the initial stretches of the drift up to about RD 480 m. Later, dolomitic limestones are encountered till the end of the drift.

ii) The contact of slate / dolomitic limestone is gradational in nature.

iii) The foliation in general, dips at moderate angles of 25°-35° towards NNW in the initial portions of the drift up to RD 525m, though the dip decreases to even 10°-20° afterwards.

iv) The general foliation shows a reverse trend after RD 590 m with moderately shallow dips of 15°-25° towards NE to ENE directions because of synclinal structure.

v) Two important sets of joints (J1 and J2) have been observed. While joint set J1 has greater continuity of more than 2–3 m, the joint set J2 has lesser continuity of about 1 m or even less.

vi) Dolomitic limestones have GSI values ranging between 25 and 70 with an average of 40, whereas the slates have a very low GSI between near 0 to 20 with an average of about 10.

Fig 3.4 Presence of slate just above the drift opening at Hat village

vii) The foliation at the contact of dolomitic limestones/slates shows reverse trend inside the powerhouse area indicating that the bedding has been folded into a broad, open and upright syncline. If the location of the powerhouse is introduced in this section horizontally extending between RD 530m and 650m it will be exactly located in the core of the syncline structure with both the limbs dip towards each other. The southeast limb dipping into hill from valley side present below the debris may cause seepage of subsurface water from debris toward the fold axis inside the powerhouse cavity. Similarly, the seepage from the northwest limb also will flow towards the fold axis causing excessive seepage inside the powerhouse area. It will be a major disadvantage in case of a syncline with fold axis present within the powerhouse. In this view it is suggested that power may be slightly shifted towards the valley side at RD 400 so that the powerhouse cavern will be located within one limb of syncline (Fig 3.5). This will help in minimization of seepage. The additional details of powerhouse drift are summarized in Table 3.14.

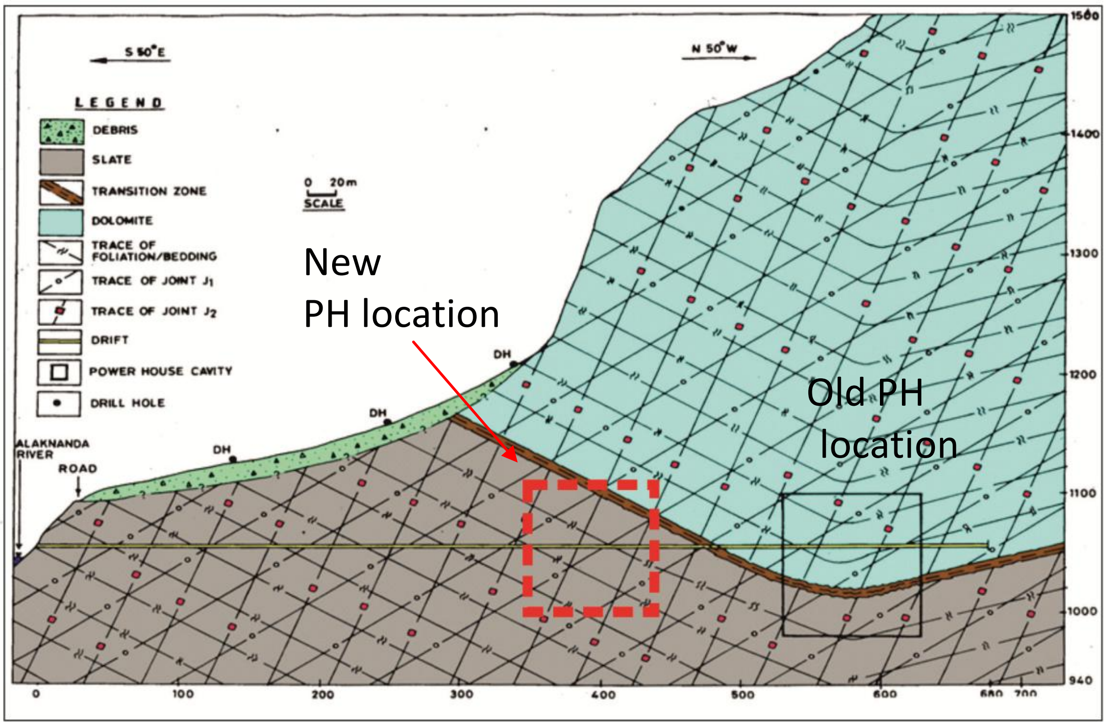

Fig 3.5 Geological cross section across powerhouse area showing the older and new PH proposed locations.

Summary of Drifts

Table 3.13 Details of Drift at Dam site

<table>
<tr><th rowspan="2">Drift No</th><th rowspan="2">Elevation
El±(m)</th><th rowspan="2">Location</th><th colspan="2">Drift Details</th><th rowspan="2">Dimension</th></tr>
<tr><td>RD
(m)</td><td>Direction</td></tr>
<tr><td rowspan="4">DL-1</td><td rowspan="4">EL.1244.32</td><td rowspan="4">Left bank of Alaknanda river near the dam axis (E3843565.806, N754309.811),</td><td>0-7</td><td>N120°</td><td rowspan="4">(2 m x 1.8)
L =33m
Unsupported</td></tr>
<tr><td>7-12</td><td>N130°</td></tr>
<tr><td>12-19</td><td>N200°</td></tr>
<tr><td>19-33</td><td>N237°</td></tr>
<tr><td></td><td colspan="5">Remarks:
The drift is self-supporting and no plant roots have been recorded.
Light grey to dark grey colored, fairly fresh, medium to coarse grained, laminated and highly jointed Quartzites with occasional iron stains has been observed.
The bedding traces / foliations are dipping 25^{o}–40^{o} in N10^{o}W to N10^{o}E in upstream direction.
Presence of moist zones along shear and some joints. The rest of the reaches are dry.
Shear up to 10 cm are present in the drift and generally contain weathered rock. In some shears ferruginous clay is present. Joints with 1-2 cm opening have been recorded in early reaches of the drift.</td></tr>
</table>

<table>
<tr><td rowspan="3">Upstream Cross Cut in Drift DL-1</td><td rowspan="2">1243.70</td><td rowspan="2">On left bank the cross cut has been excavated in N25^{o}E direction from RD 33.50 m in main drift</td><td>RD (m)</td><td>Direction</td><td rowspan="2">(2m x 1.8)
L =15m
Unsupported</td></tr>
<tr><td>0-33.5</td><td>N25°</td></tr>
<tr><td colspan="5">Remarks:
• Light grey to dark grey colored, fairly fresh, medium to coarse grained, laminated and highly jointed Quartzites with occasional iron stains has been observed.
Shear zone up to 10cm thick are present with 2cm clay gauge at places. Quartz vein 1-3 cm observed randomly.</td></tr>
<tr><td rowspan="3">Downstream Cross Cut in Drift DL-1</td><td rowspan="2">1244.12</td><td rowspan="2">On left bank the cross cut has been excavated in N220° direction from RD 33.00 m in main drift</td><td>RD (m)</td><td>Direction</td><td rowspan="2">(2m x 1.8)
L =15m
Unsupported</td></tr>
<tr><td>33.00</td><td>N220^{o}</td></tr>
<tr><td colspan="5">Remarks:
• Light grey to dark grey colored, fairly fresh, medium to coarse grained, laminated and highly jointed quartzites with occassional iron stains has been observed.
Shear zone up to 10cm thick are present with 2cm clay gauge at places. Quartz vein 1-3 cm observed randomly.</td></tr>
<tr><td rowspan="2">DL–02</td><td rowspan="2">1240.38</td><td rowspan="2">On the right bank of Alaknada river along near dam axis</td><td>RD (m)</td><td>Direction</td><td rowspan="2">(2m x 1.8)
L =27m
Unsupported</td></tr>
<tr><td>0-27m</td><td>N190^{o}</td></tr>
<tr><td>The drift has been excavated in N190^{o} direction.</td><td colspan="5">Remarks:
Off white, recrystallized, banded, medium to coarse grained (at places fine grained) sericite bearing quartzites. These</td></tr>
</table>

<table>
<tr><td>Thereafter two cross cuts have been excavated in N83°E and N260°-265° direction respectively for 2m and 55 m length.</td><td colspan="5">are dipping 32°-40° in N40°E direction in upstream randomly.</td></tr>
<tr><td rowspan="3">DL–02
Cross cut in to hill</td><td rowspan="3">1240.38</td><td rowspan="3">On the right bank of Alaknanda river along near dam axis</td><td>RD (m)</td><td>Direction</td><td rowspan="3">(2m x 1.8)
L = m
Unsupported</td></tr>
<tr><td>0-2 m</td><td>N83°</td></tr>
<tr><td>0-55m</td><td>N260°</td></tr>
<tr><td></td><td colspan="5">Remarks:
• Light grey to dark grey colored, fairly fresh, medium to coarse grained, laminated and highly jointed Quartzites with occasional iron stains has been observed.
Shear zone up to 10cm thick are present with 2cm clay gauge at places. Quartz vein 1-3 cm observed randomly.</td></tr>
</table>

Table 3.14 Details of Drift at Powerhouse

<table>
<tr><th rowspan="2">Drift No</th><th rowspan="2">Elevation
El±(M)</th><th rowspan="2">Location</th><th colspan="2">Drift Details</th><th rowspan="2">Dimension</th></tr>
<tr></tr>
<tr><td rowspan="3">PHD</td><td rowspan="3">1057.63</td><td rowspan="3">On the right bank of Alaknanda river along near Hat village.</td><td>RD (m)</td><td>Direction</td><td rowspan="3">(2m x 1.8)
L = 680m
Generally unsupported.

Supported in stretches from RD 60 to 65.5 m and RD 130 to 140 m</td></tr>
<tr><td>0-525</td><td>N55 ^{o}W</td></tr>
<tr><td>0-55 m</td><td>N260^o</td></tr>
<tr><td></td><td colspan="5">Remarks:
The drift has been started in intensely foliated phyllitic slate and the same has been met with up to RD 439, thereafter interbedded phyllitic slate and dolomitic limestone has been encountered up to RD 460m onwards the drift has been excavated in dolomitic limestone charged with water.
Shears up to 10 cm wide have been recorded in the drift. In some shear clay gouge is present. Joints are generally of tight nature. Some overbreak is recorded near RD 210 m to 220 m and RD 290 to 300 m. The drift is moist and dripping through crown and spring level from RD 42 to 64 m.</td></tr>
</table>

Based on the considerations of perennial streams in the area and the information from drill hole PT-4, it is anticipated that higher water pressures may be encountered along the PT alignment in areas around Dwing and Ghanpani streams.

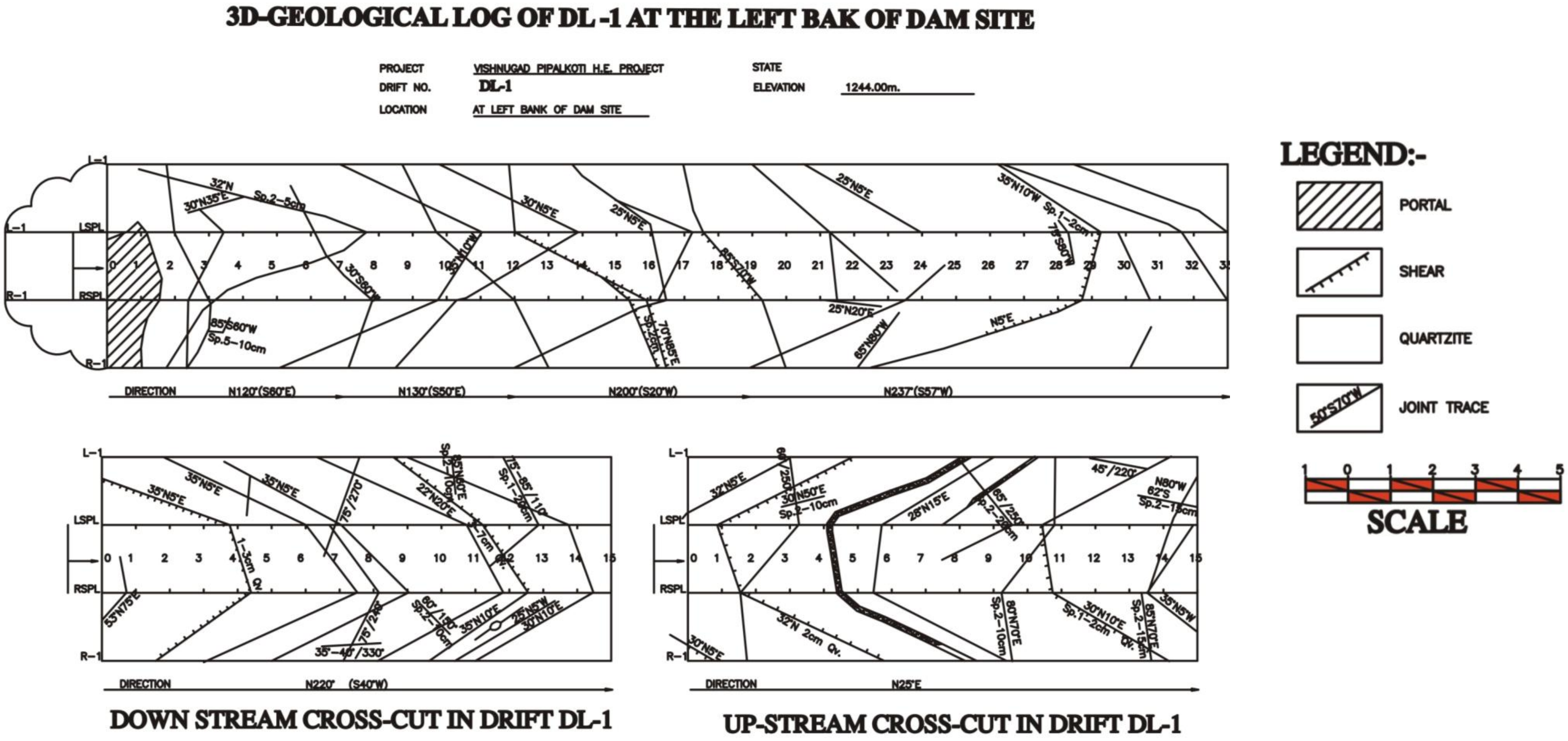

Fig 3.6 3D–Drift log of DL-01 located on the left bank near dam axis

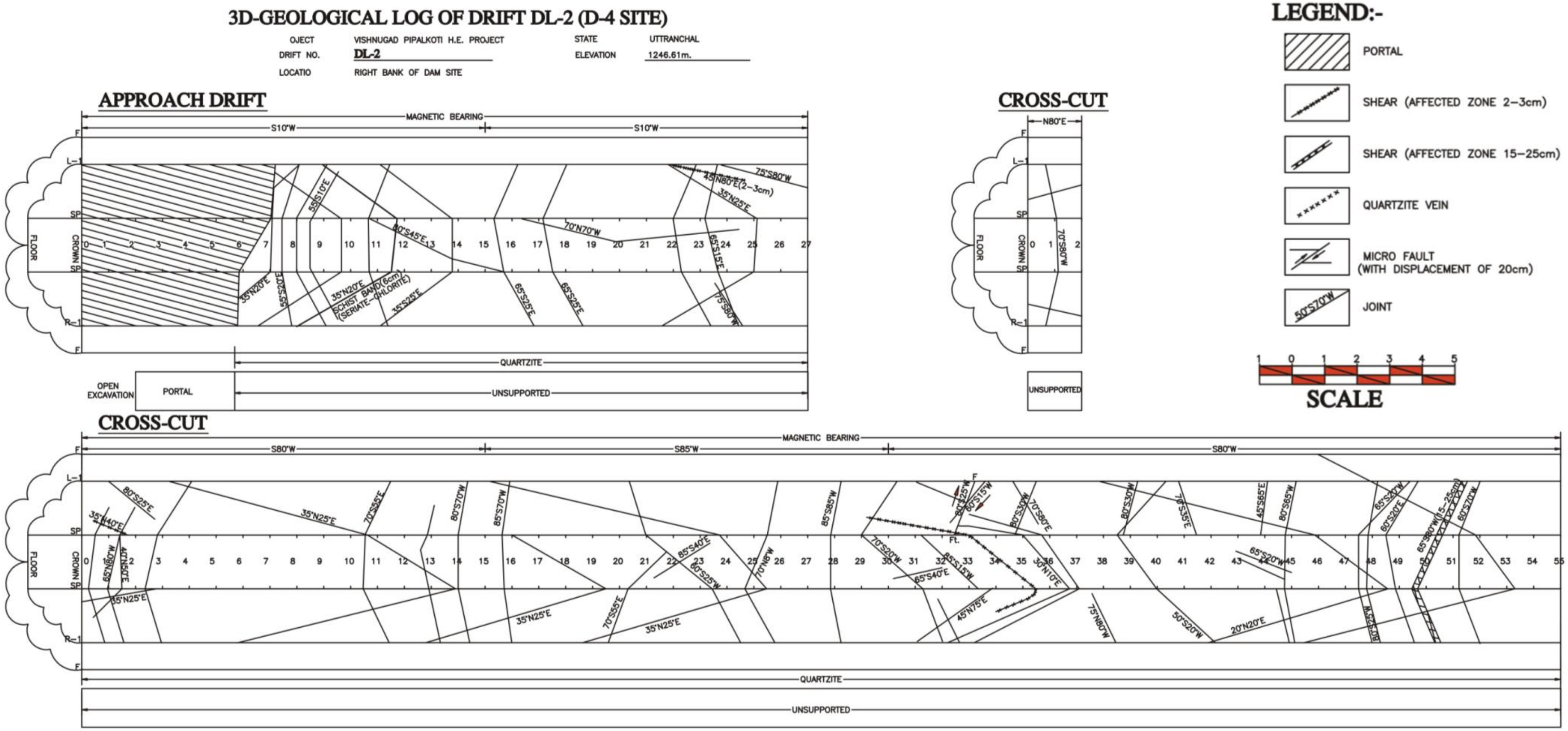

Fig 3.7 3D–Drift log of DL-01 located on the right bank near dam axis

3.3 LABORATORY DETERMINATION OF ENGINEERING PROPERTIES OF ROCKS

Determination of Engineering properties and realistic estimation of rock mass characters are essential to understand its behaviour and to carry out stability analysis. The Engineering response of rocks depends on the inherent properties such as petro-fabric assemblage of the rocks such as texture, nature of cementing material, grain shape, size and porosity. The rock sample becomes weak by the presence of discontinuities, like bedding, foliation, cleavage, macro and micro-fractures (Behrestaghi et al, 1996).

The evaluation of strength and deformation behaviour of rock masses and intact rocks can be carried out in the field and laboratory tests respectively. The important properties required for stability analysis of rock slopes and underground caverns are shear strength parameters, uniaxial compressive strength (UCS) and tensile strength of intact rocks as well as elastic moduli and Poisson's ratio (E_d, ν) of the intact rocks and rock mass (Viladkar, 1993). In order to understand the overall behaviour of rock mass, the mechanical strength parameters of intact rocks are determined from laboratory tests following standard test procedures as suggested by ISRM (1979) and then the effect of joints were incorporated to predict the overall behaviour of the rock mass. Twenty numbers of samples were collected each from dam site and powerhouse area. The tests were done both in dry and in saturated conditions. The saturation of rock specimens was done by boiling and allowing saturation for extended periods (more than 45 days) till the weight of specimens became constant. Due to lack of sample in slates the tests were conducted on dry state only.

The following experiments were carried out by the Project Authority to determine the geomechanical characteristics of rocks in laboratory:

i) Uniaxial compressive strength (UCS) tests on intact rock cores (ISRM, 1979 and IS: 9143-1979). The results of these tests shall provide the UCS, elastic modulus and Poisson's ratio of the intact rocks in dry and saturated states.
ii) Brazilian tests (ISRM (1979) and IS: 10082-1981), to get the tensile strength of the intact rocks in dry condition
iii) Triaxial tests on dry and saturated rock cores to determine Mohr-Coulomb and Hoek-Brown shear strength parameters, (ISRM, 1981 & 1983) and (IS: 13047-1991)

The number of samples collected for different tests from the dam and powerhouse area is tabulated in Table 3.15.

Table 3.15 Number of samples tested for dam and powerhouse area.

Sl. No.	Type of Test	No. of samples for Dam area and Powerhouse complex	Total no. of samples for Dam area and Powerhouse complex
1.	Uniaxial compression test (USC) for strength, elastic modulus and Poisson's ratio i. Dry condition ii. Saturated condition	20	40
2.	Triaxial compression test for determining of cohesion (c), and friction angle (Φ) i. Dry condition ii. Saturated condition	20	40
3.	Brazilian test to determine tensile strength	10	20

3.3.1 Uniaxial Compression Tests (For determination of UCS)

Uniaxial compression tests were conducted on cylindrical specimens of NX size for each rock type as per the guidelines of ISRM (1979) and IS: 9143-1979. In all experiment, the axial loading was gradually increased with a uniform rate such that the failure occurred within 5 to 10 minutes. The Elastic modulus was obtained during UCS testing by measuring the axial/lateral deformation history of the sample in addition to its load history. Poisson ratio was determined from the corresponding stress/strain curves. The average slopes obtained from stress versus strain curve for the axial and lateral were used to calculate average elastic modulus.

Loading data, recorded at same rate were converted to stress (qc)

Uniaxial compressive strength of rock samples is calculated as

$$q_c = P/A \tag{3.1}$$

Where;

q_c = uniaxial compressive strength in MPa

P = Load in MPa

A = Cross sectional area of sample in cm^2

The displacement data area is converted to strain by

$$El = \frac{\Delta L}{L} \quad \text{and} \quad Er = \frac{\Delta D}{D} \tag{3.2}$$

Where

El	=	Longitudinal strain
Er	=	Radial strain
L	=	Sample length (mm)
Δ L	=	Change in length (mm)
Δ D	=	Sample diameter (mm)
D	=	Change in diameter (mm)

And the Poisson's ratio (v) is calculated by:

$$v = -\frac{\text{Slope of axial curve}}{\text{Slope of lateral curve}}$$

The tests results for quartzite, dolomitic limestone and slates are furnished in Table 3.16a, b, c, d and e.

Table 3.16a Results of UC tests on dry samples of Quartzites-Desilting chambers area

Designation	Location	UCS, MPa	E_i GPa	Poisson's Ratio (v)	Modulus Ratio	Classification Deere-Miller
UCS_DC_1	LDC_DCH1 109	69.89	12.50	0.19	178.9	CL
UCS_DC_2	LDC_DCH1 274	108.77	12.77	0.19	117.25	CL
UCS_DC_3	LDC_DCH1 357	48.33	6.82	0.19	141.11	DL
UCS_DC_4	LDC_DCH1 377	127.72	16.87	0.20	53.70	BL
UCS_DC_5	LDC_DCH1 421	62.82	12.72	0.19	202.50	CM
UCS_DC_6	LDC_DCH1 430	62.89	10.02	0.17	159.32	CL
UCS_DC_7	UDC_DCH2 440	76.08	12.31	0.16	161.80	CL

UCS_DC_8	UDC_DCH2 486	59.20	15.91	0.16	268.75	CL
UCS_DC_9	UDC_DCH2 486	57.84	9.86	0.21	171.53	CL
UCS_DC_10	UDC_DCH2 471	73.64	10.67	0.19	144.89	CL
Average		**74.72**	**12.05**	**0.19**	**159.98**	**CL**
S.D.		**23.45**	**2.78**	**0.02**	**55.62**	

Table 3.16b Results of UC tests on saturated samples of Quartzites-Desilting chambers area

Designation	Location	UCS, MPa	E_i GPa	Poisson's Ratio (ν)	Modulus Ratio	Deere-Miller Classification
UCS_DC_1	LDC_DCH1 275	29.84	3.50	0.24	117.29	DL
UCS_DC_2	LDC_DCH1 432	49.18	9.37	0.23	190.52	DL
UCS_DC_3	UDC_DCH2 598	37.59	3.96	0.25	105.35	DL
UCS_DC_4	UDC_DCH2 634	41.17	5.04	0.26	120.86	DL
UCS_DC_5	UDC_DCH2 672	127.62	19.74	0.20	154.68	BL
UCS_DC_6	LDC_DCH1 211	35.11	10.26	0.26	292.22	DM
UCS_DC_7	LDC_DCH1 274	57.23	8.05	0.26	140.66	CL
UCS_DC_8	LDC_DCH1 279	50.60	8.34	0.26	164.82	DL
UCS_DC_9	LDC_DCH1 335	54.14	12.31	0.23	227.37	DM
UCS_DC_10	LDC_DCH1 430	49.71	8.82	0.25	177.43	DL
Average		**56.2**	**8.94**	**0.24**	**169.12**	**CL-DL**
S.D.		**26.34**	**4.48**	**0.02**	**56.95**	

Table 3.16c. UC tests on dry samples of Dolomitic limestones

Sample	Location	UCS, MPa	E_i GPa	Poisson's Ratio (ν)	Modulus Ratio	Deere-Miller Classification
UCS test-Dry-PH1	7 at Ch. 580m No. 1	219.67	16.78	0.18	76.4	BL
UCS test-Dry-PH2	9 at Ch. 560m No. 24	63.82	13.46	0.21	210.9	DM
UCS test-Dry-PH3	7 at Ch. 580m No. 2	165.33	39.13	0.20	236.7	BM
UCS test-Dry-PH4	9 at Ch. 560m No. 7	159.23	15.93	0.19	100.0	BL
UCS test-Dry-PH5	8 at Ch. 570m No. 17	137.90	12.50	0.22	90.64	BL
Average		**149.19**	**14.36**	**0.20**	**142.93**	**BL**
S.D.		**50.49**	**1.68**	**0.02**	**74.86**	

Table 3.16d. UC tests on saturated samples of Dolomitic limestones

Sample	Location	UCS, MPa	E_i GPa	Poisson's Ratio (ν)	Modulus Ratio	Deere-Miller Classification
UCS_Saturated_PH1	10at Ch. 550m No. 14	76.11	8.89	0.22	116.8	CL
UCS_Saturated_PH2	8 at Ch. 570m No. 13	92.88	14.70	0.21	158.3	CL
UCS_Saturated_PH3	8 at Ch. 570m No. 3	73.33	9.20	0.21	125.4	CL
UCS_Saturated_PH4	9 at Ch. 560m No. 17	117.2	14.00	0.20	119.5	BL
UCS_Saturated_PH5	8 at Ch. 570m No. 20	73.51	13.7	0.20	187.6	CL
Average		**86.61**	**12.90**	**0.21**	**141.52**	**CL**
S.D.		**16.93**	**2.52**	**0.01**	**30.66**	

Table 3.16e. UC tests on dry samples of Slates

Sample	Location	UCS MPa	E_i, GPa	Poisson's Ratio (ν)	Modulus Ratio	Deere-Miller Classification
UCS-Dry-PH-1-2	PHDF-1	222.64	21.19	0.18	95.17	BL
UCS-Dry-PH-1-3	PHDF-1	137.22	16.16	0.20	117.9	BL
UCS-Dry-PH-1-4	PHDF-1	119.09	9.21	0.17	113.73	BL
UCS_Dry_PH_2	PHDF-2	72.17	6.45	0.20	89.4	CL
UCS-Dry-PH-1-13	PH10 No. 13	24.11	3.84	0.21	159.0	EL
UCS-Dry-PH-1-30	PH10 No. 30	185.75	28.57	0.16	154.4	BL
UCS-Dry-PH-1-173	PH10 No. 173	43.99	6.58	0.23	149.5	DL
UCS-Dry-PH-1-194	PH10 No. 194	36.48	3.96	0.21	108.6	DL
UCS-Dry-PH-1-JGII	PH-JGII	72.17	6.45	0.20	89.4	CL
Average		**101.51**	**11.39**	**0.20**	**119.68**	**CL**
S.D.		**65.0**	**8.17**	**0.02**	**27.92**	

3.3.2 Brazilian Tests for Determination of Tensile Strength

It is difficult to achieve pulling effect on rock samples to obtaining a direct uniaxial tensile strength test. Brazilian test methods is a widely practiced indirect determination of tensile strength of rocks, though strictly not uniaxial in nature, the values obtained are comparable with those of direct test. Brazilian tests were conducted on discoidal specimens (diameter less than 45 mm and thickness approximately equal to half the diameter) of each rock type in dry condition as per the procedure given in ISRM (1979) and IS: 10082-1981. The test load was applied continuously at a constant rate so that failure of rock occurred within 15 to 30 seconds. Brazilian test enables one to determine the tensile strength of rock specimen indirectly, which is calculated using the expression,

$$\sigma_t = \frac{2P}{\pi d.t} \tag{3.3}$$

Where,

P = load applied at failure

d = diameter of the specimen and

t = thickness of specimen.

The results have been presented in Tables 3.17a, b, and c

Table 3.17a Summary of results of Brazilian tests conducted on dry Quartzite samples

Designation	Location	Weight, gm	Thickness (mm)	Diameter (mm)	Load, kN	Tensile Strength, MPa	Unit weight, kN/m^3
109/1	LDC-DCH1	185	34.3	54.8	35	11.85	22.86
109/2	LDC-DCH1	198.5	32.2	54.8	29	10.46	26.13
109/3	LDC-DCH1	200	32.5	54.8	38	13.58	26.08
155	LDC-DCH1	195	32	54.8	46	16.69	25.83
195/1	LDC-DCH1	174	31.5	54.8	35	12.90	23.41
195/2	LDC-DCH1	177	32	54.8	38	13.79	23.44
204	LDC-DCH1	180.5	32	54.8	34	12.34	23.91
275/1	LDC-DCH1	201.5	32.5	54.8	32	11.43	26.28
275/2	LDC-DCH1	202	32.5	54.8	41	14.65	26.34
279/1	LDC-DCH1	190	31	54.8	42	15.73	25.98
279/2	LDC-DCH1	198	32	54.8	51	18.51	26.22
335/1	LDC-DCH1	203	33	54.8	45	15.84	26.07
335/2	LDC-DCH1	191	31	54.8	49	18.36	26.11
377/1	LDC-DCH1	204.5	33.5	54.8	32	11.09	25.87

377/2	LDC-DCH1	164.5	27.5	54.8	32	13.51	25.35
421/1	LDC-DCH1	200.5	33	54.8	42	14.78	25.75
421/2	LDC-DCH1	190	31	54.8	50	18.73	25.98
427	LDC-DCH1	199	32.5	54.8	28	10.00	25.95
430/1	LDC-DCH1	202	33	54.8	46	16.19	25.94
430/2	LDC-DCH1	188	31.2	54.8	42	15.63	25.54
432/1	LDC-DCH1	193	31.5	54.8	60	22.12	25.97
432/2	LDC-DCH1	200	32.7	54.8	49	17.40	25.92
440	UDC-DCH2	189	30.5	54.8	44	16.75	26.26
452	UDC-DCH2	187	30.8	54.8	45	16.97	25.73
471	UDC-DCH2	198	31.8	54.8	52	18.99	26.39
495	UDC-DCH2	192	31.7	54.8	50	18.32	25.67
545	UDC-DCH2	196.5	32	54.8	48	17.42	26.02
619	UDC-DCH2	198	33.2	54.8	35	12.24	25.28
685/1	UDC-DCH2	209	34	54.8	42	14.34	26.05
685/2	UDC-DCH2	199.5	32	54.8	59	21.41	26.42
634	UDC-DCH2	194.5	30.6	54.8	32	12.14	26.94
708/1	UDC-DCH2	203.5	32.8	54.8	49	17.35	26.29
708/2	UDC-DCH2	206	32.8	54.8	28	9.91	26.62
708/3	UDC-DCH2	201.5	32.2	54.8	42	15.15	26.52
708/4	UDC-DCH2	208	32.5	54.8	31	11.08	27.12
Average						**15.08**	**25.78**
S. D.						**3.18**	**0.95**

Table 3.17b. Summary of results of Brazilian tests conducted on dry samples of Dolomitic limestone

Designation	Location	Weight, gm	Thickness mm	Diameter mm	Load, kN	Tensile Strength, MPa	Unit weight, kN/m^3
17	9 at Ch. 560m	252	43	52	60	17.08	27.58
1	7 at Ch. 580m	172.8	33.5	54	82	28.85	22.51
14	10 at Ch. 550m	232.2	34.5	57.5	65	20.85	25.91
22	7 at Ch. 580m	164.2	30	54.5	25	9.73	23.45
31	8 at Ch. 570m	156.3	24.5	54.5	50	23.83	27.34
13	8 at Ch. 570m	263.3	42.5	54.5	77	21.15	26.55
17	8 at Ch. 570m	171.3	28	54	58	24.41	26.70
40	9 at Ch. 560m	162.2	28	52	12	5.24	27.27
7	7at Ch. 580m	187.7	26	58	100	42.20	27.31
18	9 at Ch. 560m	295	40	58	40	10.97	27.90
	Average					**20.43**	**26.25**
	S.D.					**10.64**	**1.83**

Table 3.17c. Summary of results of Brazilian tests conducted on dry samples of Slates

Designation	Location	Weight, gm	Thickness mm	Diameter, mm	Load, kN	Tensile Strength, MPa	Unit weight, kN/m^3
1/1	PHDF-1	88.5	23	42	16	10.54	27.76
1/2	PHDF-1	107	29.5	42	10	5.14	26.17
2/1	PHDF-2	106.5	28.2	42	18	9.67	27.25

2/2	PHDF-2	90.5	24	42	12	7.58	27.21
2/3	PHDF-2	114.5	30	42	24	12.12	27.54
3/1	PHDF-3	102	27	42	16	8.98	27.26
3/2	PHDF-3	108	28.2	42	12	6.45	27.63
3/3	PHDF-3	104	27	42	20	11.22	27.79
3/4	PHDF-3	104	28	42	12	6.49	26.80
4/1	PHDF-4	99	33.1	38	15	7.59	26.36
	Average					**8.58**	**27.18**
	S.D.					**2.30**	**0.57**

3.3.3 Triaxial Compression Tests

Conventional axi-symmetric triaxial compression tests were conducted on rock specimens of NX size as per ISRM (1981, 1983) and (IS: 13047-1991). About twenty numbers of samples were tested for each rock type and the results are given in Table 3.18.a, b, c, d, & e. The methodology is described in (Chapter-2).

Table 3.18a. Shear strength parameters from triaxial strength tests on dry rock samples of Quartzites

Sample	Location	σ_3, MPa	σ_1, MPa	E, GPa	Shear strength parameters
TRX-DRY-DC-1	268/1	10	118.06	13.59	Mohr-Coulomb: c = 18.39 MPa ϕ = 48.1° Hoek-Brown: m_i = 16.32 σ_{ci}=148.07 MPa
TRX-DRY-DC-2	195	20	262.11	16.67	
TRX-DRY-DC-3	155	30	410.4	19.74	
TRX-DRY-DC-4	357	40	444.74	22.62	
TRX-DRY-DC-5	109	50	391.11	20.00	
TRX-DRY-DC-6	268/2	60	444.21	20.08	
TRX-DRY-DC-7	275	70	502.83	22.22	

Table 3.18.b Shear strength parameters from triaxial strength tests on saturated rock samples of Quartzites

Sample	Location	σ_3, MPa	σ_1, MPa	E, GPa	Shear strength parameters
TRX_SAT_DC_1	495/2	10	129.53	14.00	Mohr-Coulomb c = 14.47 MPa ϕ = 44.1° Hoek-Brown: m_i = 12.72 σ_{ci}=126.61 MPa
TRX_SAT_DC_2	685	20	156.05	15.35	
TRX_SAT_DC_3	452/1	30	250.36	13.64	
TRX_SAT_DC_4	452/2	40	308.07	10.03	
TRX_SAT_DC_5	495/1	50	361.20	18.02	
TRX_SAT_DC_6	452/3	60	431.20	17.72	
TRX_SAT_DC_7	440	70	404.50	21.42	

Table 3.18c. Shear strength parameters from triaxial strength tests on dry rock samples of Dolomitic limestone

Sample	Location	σ_3, MPa	σ_1, MPa	E, GPa	Shear strength parameters
Triaxial test-Dry-PH1	8at Ch. 570m No. 17	10	122.96	15.56	Mohr-Coulomb: c = 14.40 MPa ϕ = 37.1° Hoek-Brown: σ_{ci}=73.59 MPa m_i= 6.65
Triaxial test-Dry-PH1	10 at Ch. 550m No. 14	20	139.09	7.80	
Triaxial test-Dry-PH1	8 at Ch. 570m No. 1	30	151.48	12.31	
Triaxial test-Dry-PH1	7 at Ch. 580m No. 7	40	209.92	16.34	
Triaxial test-Dry-PH1	7 at Ch. 580m No. 3	50	273.60	21.4	

Table 3.18d. Shear strength parameters from triaxial strength tests on saturated rock samples of Dolomitic limestone

Sample	Location	σ_3, MPa	σ_1, MPa	E, GPa	Shear strength parameters
TRI_1_PH_ (Saturated)	8at Ch. 570m No. 20	10	127.62	10.77	Mohr-Coulomb c = 12.6 MPa ϕ = 36.9° Hoek-Brown: σ_{ci}= 56.88MPa m_i = 9.7
TRI_2_PH_ (Saturated)	7 at Ch. 580m No. 22	20	130.25	12.07	
TRI_3_PH_ (Saturated)	9 at Ch. 560m No. 18	30	126.13	8.75	

TRI_4_PH_ (Saturated)	10 at Ch. 550m No. 14	40	222.59	9.62	
TRI_5_PH_ (Saturated)	8 at Ch. 570m No. 31	50	246.70	17.65	

Table 3.18e. Shear strength parameters from triaxial strength tests on dry samples of slates

Sample	Location	σ_3 MPa	σ_1 MPa	E GPa	Shear strength parameters
TRX-DRY-PHDF-1,1	PHDF-1	10	98.86	7.35	Mohr-Coulomb: c = 11.36 MPa ϕ = 40.1° Hoek-Brown: σ_{ci}=75.1 MPa m_i= 9.52
TRX-DRY-PHDF-2,2	PHDF-2	20	171.89	14.29	
TRX-DRY-PHDF-3,1	PHDF-3	30	232.45	13.89	
TRX-DRY-PHDF-3,2	PHDF-3	40	169.10	12.86	
TRX-DRY-PH-6	PHDF-2	50	266.46	25.21	

Table 3.18f. Shear strength parameters from triaxial strength tests on saturated rock samples of slates

Sample	Location	σ_3, MPa	σ_1, MPa	E, GPa	Shear strength parameters
TRX-SAT-PH-1	PHDF-1	10	85.32	7.80	Mohr-Coulomb: c = 8.01 MPa ϕ = 35.9° Hoek-Brown: σ_{ci}=58.8 MPa m_i= 4.0
TRX-SAT-PH-2	PH10 No.61	20	115.06	113.08	
TRX-SAT-PH-3-3	PHDF-3	20	93.12	11.11	
TRX-SAT-PH-5	PH10 No.61	30	167.48	14.4	
TRX-SAT-PH-3-2	PHDF-3	30	151.87	14.11	
TRX-SAT-PH-3	PH10 No.61	40	192.10	28.85	
TRX-SAT-PH-3-1	PHDF-3	40	143.18	10.0	
TRX-SAT-PH-4	PH10 No.132	60	261.69	17.05	

3.4 RESULTS AND INTERPRETATION OF TEST DATA

Various tests related to strength parameters of intact rock specimens were carried out under dry and saturated conditions. The results obtained for different rock types were statistically analysed to obtain average and standard deviation. The averaged results for different rock types related to geomechanical properties, strength and deformation parameters from dam and powerhouse area under dry and saturated condition are summarized in Table 3.19.

Table 3.19 Averaged results of laboratory tests for different rock types.

Location	**Rock Type**	**UCS (MPa)**	**Tensile Strength (MPa)**	**Intact Rock Modulus, E_i(GPa)**
Dam area Desilting Chamber	Quartzites (Dry)	74.72±23.45	15.08±3.18	12.05±2.8
	Quartzites (Saturated)	56.20±26.34	-	8.94±4.48
Powerhouse	Slates(Dry)	101.51±65.0	8.58±2.30	11.39±8.1
	Dolomitic L.st(Dry)	149.19±50.49	20.43±10.64	14.36±1.68
	Dolomitic L.st (Sat)	86.61±16.93	--	12.90±2.5

The results of laboratory tests indicate that the dolomitic limestones show high range of values as compared to other rock types. The UCS, tensile strength and elastic modulus values for dolomitic limestones of powerhouse area range from strong to very strong, whereas the quartzite rocks from the dam area and the slates from the powerhouse area fall in strong rock category (Bieniawski, 1979).

In order to understand the relation between the UCS (σ_c) and the tangent modulus of deformation, E_t (at 50% of σ_c), it is plotted on Modulus-Strength Classification of Deere and Miller (1966) (Fig 3.8) for representative rock samples (Table 3.20). This logarithmic plot illustrates that a wide overlap in strength and deformation properties can be seen for individual rock types. In case of slates, the tests on dry samples indicate that they fall under the category of low to medium, though sporadic values fall under high category also. The dry dolomitic limestone samples shows high UCS values, while the saturated samples fall between medium to high range.

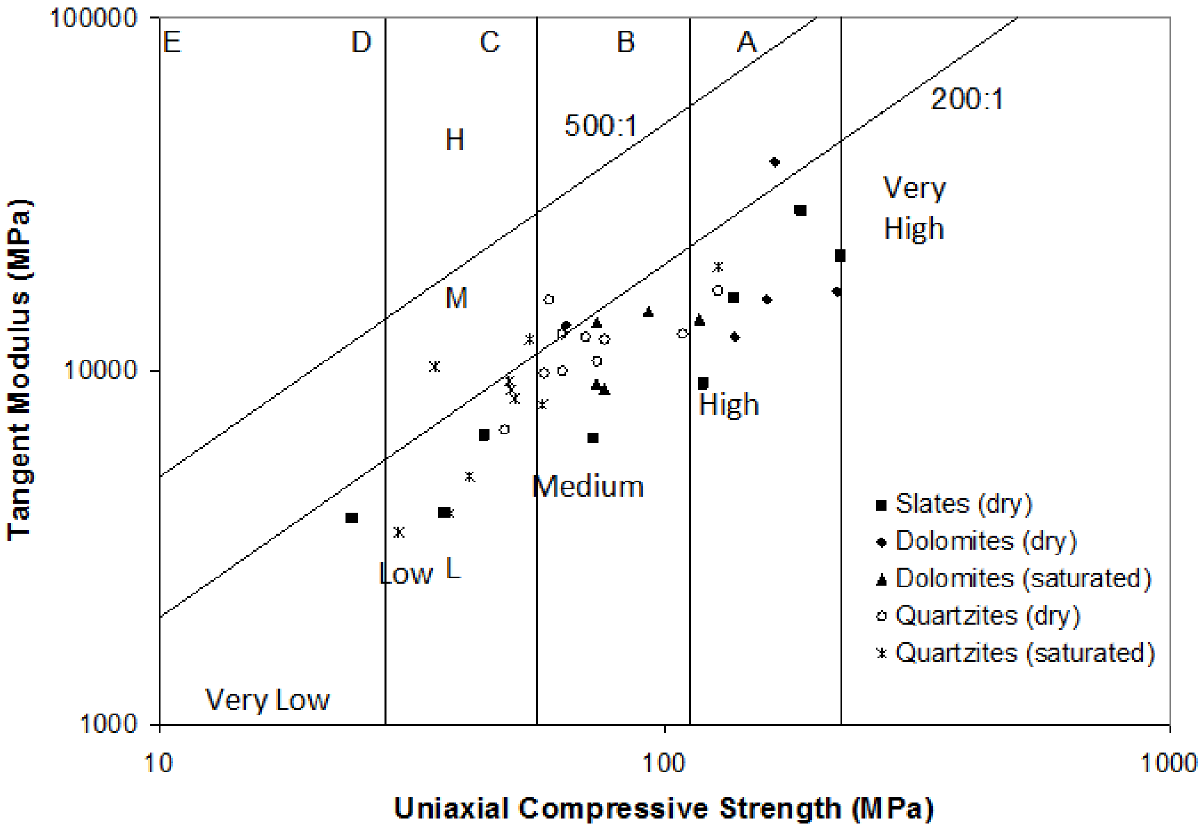

Fig 3.8 Deere–Miller (1966) Classification of Rocks

The dry samples of quartzite are mostly clustered around medium strength, though the saturated samples range between low to medium. Over all the quartzite rank lower than that of dolomitic limestones. This can be mainly attributed to the fact that very coarse grains to coarse grained quartzites tend to easily break around the grain boundaries under loading.

Table. 3.20 Summary of mechanical properties for major rock type in the project area

Location	Rock Type	UCS (MPa)	Tensile Strength (MPa)	Intact Rock Modulus, E_i(GPa)	Deere-Miller Classification
Dam area Desilting Chamber	Quartzites (Dry)	74.72±23.45	15.08±3.18	12.05±2.8	CL
	Quartzites (Saturated)	56.20±26.34	-	8.94±4.48	CL-DL
Powerhouse	Slates(Dry)	101.51±65.0	8.58±2.30	11.39±8.1	CL
	Dolomite(Dry)	149.19±50.49	20.43±10.64	14.36±1.68	BL

	Dolomite(Sat)	86.61±16.93	--	12.90±2.5	CL

The Brazilian tests were conducted on representative samples of quartzite rock collected from dam area, slate and dolomitic limestone from the powerhouse area. Total 20 numbers of samples for each rock types were tested consisting of 10 samples under dry condition and 10 samples under saturated condition. The tensile strength values for the quartzites and slates ranges between 3.18 to 15.08 MPa indicating that their intact rock strength range between strong to very strong category (Bieniawski, 1979). Whereas dolomitic limestone falls on very strong category with the tensile strength ranges between 10.64 to 20.43 Mpa.

The triaxial test results shown in Table 3.18 indicate that quartzite rocks in general show maximum peak strength followed by dolomitic limestone and then slates. The results of triaxial compression test for quartzites, dolomitic limestone and slates (in terms of major principal stress, σ_1 and minor principal stress, σ_3 at failure) for both dry and saturated rock cores are tabulated in Table 3.20

Shear strength of intact rock

The shear strength parameters for intact rocks have been obtained using two failure criteria namely, Mohr-Coulomb and Hoek-Brown criterion. The Mohr-Coulomb parameters, c and ϕ have been obtained by plotting p-q diagram and fitting best straight line (Fig 3.9, 3.10 and 3.11). The original Hoek-Brown (1980) criterion has been used to describe the non-linear strength behaviour of intact rocks (Fig 3.12, 3.13 & 3.14). The confined strength of the intact rock is represented as follows:

$$\sigma_1 = \sigma_3 + \sqrt{m\sigma_{ci}\sigma_3 + \sigma_{ci}^2} \tag{3.2}$$

Where

m and σ_{ci} are the criterion parameters,

σ_1 = the major principal stress at failure,

σ_3 = the minor principal stress at failure,

m = is the value of the Hoek-Brown constant m for the rock mass

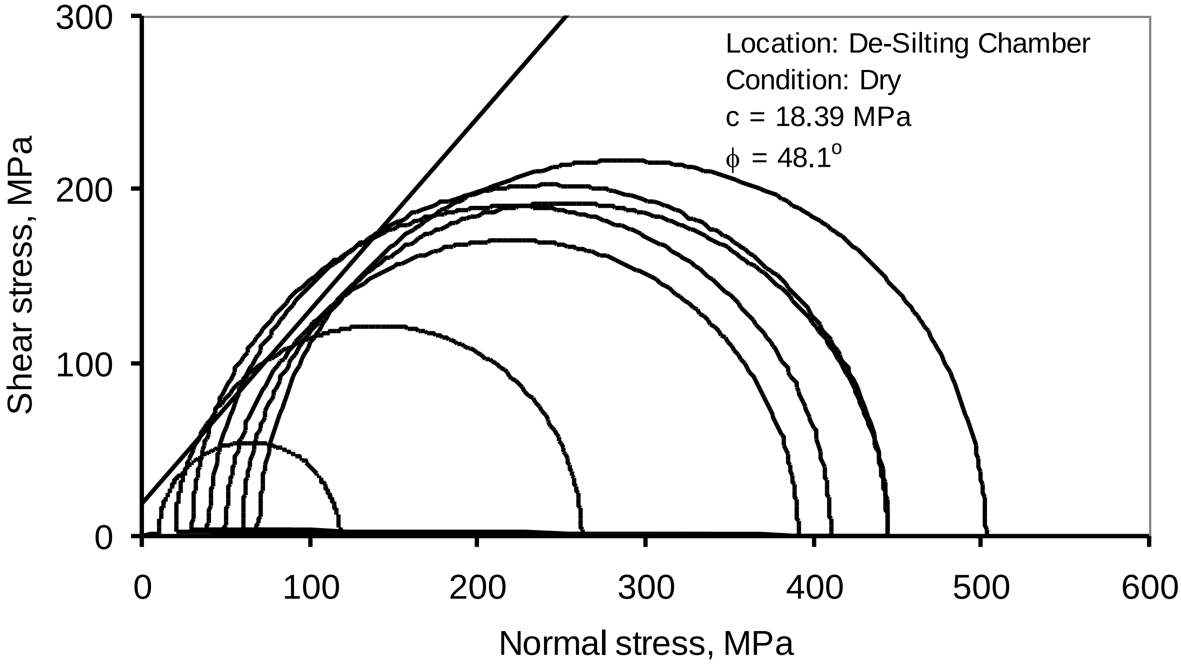

Fig 3. 9a Mohr's Envelope for Quartzites (Dry)-Desilting Chambers Area

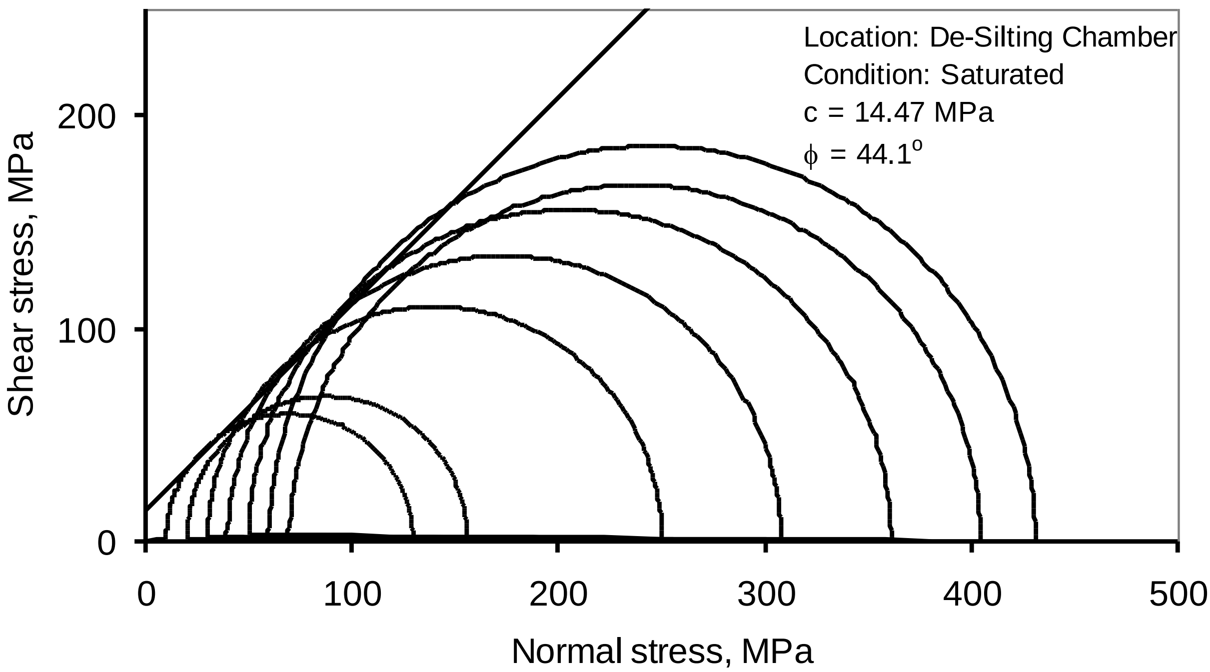

Fig 3.9b Mohr's Envelope for Quartzites (Saturated)-Desilting Chambers Area

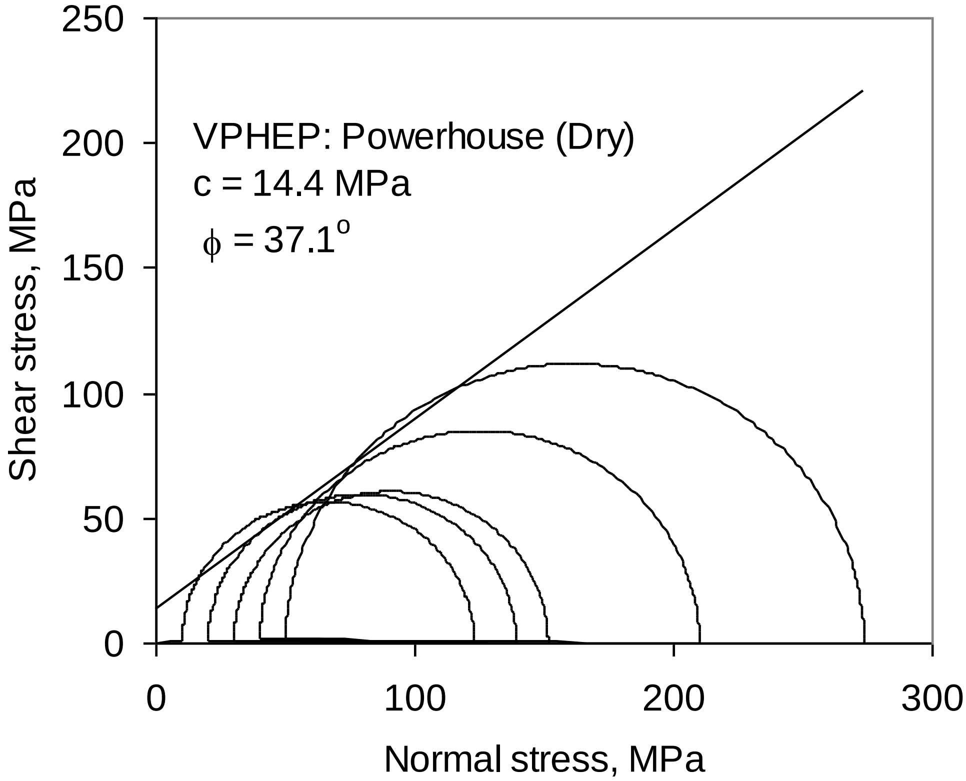

Fig 3.10a Mohr's Envelope for Dolomitic limestone (Dry)-Powerhouse

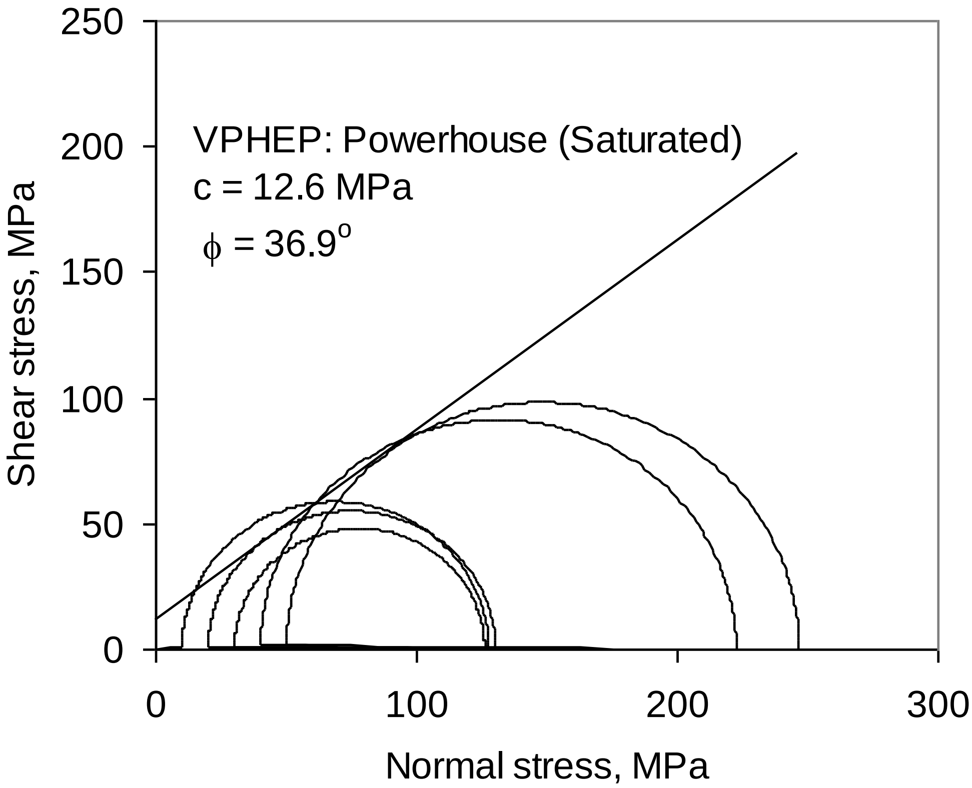

Fig 3.10b Mohr's Envelope for Dolomitic limestone (Saturated)-Powerhouse

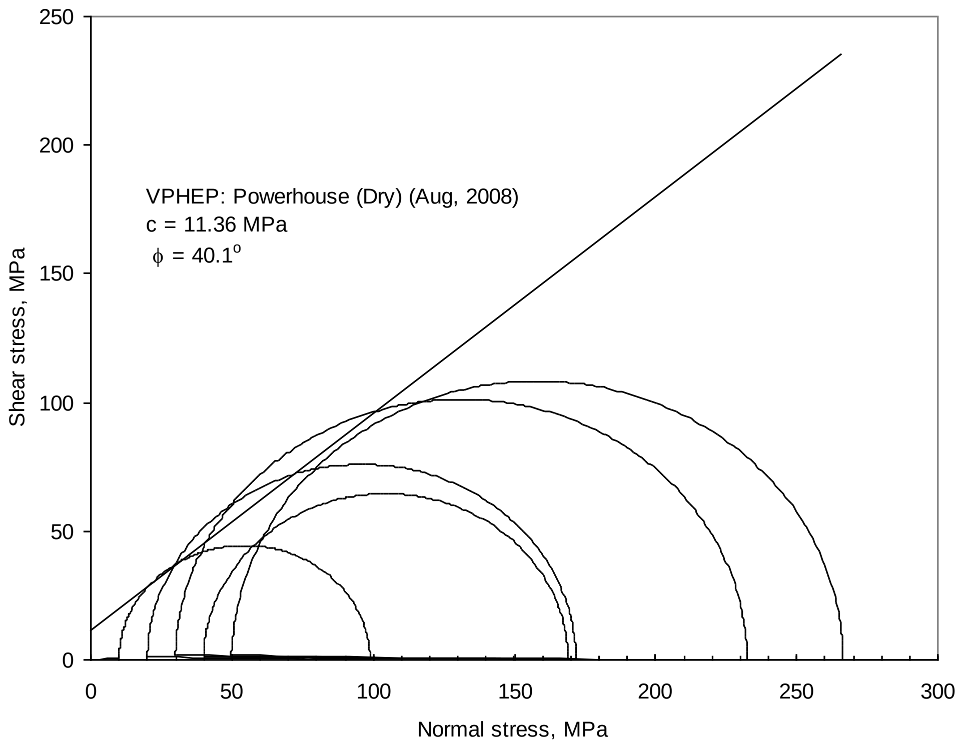

Fig 3.11a Mohr's Envelope for Slates (Dry)-Powerhouse

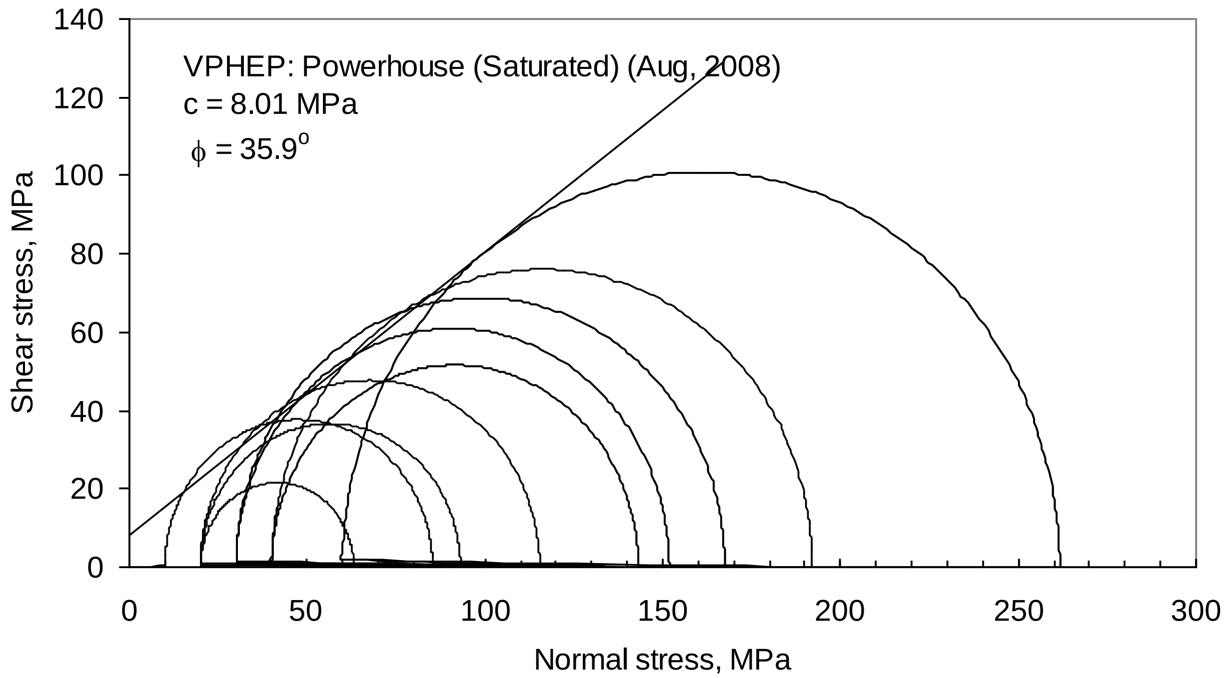

Fig 3.11b Mohr's Envelope for Slates (Saturated)-Powerhouse

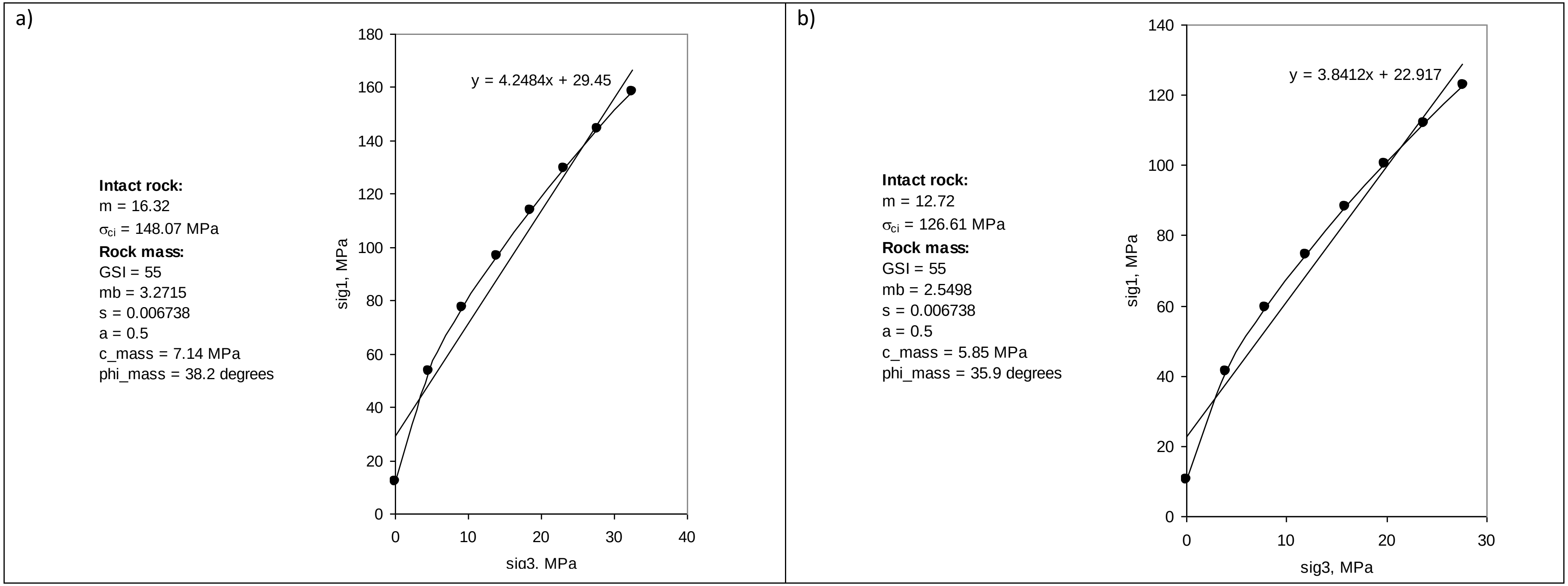

Fig 3.12 Hoek-Brown parameters for intact rock and jointed rock masses of Quartzites a) Dry Condition and b) Saturated Condition

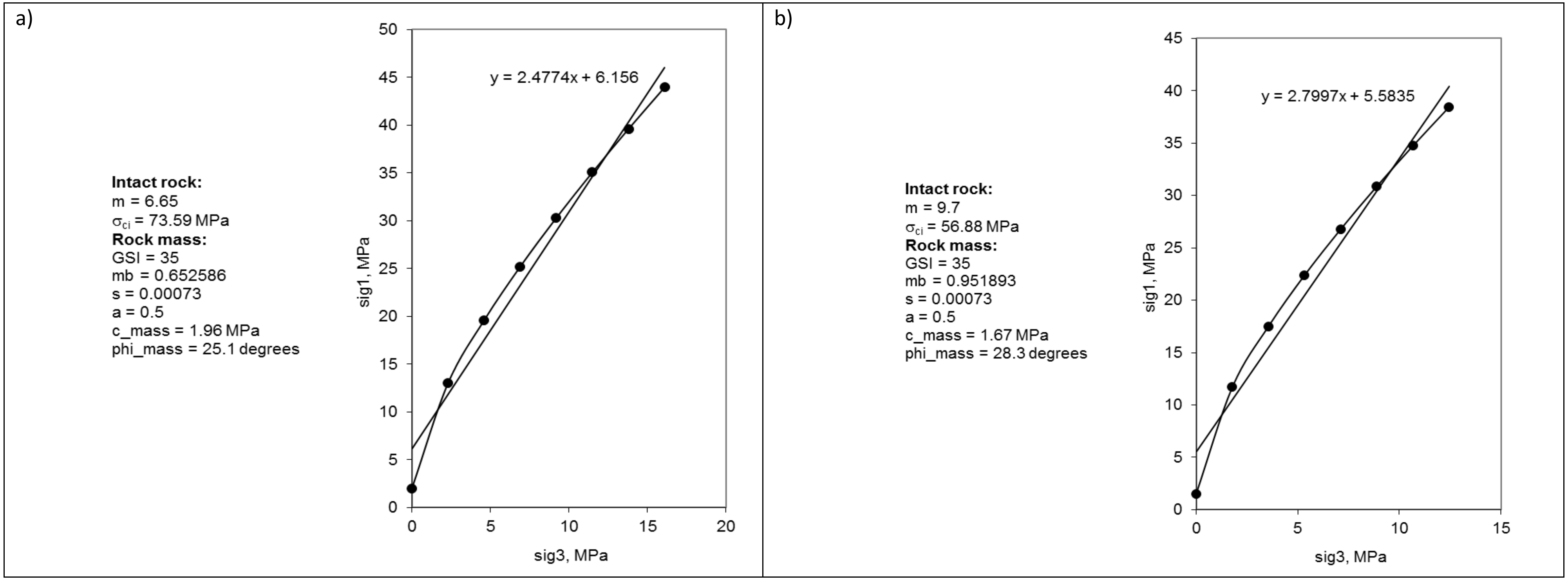

Fig 3.13 Hoek-Brown parameters for intact rock and jointed rock masses of Dolomitic limestone a) Dry Condition and b) Saturated Condition

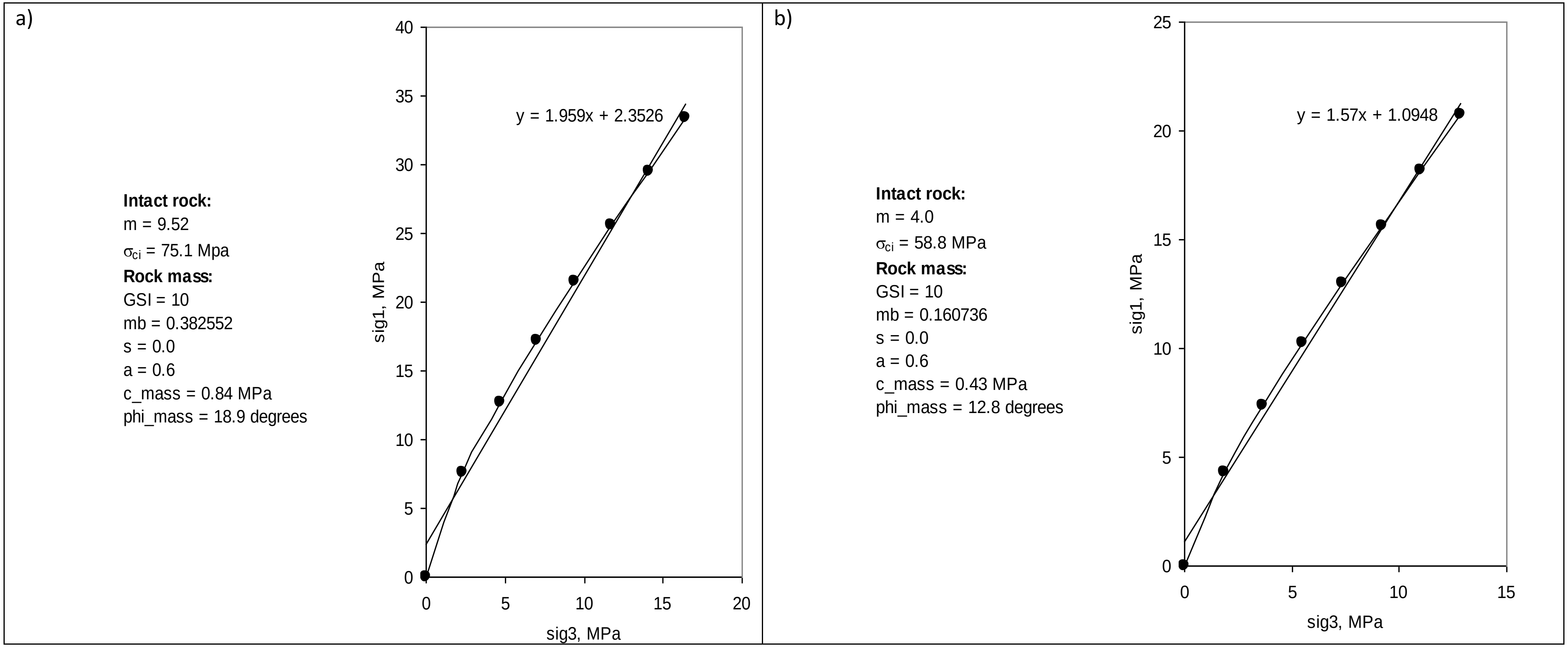

Fig 3.14 Hoek-Brown parameters for intact rock and jointed rock masses of Dolomitic limestone a) Dry Condition and b) Saturated Condition

3.5 GROUND CHARACTERIZATION

Rock mass refers to in-situ rocks with all inherent geo-mechanical anisotropies like bedding planes, fault, joint, fractures and shears, which directly affects the strength properties of the rock. Rock mass is a huge in-situ rock traversed by network of discontinuities forming many rock blocks. In geology, we are interested with inherent anisotropies of the rock, which has to be accounted in the scheme of rock mass classification in quantified numbers (Singh & Goel, 1999).

Rock mass characterization by empirical approach provides guidelines for the estimation of support pressure for subsurface Engineering structures. In the present study, the ground characterization was determined based on the widely followed geomechanical classifications like RQD (Deere, 1964), RMR (Bieniawski, 1973), Q system (Barton et al (1974) and GSI (Hoek et al. 1998; Marinos and Hoek 2000, 2001). In 1973, Bieniaswski proposed the RMR System, which is widely applied for stability analysis and to ascertain the strength properties of rocks. Barton et al (1974) proposed the Q system, which is the best system, so far, for support pressure evaluation and required support system of tunnels. The RMR and the Q classifications directly rely upon the RQD classification. Whereas RQD at some geological condition becomes negligible and essentially zero. An alternate rock classification GSI (Hoek et al. 1998; Marinos and Hoek 2000, 2001) was developed without involvement of RQD that more effectively reflects the ground geological condition and estimation of rock mass properties.

Extensive in-situ and laboratory tests were carried out for determining the strength properties. The structural discontinuities and hydrogeological condition that coexists within the rock mass plays a key role in determining the mechanical characteristics of the rock mass (Behrestaghi et al, 1996). In order to carry out ground characterization, it is essential to obtain data related to lithological and structural parameters. For that purpose, Engineering Geological mapping on 1:1000 and 3D drift logging were carried out in dam and powerhouse area. The structural details of lithology exposed on ground at dam and power areas like attitude of foliation, joints and shears were recorded and summarized in Table 3.21 & 3.22. In addition, in order to estimate the geomechanical properties, the characteristics of discontinuities like spacing, opening, persistence/continuity, roughness, and water condition were recorded and simultaneously samples for laboratory experiments were also collected. Water inflow in the exploratory drifts at dam site and powerhouse area has been vigilantly observed and the details are tabulated in Table 3.23.

Table 3.21 Structural details Recorded at Dam site

Planes	Dip amount & Dip direction	Spacing (cm)	Smoothness	Opening	Water Condition
Foliation/J1	34º/N10º	10-15	Smooth planar	Slightly open	Dry
J2	85º/N270º	50-80	Rough	Tight	Dry
J3	60º/N200º	30-80	Smooth undulatory	Tight	Dry
J3	30º/N200º	25-95	Rough planar	Closed	Dry

Table 3.22 Structural details Recorded at powerhouse site

Sl. No	Dip amount & Dip Direction	Spacing (cm)	Smoothness	Water condition
Slates				
Foliation	25°-30°/N80°W	15-30	Smooth	Dry
J1	55°-70°/N20°E	2-30	Smooth planar	Dry
J2	Vertical	5-10	Smooth undulatory	Dry
J3	30-45/N40°E	5-10	Smooth planar	Dry
Dolomitic limestone				
J1	60°/N65°E	50-100	Smooth planar	Wet at places
J2	60°-65°/S25°W	25-40	Smooth undulatory	Damp
J3	Vertical	15-50	Smooth planar	Wet

Table 3.23Water inflows in exploratory drifts

Drifts	Length (m)	Rock types	Inflow
Dam site DL-01	33	Quartzite	Damp–dry
DL-01 u/s cross cut	15	Quartzite	Damp–dry
DL-01 d/s cross-cut	15	Quartzite	Damp
U/S Surge Shaft U/SSD-1	211	Dolomitic limestone	Mostly dry and damp at places
Powerhouse PHD-1	0-439	Shale/slates	Generally damp and dripping from RD 42 to 64m.
	439-460	Shale/slates and Dolomitic limestone	Generally dripping condition
	460-650	Dolomitic limestone	Generally dripping and at RD 500m, heavy inflow of 80 litres/min

3.5.1 Characterization of Rock Mass–RQD, RMR and Q

3.5.1.1 Rock Quality Designation (RQD)

The Rock Quality Designation (RQD) values obtained from various drill holes at different depths for various rock types were studied and the average values obtained are provided in Table 3.24. In dam area, the RQD values for quartzite range from 75% to 80% indicating good rock. While in surge shaft and powerhouse areas, the RQD values of slate range from 50%-55% indicating fair rock. The RQD values dolomitic limestone in general have high range between 60% to 90% indicating fair to good rock.

Table 3.24 Rock Quality Designation (RQD) values obtained for different rock types.

Rock type	RQD (%)	Rock Quality
Quartzites	88.6	Good
Dolomitic limestones	80.1	Good
Slates	55	Fair

3.5.1.2 Evaluation of Rock Mass Rating (RMR)

The geomechanical properties of the rocks were studied at dam site, powerhouse and other locations in order to evaluate RMR. In the present study, Bienieawski 1984 method was followed to evaluate the geomechanical properties of the rocks of the project area. In the dam area, including desilting chamber, observations related to geomechanical properties of quartzites were carried out in 10 locations. Similarly, the geomechanical properties of slate and dolomitic limestone were noted in powerhouse and surge shaft area in another ten locations. The average values of geomechanical properties and final RMR obtained from the study has been shown in Table 3.25.

Table 3.25 Estimation of RMR for different rock type (Bineiawski, 1984)

Parameters	**Rock type**		
	Quartzite	**Slate**	**Dolomitic limestone**
UCS (MPa)	108	101.5	149.19
Rating	12	12	12
RQD	88.6	52	78.2
Rating	20	13	17
Spacing of Discontinuities (m)	0.2-0.6	0.06-0.2	0.06-0.2
Rating	10	8	10
Condition of discontinuities	Very rough and unweathered, wall rock tight and discontinuous, no separation		
Rating	30	30	30
Ground water condition	Dry	Damp	Damp
Rating	15	10	10
RMR_{basic}	82	73	79
Class	I	II	II
Description	Very good rock	Good rock	Good rock

3.6 Q-SYSTEM

The Q system is one of the popular rock mass classification systems that is been widely followed all over the world for planning underground structures. It was introduced and developed by Barton, Lien and Lunde in the year 1974. The Q values were evaluated for different rock types exposed at the dam site, powerhouse, surge shaft and in power tunnel locations. The results are summarized in Table 3.26.

Table 3.26 Summary of Q values calculated for quartzites, slate and dolomitic limestones

<table>
<tr><th>Parameters</th><th colspan="2">Quartzite</th><th colspan="2">Slate</th><th colspan="2">Dolomitic limestones</th></tr>
<tr><td rowspan="2">RQD</td><td colspan="2">88.6</td><td colspan="2">52</td><td colspan="2">78.2</td></tr>
<tr><td colspan="2">Good</td><td colspan="2">Fair</td><td colspan="2">Good</td></tr>
<tr><td>Joint set no. (Jn_)</td><td colspan="2">Three sets</td><td colspan="2">Three sets</td><td colspan="2">Three sets</td></tr>
<tr><td>Rating</td><td colspan="2">6</td><td colspan="2">6</td><td colspan="2">6</td></tr>
<tr><td>Joint roughness no. (J r)</td><td colspan="6">Smooth planar</td></tr>
<tr><td>Rating</td><td colspan="2">1</td><td colspan="2">1</td><td colspan="2">1</td></tr>
<tr><td>Joint alteration no. (Ja)</td><td colspan="6">Unaltered joint walls, surface staining only</td></tr>
<tr><td>Rating</td><td>1</td><td>1</td><td>1</td><td>1</td><td>1</td><td>1</td></tr>
<tr><td rowspan="2">Joint water reduction factor (JW)</td><td colspan="6">Dry excavation or minor inflow</td></tr>
<tr><td>1</td><td>1</td><td>1</td><td>1</td><td>1</td><td>1</td></tr>
<tr><td>Stress reduction factor (SRF)</td><td colspan="6">Single weakness zones containing clay or chemically disintegrated rock (depth of excavation > 50m)</td></tr>
<tr><td>Rating</td><td colspan="2">2.5</td><td colspan="2">2.5</td><td colspan="2">2.5</td></tr>
<tr><td>Q</td><td colspan="2">6</td><td colspan="2">3.44</td><td colspan="2">5.21</td></tr>
<tr><td>Group</td><td colspan="2">2</td><td colspan="2">2</td><td colspan="2"></td></tr>
<tr><td>Description</td><td colspan="2">Fair</td><td colspan="2">Poor</td><td colspan="2">Fair</td></tr>
</table>

3.7 ROCK MASS STRENGTH

Reliable estimates of the strength and deformation characteristics of rock masses are required for all types of analyses used for the design of slopes, foundations and underground excavations. Mechanical behaviour, deformation characteristics of rock mass and strength parameters are essential for stability analysis related to foundations, slopes and underground caverns.

3.7.1 Geological Strength Index (GSI)

Geological Strength Index (GSI) is a method for rock-mass characterization that has greater importance for geological condition of the rock mass (Fig 3.15).

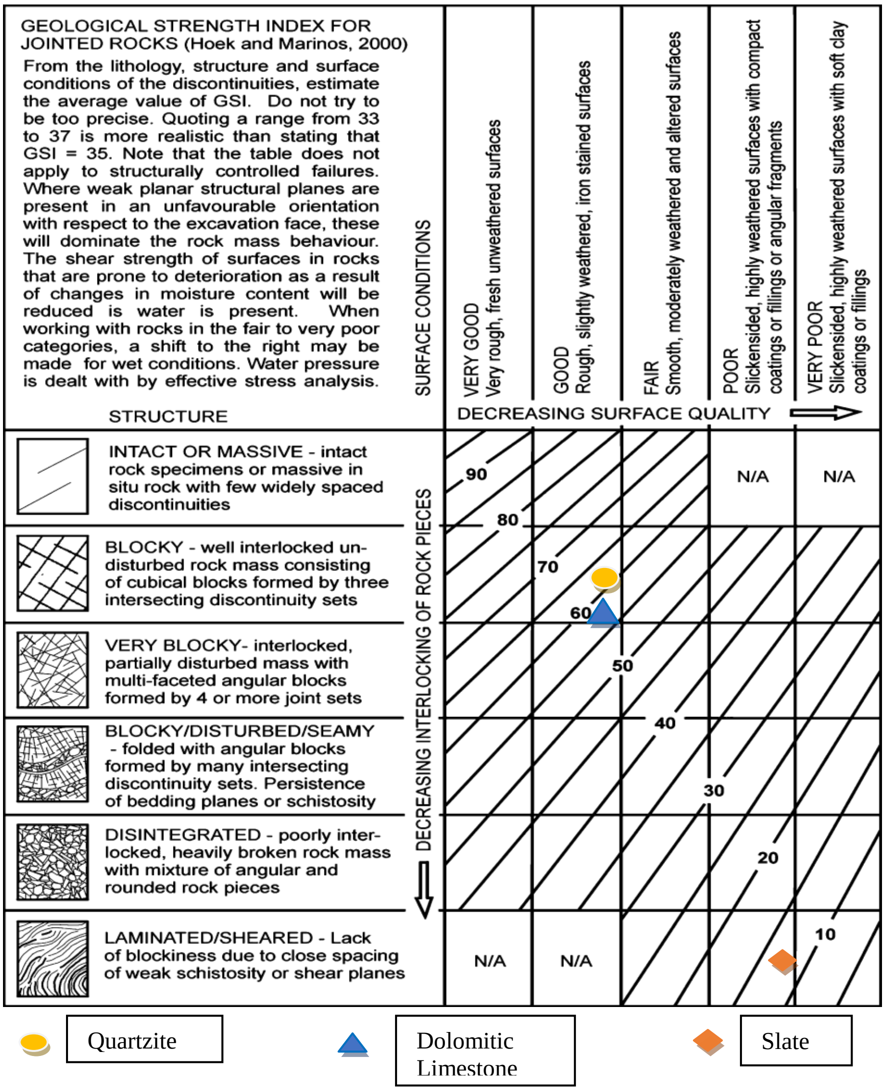

Fig 3.15. General chart for GSI estimates from the geological observations (Hoek et al.1992)

The blockiness, the geological process of the rock mass and the conditions of discontinuities are quantified effectively (Marinos et al., 2005). As GSI approach can be directly correlated with rock mass ground conditions, the values of GSI are highly reliable for the estimation of rock mass shear strength parameters. The GSI values were estimated from the dam, power tunnel and powerhouse area. The quartzite rocks present in the dam area appeared to be well interlocked, undisturbed, joints were rough, unweathered and observed with iron strains and these quartzite rocks are categorised on the GSI chart (Hoek & Marinos 2000) with GSI value 60. The dolomitic limestones of powerhouse area appeared blocky, interlocked, with slight disturbance were assigned estimated value of 58. The slate from the powerhouse area appears with phyllitic shine, intensely folded, closely spaced joints sets with shear bands at places. The GSI value for slate were estimated to be 15 that fall under fair to poor in strength the values obtained are given in Table 3.25. The estimated GSI values are plotted over GSI chart (Hoek & Marinos 2000).

3.7.2 Hoek-Brown shear strength parameters

The Hoek-Brown shear strength parameters for the rock mass have been obtained following the procedure suggested by Hoek and Brown (1997). As per this approach, the strength of the rock mass is represented by the generalised criterion as:

$$\sigma_1 = \sigma_3 + \sigma_{ci}\left(\frac{m_j\sigma_3}{\sigma_{ci}} + s_j\right)^a \tag{3.3}$$

The parameters, m_j, s_j and ‘a’ are estimated from the following relationships:

$$m_j = m_i e^{\left(\frac{GSI-100}{28}\right)} \tag{3.4}$$

i) For undisturbed rock masses i.e GSI > 25

$$s_j = e^{\left(\frac{GSI-100}{9}\right)} \tag{3.5}$$

$$a = 0.5$$

ii) For disturbed rock masses, GSI < 25

$$s = 0$$

$$a = 0.65 - \frac{GSI}{200} \tag{3.6}$$

Where, GSI is the geological strength index.

By following the above expressions, parameters, m_j , s_j and 'a' were obtained. Now the values of simulated tri-axial strength were generated for eight confining stresses in the range of $0<\sigma_3<0.25\ \sigma_{ci}$ as suggested by Hoek and Brown (1997). The equivalent Mohr-Coulomb shear strength parameters, c_{mass} and ϕ_{mass} were now obtained by fitting a straight line into the simulated tri-axial tests data and using the following expressions:

$$\phi_{mass} = \sin^{-1}\left(\frac{k-1}{k+1}\right) \tag{3.7}$$

$$c_{mass} = \frac{\sigma_{cm}}{2\sqrt{k}} \tag{3.8}$$

where the best fitting straight lie is given as:

$$\sigma_1 = \sigma_{cm} + k\sigma_3 \tag{3.9}$$

The summary of the results thus obtained has been presented in Table 3.27

Table 3.27 Rock mass strength parameters as per Hoek and Brown (1997) criterion obtained from Triaxial tests

Rock Type	Condition	GSI	m_i MPa	σ_{ci}	m_j	s_j	a	c_{mass} MPa	ϕ_{mass} (°)
Slates	Dry	20	9.52	75.1	0.38	0.0	0.6	0.84	18.9
	Saturated	17	4.0	58.8	0.16	0.0	0.6	0.43	12.8
Dolomitic limestone	Dry	58	6.65	73.59	0.65	0.00073	0.5	1.96	25.1
	Saturated	58	9.7	56.88	0.95	0.00073	0.5	1.67	28.3
Quartzites	Dry	60	16.32	148.07	3.27	0.00674	0.5	7.14	38.2
	Saturated	55	12.72	126.61	2.55	0.00674	0.5	5.85	35.9

3.7.3 Rock Mass Deformability and Shear Strength

Rock mass deformability is considered to be one of the primary parameters governing the behaviour of rock masses (Deere et al, 1967). Deformability is categorised by a modulus relating the relationship between the applied load and the resulting deformation (Bieniawski, 1978). The plate load tests were done at the dam site and in the powerhouse drift to determine rock mass deformability. The obtained results are summarised on Table 3.28. In-situ shear tests were also carried out to assess the sliding resistance of concrete on rock.

Table 3.28 Results of in situ tests on deformability and shear strength

Plate load tests			**Average results for 80 tonne load on 60cm plate**		
Location	**Rock type**	**Orientation**	**Modulus of deformation GPa**	**Modulus of elasticity GPa**	
Left bank drift	Quartzite	Vertical	2.7	3.9	Left bank drift
Right bank drift	Quartzite	Horizontal	1.2	5.1	Right bank drift
Right bank drift	Quartzite	Vertical	10.2	13.7	Right bank drift
PH drift	Dolomitic limestone	Vertical	3.4	5.2	PH drift
PH drift	Dolomitic limestone	Horizontal	1.2	2.0	PH drift
In-situ shear tests		In-situ shear strength			
		Peak		Residual	
		Cohesion (c) kPa	**Friction (φ°)**	**Cohesion (c) kPa**	**Friction (φ°)**
Left bank drift	Concrete/rock	775	55°	470	50°
Right bank drift	Concrete/rock	295	59°	215	57°

3.7.4 Empirical estimation of Rock Mass Modulus

Hoek and Diederichs (2006) have suggested the following expressions for the rock mass modulus based on GSI.

$$E_{mass} = E_i\left(0.02 + \frac{1 - D/2}{1 + \exp((60 + 15D - GSI)/11)}\right) \tag{3.10}$$

$$E_{mass} = 1x10^5\left(\frac{1 - D/2}{1 + \exp((75 + 25D - GSI)/11)}\right) \tag{3.11}$$

Where E_i is the intact rock modulus and D is the damage factor.

The obtained results for different rock types are summarized in Table 3.29

Table 3.29 Summary of rock mass modulii values using GSI: Hoek and Diederichs (2006)

Sl	Rock type	E_{mass}, GPa
1	Quartzites	4.919 & 5.635
2	Slate	0.270 & 0.342
3	Dolomitic limestone	1.630 & 2.567

CHAPTER IV

ENGINEERING GEOLOGICAL APPRAISAL OF PIPALKOTI DAM SITE

Vishnugad-Pipalkoti Hydroelectric Project is a run-off-the-river (ROR) hydropower project on the river Alaknanda, which involves construction of a 65m high diversion dam. The dam is located near the village Helong (79º 29’30” E and 30º 30’50” N) in Chamoli District. The dam area includes project components such as main dam, intake portal, desilting chambers, upstream and downstream coffer dams. The National Highway, NH-58 (El±1307m), passes just above the dam top (El±1270m) on the left bank (Fig 4.1 & 4.2). The dam is located in a narrow river valley section with chord–height ratio of 1.37. In the immediate upstream of the dam site, the valley opens up with a wider river section. Since the project envisages an overflowing spillway, the available width at the top of the dam may not be sufficient to accommodate flood season discharge and hence may involve widening of the river section. The right bank slopes are steeper (65º) as compared to left bank (60º) though the slopes above dam site on the left bank becomes more flatter (40º). Two diversion tunnels will be excavated on the left bank to facilitate the construction of the dam. The inlet portals of these tunnels will be located in the wider section of the river just upstream of the dam site. The Engineering Geological evaluation of the dam site includes the following work components.

Field Studies

a.) Detailed Geological mapping of the dam area on 1:1000 scale.
b.) Preparation of Geological cross sections along dam axis, 100m upstream and 100m downstream of dam axis.
c.) Subsurface geotechnical investigations including i) drill core logging, ii) 3D drift mapping, iv) Water pressure tests in drill holes v) Plate load tests and Block shear tests in drifts.
d.) Empirical approaches (Hoek and Diederrich, 2006) (Sigh et al, 2002) were followed for determination of rock mass modulus.
e.) Stability analysis of the dam abutments.

Laboratory Studies

a.) Determination of geomechanical properties such as specific gravity, uniaxial compressive strength (σ_c), tensile strength (σ_t) and other properties.
b.) Estimation of shear strength parameters like cohesion and friction using triaxial tests.

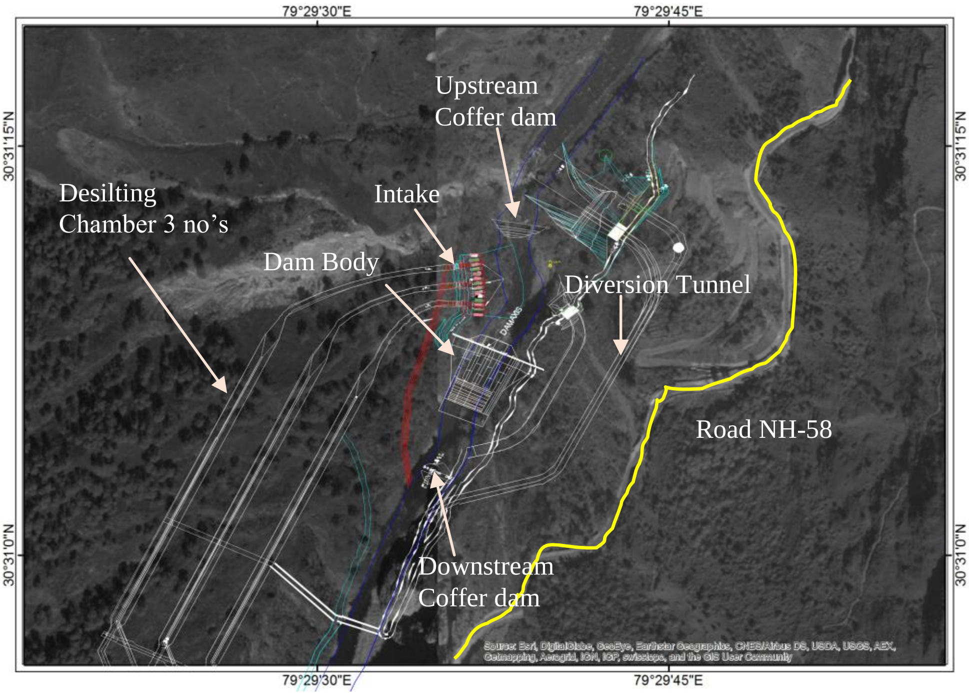

Fig 4.1 Dam, Intake, Desilting chamber and Diversion tunnel plan laid over satellite imagery(ArcGIS10.2 Base map image)

Fig 4.2 Steep narrow gorge of VHEP dam area with massive Garhwal quartzites

4.1 DETAILED GEOLOGICAL MAPPING OF DAM AREA

Detailed mapping of the dam area has been carried out on 1:1000 scale covering dam site, diversion structure, intake portal, desilting chambers and coffer dams (Fig 4.3). The river at the dam site flows from northeast towards southwest. The right bank slopes are steep occupied by quartzite rocks of Garhwal Group. Thin slope wash materials can be seen at places on the rock surface. On the other hand, the left bank has rock exposures up to El ± 1300m and further above debris materials are seen occupying most areas with intermittent rock exposures. One major patch of debris materials is seen over a length of about 230m and having a width of about 20m above the dam site. The important regional feature namely MCT is present about 2km upstream of dam site at the tail end of the reservoir and hence poses no problem.

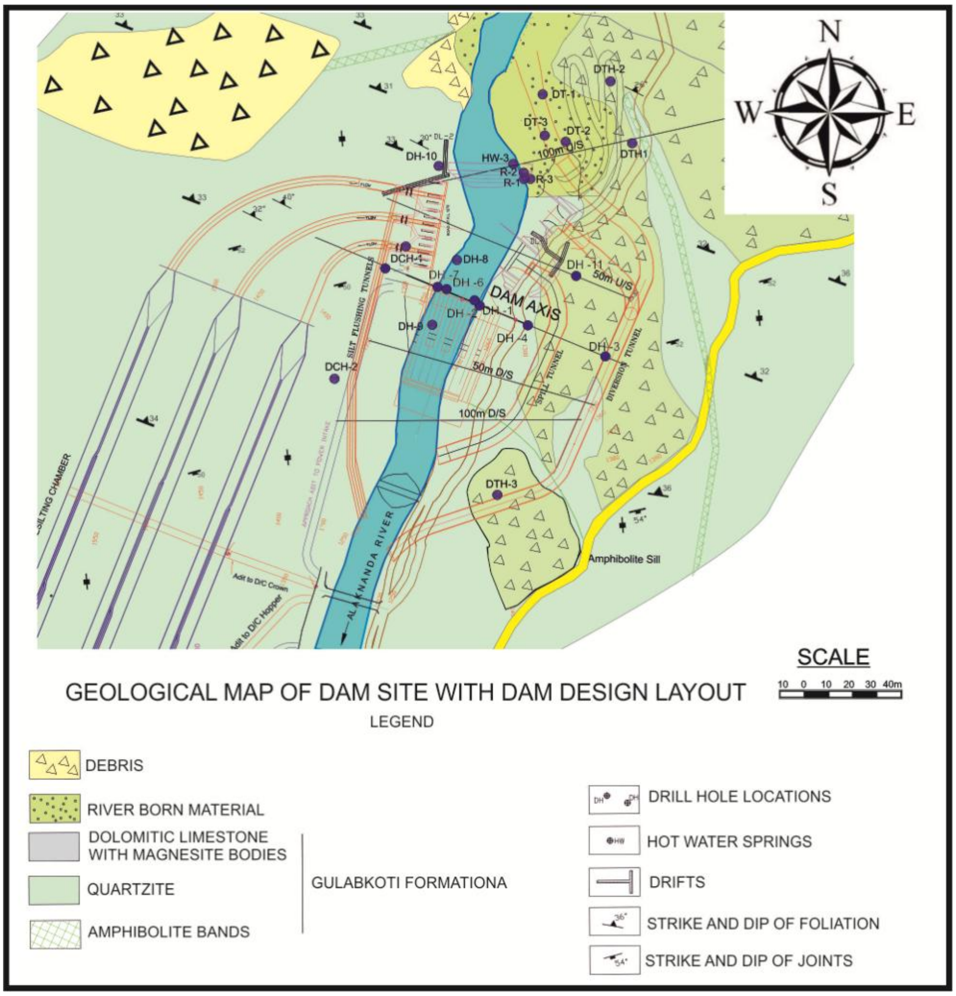

Fig 4.3 Geological map of Dam area with major project structures

4.1.1 Lithology

The rock type exposed at the dam site is quartzite which is seen on both the banks. In general quartzites are massive in nature, hard and competent with foliation being observed as a dominant discontinuity. The rocks are often interbedded with thin bands of biotite mica schist. A chlorite schist band with thickness varying from a few centimetres to a meter (Fig 4.4) were traced and mapped. The quartzites are fine to medium grained, dirty white in color showing reddish brown patches along the joint surfaces due to iron stains. When the rocks are broken, they are generally milky white on fresh surface. Fresh hand specimen appears light grey coloured, hard, compact, and medium to fine grained. The major constituent minerals of the rock are quartz and mica (Fig 4.6).

4.1.2 Thin Section Description

In thin section the quartzites show a mosaic of quartz minerals which are undeformed in nature. The quartz grains are dirty white colour, medium grained and appear grey to dark grey colour in cross nicol (Fig 4.6a). The quartz mineral do not show any preferred orientation that the effects of metamorphism are very limited. The quartz minerals are seen in association with mica which show dark colours in cross nicol. The mineral grains are mostly equi-granular in nature.

4.1.3 Structure

The structural discontinuities were observed on either bank in dam area. The geological discontinuities including foliation, joints, shear zones, etc. were recorded in dam site and its vicinity. The foliation is the dominant geological discontinuity of the area. Its strike varies between N260º and 290º and dips from 28º-45º in northern quadrant. The rocks are also traversed by two major sets of joints (J1 & J2) apart from foliation (FJ). The joints in general have less strike continuity, mostly less than a meter. Hence, the attitude of the dominant structure, namely foliation is an important factor in stability assessment.

Amongst the two major joint sets observed in dam area, the joint J1 is vertical to sub-vertical and nearly perpendicular to the river flow direction showing continuity more than

30m on the valley face. The joint J2 shows opening close to surface at many places and as such vulnerable to rock failure. The joint set FJ and J1 combine to from wedges at places. The details of the joint sets are tabulated in Table 4.1.

Minor shear bands parallel to the foliation plane are seen commonly at many places with wide range of thickness from 2 to 15cm. At places these shears are found associated with chlorite schist and they often have larger strike continuity of more than 30m. The shears remain dry with gauge and crushed angular fragments.

Fig 4.4 Garhwal Group Quartzites with bands of cholrite schist exposed on the left abutment

The foliation, which dips upstream and slightly towards the valley on the left bank, is unfavourably oriented with reference to its general stability. The intersections of observed joint sets lead to formation of rock wedges with some of them being unstable with reference to local slopes. Hence, rock slope stability analysis was carried out in dam area in order to understand the existing status of stability and also the impacts of stability after stripping. The major discontinuities recorded at the dam site were projected on stereonet. The structural details obtained based on stereonet analysis are given in Table 4.1. Three hot water springs at the river bed level, two close to right bank and one close to left bank were also observed on the upstream of dam site.

Fig 4.5 Quartzite Core samples from Dam area showing foilation traces

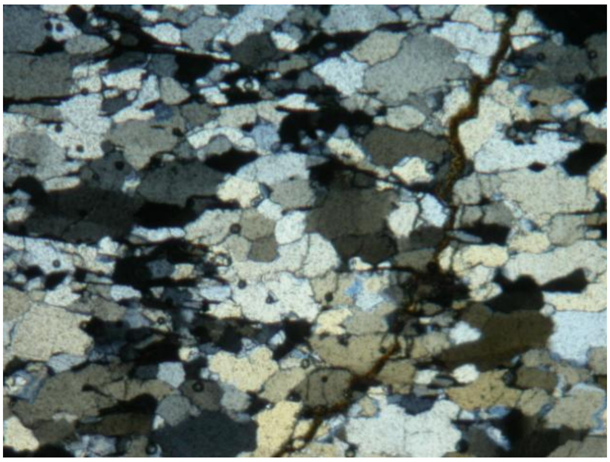

Fig 4.6a Tightly packed angular quartz grains in quartzite. (Mgf. X 20 cross nicol)

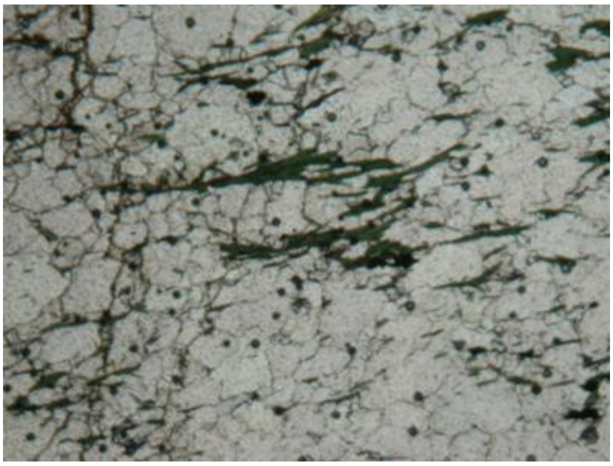

Fig 4.6b Mica defining the foliation in the rock. (Mgf. X 20 PPL)

On the basis of stereographic plotting of geological discontinuities (Fig 4.7), various sets obtained are shown in Table 4.1.

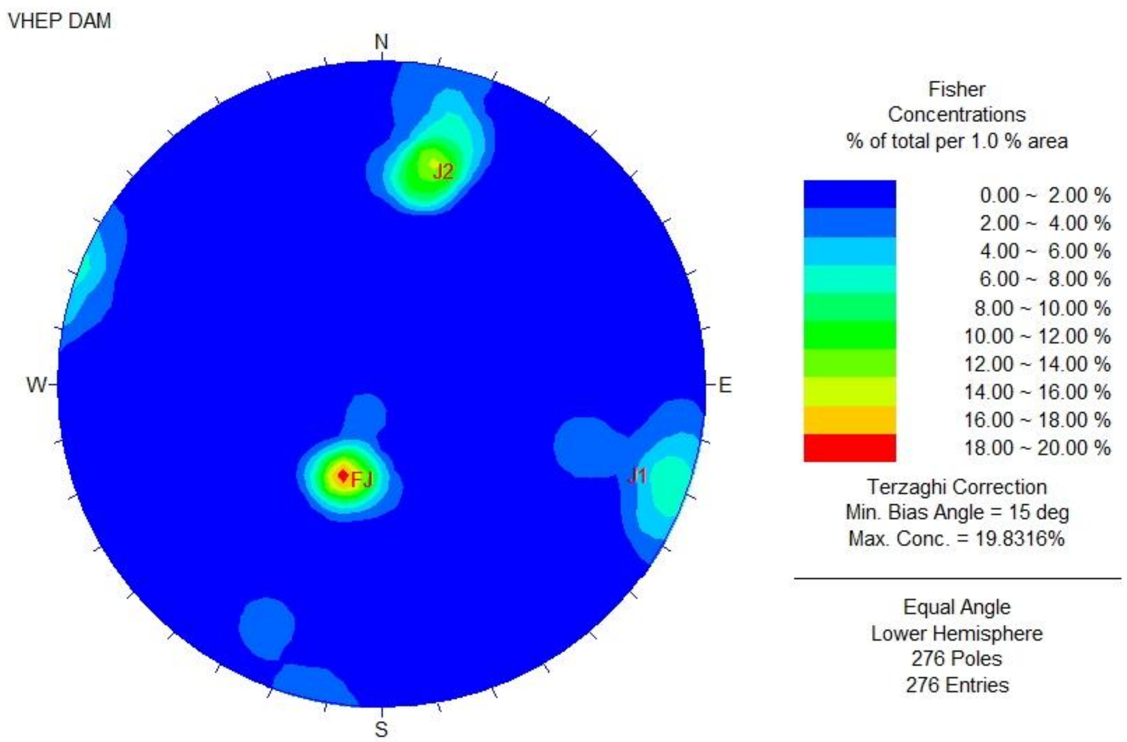

Fig 4.7 Stereonet showing the pole concentration of major discontinuities in dam area (Dips version 5.1)

Table 4.1 Structural discontinuities (Dam site) obtained from field and stereographic analysis.

Planes	Dip amount & Dip direction	Spacing (cm)	Smoothness	Opening	Water Condition
Foliation Joint FJ	34º/N13º (Upstream dipping)	10-15	Smooth planar	Slightly open	Dry
J1	85º/N270º Sub-vertical to vertical	50-80	Rough	Tight	Dry
J2	60º/N200º Parallel to river	30-80	Smooth undulatory	Tight	Dry

4.2 SUBSURFACE INVESTIGATIONS

Foundation refers to the natural surface on which the dam rests and embraces the whole length and width of the superstructure at the general level of fresh rocks. The construction of dam generates pressure on the foundation resulting from the load of the structure as well as the impounded water (Anbalagan, 1986). The safety of the structure depends on the stress deformation properties of the rocks constituting the foundation. Subsurface investigations were carried out in order to evaluate the overall foundation characteristics.

4.2.1 Drill Holes

The subsurface investigation through drill holes provide information on the nature of soil overburden, its depth up to rock contact, rock type and other related informations. Seventeen number of drill holes were drilled and two exploratory drifts were excavated in the dam site. Seven drill holes were drilled along the proposed dam axis in the river bed and on the abutments A detailed summary of drill holes done at dam site is presented in Table 3.2. Based on exploration, it is estimated that the depth of overburden thickness in riverbed is of the order of 20m. The details of drill hole are presented in Table 4.2. The drill core log reveals that quartzite rocks of Gulabkoti Formation (Fig 4.8) with minor shear bands of chlorite schist are present in the dam area. The average RQD ranges from 75-80% indicating good rock (Deere et. al., 1988). The water pressure tests were done in different segments of drill holes along and close to dam axis to evaluate the foundation condition of the dam site (Houlsby, 1976) and results are presented in Table 4.3. The water pressure tests indicate values more than 4 Lu even at a depth of 60m. In view of this, it can be estimated that the depth of grout curtain should extent up to a minimum depth of 1H of dam (65m) at deepest foundation level.

The rock samples for laboratory tests were simultaneously collected and laboratory tests were carried out. The obtained geomechanical properties for quartzite rocks like UCS, tensile strength, elastic modulus, cohesion and friction are presented in Table 4.4. The average UCS values ranges from 74MPa to 88MPa and the tensile strength values for the quartzites ranges between 3.18MPa and 15.08MPa indicating that there intact rock strength range between strong to very strong (Bieniawski, 1979). Rock mass strength parameters following Hoek and Brown (1997) criterion obtained from triaxial tests are tabulated in Table 4.5. These parameters were used as the input parameters for the stability analysis of abutments.

4.2.2 Drifts

In order to explore the rock condition at the dam site, two exploratory drifts, one each on the left and right bank of the Alaknanda at EL ± 1244.32m and EL ± 1246.61m were excavated. These drifts were examined and 3D geological logging done.

The summary of drift DL-01 and DL-02 (Fig 4.9 and 4.10) are given in Table 4.6. The 3D drift logs of exploratory drift DL-01 on the left bank at EL ± 1244.32, (Fig 3.6 & 3.7) indicates a glide crack at a depth of 12m from surface. Its continuity in space has been studied and plotted (Fig 4.12). The slope material up to the glide crack constitutes unsound rock and has to be removed as part of stripping. The stripping limit was identified as 13m for the left bank using glide cracks and weathering of rock mass. As the right bank is free from any glide crack it requires only optimum stripping up to 5m the level of sound rock as per site condition based on weathering of rock mass. In order to strip out up to the identified depth, a slope excavation design is proposed (Fig 4.12) based on the slope optimization (Anbalagan and Singh, 1996). The excavated slope will have a general slope angle of 55 after stripping. During stripping, the excavation of rock slopes using explosives may cause instability, particularly on the left bank along the foliation planes. A carefully controlled blasting with planned blast design will help in minimising the impacts on the surrounding rock slopes, particularly keeping in view the presence of NH-58 just above the dam site.

The rock mass deformability was determined by the project authorities in drifts by plate load and block shear tests and their results are presented in Table 4.4. The test results indicate that the rock mass is sound in general. The RMR (Bienieawski 1984), Q system (Barton et al, 1974) and GSI (Hoek and Brown, 1992) obtained from the site surface and subsurface investigations are described in detail in Chapter 3. The RMR obtained for quartzite was 82 that falls under class I, very good rock. The obtained Q and GSI vales are 6 and 55 indicating fair and good rock respectively. The results are presented in Table 4.4 & 4.5. The data obtained from the surface and subsurface investigations, laboratory and field tests like USC, tensile strength, Poisson’s ratio, cohesion, friction, elastic and deformation modulus were used as input parameter for the stability analysis and calculation of factor of safety for the left and right dam abutments.

Fig 4.8 Quartzite of Gulabkoti Formation Exposed at Dam site

Fig 4.9 Drift–DL-01 on the Left bank at dam site

Fig 4.10 Drift-DL-02 on Right bank at dam site

Fig 4.11Fresh light grey colored quartzite seen in diversion tunnel near dam site

Table 4.2 Summary of Drill Holes at Dam Site

Drill Hole No	Collar Elevation El±(m)	Location	Over Burden Depth (m)	Nature of Over Burden	Total Depth Drilled El±(m)	Nature of Rocks	Remarks
DH-1	1231.85	On left bank 50m u/s of dam axis	7.40m	Pebble, cobble and boulders of quartzite and schist in sandy matrix.	30.20	Dirty white colour, fine grained sericite banded quartzite with thin interbands/ partings of sericite-chlorite schist.	Core recovery in the bed rock varies from 84% to 100% with RQD varying 56% to 100%
DH-2	1230.30	On left bank 50m u/s of dam axis	10.65m	Pebble, cobble and boulders of quartzite, gneiss and schist in sandy matrix.	50.30	Medium to fine grained recrystallized banded quartzite with thin interbands of sericite-chlorite schist along with quartz vein	At 28.50 m (El. 1201.8 m) depth hot water discharge of 25 litres/5 minutes with temperature of 54C has been observed. Core recovery in the bed rock varies from 69% to 100% with RQD varying 70% to 100%.

DH-3	1319.00	50m upstream on the left bank of the river, from the dam axis	12.0	Hill slope debris material compositing of quartzites	30	White to off-white banded, cross bedded, laminated, sericite bearing quartzite	Core recovery in the weathered rock mass (below the debris) is 25% while below it varies from 52% to 100% with RQD varying 11% to 74%.
DH-4	1291.0	50m upstream on the left bank of the river, from the dam axis	1.60	Scree and debris	61.10	Banded, off-white, recrystallized, sericite bearing quartzite with 2-5 cm thick quartz veins	The core shows the splitting along sub-vertical to vertical joints. Core recovery in the bed rock varies from 50% to 100% with RQD varying 10% to 99%.
DH-5	1230.45	Located in the main channel of the river towards the right bank 50m u/s of dam axis	13.20	River borne material composed of coarse sand, grit, gravel, pebble cobble and boulders of quartzite, gneiss and schist	36.80	Fresh, off-white, recrystallized, banded, sericite bearing quartzite with thin interbands of sericite-chlorite schist	Pot holes/cavities at 16.70m, 17.30m, 18.25m-18.80m and 20.20m–20.70m depth were observed. Core recovery in the bed rock varies from 75% to 98.88% with RQD varying 33% to 90%. The presence of hot water from 13.20 m depth under artesian conditions

							with temperature of 49°C while at 25.30 m the temperature of the hot water is 68°C
DH-6	1231.15	Located on the right bank of the river 50m u/s of the dam axis	25.10	River borne material composed of coarse sand, grit, gravel, pebble cobble and boulders of quartzite, gneiss and schist	38.20	Greenish to off-white, sericite bearing quartzite	Core recovery in the bed rock varies from 80% to 100% with RQD varying 9.09% to 98.66%. At 24.30 m depth discharge of hot water under artesian conditions with temperature of 55C has been reported. Further down discharge of hot water increased 5 litres to 20 litres / minute.
DH-7	1229.27	Located in the river channel near the right bank 25 m U/S of dam axis	21.50	River borne material composed of coarse sand, grit, gravel, pebble cobble and boulders of quartzite and schist	51.80	Fine grained greyish white quartzite with a quartz vein	Core recovery in the bed rock varies from 80% to 100% with RQD varying 24.00% to 97.00%. The hot water was recorded from 8.0 m depth under artesian conditions with temperature of 65°C

DH-8	1229.33	Located 30m D/S of dam axis at right bank of river bed	8.0	River borne material composed of coarse sand, grit, gravel, pebble cobble and boulders of quartzite	50.70	Fine grained greyish white quartzite	Core recovery in the bed rock varies from 50% to 100% with RQD varying nil to 92.00%
DH-9	1257.5	Located 105 m U/S of dam axis at the right bank of the river	Nil	Nil	50.40	Fine grained greyish white quartzite	Core recovery in the bed rock varies from 85% to 100% with RQD varying 24.00% to 98.00%.
DH-10	1303.73	Located 50m U/S of the dam axis on the left bank	1.0	Colluvial material	100.25	Fresh, off-white, recrystallized, banded quartzite with thin interbands of sericite-chlorite schist from 59-60 m	Minor shear zones were observed from 17.10-17.20m, 18.90-19.00m, 48.40-48.50m, 49.00-49.15m, 74.60-75.00, 70.80-71.00m, 86.00–86.50m and 87.30–87.60m. Core recovery in the bed rock varies from 80.00% to 100.00% with RQD varying nil to 100.00%

Table 4.3 Frequency distributions of Lugeon values by rock type (after Heuer, 1995)

Rock type	Lugeon numbers					
	0–1	**1–3**	**3–10**	**10-30**	**30–100**	**>100**
Quartzite	0%	15%	84%	1%	0%	0%
Permeability cm/sec	$6x10^{-6}$	$2x10^{-5}$	$6x10^{-5}$	$2x10^{-4}$	$6x10^{-4}$	$2x10^{-3}$

Table 4.4 Details Geomechanical properties and rock mass properties

Rock Type	UCS (MPa)	Tensile (MPa)	Triaxial Results	Poisson's Ratio (ν)	Modulus Ratio	Intact Rock Modulus, E_i (GPa)	RQD	RMR	Q
Quartzite	74	15.08	Mohr-Coulomb: c = 18.39 MPa ϕ = 48.1° Hoek-Brown: m_i = 16.32 σ_{ci}=148.07 MPa	0.24	169.12	12.05±2.8	88.6%	82 Class-I	6 Fair

Table 4.5 Rock mass strength parameters as per Hoek and Brown (1997) criterion obtained from Triaxial tests

Rock Type	Condition	GSI	m_i (MPa)	σ_{ci}	m_j	s_j	a	c_{mass} (MPa)	ϕ_{mass} (°)
Quartzites	Dry	60	16.32	148.07	3.27	0.00674	0.5	7.14	38.2
	Saturated	55	12.72	126.61	2.55	0.00674	0.5	5.85	35.9

Table 4.6 Details of Drift at Dam site

<table>
<tr><th rowspan="2">Drift No</th><th rowspan="2">Elevation El±(M)</th><th rowspan="2">Location</th><th colspan="2">Drift Details</th><th rowspan="2">Dimension</th></tr>
<tr></tr>
<tr><td rowspan="5">DL-1</td><td rowspan="5">EL.1244.32</td><td rowspan="5">Left bank of Alaknanda river near the dam axis (E38°43’56.806”, N75°43’09.811”)</td><td>RD (m)</td><td>Direction</td><td rowspan="5">(2 m x 1.8)
L = 33m
Unsupported</td></tr>
<tr><td>0-7</td><td>N120°</td></tr>
<tr><td>7-12</td><td>N130°</td></tr>
<tr><td>12-19</td><td>N200°</td></tr>
<tr><td>19-33</td><td>N237°</td></tr>
<tr><td>Remarks:</td><td colspan="5">The drift is self-supporting and no plant roots have been recorded.
• Light grey to dark grey colored, fairly fresh, medium to coarse grained, laminated and highly jointed Quartzites with occasional iron stains has been observed.
• The bedding traces/foliations are dipping 25°–40° in N10°W to N10°E in upstream direction.
• Presence of moist zones along shear and some joints. The rest of the reaches are dry.
• Shear up to 10 cm are present in the drift and generally contain weathered rock. In some shears ferruginous clay is present. Joints with 1-2 cm opening have been recorded in early reaches of the drift.</td></tr>
<tr><td colspan="6"></td></tr>
</table>

Upstream Cross Cut in Drift DL-1	1243.70	On left bank the cross cut has been excavated in N25°E direction from RD 33.50 m in main drift	**RD (m)** 0-33.5	**Direction** N25°	(2m x 1.8) L = 15m Unsupported
Remarks:	• Light grey to dark grey colored, fairly fresh, medium to coarse grained, laminated and highly jointed Quartzites with occasional iron stains has been observed. • Shear zone up to 10cm thick are present with 2cm clay gauge at places. Quartz vein 1-3 cm observed randomly.				
Downstream Cross Cut in Drift DL-1	1244.12	On left bank the cross cut has been excavated in N220° direction from RD 33.00 m in main drift	**RD (m)** 33.00	**Direction** N220°	(2m x 1.8) L =15m Unsupported
Remarks:	• Light grey to dark grey colored, fairly fresh, medium to coarse grained, laminated and highly jointed quartzites with occassional iron stains has been observed. • Shear zone up to 10cm thick are present with 2cm clay gauge at places. Quartz vein 1-3 cm observed randomly.				
DL–02 The drift has been excavated in N190° direction. Thereafter two cross cuts have been excavated in N83°E and N260°-265° direction respectively for	1240.38	On the right bank of Alaknada river along near dam axis	**RD (m)** 0-27 m	**Direction** N190°	(2m x 1.8) L =27m Unsupported

2m and 55 m length.					
Remarks:	• Off white, recrystallized, banded, medium to coarse grained (at places fine grained) sericite bearing quartzites. These are dipping 32^o-40^o in $N40^oE$ direction in upstream randomly.				
DL–02 Cross cut in to hill	1240.38	On the right bank of Alaknanda river along near dam axis	**RD (m)**	**Direction**	(2m x 1.8)
			0-2 m	$N83^o$	L = m
			0-55 m	$N260^o$	Unsupported
Remarks:	• Light grey to dark grey colored, fairly fresh, medium to coarse grained, laminated and highly jointed Quartzites with occasional iron stains has been observed. • Shear zone up to 10cm thick are present with 2cm clay gauge at places. Quartz vein 1-3 cm observed randomly.				

Table 4.7 Estimation of RMR (Bineiawski, 1984)

Parameters	Quartzite
UCS (MPa)	108
Rating	12
RQD	78
Rating	20
Spacing of Discontinuities(m)	0.2-0.6
Rating	10
Condition of discontinuities	Very rough and unweathered, wall rock tight and discontinuous, no separation
Rating	30
Ground water condition	Dry
Rating	15
RMR_{basic}	82
Class	I
Description	Very good rock

Table 4.8 Results of in situ tests on deformability and shear strength

Plate load tests			**Average results for 80 tonne load on 60cm plate**		
Location	**Rock type**	**Orientation**	**Modulus of deformation (GPa)**	**Modulus of elasticity (GPa)**	
Left bank drift	Quartzite	Vertical	2.7	3.9	Left bank drift
Right bank drift	Quartzite	Horizontal	1.2	5.1	Right bank drift
Right bank drift	Quartzite	Vertical	10.2	13.7	Right bank drift
In-situ shear tests		**In-situ shear strength**			
		Peak		**Residual**	

		Cohesion (c) kPa	Friction (φ°)	Cohesion (c) kPa	Friction (φ°)
Left bank drift	Concrete/rock	775	55°	470	50°
Right bank drift	Concrete/rock	295	59°	215	57°

4.2.3 Geological Cross Sections

Geological cross sections on 1:1000 scale were prepared, one along the dam axis (Fig 4.12) and two more at 100m upstream and 100m downstream of the dam axis (Fig 4.13 & 4.14). The structural details obtained from stereonet analysis were used for the preparation of geological cross sections taking into consideration the apparent dip of these discontinuities (Figs 4.13 & 4.14). The geological section along the dam axis (Fig 4.12) illustrates a 'V' shaped valley section with slope angles 60° dipping towards N295° on left bank and 65° dipping towards N115° on right bank. The major geological discontinuity foliation dips 28° to 35° with slight variation in direction between N355° and N015° in upstream direction.

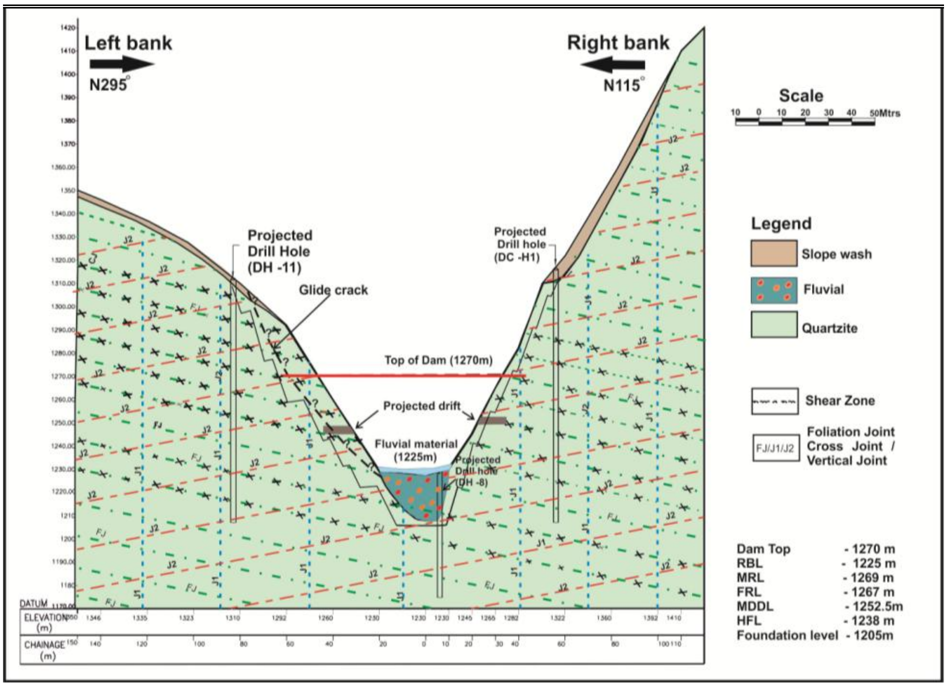

Fig 4.12 Geological cross section across dam axis

Two major joint sets in addition to foliation joint FJ are present. One joint (J1) is very steep with a dip of 78°-85° dipping between N265 and N275°. Another joint J2 has a dip 55°-

60° dipping between N195° and N205°. Minor shear bands inferred from the drill core logs are projected parallel to foliation plane. The identified stripping limits of 13m on the left bank and 6m for the right bank were transferred to geological cross and a slope excavation design is proposed (Fig 4.12). Accordingly, slope stability analysis was carried out for natural slope conditions as well as stability of slopes after stripping excavations

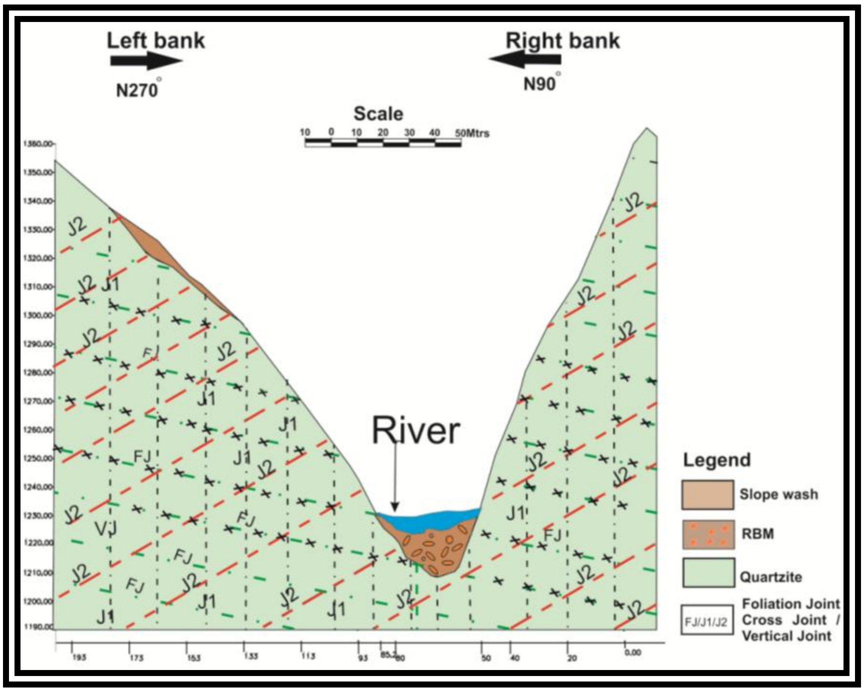

Fig 4.13 Geological section 100m d/s of Dam axis

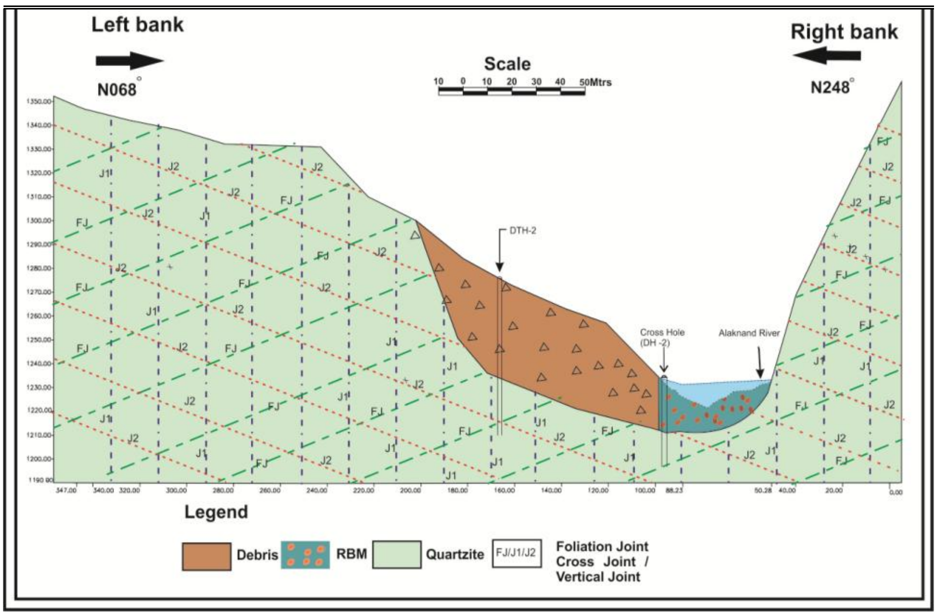

Fig 4.14 Geological cross section 100m Up/s of dam axis

4.3 SLOPE STABILITY ANALYSIS OF ABUTMENTS

In view of narrow gorge, the construction of dam may entail a huge excavation in order to accommodate spillway within the dam body. Recognition of potential slope instability in the initial stage of project planning is of great value in order to design the structure. The extent of stripping limit and the rock type are the two important factors involved in the excavation of cut slopes for stripping out the weathered rock mass to lay the foundation of the dam (Anbalagan, 1986). The stability behaviour of rock masses is controlled by the nature and disposition of structural discontinuities like bedding planes and joints. Hence, it was essential to carry out stability analysis in order to work out its impact on the rock slope stability. Simple kinematic analysis, a graphical technique using the plot of the poles on a stereonet was used to assess the pattern of slope failures.

Kinematic analysis of rock Slope:

Stereographic projection of structural data with respect to local slope provides interactive information and the possible mode of failure. The data on structural discontinuities recorded from the field, such as nature of discontinuity, orientation, spacing, continuity, roughness and filling material in addition to joint shear strength parameters following Barton et al, 1982 model were used as input parameters. The concentration of poles was delineated by contoured plots (Fig 4.7).

The representative values for foliation joint FJ and joints J1 and J2 obtained from contoured plots are given in Table 4.9:

Table 4.9 Attitude of foliation and joints of the Dam site obtained from contour plot

Discontinuities	***Strike***	***Dip***	***Dip direction***
FJ (Foliation)	N103°	34°	N013°
J2 (Joint)	N180°	85°	N270°
J3 (Joint)	N290°	60°	N200°

Inclination of Slope–Left bank 60°/N295°; Right Bank 65°/N115°.

The structural discontinuities such as bedding, foliation, joints and shears play a significant role in determination of stability of rock slopes. The nature of discontinuity characters like orientation with respect to slope, dip amount, spacing, persistence, roughness, opening, water condition and filling materials influence the stability condition of rock slopes.

In view of presenting a comparative study on topple, planar and wedge failure the kinematic analysis were carried out for all three mode of failure for both the banks of the dam area. The relation between the joints and the slope was studied in detail through kinematic analysis. In the kinematic analysis the attitude of the joints as compared to the inclination of the slope was studied to understand and identify the unstable planes and wedges on both the banks.

<u>Stability Analysis for Planar failure:</u>

The kinematic analysis has been done separately for left bank (Fig 4.15) and right bank (Fig 4.16). For the left bank, the stereoplot shows three sets of joints in addition to the slope. Since the attitude of the foliation shows that it dips in the direction of the slope at an angle less than that of the slope inclination, this indicates that the attitude of foliation provides a favourable condition for slope instability. In this context, the joint J1, which dips steeply at 85°/N270°, acts as a release joint to facilitate the plane failure along the foliation. For this purpose, the software Dips version 5.1.3 (Rocscience) was used.

The plane failure analysis in Dips version 5.1.3 (Rocscience) uses variability cone, frictional cone, and a Daylight Envelope, to test for combined frictional and kinematic possibility of planar sliding. The daylight envelope essentially represents all planes, which may get theoretically daylighted on a given slope. The kinematic analysis for planar slide for left bank (Fig 4.15) indicates that there is no overlap of FJ joint in the planar sliding region represented by crescent shaped zone formed by the friction cone and the day light envelope. The kinematic analysis for the left bank reveals that there is a low possibility of planar sliding hazard.

On the right bank, the foliation joint FJ dip favorably with respect to the slope direction that is it does not dip in the same direction as that of the slope to cause plane failure (Fig. 4.16). Similarly, in the plane failure analysis using Dips software, the poles of FJ do not fall within the shaded area friction cone and the day light envelope indicating the right bank is free from planar failure.

The J2 joint on the left bank dips at a steeper angle inside the hill without any free end face that tend to slide. The kinematic analysis results shows that the window set obtained for the pole concentration does not overlap with the friction cone and the daylight envelope. On the right bank the joint J2 though it appears to be vulnerable in geological section, in kinematic analysis the set window of J2 does not has any influence with the friction cone/ day light envelope as J2 dips away from the slope direction forming it a stable plane.

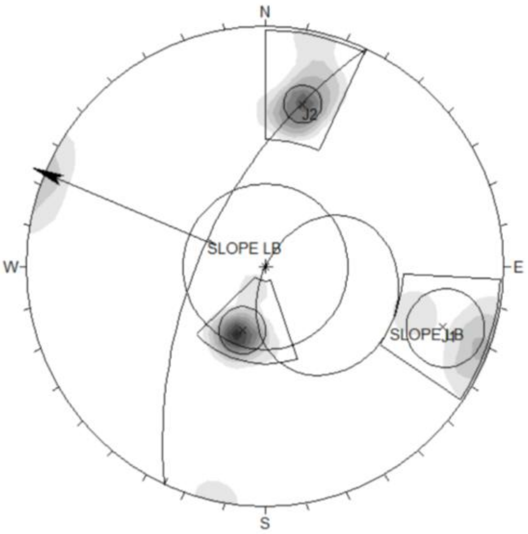	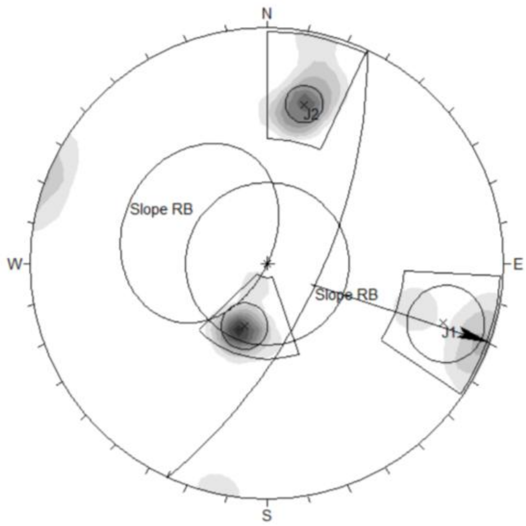
Fig 4.15 Planar analysis for left bank showing with friction cone and day light envelope	**Fig 4.16 Planar analysis for right bank showing with friction cone and day light envelope**

The planar analysis for both the bank slope indicates that the structural discontinuities except for the foliation on the left bank, dip favorably with respect to the slope direction that is they do not dip in the same direction as that of the slope for planar failure. Hence it can be concluded as follows:

i) There is a low possibility of plane failure on the left bank.
ii) For other geological discontinuities, both the left and the right bank slopes are stable under natural condition. After stripping as the general slope gets flattened the stability has not been adversely affected in case of plane failure.

Stability Analysis for Wedge failure:

In the kinematic analysis for wedge failure, the friction angle was taken from the equator of the stereonet as this provides the actual sliding surface. The intersections of the geological discontinuities observed in the area result in number of wedges namely FJ–J1 wedge, FJ-J2 wedge and J1-J2 wedge.

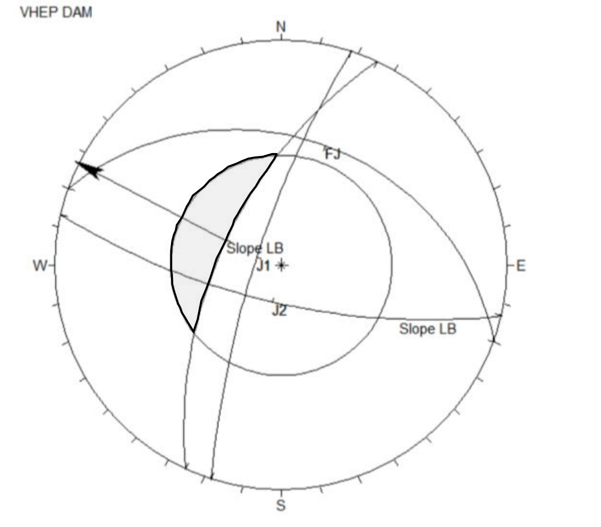	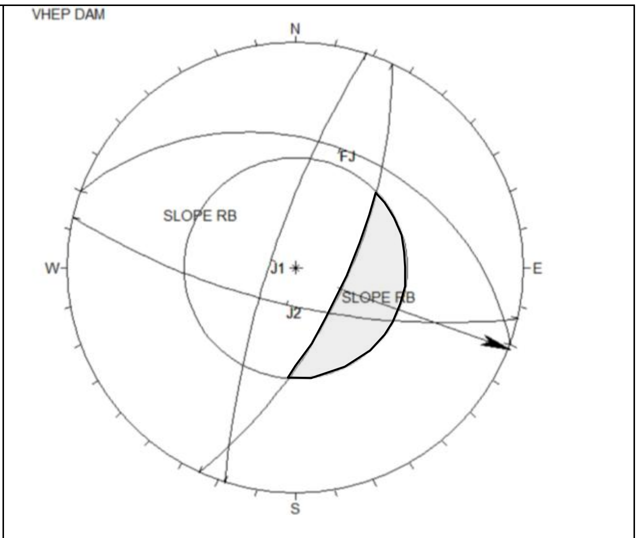
Fig 4.17 Analysis for Wedge for left bank	**Fig 4.18 Analysis for Wedge for right bank**

The wedges formed by FJ and J1 intersects at the northern quadrants falls away from the crescent shaped vulnerable region formed by the friction cone and slope on both the banks, thus making it a stable wedges. The combination of FJ with J2 intersects at the south eastern quadrant falling much away from the potential zone of failure, forming stable wedges on both the banks. Similarly the wedges formed by the intersection of J1 and J2 joints falls on the south-western quadrant within the friction cone but not within the crescent shaped shaded area potential for wedge failure. Thus making the wedges formed by J1 and J2 stable on both the banks (Fig. 4.17 & 4.18).

The wedge analysis for both the banks indicates that the directions of line intersections of the wedges formed by J1 and J2 are aligned reasonably away from the slope directions. And as such the intersection points of the wedges do not fall within the shaded area between the slope and the friction cone (Fig. 4.17 and Fig 4.18). Hence, it can be concluded that the slopes of both the banks are stable under natural condition. After stripping as the general slope gets flattened while the direction remains the same and hence, the stability has not been adversely affected.

Stability Analysis for Toppling failure:

The kinematic analysis for toppling failure was carried out using Dips software. It follows the method as indicated by Goodman, 1980, which is based on i) Variability cones indicating the extent of the joint set population. ii) Slip limit based on the joint friction angle and slope angle and iii) Kinematic considerations. The topple analysis were carried out for joint J1 only as it dips at very steep angles (85°).

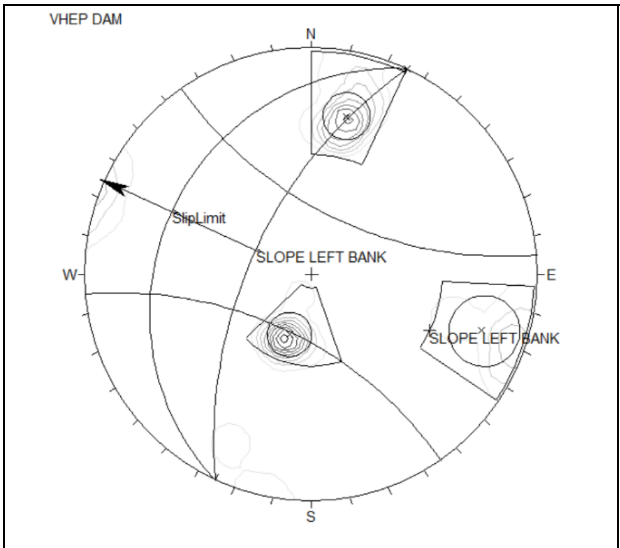

Fig 4.19 Topple Analysis result for left Bank

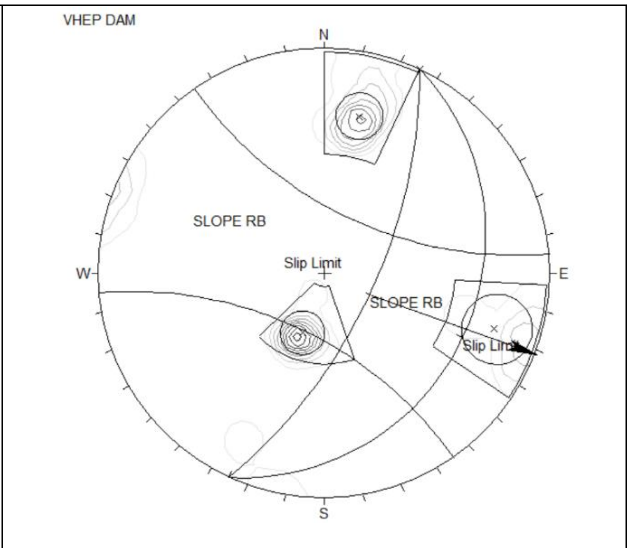

Fig 4.20 Topple Analysis result for right Bank

The analysis was done for the left bank considering the presence of basal plane FJ and steeply dipping joint J1. For the right bank the basal plane, which may aid in toppling failure is J2.

The result for topple failure indicates that the pole concentration of J1 on the left bank defined by the variability cone boundary has 15% toppling hazard (Fig 4.19) and 10-15% toppling hazard on the right bank (Fig 4.20). These concentrations are considerably low to effect toppling failure.

Considering the kinematic analysis done for both the banks the following can be concluded.

i) The left bank has the potentiality of causing low probability of plane failure along foliations. In view of this, detailed plane failure stability analysis was carried out for the left bank using the program SASP.

ii) The left bank has no potentiality for wedge and toppling failures.

iii) The right bank has no potentiality for plane wedge and toppling failures.

ROCK SLOPES STABILITY ANALYSIS USING SOFTWARE "SASP"

The SASP software (STABILITY ANALYSIS OF ROCK SLOPE WITH PLANAR SLIDE) (Sing and Goel, 2002) is based on Barton and Bandis (1990) theory of shear strength of joints and Hoek and Bray (1981). The program has a salient feature for estimation of dynamic settlement (from pseudo-static analysis) of rock/ soil slopes which depends strongly upon the earthquake magnitude on Richter's scale. The program is designed to automatically identify the critical failure surface both in soil and rock slopes.

The input variables for SASP program are mentioned below.

ZW	=	Depth of Water In Tension Crack
Z_C	=	Depth of Tension Crack (If 0, Program will calculate it)
FAL	=	Fixed Anchor Length
P	=	Safe Anchor Capacity
THETA	=	Angle of Anchor with respect to Normal of Joint Plane
T	=	Normal Force
H	=	Height of Slope
SIF	=	Slope Angle
SIP	=	Dip of Joint Plane
GAMA	=	Unit Weight of Rock Mass
GAMA W	=	Unit Weight of Water
C	=	Cohesion
Φ	=	Residual Sliding Angle of Friction
$\bar{B}$	=	Bishop's pore pressure parameter
α_h	=	Horizontal seismic coefficient
α_v	=	Vertical seismic coefficient

In the theory of shear strength of joints (Barton and Bandis, 1990) it is assumed that joints having $\Phi_j \leq 45°$ are weathered in nature. In Hoek and Bray (1981) theory, the drawback is that the depth of tension crack (Zc) is predicted to be equal to the height of slope (H) where the slope angle is vertical whereas in nature it is observed that Zc < 2H/3. The above mentioned checks are considered in SASP.

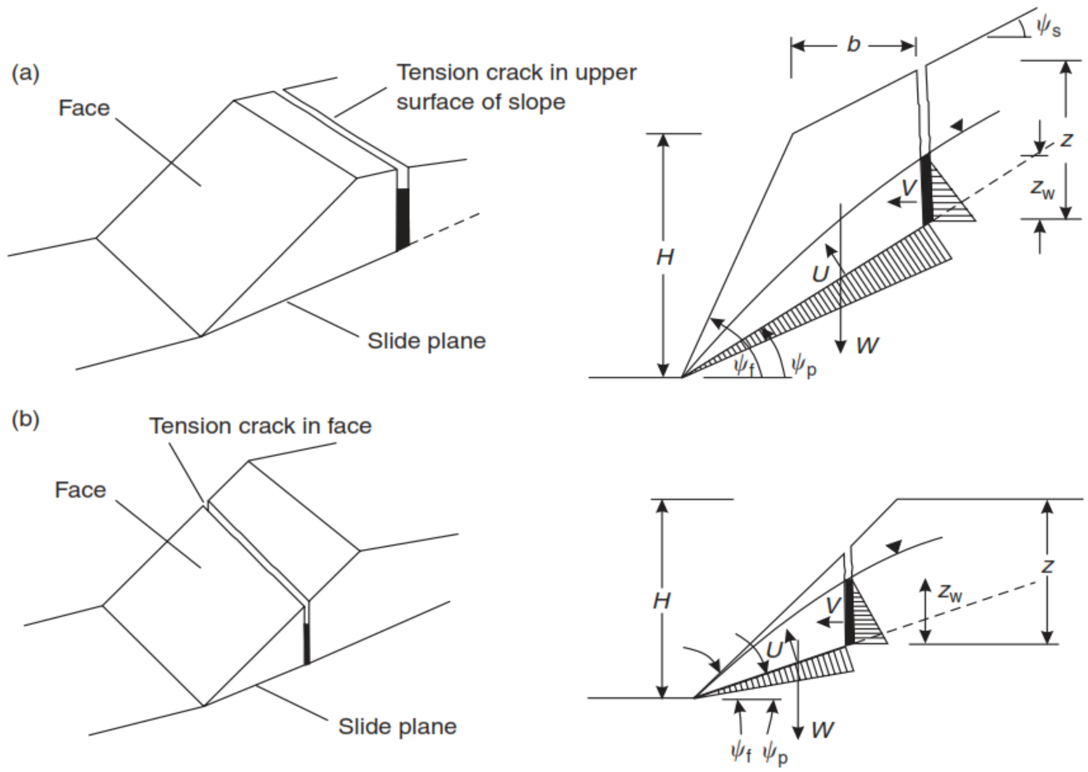

Fig 4.21 Geometric plane Geometries of plane slope failure: (a) tension crack in the upper slope; (b) tension crack in the face. (Hoek and Bray 1981)

The detailed stability analysis of each rock slope for four different slope conditions were carried out using SASP software program form the mechanics point of view. The two different slope conditions are:

i) Dry slope, static analysis

ii) Dry slope, seismic analysis

The expressions of factor of safety are mentioned by the Equations (4.1 & 4.3) for the above mentioned slope conditions respectively. These expressions were derived with respect to the Fig 4.21 (Hoek and Bray 1981)

Dry Static condition

$$FOS = (C.A + W \cos \psi_P \,.\, \tan \Phi) / W \sin \psi_P \qquad \text{[Eq 4.1]}$$

Dry Seismic condition

$$FOS = \frac{W \cos(\psi_P + \Theta) \tan \Phi - \{U_1 (\sin \psi_P + U_2) \tan \Phi - C\} / k}{W \sin(\psi_P + \Theta) + (U_1 \cos \psi_P) / k} \qquad \text{[Eq 4.2]}$$

Where, $k = \sqrt{\{A_H{}^2 + (1 + Av)^2\}}$ Seismic condition

Based on the above mentioned method the analysis was carried out for the left and right bank and their results are as follows

Case 1 Dry Static condition

```
STABILITY ANALYSIS OF ROCK SLOPE WITH PLANAR FAILURE LEFT BANK

*************************************************************
           UNITS USED           -> TONNE - METER - DEGREE
           INPUT FILE NAME      ->isasp.pip
           OUTPUT FILE NAME     ->osasp.pip

*************************************************************
                              CASE NO.    1

*************************************************************

           COHESION                                =   40.0000
           RESIDUAL ANGLE OF FRICTION              =   45.0000
           JOINT ROUGHNESS COEFFICIENT             =   10.0000
           JOINT WALL COMP. STRENGTH               = 2900.0000

           HEIGHT                                  =   65.0000
           DIP OF JOINT PLANE                      =   35.0000
           DEPTH OF WATER IN TENSION CRACK         =   23.6719
           COEFF. OF HORIZONTAL ACCELERATION       =     .1000
           FOR EARTHQUAKE MAGNITUDE(RICHTER SCALE)=    7.0000
           UNIT WEIGHT OF ROCK                     =    2.5000
           UNIT WEIGHT OF WATER                    =    1.0000
           DEPTH OF TENSION CRACK                  =   23.6719
           SLOPE ANGLE                             =   60.0000

*************************************************************
           STATIC FACTOR OF SAFETY                 =    2.1182
           DYNAMIC FACTOR OF SAFETY                =    1.7981
           DYNAMIC SETTLEMENT IN METER             =     .0000
           CRITICAL ACCELERATION                   =     .8026
           FACTOR OF SAFETY - DRAINED SLOPE        =    2.8667
           DYNAMIC FACTOR OF SAFETY-DRAINED SLOPE  =    2.4210
           SLIDING ANGLE OF FRICTION               =   45.0000

*************************************************************
```

Case 2. Dry Seismic condition

```
************************************************************
STABILITY ANALYSIS OF ROCK SLOPE WITH PLANAR FAILURE- LEFT
     BANK-AFTER STRIPING


************************************************************
           UNITS USED           -> TONNE - METER - DEGREE
           INPUT FILE NAME      ->isasp.pi1
           OUTPUT FILE NAME     ->osasp.pi1

************************************************************
                              CASE NO.    1

************************************************************

           COHESION                                =   40.0000
           RESIDUAL ANGLE OF FRICTION              =   45.0000
           JOINT ROUGHNESS COEFFICIENT             =   10.0000
           JOINT WALL COMP. STRENGTH               = 2900.0000

           HEIGHT                                  =   65.0000
           DIP OF JOINT PLANE                      =   35.0000
           DEPTH OF WATER IN TENSION CRACK         =     .0000
           COEFF. OF HORIZONTAL ACCELERATION       =     .1000
           FOR EARTHQUAKE MAGNITUDE(RICHTER SCALE)=    7.0000
           UNIT WEIGHT OF ROCK                     =    2.5000
           UNIT WEIGHT OF WATER                    =    1.0000
           DEPTH OF TENSION CRACK                  =   19.4865
           SLOPE ANGLE                             =   55.0000


************************************************************
           STATIC FACTOR OF SAFETY                 =    3.1757
           DYNAMIC FACTOR OF SAFETY                =    2.6913
           DYNAMIC SETTLEMENT IN METER             =     .0000
           CRITICAL ACCELERATION                   =    1.4534
           FACTOR OF SAFETY - DRAINED SLOPE        =    3.1757
           DYNAMIC FACTOR OF SAFETY-DRAINED SLOPE =    2.6913
           SLIDING ANGLE OF FRICTION               =   45.0000

************************************************************
```

4.4 DISCUSSION

The rock slopes stability analysis for planar failure on the left bank indicates that the natural slope of height 65m with slope angle 60º is stable under static condition with the factor of safety (FOS) 2.11 and under dynamic factor of safety (FOS) 1.7.

The rock slope analysis for modified slope with a slope angle 55º after stripping was also done. This indicates that the FOS has doubled due to suitable optimization of slope angle. The obtained FOS for slope is 3.17 under static condition and 2.69 under dynamic condition.

From the slope stability analysis carried out for left bank it can be concluded that the natural slope remains under stable with FOS 1.7 to 2.7. And after adopting the proposed slope design the rock slope shows increased in FOS from 1.7 and 2.7 to 2.69 and 3.17.

CHAPTER V

GEOTECHNICAL EVALUATION OF POWER TUNNEL

Tunnels play a key role in water resource management projects. In recent years, a large number of power tunnels were constructed, some are under progress and many are proposed to harness the energy potential of the rivers flowing from Himalaya (Goel et al., 1995). Sound knowledge on geology of the area, topography and nature of rock mass conditions are some of the important parameters that help in the selection of tunnel alignment and design a support system. Tunnelling in Himalaya, a tectonically disturbed and active terrain with varying rock formations and competencies traversed by adverse geological features may lead to unstable conditions during excavations. These problems to a large extent can be tackled during tunnelling with the help of detailed geological mapping (Jayabalan et al, 2015). Water seepage problems, squeezing, cavity formation, swelling, thermal springs and methane gas are the general adverse problems associated with tunnelling (Lakshmanan et al, 2015). The evaluation of intact rocks and rock mass properties along the tunnel section are essential, in addition to estimation of the joint shear strength parameters (Barton & Bandis 1990). The rock mass characters and the weak zones in them such as shears and highly fractured rocks are mainly responsible for unstable condition during tunnelling (Anbalagan et al, 2013).

In the present work, the geotechnical evaluation of the power tunnel (PT) includes the following work components.

a. Preparation of Geological map along PT on 1:15,000 Scale
b. Preparation of a geological cross section along PT
c. Characterization of Rock Mass using RQD, RMR, Q & GSI
d. Evaluation of stability in different segments of PT & support requirements

5.1 VISHNUGAD-PIPALKOTI POWER TUNNEL (PT)

A 13.4km long and 8.8m diameter horse shoe shaped power tunnel (PT) off-taking from inlet portal through desilting chamber up to surge shaft is proposed through a rough and steep rugged terrain on the right bank of Alaknanda river. These hills have moderate to very steep slopes, which are characterised by different types of rocks and debris and slope wash materials seen on surface at many places. The PT alignment crosses many perennial streams such as Tapon, Dwing, Tiroshi, Hyuna, Maina Nadi and Ghanpani.

The tunnel section extending between A (intake) to F (surge shaft) has five segments (1 to 5) with four kinks (B, C, D & E) (Fig. 5.1). The tunnel is aligned in a general southwesterly direction from A to B. Later it takes a mild turn (25º) towards WSW up to C, where it crosses Maina river for a short distance in SSW direction up to D. Further ahead, it swerves in a general direction towards south up to F. The maximum rock cover above the tunnel is of the order of 825m and the minimum rock cover is encounter in Maina river area (20m) (Fig. 5.3) has been estimated from drilling data given in Table 5.1. The Power Tunnel layout has been made in such a way that the rock cover is kept below 500m as far as possible. But in small stretches it exceeds 500m. The minimum rock cover is of 20m at Maina river crossing in addition to the fluvial material (10m) above. Utmost care has been taken to suitably locate the tunnel crossing points in the Maina river section keeping in view the topography and the geology of the area.

The proposed layout of Power Tunnel has a provision four adits to facilitate tunnel construction. Adit-01 is located adjoining the desilting chambers, the Adit-02 is located just below the Dwing village, just opposite of Patal Ganga confluence, Adit-03 is located on the right bank of Maina river and Adit-04 will be the approach to bottom of surge shaft located at surge shaft area.

Table 5.1 Structural details observed in Quartzite

Sl. No.	**Dip/Dip Direction**	**Spacing (cm)**
FJ	28°-35°/N355°–N010°	30-50
J1	55°-60°/N190-205°	50-100
J2	75°-85°/N265°-275°	80-100
Structural details observed in Dolomitic limestone		
FJ	25°-20°/N010°-N020°	10-30
J1	50°-58°/N190°-N180°	20-50
Structural details observed in Slates		
FJ	28°-32°/N025°-N030°	30-50
J1	50°-58°/N190°-N180°	20-50
J2	75°-85°/N265°-275°	80-100

5.2 GEOLOGICAL MAPPING

The geological mapping was carried out between Intake and powerhouse (PH) area on 1:15,000 scale (Fig. 5.2). For that purpose a number of traverse were taken in the area to cover mapping in different segments. In general, rock exposures are present along the tunnel alignment debris pockets at places.

Three numbers of intake tunnels 6m modified horse shoe are proposed on the right bank of the river Alaknanda. They are located in hard and massive quartzites of Garhwal Group with thin bands of chlorite schist varying from a few centimetre to a meter. From the surface mapping, drill hole and drifting it is anticipated that the rock to be encountered in the desilting chamber shall be greyish, white, banded, and medium to coarse grained quartzites dipping at 32^o-40^o in N30^oE direction i.e upstream. The exploratory drill holes DCH-01 and 02, has been proved overburden up to 9.0 m. Thermal springs has been recorded in the dam site area may be have its influence in this area also.

Quartzites with intercalated shear and schist of Golabkoti Formation are encounter in the initial reaches. Further south, Pipalkoti Formation consisting of alternate bands of slates intercalated with phyllites, dolomitic limestone, bands of talc quartzite and magnesite are present for quite some distance up to Belakuchi village. Further south slates intercalated with phyllites of Pipalkoti Formation are present up to Maina river. Further south of Maina river, thick bands of slates and dolomitic limestones are seen alternately with slates being dominantly seen close to Maina river and dolomitic limestones seen dominantly close to surge shaft area.

Maina River is present almost in the middle of the tunnel alignment. It follows towards N 100 directions. It is nearly a straight river course possibly indicating some structural control. The Maina River falls in the segment 3(Fig 5.1). The Maina River flows along a tight narrow gorge with fluvial and colluvial materials occupying the floor of the river. Since the river course is nearly straight with tight valley slopes, it possibly follow a major shear zone in this reach. The explorations using drill holes indicate that the rock cover above the tunnel is about 20m, which is inadequate considering the size of the tunnel (8.8m dia). Since 3D rock cover is essentially required for a stable tunnel conditions, the stability of the tunnel during excavation is a major problem. The entire stretch should be excavated using forepolling methods, by which the roof will be supported while carrying out the excavation. In view of extensively sheared rocks with inadequate rock cover, the tunnel shall be supported with continuous steel ribs placed at close spacing as required at the site.

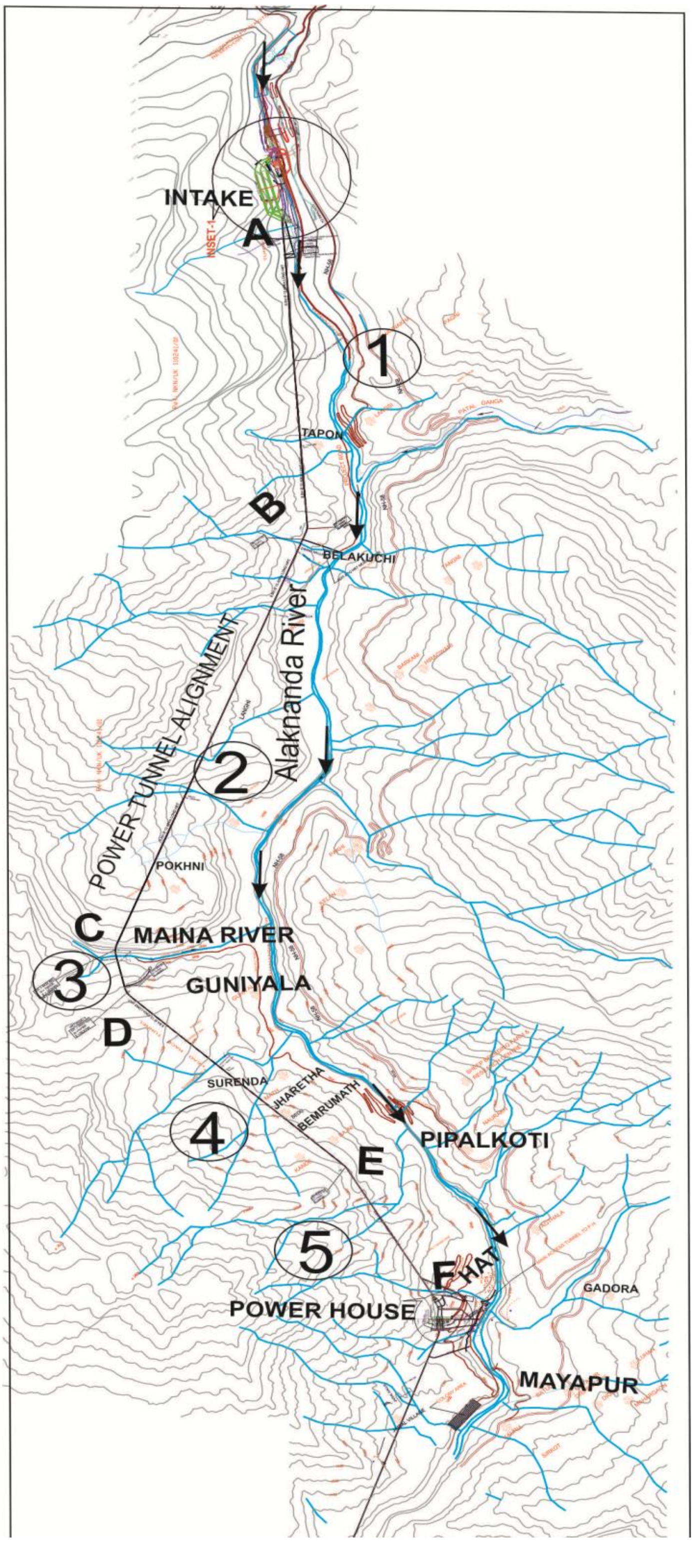

Fig 5.1 Layout map of the Vishnugad–Pipalkoti HEP showing the power tunnel alignment along the right bank of Alaknanda river

Structurally the quartzite of Golabkoti Formation is massive with least development of foliations and well developed joints. In addition to foliation (FJ), two sets of joints were observed at the site. Further south, the structural details were noted for different lithologies present in Table 5.1. It is expected that during the tunnelling two shear zones namely Maina Nadi and Bamru are expected to be encountered along the tunnel alignment. The details observed and recorded from drill holes PT-1,2 & 3 are given in Table 5.2 and 5.3

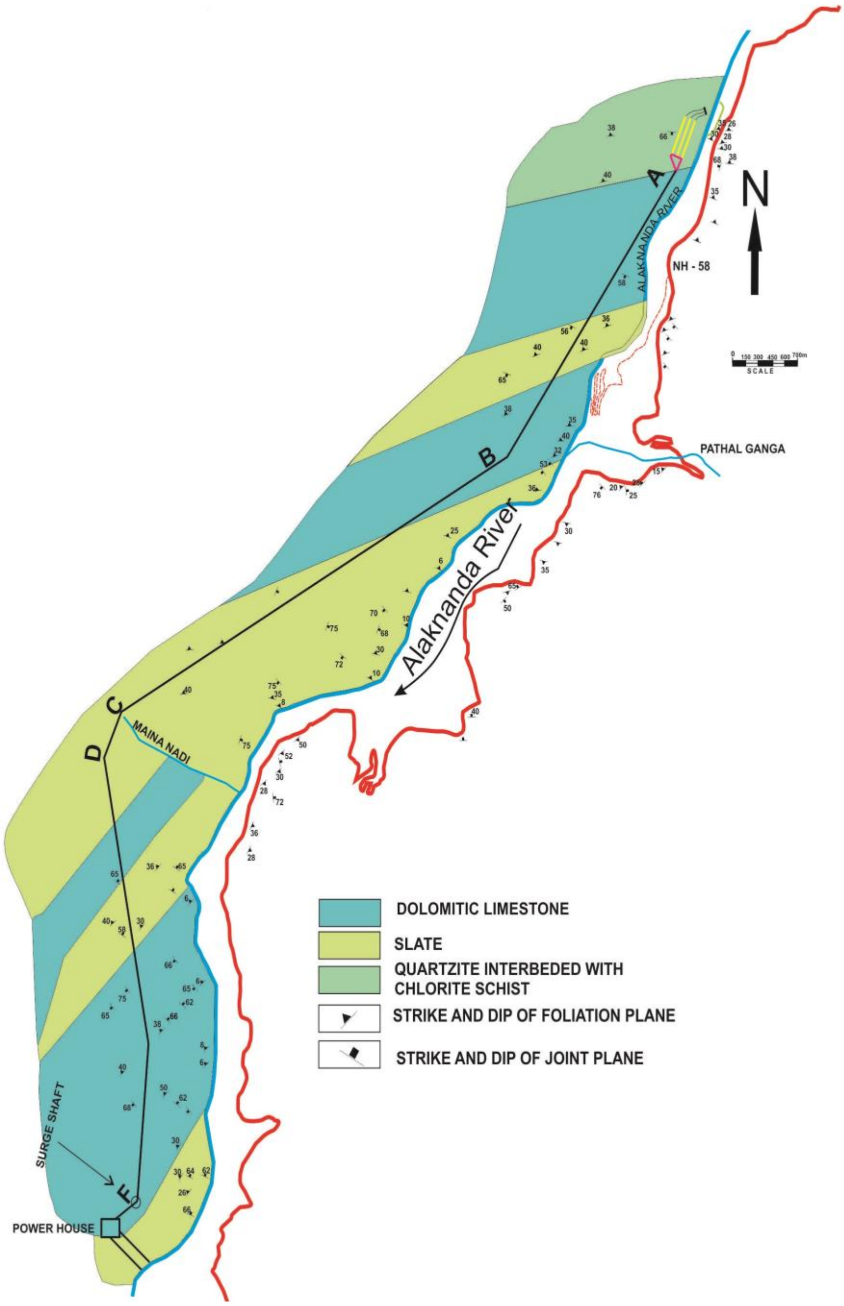

Fig 5.2 Geological map along power tunnel (PT) alignment passing through various litho units.

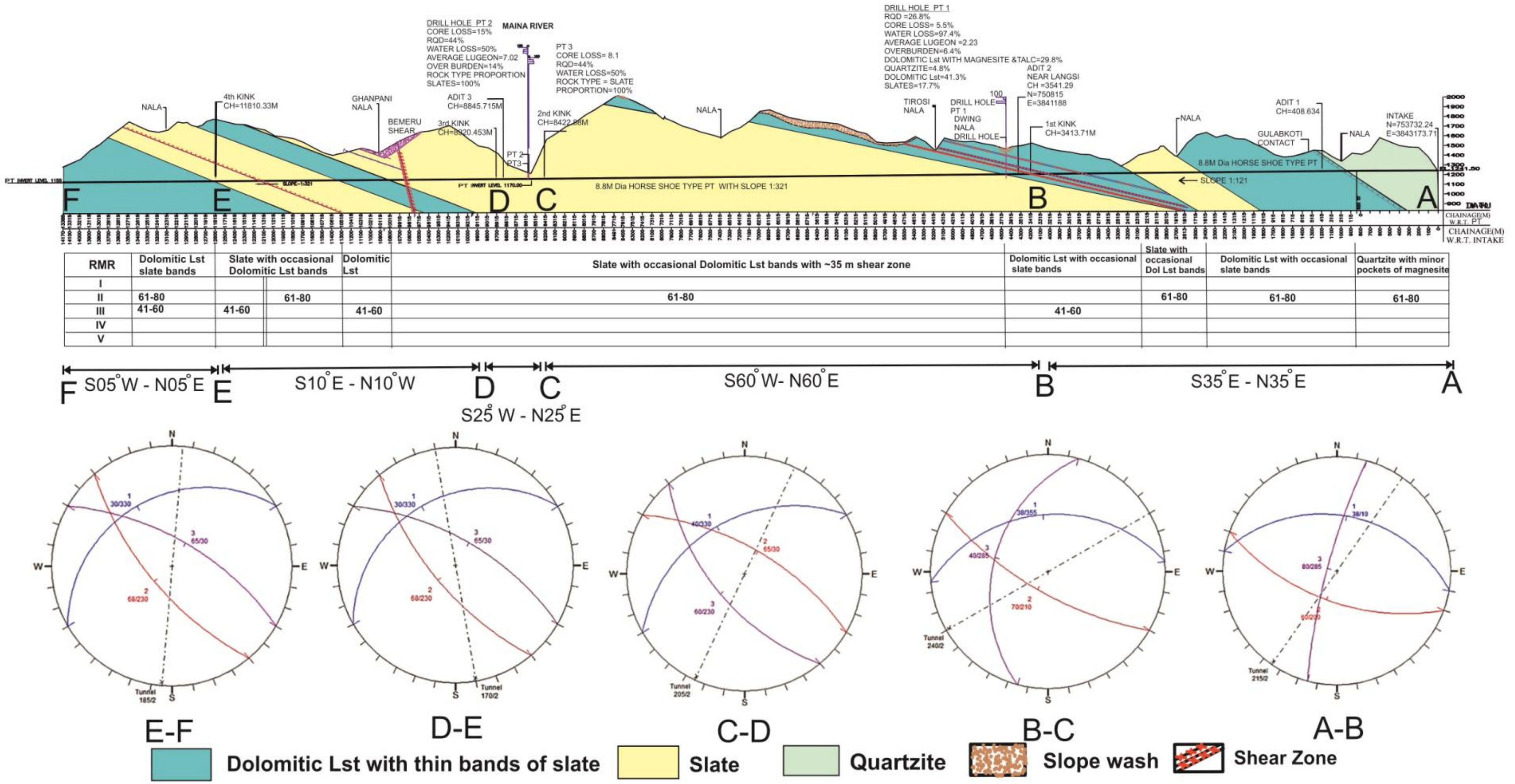

Fig 5.3 Geological cross-section along the Power Tunnel alignment with stereonet kinematic analysis with respect to tunnel orientation and structural discontinuities

Table 5.2 Summary of Drill Holes at Dwing Pt Crossing Point

Drill Hole No	**Collar Elevation El±(m)**	**Location**	**Over Burden Depth (m)**	**Nature of Over Burden**	**Total Depth Drilled El±(m)**	**Nature of Rocks**	**Remarks**
PT 1	1501m	Centre of Dwing nala	18.50	The overburden consist of river borne and colluvial material containing gravels pebbles and boulders of gneiss, schist, shale/ slate and dolomitic limestone.	285.05	Medium grained greyish white quartzite with a biotite chlorite schist band between 18.50-22.50 m. Further below up to 28.6m talc. From 28.6 m to 71.5 (EL.1429.55 m) the quartzite with minor bands of talc and dolomitic limestone has been met.	Thin shear zone have been recorded from 49.50-49.70 m, 57.47-57.65 m, 78.50-78.70 and 91.70-92.40. The percentage core recovery ranges from 80 to 100 percent while the RQD varies from 10 to 100% percent.

Table 5.3 Summary of Drill Holes at Maina Pt Crossing Point

Drill Hole No	Collar Elevation El±(m)	Location	Over Burden Depth (m)	Nature of Over Burden	Total Depth Drilled El±(m)	Nature of Rocks	Remarks
PT 2 & 3	1240.01m & 1238.94m	In Maina river PT crossing area	7.0 & 9.5	The overburden consist of river borne material containing sand, grit, gravels pebbles and boulders of gneiss, schist, shale/ slate and dolomitic limestone.	50 & 56	Rocks of thinly foliated, greyish black shale/slate with interbands of dolomitic limestone has been met up to a depth of 12.18 m, below this level splintery, grayish black shale/slate has been met upto drilled depth of 56.00m.	General dip of bedding / foliation varies from 45-80 due to folding. The percentage core recovery varies from 80% to 100% while the RQD percentage varies from 10 to 84%.

5.3 CHARACTERIZATION OF ROCK MASS USING RQD, RMR, Q AND GSI

The necessary parameters required for rock mass characterization obtained from field and laboratory tests are discussed in Chapter 3. The obtained results are presented in Table 5.4 to 5.8 for reference. The shear strength parameters required for further analysis were obtained from these tables.

Table 5.4 Rock Quality Designation (RQD) values obtained for different rock types.

Rock type	RQD (%)	Rock Quality
Quartzites	88.6	Good
Dolomitic limestones	80.1	Good
Slates	55	Fair

Table 5.5 Estimation of RMR for different rock type (Bineiawski, 1984)

Designation	Rock type		
	Quartzite	**Slate**	**Dolomitic limestone**
RMR_{basic}	82	73	79
Class	I	II	II
Description	Very good rock	Good rock	Good rock

Table 5.6 Summary of Q values calculated for quartzites, slate and dolomitic limestone

Designation	Quartzite	Slate	Dolomitic limestones
Q	6	3.44	5.21
Group	2	2	
Description	Fair	Poor	Fair

Table. 5.7 Summary of mechanical properties for major rock type in the project area

Rock Type	UCS (MPa)	Tensile Strength (MPa)	Intact Rock Modulus, E_i(GPa)	Deere-Miller Classification
Quartzites (Dry)	74.72±23.45	15.08±3.18	12.05±2.8	CL
Quartzites (Saturated)	56.20±26.34	-	8.94±4.48	CL-DL
Slates(Dry)	101.51±65.0	8.58±2.30	11.39±8.1	CL
Dolomie(Dry)	149.19±50.49	20.43±10.64	14.36±1.68	BL
Dolomitic limestone(Saturated)	86.61±16.93	--	12.90±2.5	CL

Table 5.6 Shear strength parameters as per Hoek and Brown (1997) criterion

Rock Type	Condition	GSI	m_i MPa	σ_{ci}	m_j	s_j	a	c_{mass} MPa	ϕ_{mass} degrees
Slates	Dry	20	9.52	75.1	0.38	0.0	0.6	0.84	18.9
	Saturated	17	4.0	58.8	0.16	0.0	0.6	0.43	12.8
Dolomitic limestone	Dry	58	6.65	73.59	0.65	0.00073	0.5	1.96	25.1
	Saturated	58	9.7	56.88	0.95	0.00073	0.5	1.67	28.3
Quartzites	Dry	60	16.32	148.07	3.27	0.00674	0.5	7.14	38.2
	Saturated	55	12.72	126.61	2.55	0.00674	0.5	5.85	35.9

Table 5.9 The representative values of JRC and JCS for Quartzites Slates and Dolomitic limestone (Barton and Choubey, 1977) and ISRM (1978)

Structural Discontinuities	Quartzites		Slates		Dolomitic limestones	
	JRC	JCS	JRC	JCS	JRC	JCS
Foliation (FJ)	8	20	8	24	8	22
Joint J1	8	10	6	22	8	22
Joint J2	8	20	10	18	8	25

5.4 STABILITY ANALYSIS OF POWER TUNNEL

The assessments of rocks to be encountered in the tunnels are carried out based on surface geological mapping and other parameters related to rock mass characters. However the actual rock conditions encountered during tunnelling may differ due to complicated tectonic and structural set up of the area. This is true in most cases of tunnels in Himalaya, where the tunnels are excavated with huge rock over burden cover.

Among the geological discontinuities foliation is the most dominant and is profusely present within the rock. In addition there are two more sets of joints observed in the rocks. In addition shear zones are often encountered mainly parallel to the foliation planes. They show varying size ranges from few cms up to 30cms. The size may increase at places because of swelling and pinching tendencies due to tight folding. . Depending up on the location of the shear zones, their size and disposition, they are often responsible for overbreak seen associated with excavation. In general, the orientation of geological discontinuities with respect to the tunnel alignment is a major factor in resulting unstable wedges within the tunnel. The more, the geological discontinuities are parallel to tunnel alignment more unfavourable conditions may result during excavation. Similarly, if more than one set of discontinuities are present, the rock wedges formed may be stable or unstable depending upon the direction of plunge of rock wedge. The more the plunge direction of wedge line is parallel to the tunnel alignment, the wedges may become unfavourable. Similarly, if the amount of plunge is more, the instability tendency will also increase.

Kinematic analysis was carried out for all five segments with respect to their tunnel orientation and structural discontinuities on stereonet. Similarly wedges analysis was done for all five segments to identify the nature of wedge position, its size, volume and factor of safety (FOS). Joint properties obtained from field such as Joint Roughness Coefficient (JRC) based Barton and Choubey (1977) and Joint wall compressive strength (JCS) (ISRM, 1978) were incorporated as primary input parameters for the analysis.

5.4.1 Segment A-B of Power Tunnel

Hard, massive quartzites with well-developed joints are mainly exposed in the initial reaches of this segment. These rocks are delimited towards south by fairly hard, grey colored and well jointed dolomitic limestones. The rocks have minor intercalations of greyish black slates at places. Further ahead thick bands of dolomitic limestones and slates are interbanded till the end of segment A-B.

The bedding planes are parallel to the foliations seen in the rocks in almost all the areas of the project site. The foliation are the major geological discontinuity in inducing instability within the tunnel, The kinematic analysis reveals that the foliation is intersecting tunnel alignment at an angle of 35º (angle between strike of bedding and tunnel alignment). Since it is less than 45º the condition can be termed as fairly suitable. The tunnel stretch may face overbreaks due to foliation shears intersecting the joints within the tunnel.

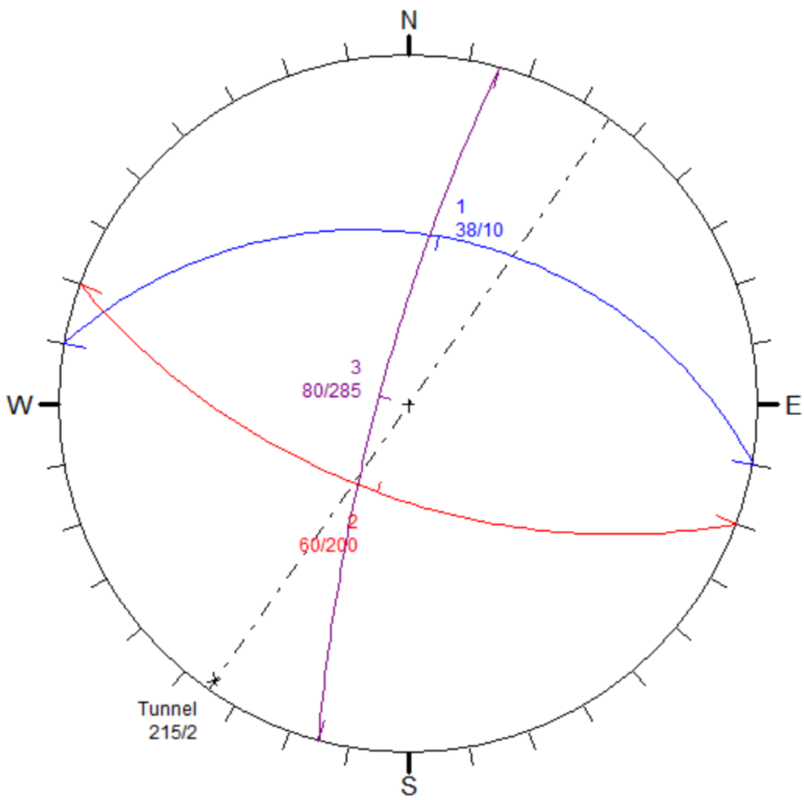

Fig 5.4 Kinematic analysis for PT segment A-B

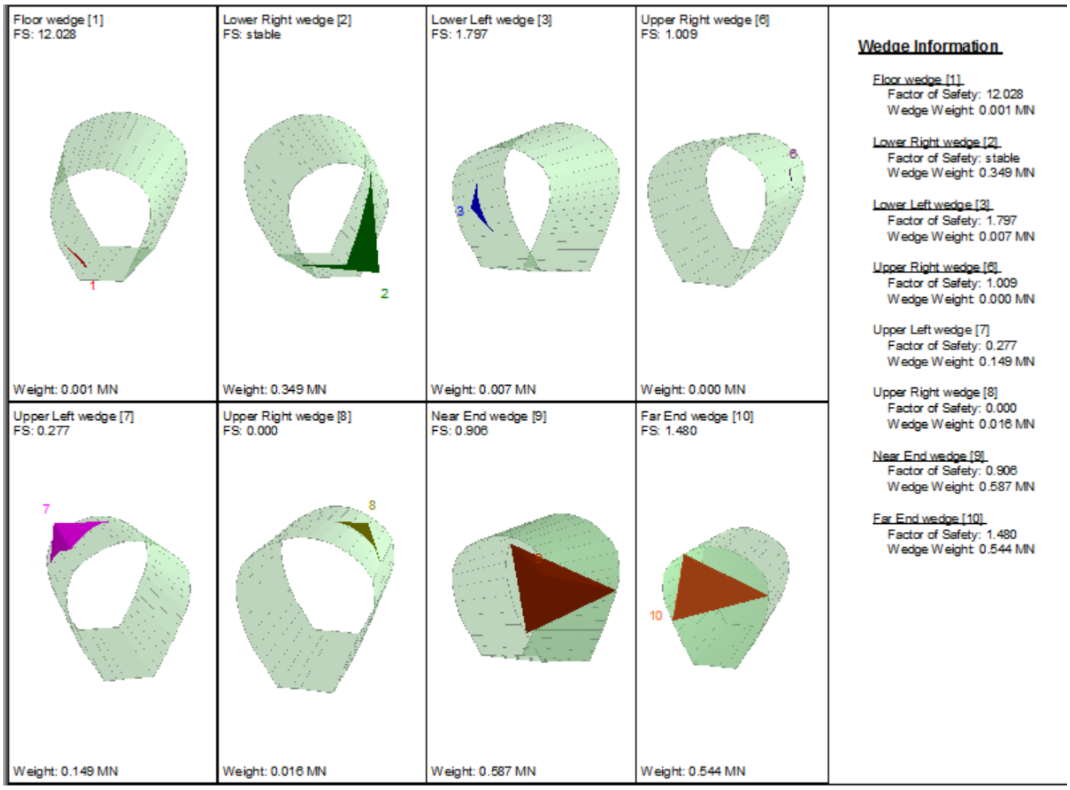

Fig 5.5 Wedges formed between A–B Segment 1

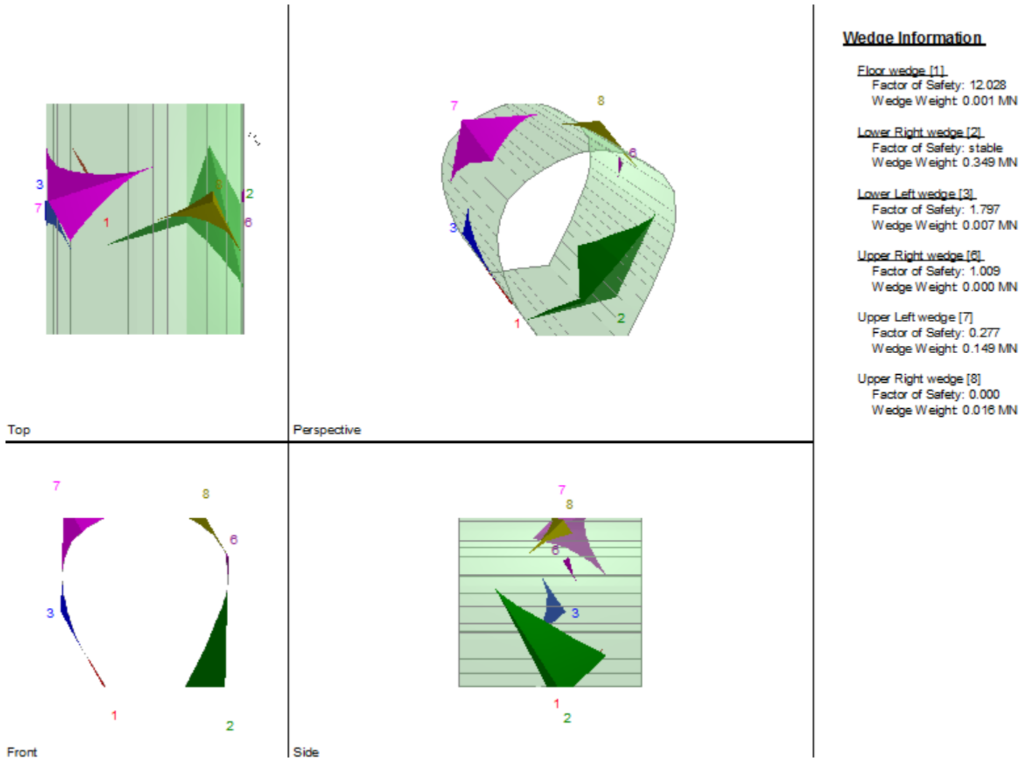

Fig 5.6 The unstable wedges formed on the top right roof corner and top left roof corner of the PT in segment A-B

The intersection of various geological discontinuities results in rock wedges, some of which may be unstable in nature. In order to predict possible unstable rock wedges the program Unwedge (Rocscience) was used. The program takes into consideration the attitude of the plunge line of various rock wedges formed with reference to the tunnel orientation. The program indicates graphically various rock wedges formed along with their factor of safety (FOS). The rock wedges with low FOS can be identified. The program has a provision to include the seismic coefficient of the area, which has relevance to Himalaya. The basic factor of safety as identified by the program is 1.5 for stable wedges and the wedges less than 1.5 will fall in unstable category.

In segment A-B, ten wedges are formed in total along the PT orientation at N215° due to intersection of the bedding/ foliation (FJ), the joint J1 and the jointJ2 (Fig 5.5). Those wedges are identified as follows:

Among these ten wedges two wedges namely wedge no 7, 8 and 9 are unstable with FOS less than one located on the roof up right corner and roof up left corner, whereas the reaming wedges are just stable. The wedge analysis were done considering the seismic coefficient as the area fall on seismic zone V [IS 1893 (Part 1) 2002].

5.4.2 Segment B-C of Power Tunnel

In this segment the dolomitic limestones are exposed for short distances close to location B. Later dense and dark grey colored slates having well developed cleavage/foliation planes are seen in the remaining portion of this segment. Since the tunnel is aligned in WNW–ESE direction in this segment, it tends to become more parallel to the foliation of the rocks. Probably this is one segment where the foliations may be more closely parallel to the power tunnel orientation. A perusal of the segment indicates that the maximum depth of rock overburden (825 m) above the tunnel close to Pokhani village is the maximum in the entire tunnel alignment. The foliation plane within slates is the major geological discontinuity in this segment. It intersects the tunnel alignment at an angle of less than 20° (Fig 5.3). Because of this factor, the condition with respect to stability can be termed as unfavourable, as it may favour more overbreaks (Fig 5.7).

The wedge analysis indicates that four major critically stable and unstable wedges are formed along B-C segment. The wedges are namely lower right wedge no.2, Upper right wedge no.6 with FOS = 0.44, Upper left wedge no. 7 (critically stable) FOS = 1.6 and the roof wedge no.8 with FOS =0.

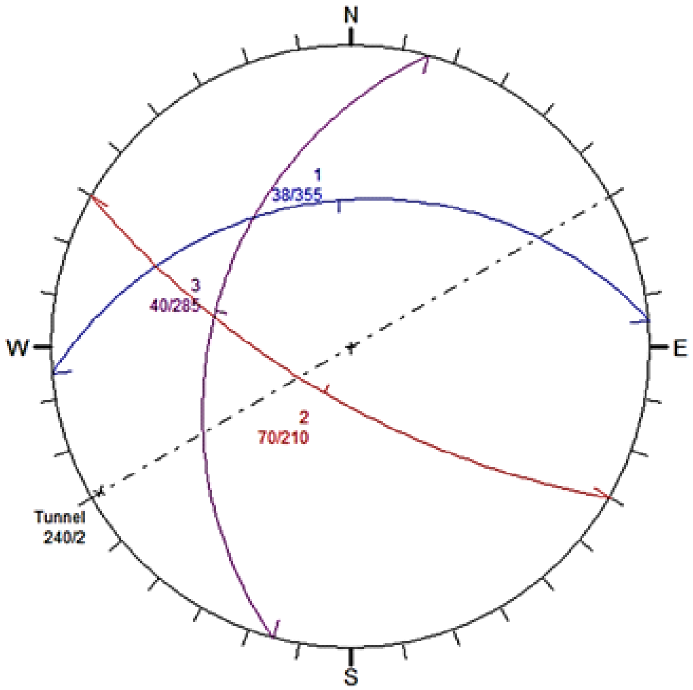

Fig 5.7 Kinematic analysis along B-C segment.

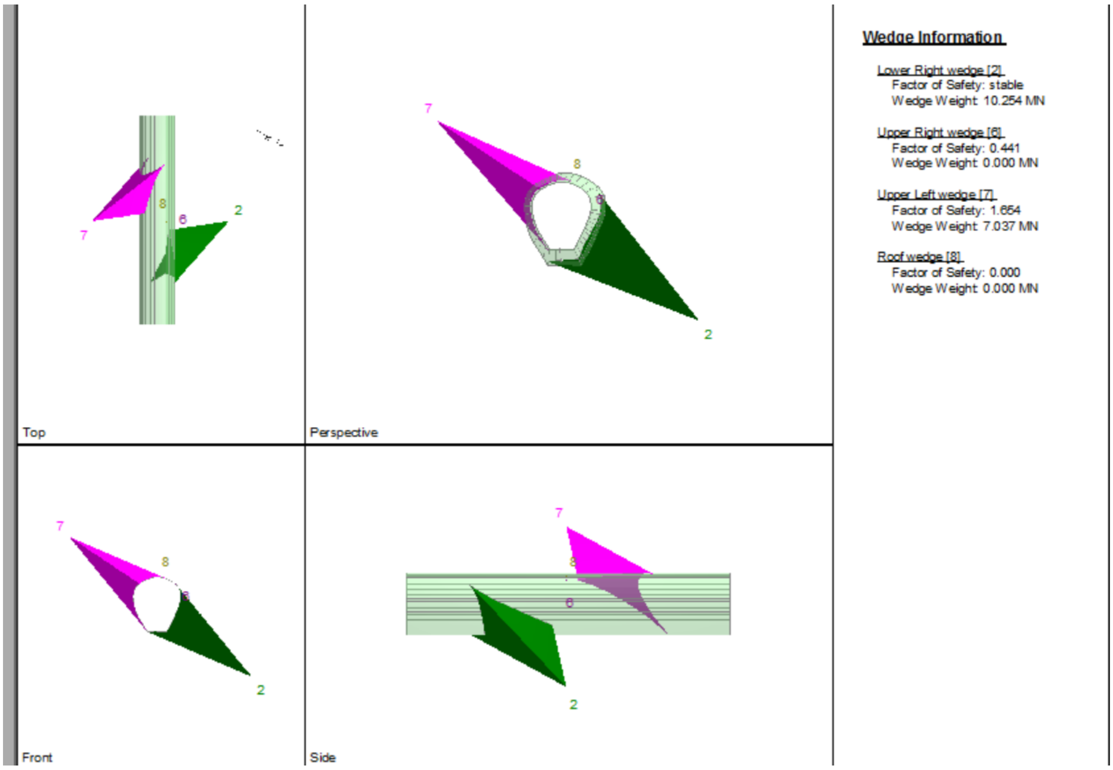

Fig 5.8 Wedges formed along B–C Segment

Summarizing the overall condition, more overbreak conditions may be anticipated mainly due to unfavourable orientation of foliation. Hence it is essential that the tunnelling in this segment should be carried out with more care to minimize the overbreaks.

5.4.3 Segment C-D of Power Tunnel

The segment C-D represents a very small stretch within the power tunnel, where the trend of tunnel alignment is N025°E–S025°W. Geologically, the slates of B-C section continue in this stretch also. The Maina River, which is an important tributary of Alaknanda, cut across the tunnel alignment in this segment. In view of deep undercutting of the river, the cover above the tunnel seems to be very less. From geological section (Fig 5.9), it can be inferred that the maximum cover in the intersection zone of Maina River with the tunnel, is of the order 20-25m. This may include boulders on the top, followed highly weathered rock, both extending to a depth of at least 10 -15m from surface. This possibly leaves fairly fresh to fresh rock cover of about 10m above the tunnel, which in anyway is less than the 3D cover (about 27m) above the tunnel roof. Moreover strong evidences are seen to suspect the presence of a shear zone along the river course. As the 3D cover is less in this stretch, the formation of wedge in combination with insufficient rock over burden cover and shear zones may result in heavy overbreak leading to collapse of the tunnel.

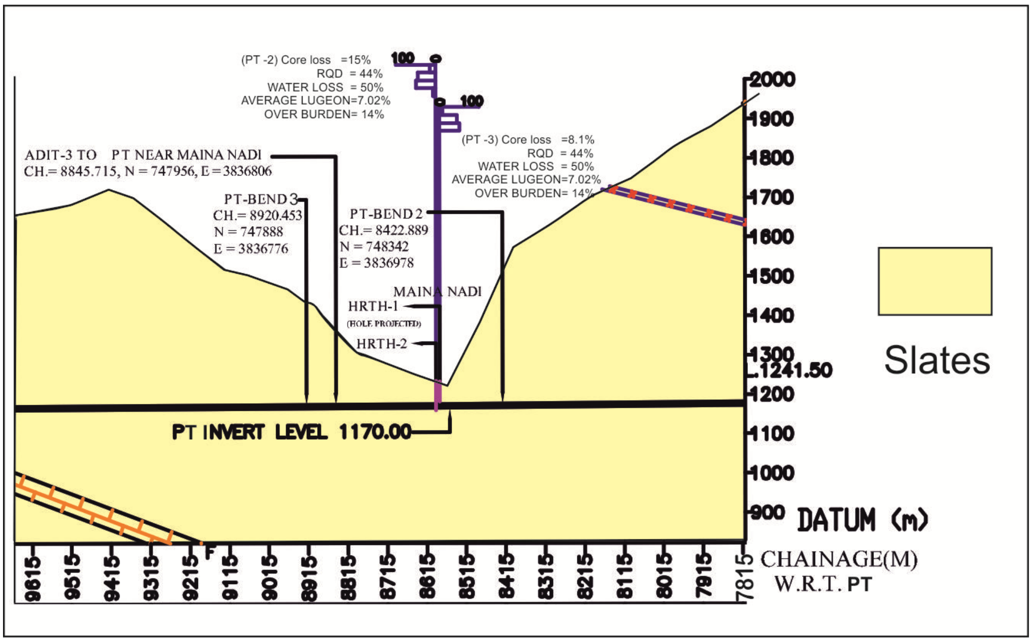

Fig 5.9 Geological cross-section along PT crossing point at Maina River (Section Direction S25°W–N25°E)

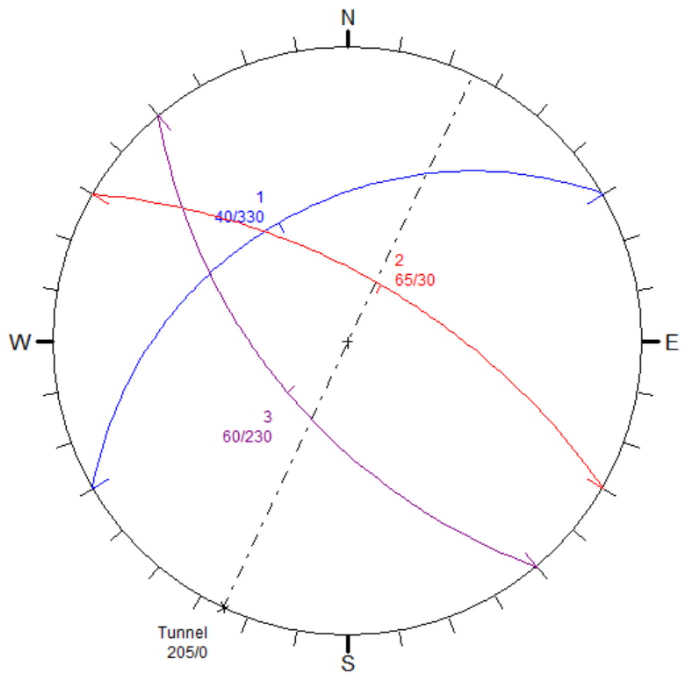

Fig 5.10 Stereonet kinematic analysis along C-D segment.

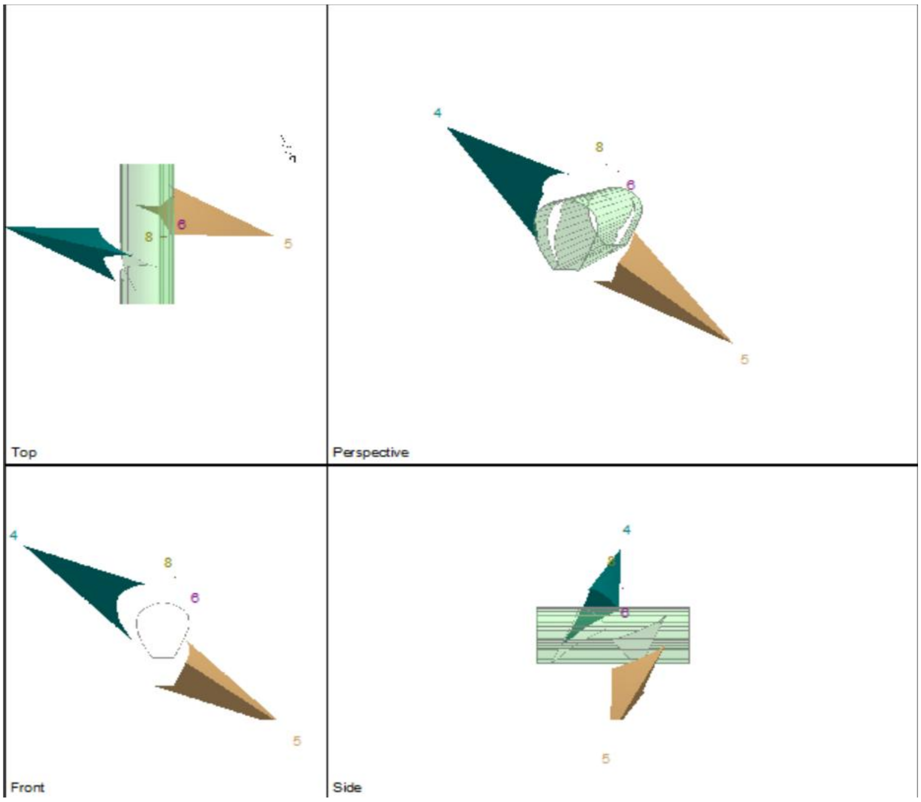

Fig 5.11 Wedges formed along C–D Segment 3

The kinematic analysis show that the wedge formed due to the intersection point of FJ, J1 and J2 falls far away from the tunnel alignment (Fig 5.10)

It is seen from the 3D wedge analysis that a total of ten wedges .are formed out of these wedges wedge no. 6 and 8 are negligible due to their small scale. The Upper left wedge no 4 likely to cause problem as it FOS <1.5 (Fig 5.11)

5.4.4 Segment D-E of Power Tunnel

In this segment, two major bands each of slates and dolomitic limestones are present, each occupying nearly equal distance along the tunnel alignment. The stereonet kinematic analysis (Fig 5.12) reveals that the strike of bedding/foliation is nearly parallel with the tunnel alignment, which is favourable condition for tunnelling. The strike joint sets J1 and J2 makes an angle with the tunnel alignment is 30° (unfavourable) and 40° (fairly favourable) respectively (Fig 5.12). The line of intersection between joint J_1 and bedding/ foliation (FJ) is plunging towards N300°, intersects the tunnel alignment at an angle of 50° (favourable). The line of intersection between joint J_2 and bedding/foliation (FJ) is plunging towards N332°, intersects the tunnel alignment at an angle of 18°(very unfavourable).Summarizing the overall condition, the tunnelling in segment may pose some problems of overbreak conditions particularly within slates.

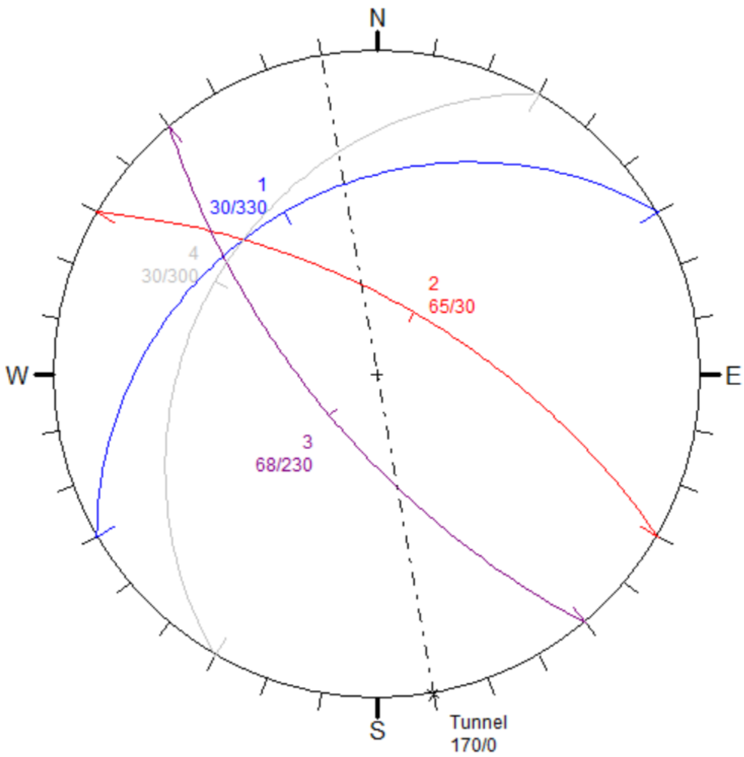

Fig 5.12 Stereonet kinematic analysis along D-E segment.

The wedge analysis shows that in total ten stable wedges are formed in this segment. Out of which the wedges with comparatively less FOS are delineated and discussed here. The wedges namely upper left wedge no4 and lower right wedge no 5 are with FOS 2.4 (Fig 5.13). As the wedge no 5 is located in between the lower right side wall and the floor this is a stable wedge. The wedge no4 may have some adverse effect on tunnel stability during excavation.

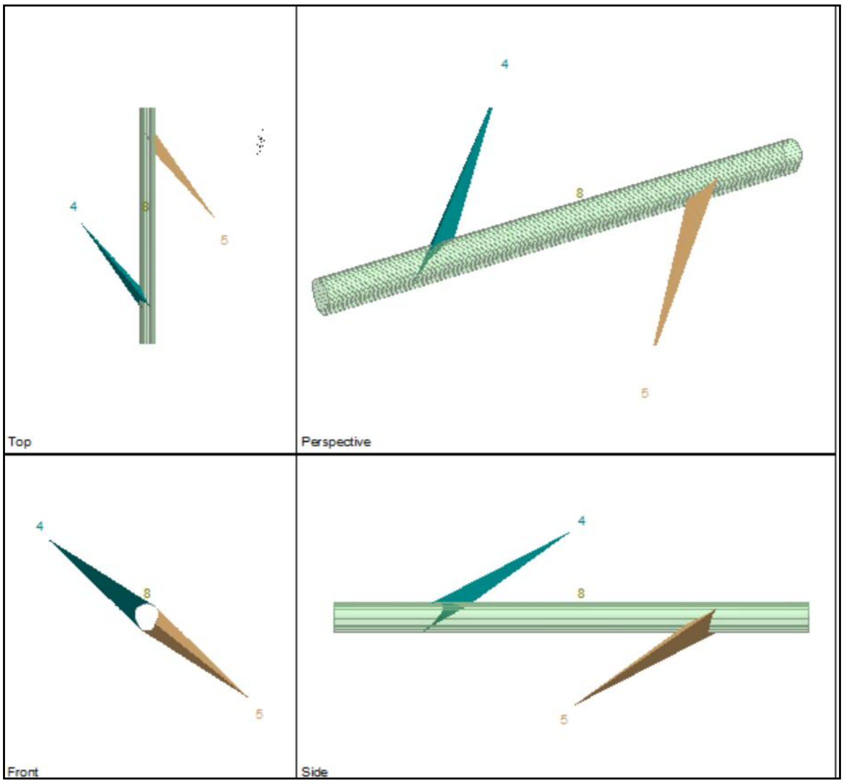

Fig 5.13 Wedges formed along D–E Segment

5.4.5 Segment E-F of Power Tunnel

Hard fairly dense dark to light grey colored, well jointed dolomitic limestones with minor bands of slates are mainly exposed in these area. The stereonet kinematic analysis indicates that the bedding plane of dolomitic limestone intersects the tunnel alignment at an angle 40˚ that is fairly favourable for tunnelling condition. The wedge formed due to intersection of joint J_1 with the bedding plane is plunging towards N 302°, i.e. intersecting the tunnel alignment at an angle of 63° (favourable) (Fig 5.14) Overall, the tunnel excavation in this segment is not likely to face major problems of overbreak and hot water encounters.

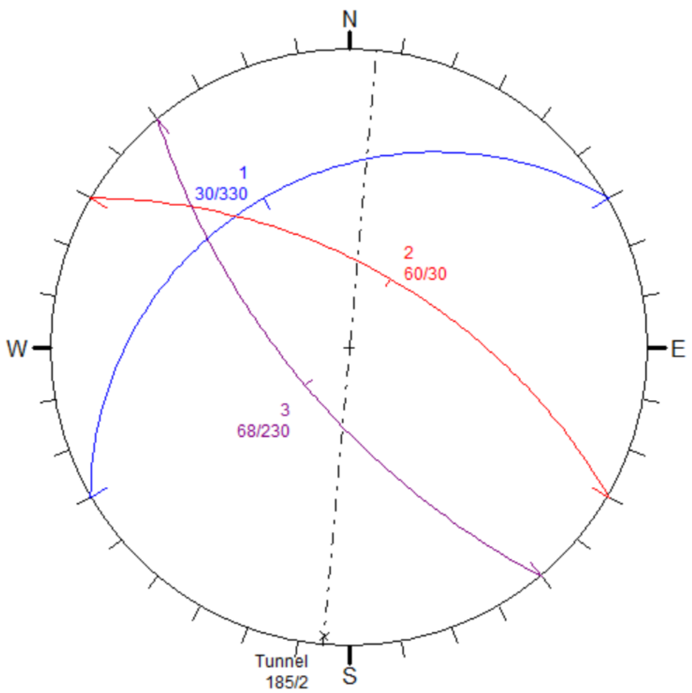

Fig 5.14 Stereonet kinematic analysis along E-F segment.

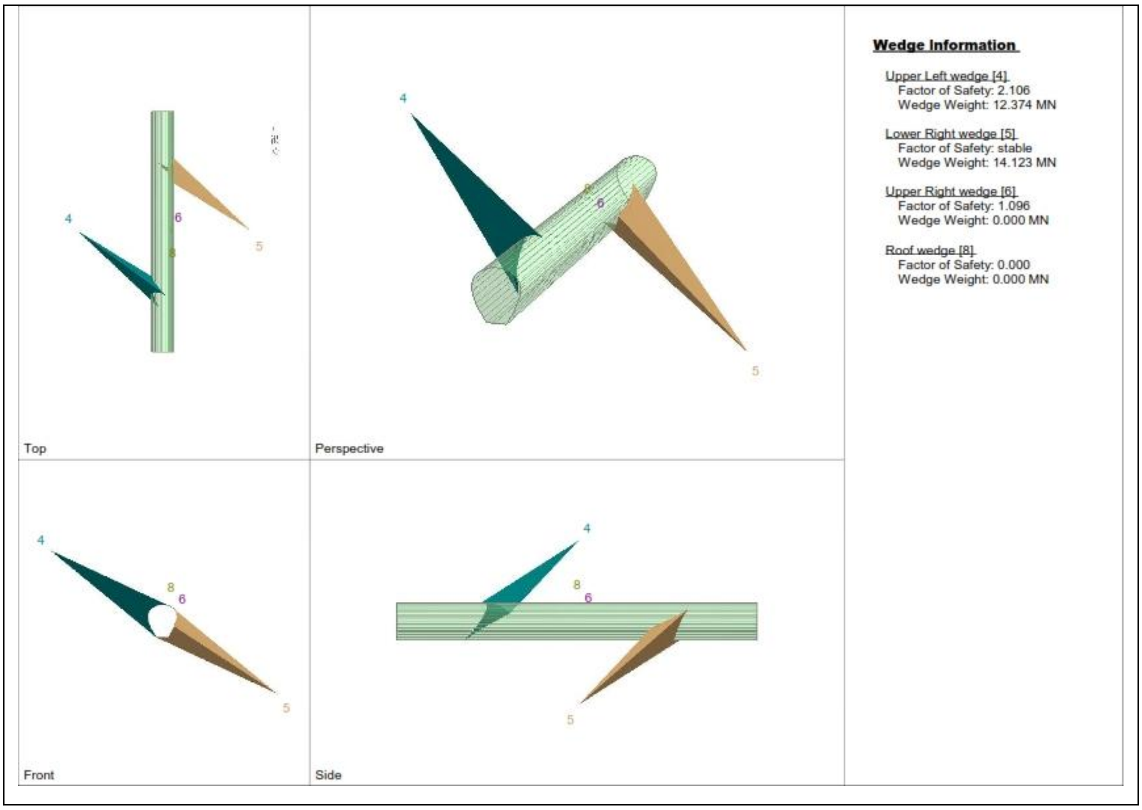

Fig 5.15 Wedges formed along E-F Segment

The wedge analysis indicates one critical stable wedge is likely to be formed in this segment. The wedges number 6 formed on the up right roof corner.(Fig 5.15)

Though the Unwedge software has an inbuilt option for modelling support design and to estimate the required support pressure from combination analyser. Evaluation of support pressure was carried out using Goel and Jethwa (1991) as these are based on the case histories of Himalaya.

EVALUATION OF SUPPORT PRESSURE

Using the measured support pressure values from 30 instrumented Indian tunnels, Goel and Jethwa (1991) have proposed the following Equation (5.1) for estimating the short-term support pressure for underground openings in both squeezing and non-squeezing ground condition in the case of tunneling by conventional blasting method using steel rib support (but not in rock burst condition).

$$P_v = \frac{\left(7.5B^{0.1}H^{0.5} - RMR\right)}{20\left(RMR\right)} \qquad \text{(Eq. 5.1)}$$

The Q system developed by Barton et al. (1974) is one of the widely used empirical approaches all over the world for choosing support system for underground excavations. They modified Q system by introducing the term ultimate support pressure and short term support pressure and plotted support capacities of 200 underground openings against the rock mass quality (Q) as shown in (Fig. 5.15). They found the following empirical correlation for roof and wall pressures.

$$P_v = \left(0.2 / J_r\right) Q^{-1/3} \qquad \text{(Eq. 5.2)}$$

$$P_h = \left(0.2 / J_r\right) Q_w^{-1/3} \qquad \text{(Eq. 5.3)}$$

Where,

P_v = Ultimate roof support pressure in MPa,

P_h = Ultimate wall support pressure in MPa,

Q = Rock mass quality (Equation 1), and

Q_w = Wall rock mass quality

It may be noted that dilatant joints or J_r values play a dominant role in the stability of underground openings.

The wall factor (Q_w) is obtained after multiplying Q by a factor which depends on the magnitude of Q as given below:

Range of Q	Wall Factor Q_w
> 10	5.0 Q
0.1–1	2.5 Q
< 0.1	1.0 Q

Barton et al. (1974) further suggested that if the number of joint sets is less than three, then

$$P_v = \frac{\left[0.2\left(J_n\right)^{1/2} \times Q^{-1/3}\right]}{3\left(J_r\right)} \qquad \text{(Eq. 5.4)}$$

$$P_h = \frac{\left[0.2\left(J_n\right)^{1/2} \times Q_w^{-1/3}\right]}{3\left(J_r\right)} \qquad \text{(Eq. 5.5)}$$

They felt that the short-term support pressure can be obtained after substituting 5Q in place of Q in Equation (5.2). Thus the ultimate roof support pressure is obtained as 1.7 times the short term support pressure.

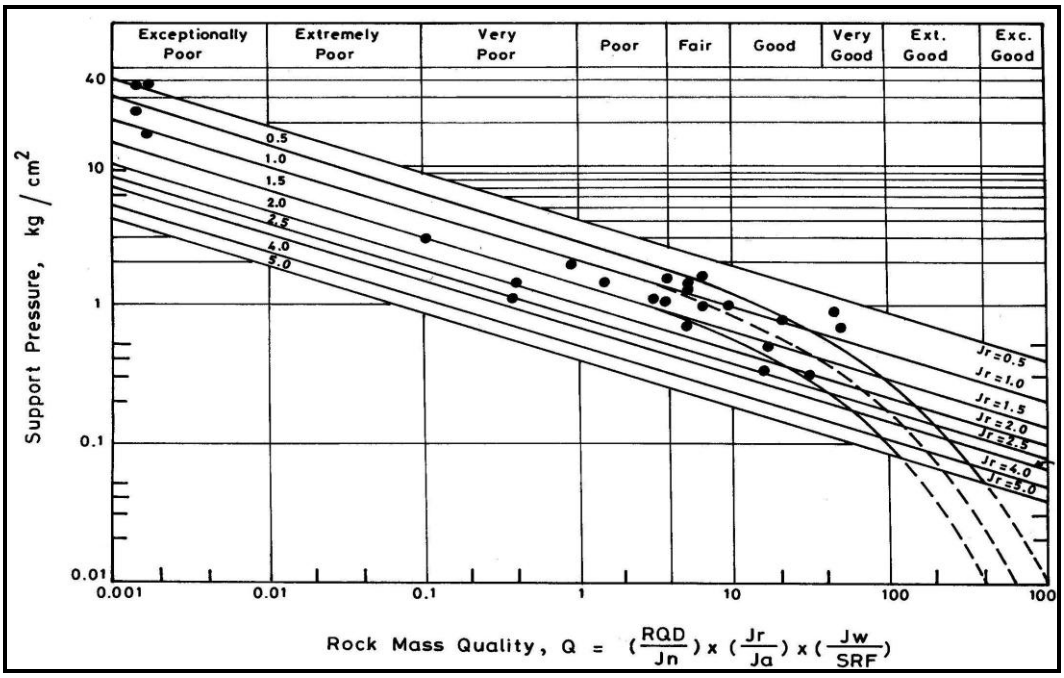

Fig 5.16: Correlation between support pressure and rock mass quality (Q) Q-system (Barton et al., 1974)

Modifications in Q-System by Singh et al. (1992)

Singh *et al.* (1992) have actually compared the measured support pressure values with the support pressure values estimated by Equation (5.2) of Barton et al. (1974) in the Himalayan tunnels. They have observed that the support pressure estimated from the Barton’s approach is unsafe in case of Himalayan tunnels which have a high overburden pressure. Based on their experiences, in the Himalayan tunnels, they proposed a couple of correction factors in Barton’s equation to propose new equations for estimating support pressure:

$$P_v\left(ult\right)=\frac{\left(0.2\times Q^{-1/3}\times f\times f^{'}\right)}{J_r} \qquad \text{(Eq. 5.6)}$$

It is measured in MPa

$$f=\frac{1+\left(H-320\right)}{800}\geq 1 \qquad \text{(Eq. 5.7)}$$

Where,

Q = Rock mass quality,

P_v (ult) = Ultimate tunnel support pressure,

f = Correction factor,

$f^{''}$ = Correction factor for tunnel closure (Table 5.10),

H = Overburden above crown or tunnel depth below ground level (m)

Horizontal or wall support pressure

For estimating wall support pressure following equation is used

$$P_v\left(ult\right)=\frac{\left(0.2\times Q_w^{-1/3}\times f\times f^{'}\right)}{J_r} \qquad \text{(Eq. 5.8)}$$

The wall factor (Q_w) is obtained after multiplying Q by a factor which depends on magnitude of Q as given below:

Range of Q	Wall Factor Q_w
>10	5.0Q
0.1-10	2.5Q
<0.1	1.0Q

Using approach of Singh et al. (1992)

The modified equation of Singh is used in estimating support pressure Equation (5.5)

Table 5.10 Correction factor for overburden f and tunnel closure f' by using approach of Singh et al. (1992)

Rock Type	Depth of overburden (H) in m	Correction for overburden f=1+(H-320)/800$\geq$1	Rock Condition	Tunnel Closure (ua),%	Correction factor (f')
Slate	495	1.218	Non-Squeezing $H<350Q^{0.33}$	<1	1.1
Slate	600	1.350	Non-Squeezing $H<350Q^{0.33}$	<1	1.1
Slate	825	1.631	Non-Squeezing $H<350Q^{0.33}$	<1	1.1
Dolomitic Limestone	375	1.068	Non-Squeezing $H<350Q^{0.33}$	<1	1.1
Dolomitic Limestone	495	1.218	Non-Squeezing $H<350Q^{0.33}$	<1	1.1
Dolomitic Limestone	450	1.162	Non-Squeezing $H<350Q^{0.33}$	<1	1.1

Table 5.11 Support pressure using equation of Singh et al.(1992)

Rock Type	Depth of overburden (H) in m	Q_{av}	Ultimate Roof Support Pressure By Singh et al. (1992) P_v (ult) (Mpa)	Ultimate Wall Support Pressure by Singh et al. (1992) P_h (ult) (Mpa)
Slate	495	12.77	0.03877	0.02277
Slate	600	12.77	0.04298	0.02524
Slate	825	12.77	0.05193	0.03053
Dolomitic Limestone	375	16.07	0.03132	0.01842
Dolomitic Limestone	495	16.07	0.03572	0.02100
Dolomitic Limestone	450	16.07	0.03408	0.02003

For present purpose the excavation span = 8 m

5.5 ESTIMATION OF SUPPORT REQUIREMENT

5.5.1 Determination of Maximum Unsupported Span

Barton et al. (1974) proposed the following equation for estimating equivalent dimension (D_e') of a self-supporting or an unsupported tunnel.

$$D_e^{'} = 2\left(Q^{0.4}\right) meters \qquad \text{(Eq. 5.9)}$$

If H < 350 Q $^{1/3}$ meters

Where

$$D_e^{'} = \frac{Span}{Excavation\ Support\ Ratio\left(ESR\right)} \qquad \text{(Eq. 5.10)}$$

D_e'= Equivalent dimension, Span = Diameter or Height of tunnel in meters, ESR = Excavation support ratio

5.5.2 Length of Bolts and Anchors

Bolt length is determined by the following equation given by Barton et al. (1974)

$$L_b = 2 + 0.15 D_e^{'} \qquad \text{(Eq. 5.11)}$$

Where, L_b = Bolt length (m)

Anchor relation is given by the following relation

$$L_a = \frac{0.4D}{ESR} \qquad \text{(Eq. 5.12)}$$

The spacing between the anchors is taking as half the length of anchor.

In the studied area the span or diameter of tunnel (D) is 8.8m and taking ESR = 1.6 (Table 6), we can get the value of D_e' from Equation 5.10.

$$D'_e = (8.8/1.6) = 5 \qquad \text{(Eq. 5.13)}$$

Hence

Putting the value of D_e' in Equation 5.11, we get,

$$L_b = 2 + (0.15 \times 5) = 2.75m \qquad \text{(Eq. 5.14)}$$

Thus the length of the bolt work out is 2.75 m in an opening with 8.8m width.

The length of the anchor

$$L_a = 0.4 \times 5 = 2.0m \qquad \text{(Eq. 5.15)}$$

As the anchor spacing is half of the anchor length. Thus the anchor spacing will be 1m.

5.5.3. Types of Support by Q-System

Support system has also been evaluated by Q-System (Table 5.14)

Table 5.12. Estimation of support by Q-System

Rock Type	Q_{av}	Conditional Factors		Span/ESR (m)	Type of support	Support category
		RQD/ J_n	J_r / J_n			
Slate	12.77	10.89	0.5	5	B(utg) 1.5-2 m	13
Dolomite	16.07	13.39	0.5	5	B(utg) 1.5-2 m	13

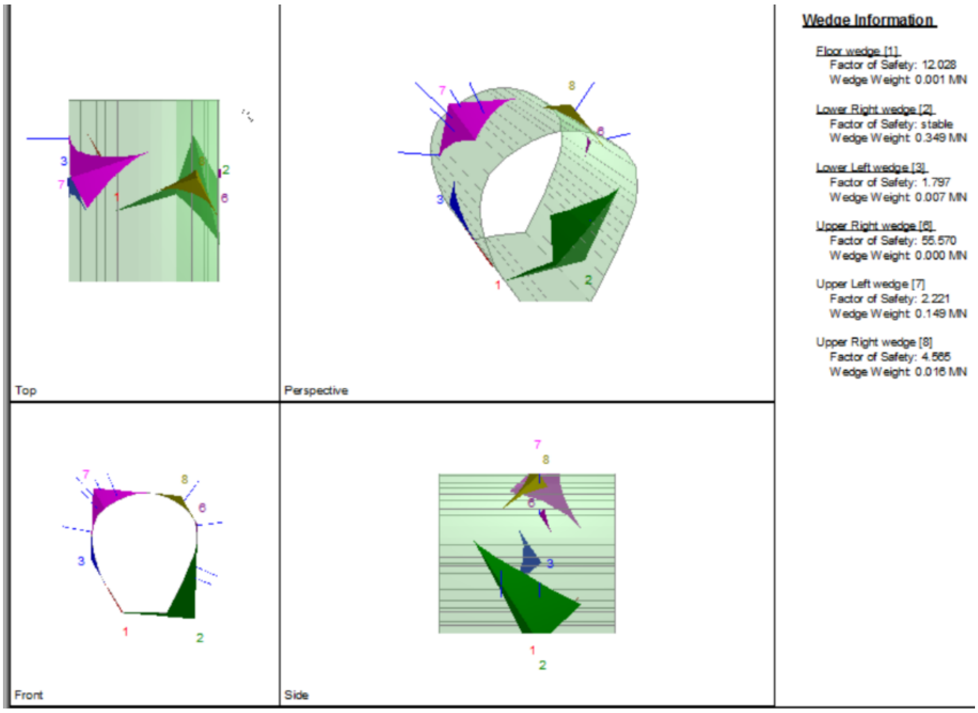

Fig 5.17 The stabilized wedge after providing the required support pressure (A-B Segment)

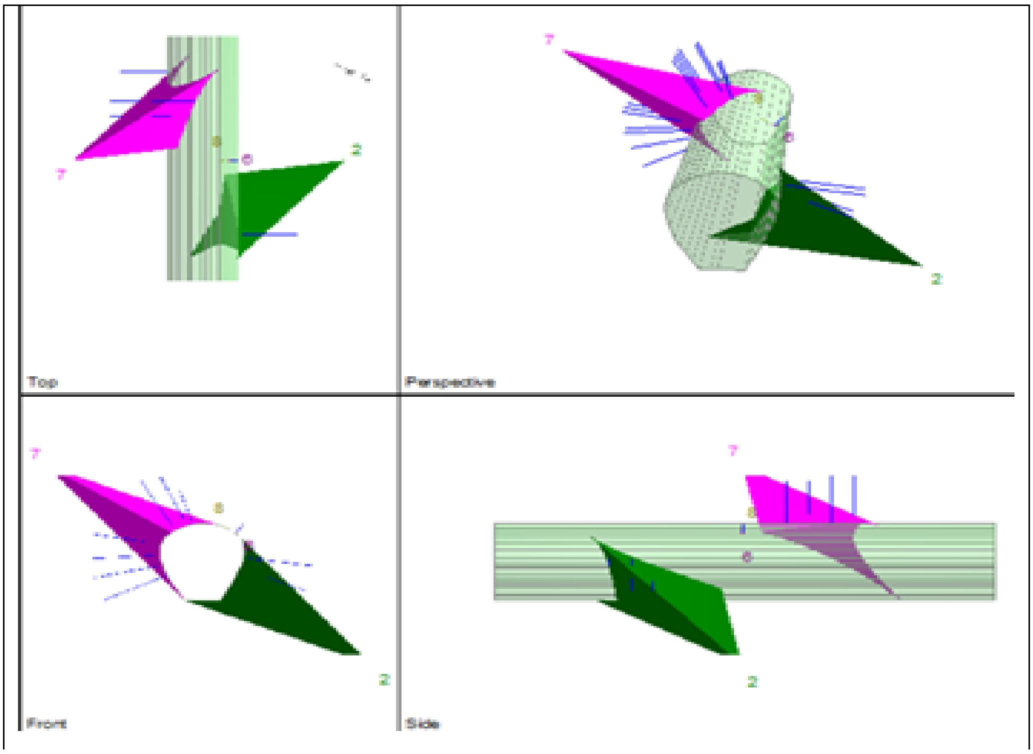

Fig 5.18 The stabilized wedge after providing the required support pressure (B-C Segment)

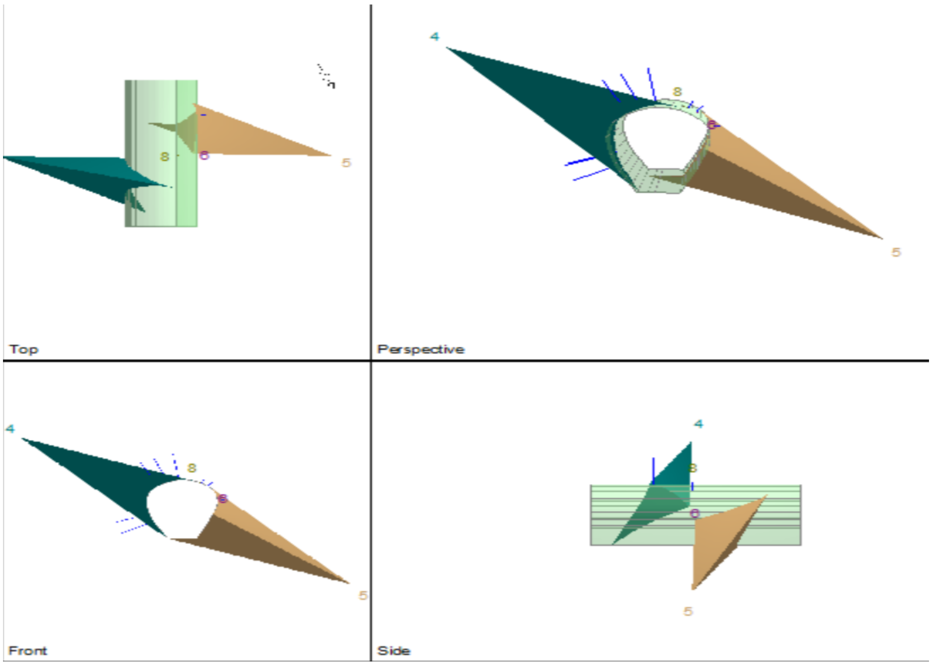

Fig 5.19 The stabilized wedge after providing the required support pressure (C-D Segment)

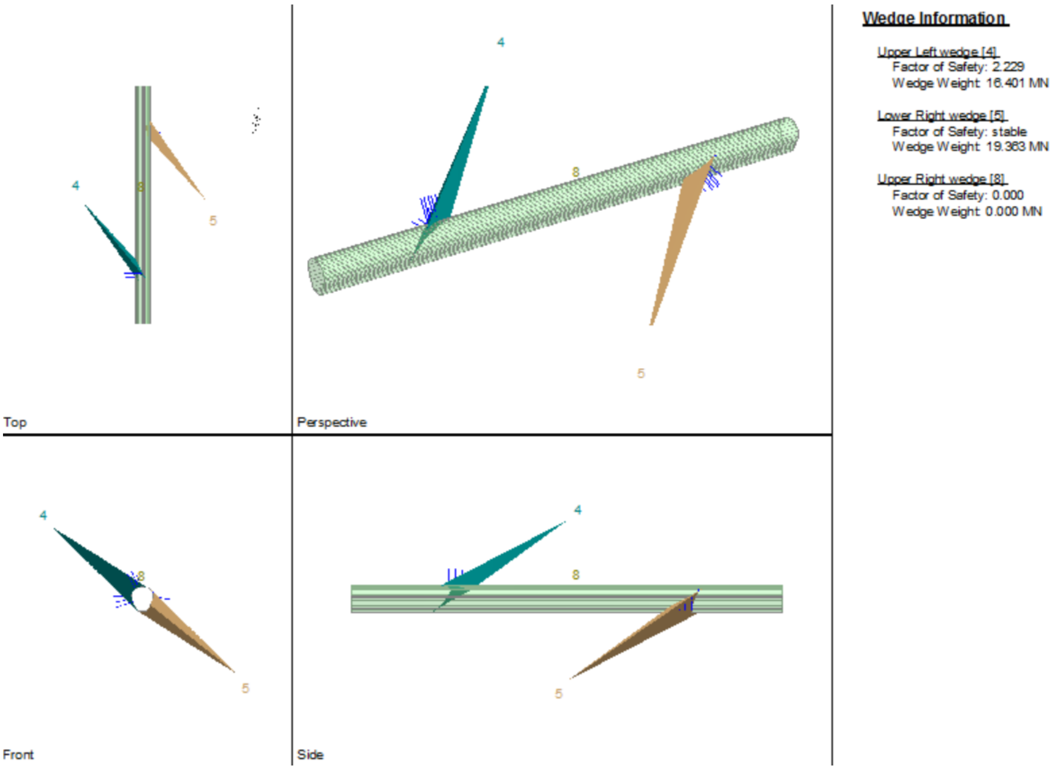

Fig 5.20. The stabilized wedge after providing the required support pressure (D-E Segment)

CHAPTER VI

EVALUATION OF IMPACTS OF BLASTING ON STABILITY OF GROUND AND CIVIL STRUCTURES ABOVE HRT & TRT

Vishnugad–Pipalkoti project involves underground excavations on a larger scale including power tunnel, tail race tunnel and other accessory structures. It is felt that the blasting associated with underground excavations may also cause vibrations of the ground, which may lead to damage the ground and civil structures in the vicinity (Yan et al., 2014). However, these vibrations can be kept under control if planned blasting is carried out.

The excavations for power tunnel (8.8m dia), approach adits, surge tank, power house and other accessory structures will involve blasting of rocks like quartzites, dolomitic limestones and slates. The blasting is likely to produce vibrations in the surrounding rock mass and these may be propagated for longer distances before being attenuated (Djordjevic et. Al., 1999). The impacts may be pronounced, where the depth of rock cover above the tunnel is less in nature. The vibrations created due to blasting can cause two major types of damages– i) damages to the existing infrastructures like buildings in the form of cracks and/or collapse of some portions of civil structures and ii) instability of hill slopes and landslides on surface as well as subsidence of ground surface. Though these impacts cannot be exactly quantified due to complicated geological and tectonic set up of the area, the amplitude of vibrations at different distances from the place of blasting can be estimated and used for studying the impacts on the existing civil structures.

A number of villages are located close to the power tunnel and tail race tunnel. Based on the actual site examination, villages like Lanji, Tirosii, Tapovan, Dhari, Math Dadhera, Surenda, Jharetha, Hyuna, Pokhani and Jaisal located close to the alignment of HRT and TRT have been considered for detailed analysis(Fig 6.1).Various types of houses including dry stone masonry houses, cement stone masonry houses and framed houses are present in these villages.The threshold value of any damage due to blasting is the function of transmitted frequency of the vibration into different types of constructions. Particularly serious concern lies to the low-frequency vibrations that exist in soft foundation materials resulted from long blast distances (Siskind et. Al., 1983). The present chapter deals with stability aspects of the terrain as well as the civil structures due to blasting for underground excavations including measures for controlled blasting.

The Alaknanda River in general flows towards southwest in the vicinity of the project area though changing its course locally towards south or west or southwest directions. A number of tributaries form both the banks join Alaknanda river in this stretch. Maina river is an important river on the right bank, which has steep water cut slopes on both the banks.

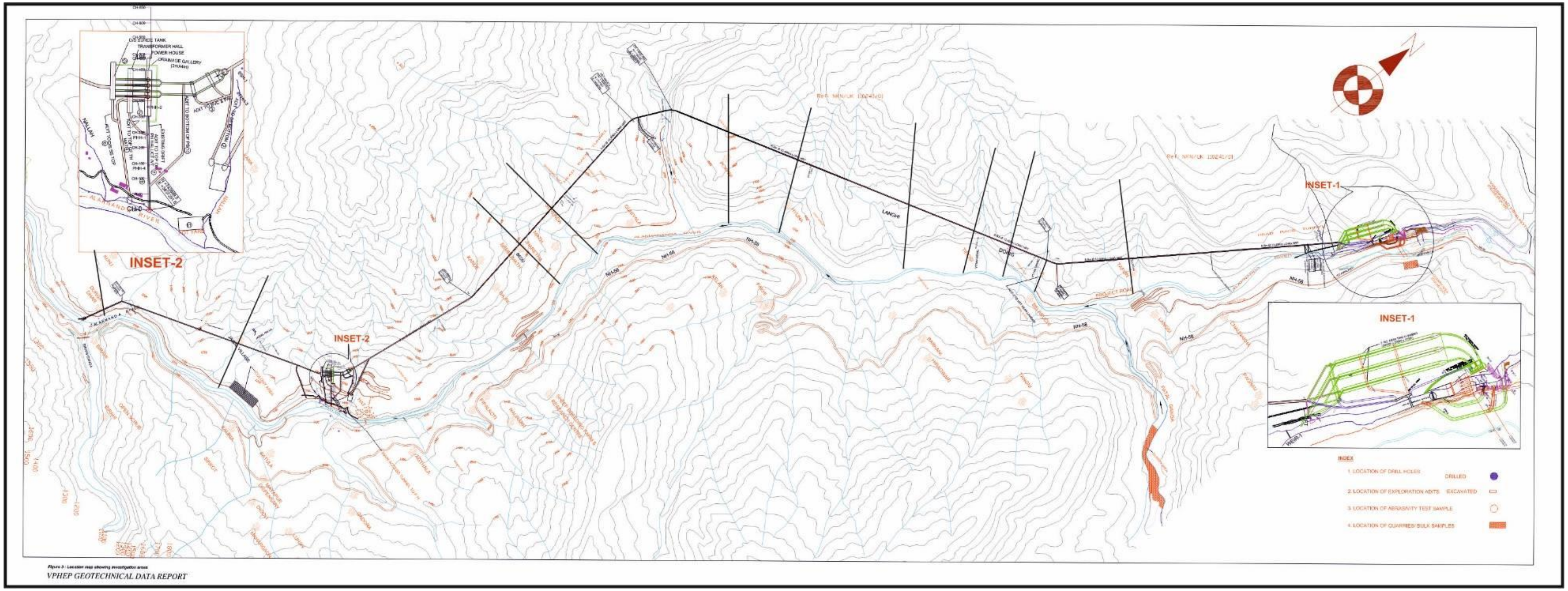

Fig 6.1 Location Map of the study area with section lines of villages

On the western side of the area particular on the right bank of the Alaknanda River, the topography generally rises steeply from the river bed level due to continuous presence of rock exposures. Locally, thin to moderate (4-40m) cover of debris can be seen at places, where the villages are located. However, the lower levels on the left bank are generally occupied by terraces either created by river, that is RBM terraces or agricultural terraces created on debris. The power tunnel located on the right bank runs nearly parallel to the river course. The villages are located close to the tunnel alignment on the slopes inclined towards east on the right bank.

6.1 GEOLOGY OF AREA

The power tunnel on the right bank passes through various types of rocks including quartzite, slates and phyllites as well as dolomitic limestone. In view of steeply rising topography of the area from river bed towards the ridge, the tunnel has good rock cover above. However, the villages under consideration are mostly located on debris cover in view of better life supporting advantages of these areas. The geological cross section prepared across these villages (Fig 6.2 to 6.12) show that the debris cover ranges from few meters to about 40m, but in general between 20-30m. The further details about these villages are discussed below.

<u>Jharetha Village</u>

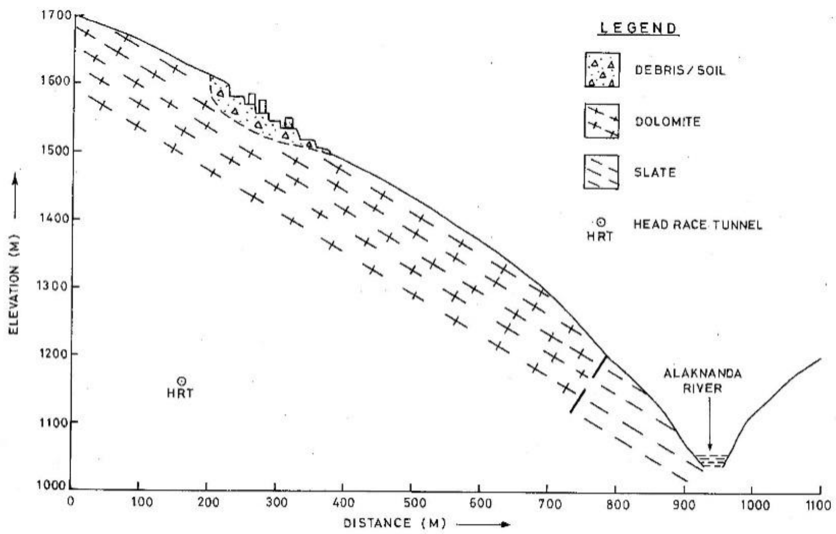

Fig 6.2 Geological section across slope in Jharetha village

This village is located on a fairly steep slope (Fig 6.2). The houses are located on thin debris cover extending as a pocket within dolomitic limestone rocks. The hill slope having rocks just below the debris has a moderate angle of 35°. However, the hill slope becomes steeper (>50°) close to river bed. The power tunnel is located deeper below the village by more than 300m. The thickness of the debris varies from few meters to about 40m. In view of presence of debris below the civil structures, it is essential to carry out stability analysis in order to establish the existing condition of stability of the area.

Surenda Village

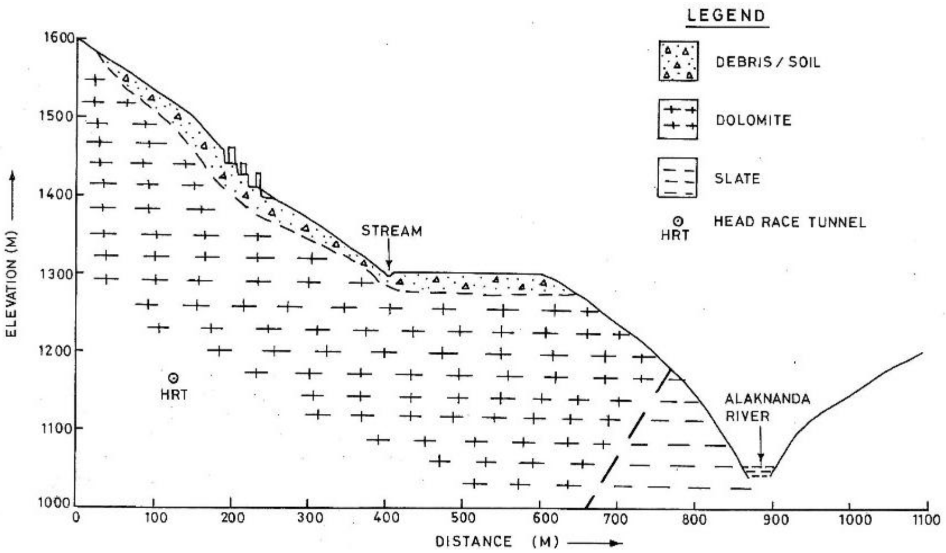

Fig 6.3 Geological section across slope in Surenda village

The village is located above Ghanpani stream between elevations 1400m and 1500m (Fig 6.3). The village is located on a fairly steep slope of about 35°. The Ghanpani stream is located on the northern edge of a terrace. The terrace is located above a steep slope, which extends down to river bed. The village Surenda and its vicinity have debris cover of the order 32 to 40m and terraced agriculture is being practiced on the debris area. The terrace adjoining Ghanpani stream also has terrace agriculture.

Tirosi Village

The village Tirosi is a small one and is located on a small terrace close to Alaknanda River (Fig 6.4). The terrace having a thickness of 25-30m extends up to the valley face.

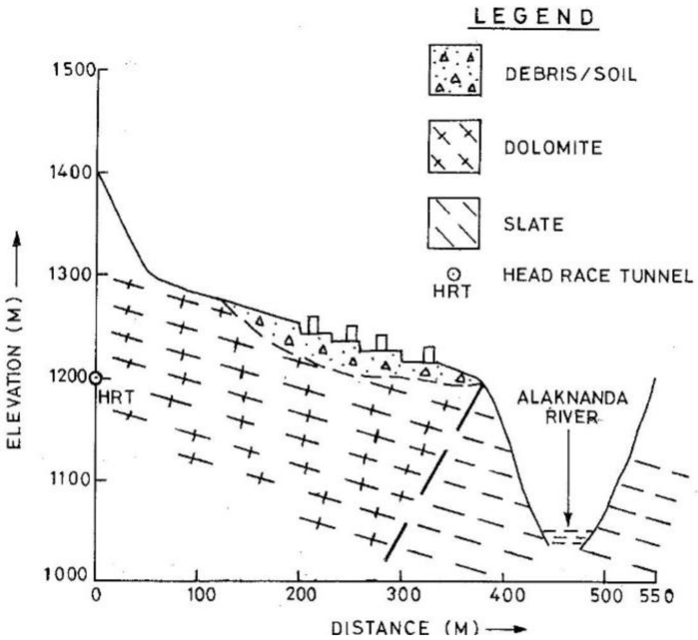

Fig 6.4 Geological section across slope in Tirosi village

Slates and phyllites are exposed on the valley face on right bank with the contact dipping into the hill. The village is located between elevations 1200m. Though the surface inclination is less (<20°) close to the village, the inclination of the slopes adjoining valley are steeper (>60°).

<u>Hyuna Village</u>

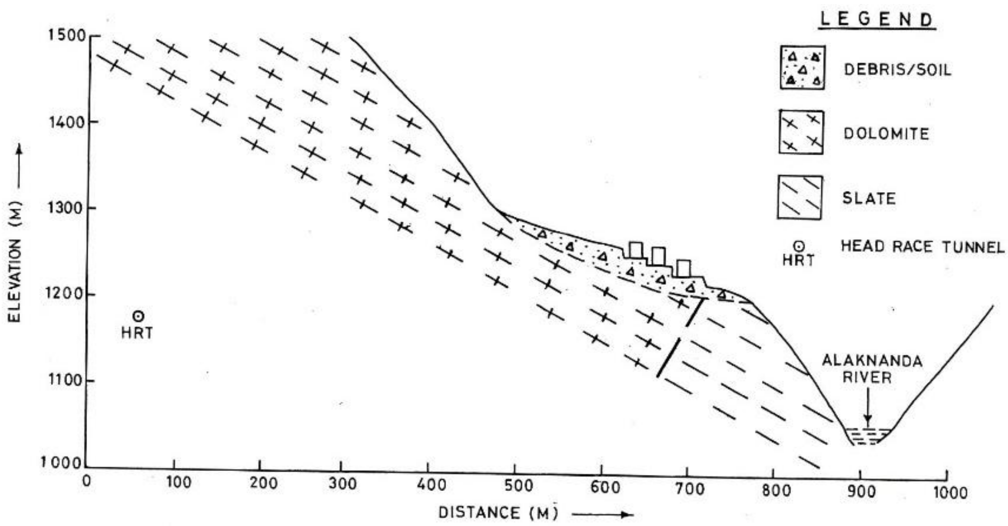

Fig 6.5 Geological section across slope in Hyuna village

The village Hyuna is located in between two boundaries of south flowing streams (Fig 6.5). It is located below Pokani, another well known village, at lower elevations. It is a small village, located on debris materials, which have been suitably modified into agricultural terraces. The thickness of the terrace apparently varies widely in different sections with a maximum of about 25m. Though the surface inclination of the debris is gentle (<20°), the rock slope having slates and phyllites on the valley side is very steep of the order of more than 45°. The hill slope present further west of Hyuna has dolomitic limestone rock with steep (>45°) slope inclination.

Tapon Village

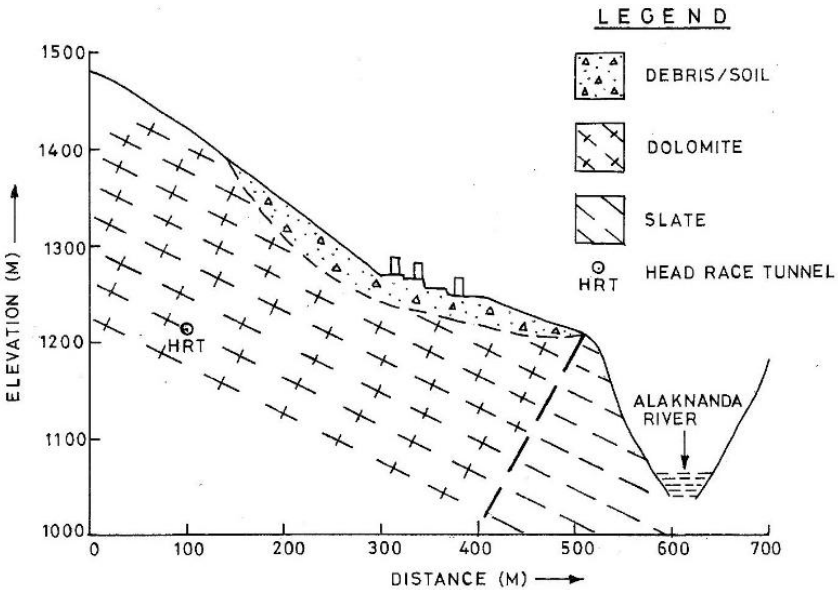

Fig 6.6 Geological section across slope in Tapon village

The village Tapon is located on a gentle hill slope (<20°) within a pocket of debris deposit (Fig 6.6). Though the village is located within the terrain of dolomitic limestone rocks, the contact with slate and phyllite rocks is also very close to the village but on the southern side towards the river Alaknanda. The debris slope at the village site and further below is moderate (20-25) and the slope increases at the back side of the village on the northwest side.

Math-Dadheta village

It is a fairly big village and located to the south of a prominent east flowing stream (Fig 6.7). This village is located within the debris materials lying over dolomitic limestone rocks. The thin debris cover is being presently used as agriculture terraces.

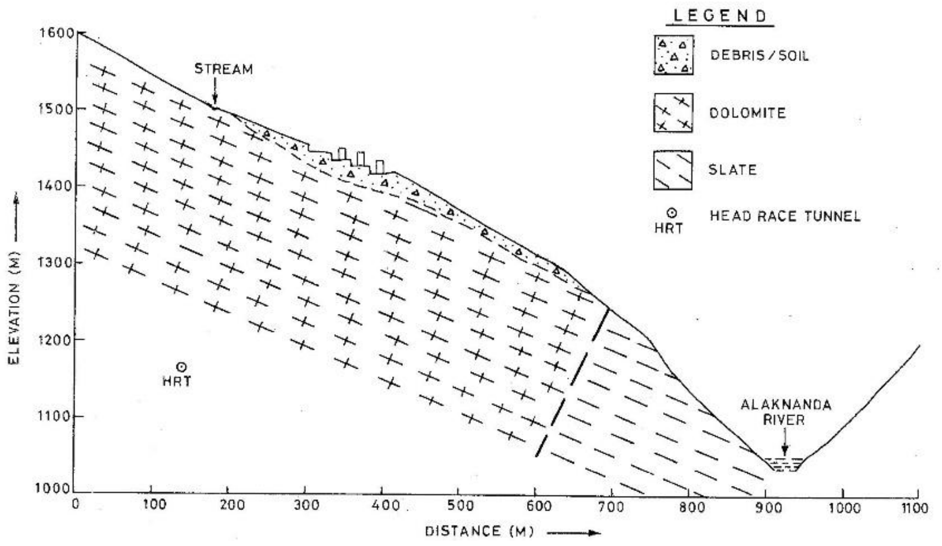

Fig 6.7 Geological section across slope in Math Dadhera village

The thickness of the debris materials may vary from 20 to 30m below the village. The slope angles are gentle to fairly steep close to the village area. However the slopes are steeper close to Alaknanda river. The contact of slate\dolomitic limestone is also present close to the river section.

Pokhani village

This village is located on the left bank of Maina River at a comparatively higher elevation between 1600 and 1700m (Fig 6.8). The village has two important segments–one located just close to the Maina River and another located about a km northeast of this location. The one on the northeast is fairly a big village and located just on the alignment and hence being considered for the analysis. The terraces are present nearly continuously between the two pockets of habitations. The slope is moderate to fairly steep (25°-30°) in the vicinity of the village, while it increases to more than 40° near Alaknanda River.

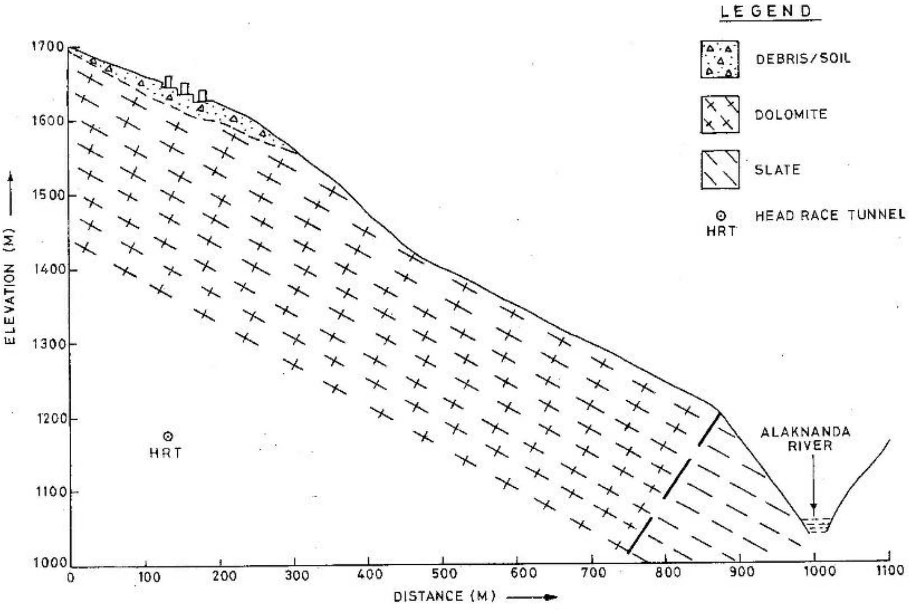

Fig 6.8 Geological section across slope in Pokhani village

<u>Lanji Village</u>

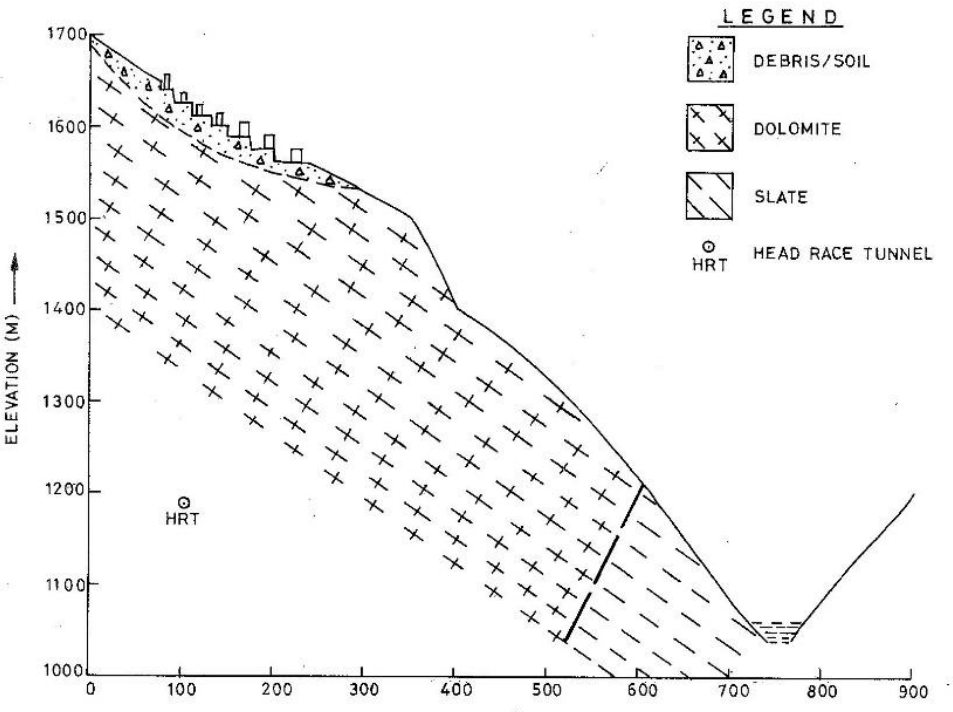

Fig 6.9 Geological section across slope in Lanji village

This village is also located in the high mountains much above the Alaknanda River (Fig 6.9). The elevation (~1600m) is comparable to Pokhani village. This village extends over a large area, being occupied by agricultural terraces. The village is just located just above the Power tunnel alignment with elevation difference of about 350m. The village is comfortably located on a gentle slope of 15°-20° with a number of terraces, where agriculture is being practiced. However, further the slope increases to >40° up to Alaknanda River. Though the entire village is located within dolomitic limestone terrain, the slates are exposed close to Alaknanda River.

Dwing Village

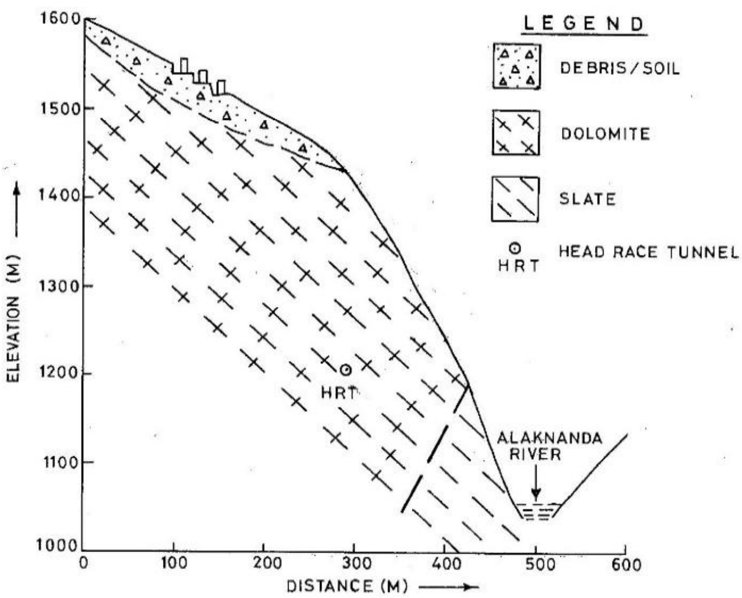

Fig 6.10 Geological section across slope in Dwing village

This village is located in between two well known streams namely Tirosi Gad and Dwing Gad within a pocket of debris (Fig 6.10). This is one location where the tunnel passes to the southeast of the village on the down slope direction. The terraces are located on the top level in the vicinity of the village, where the slope has an angle of about 20°. However, just further down, the slope increases suddenly to >45°. Though dolomitic limestones are present in the vicinity of village, it is delimited by slates on the southeastern direction towards Alaknanda River.

Jaisal Village

This village is located just adjoining Jaisal stream within a well defined debris pocket with a series of agricultural terraces (Fig 6.11). The entire village is located within a gentle slope with an overall slope angle of less than 15°. The thin debris present below the village extends in down slope direction obscuring the dolomitic limestones present below. However, close to the River Alaknanda, slates are exposed with steep slopes of more than 60°.

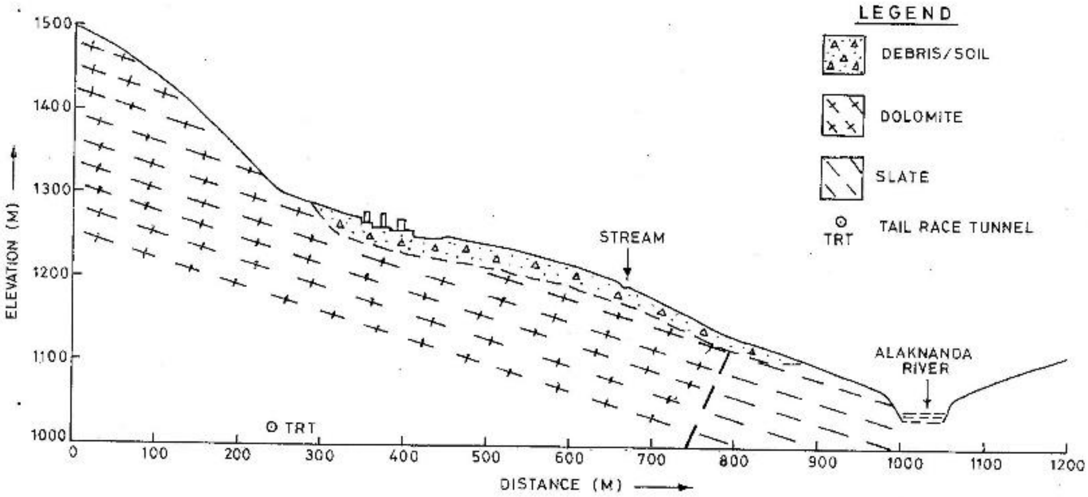

Fig 6.11 Geological section across slope in Jaisal village

<u>Dhari Village</u>

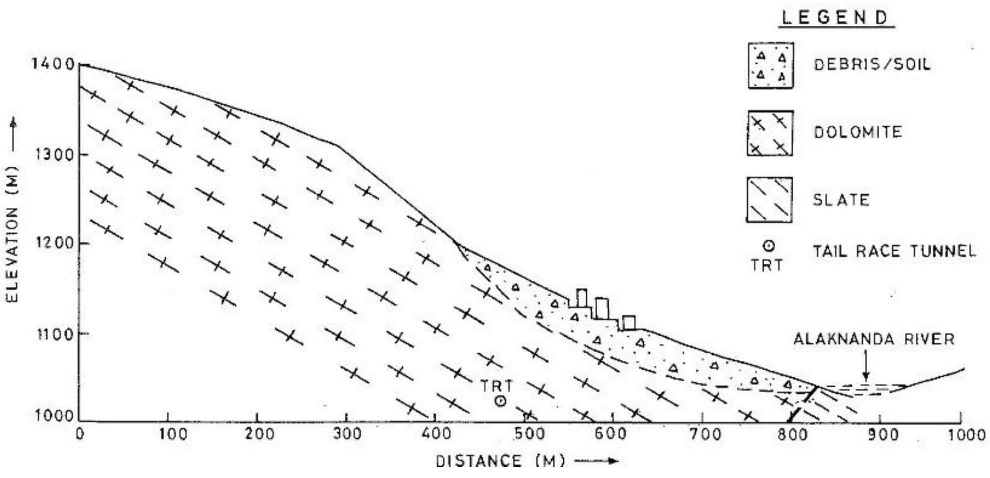

Fig 6.12 Geological section across slope in Dhari village

This village is located just close to outlet of TRT. The village is located on a thin debris zone present over dolomitic limestone rocks (Fig 6.12). The general slope angle is of the order of 25°-30° with local pockets of >45°. Since the TRT will be located close to the surface, the village has an important location from the point of view of stability of hill slopes due to blasting.

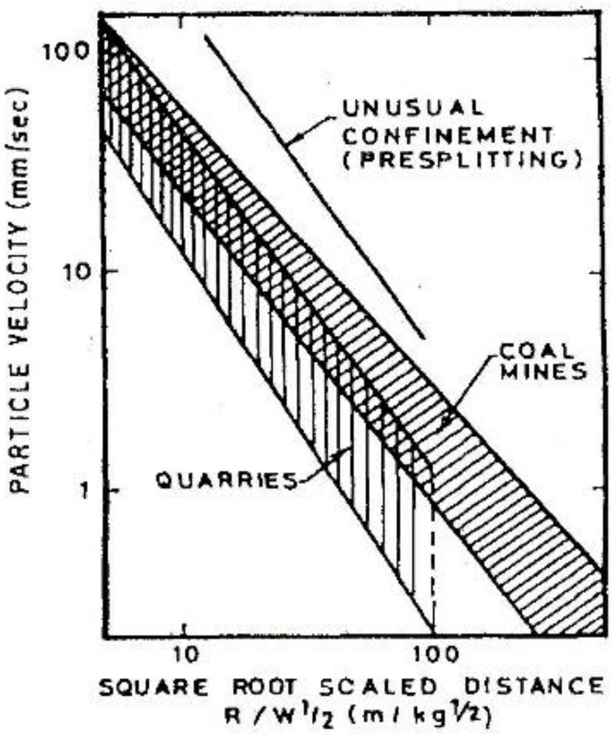

Fig 6.13 Attenuation relationships showing scatter

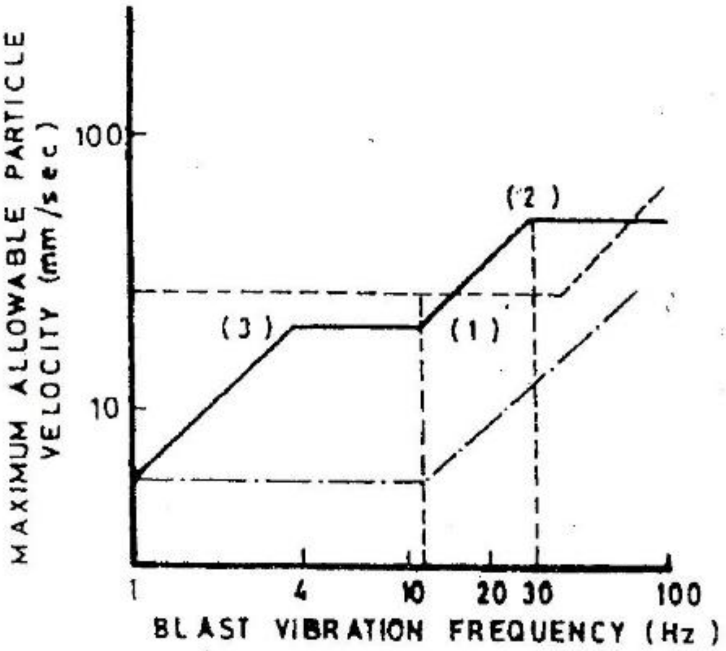

Fig 6.14 Frequency based blast vibration control to protect Residential structures

6.2 STABILITY ANALYSIS OF SLOPES

The terraces, on which the villages are located, have debris of varying thickness with bed rocks exposed below the debris. The instability of the terrain particularly within the debris may be caused mainly due to failure of the debris at its contact with the rock. Hence the general failure in the area will follow talus mode. Though failure may start with local slip circles initially, these circles will be delimited at depth due to presence of rocks at shallow depths. Hence, the failure surface will be essentially along the rock surface lying below the debris. Accordingly, talus failure analysis using computer program SAST has been carried out for these slopes. The program SAST (Stability analysis of slopes with talus mode of failure) is a versatile program to carry out analysis of slopes with possible talus mode of failure (Singh & Goel, 2002).

The input parameters used in the analysis have been indicated in the result outputs as the parameters differ from site to site. The results of stability analysis have been given in Annexures 1 to 11. The values of factor of safety obtained under different conditions of analysis have been given in Table 6.1. The result indicates the following:

i) All the slopes are stable under dry condition as well as under saturated conditions

ii) Most of the slopes are stable under dynamic condition as the factor of safety values are more than unity. Though these values for Jharetha, Surenda, and Dwing are marginally less than unity, in view of least displacement indicated, the slopes can be considered as moderately safe.

iii) The dynamic and saturated condition is unique and rare and hence generally not considered for the overall stability studies of the slopes.

Table 6.1:Results of Stability Analysis of Village Slopes Close to Power Tunnel

Village	Static Dry Condition	Static Dry +Saturated	Earthquake Dynamic	Earthquake Dynamic +Saturated	Safety of slope in terms of displacement
Jharetha	1.164	1.097	0.949	0.836	Moderately Safe
Surenda	1.139	1.070	0.927	0.815	Moderately Safe
Tirosi	2.055	1.773	1.513	1.292	Safe
Hyuna	1.834	1.550	1.407	1.175	Safe

Tapovan	1.594	1.305	1.228	0.989	Safe
Math-Dadheta	1.581	1.367	1.233	1.054	Safe
Pokhani	1.794	1.634	1.411	1.277	Safe
Langi	1.281	1.112	1.037	0.889	Safe
Dwing	1.147	1.081	0.936	0.820	Moderately Safe
Jaisal	2.465	2.013	1.799	1.452	Safe
Dhari	1.410	1.025	1.090	0.769	Safe

6.3 IMPACTS OF BLASTING IN AREA

A number of villages are located in the vicinity of the alignment of power tunnel, some of them close to the alignment and some of them sufficiently away from the alignment. For the villages considered above, the distance ranges between 140m to 580m. The village Dhari is located at a distance of 140m, which is closest of all the villages. In fact it is located close to the outfall of TRT. The village Hyuna is located far away (580m) from tunnel alignment. Inside the village, the houses are located in clusters. The impacts of blasting have been studied taking into consideration the nature of houses. The ground motion created due to blasting decrease with increasing distance. Based on a large number of vibration studies, it has been found that square root scaling or plotting peak particle velocity as a function of Distance R divided by the square root of the charge weight per delay ($R/W^{1/2}$) is the most reliable way (Mohamed M. T., 2010). Several square root attenuation relations are shown in the Fig 6.13. Here the maximum particle velocity is plotted as a function of scaled distance from the blast distance divided by the square root of the charge weight per delay

i.e.. PPV Vs $R/W^{1/2}$

Where

PPV = peak particle velocity (mm/sec),

R = scaled distance (m), and

W = Charge weight per delay

Though accurate estimation of safe charge weight per delay can be obtained for individual sites from blast tests at the sites, the same can also be estimated from already available data obtained on the basis of large numbers of case studies. The Fig 6.13 (I.S Code–14881:2001) indicates 3 specific cases namely quarries, coal mines and controlled blasting. In the present case, pre-splitting can be employed in order to keep the PPV under control mainly to protect the weak civil structures.

The maximum allowable PPV for various types of residential structures has been shown in terms of blast vibration frequency in Fig 6.14 (I.S Code–14881:2001). The dashed line in the figure corresponds to engineered structures and the dashed line (Corresponding to PPV=5) is recommended for older homes. However the experience shows that it may vary from 5 to 10. Accordingly analysis has been done taking lower to upper limits to be 5 to 10.

The villages have a cluster of houses. Hence the value R has been calculated from the location of the power tunnel and the centre of the village cluster. This value has been used in the analysis. Similarly the value of W has been obtained for both values of PPV (5 and 10mm/sec). In fact, the value $R/W^{1/2}$ can be obtained from graph in the Fig 6.13 for PPV values of 5 and 10mm/sec.

The values obtained have been given in Table 6. 2.

Table 6.2:Analysis of blasting impact for calculating safe charge weight per delay

Village	Peak Particle Velocity (PPV) mm/sec	Scaled Distance (R) m	$R/W^{1/2}$	Charge Weight per delay (W) kg	Recommended max. charge per hole kg	No. of holes per delay
Jharetha	10	400	47	72.4	10-15	7-8
	5	400	77	26.9	10-15	7-8
Surenda	10	275	47	34.2	10-15	7-8
	5	275	77	12.7	10-15	7-8
Tirosi	10	215	47	20.9	10-15	7-8
	5	215	77	7.8	7.8	6
Hyuna	10	580	47	152.28	10-15	7-8
	5	580	77	56.73	10-15	7-8
Tapovan	10	220	47	21.9	10-15	7-8
	5	220	77	8.2	8.2	6
Math-Dadheta	10	340	47	52.3	10-15	7-8
	5	340	77	19.49	10-15	7-8
Pokhani	10	450	47	91.67	10-15	7-8
	5	450	77	34.15	10-15	7-8
Langi	10	385	47	67.1	10-15	7-8
	5	385	77	25	10-15	7-8
Dwing	10	425	47	81.76	10-15	7-8
	5	425	77	30.46	10-15	7-8
Jaisal	10	275	47	34.2	10-15	7-8
	5	275	77	12.75	10-15	7-8
Dhari	10	140	47	8.87	8.87	7
	5	140	77	3.3	3.3	4-5

It is recommended to have controlled blasting (Grothe and Reinders, 2007) with individual pulls upto 3.5m, which indicates that the depth of drill holes to be charged will be limited to 2 to 2.5m. The length of individual cartridge is about 20cm with a weight of about 200gm. The total number of cartridges in a hole may range between 7-8. It indicates that the total weight of all cartridges within a hole will be 1.4kg. Since the total weight permitted per delay is 10-15kg, one delay has to be used for every 7-8 holes in general. In case of controlled blasting, it may be planned to have 5-7 holes per delay in cut holes with Easers 15-20 holes on the periphery. Stemming length in each hole shall not be less than 0.8m.

In fact the total charge weight per delay is much more as per the actual calculation. But since the permitted weight of charge weight per delay is only 10-15kg, the Table 6.2 does not show any difference in terms of weight of explosives and number of holes for 10PPV as well as 5PPV. There is only one exception that is Dhari village. Since Dhari village is located close to the alignment, it indicates W to be 3.3kg and Number of holes per delay to be 4-5 for drillhole length of 1-1.5m inside the tunnel. It is manageable since the length of the reach is much limited and hence may not create any undue field problems.

6.4 CONCLUSIONS AND RECOMMENDATIONS

The study related to the impacts of blasting in underground excavations indicates the following aspects.

1. A number of villages are located close to the power tunnel and tail race tunnel.

2. These villages are mostly located on debris materials, which are comparatively thin (as compared to the size of the slope and extension of rocks below) with the maximum thickness ranging from 15 to 40m.

3. These slopes were analyzed using computer program SAST for different conditions like static dry, static saturated, dynamic dry and dynamic saturated conditions.

4. The stability analysis of these slopes indicates that the slopes are stable in static condition. However the slopes around villages Jharethat, Surenda Tapovan, Lanji,

Dwing and Dhari indicate possible unstable conditions during dynamic saturated conditions. Though this condition (dynamic and saturated) is a very rare combination and generally not considered, In view of importance of study area, these slopes were studied with respect of nature of displacement in dry and wet conditions. On that basis, most of the villages fall in safe zone. The villages Jaretha, Surenda and Dwing, fall in moderately safe zone indicating that they are just stable in dynamic conditions considering the least displacement during earthquakes. (Table 6.1).

5. The impact of blasting from the underground excavations has been analyzed by preparing cross sections of the slope of the villages and projecting the location of the underground structure namely power tunnel in the cross section.

6. The analysis has been done using the distance between the underground structure and the houses. Similarly analysis has been done with PPV values of 5 and 10mm/sec.

7. Based on the analysis and taking into consideration the existing site conditions, it is recommended to use charge weight per delay value of 10-15kg, which may be distributed in 7-8 holes with a delay detonator. This will help in the excavation of power tunnel without creating any cracking of the buildings located in adjoining villages.

8. Controlled blasting is recommended for tunnel blasting with individual pulls upto 3.5m. In case of controlled blasting, it may be planned to have 5-7 holes per delay in cut holes with Easers 15-20 holes on the periphery. Stemming length in each hole shall not be less than 0.8m.

9. Since the permitted weight of charge weight per delay is only 10-15kg, there is no difference in terms of weight of explosives and number of holes for 10PPV as well as 5PPV.

10. The village Dhari is located close to the alignment in the tail reaches of TRT, the analysis indicates the value for W to be 3.3kg and number of holes per delay to be

4-5 for drill hole length of 1-1.5m inside the tunnel. Since the length of the reach is much limited, the above restrictions in blasting can be easily managed.

11. Regarding the actual damages due to blasting in power tunnel, if the recommended weight per delay is adopted, no adverse impacts are anticipated due to blasting at these locations as substantial attenuation of seismic waves may take place on surface.
12. It may be noted that construction blasts involve smaller explosions with small travel distance. Moreover the rock to rock transmission paths tend to produce high frequency waves with less potential for cracking adjacent structures. However it is recommended to monitor the actual blast vibration and assess the damage potential of the vibrations of ground settlement during construction stage.

13. There are several peaks of acceleration in the seismic vibrations, whereas there is only single peak of acceleration in blast induced vibrations. Thus the later ones are less dangerous to the houses compared to earthquakes. The real danger to the houses is from the earthquake induced vibrations and differential settlements due to excessive water saturation. In this context, the villages Jaretha, Surenda and Dwing are worth mentioning, which show tendency for failure during earthquake with saturation.

CHAPTER VII

STABILITY STUDIES OF UNDERGROUND POWERHOUSE

In the recent times, the underground space technology has gained greater importance to overcome the problems of space shortage and to accommodate the strategically important projects. It is an engineering challenge to design and construct a powerhouse cavity in tectonically active, rough topographic terrain with complex geological condition like Himalaya. The excavation for power house cavern in a tectonically distrusted hilly terrain poses adverse stability problems that are governed by the geological discontinuities, rock mass properties, size and shape of the powerhouse, in-situ stresses, support measures, method of excavation and the sequence of construction (Anabalagan et al, 1996). The strength and deformational response of jointed rock masses is an essential requirement in the site selection, design and successful execution of Engineering projects (M Singh at al, 2002). To design and construct economically it is necessary to study and evaluate the rock mass condition, strength parameters and stability problems.

In the present work, the above mentioned parameters have been evaluated as part of stability studies. Hence, the stability of powerhouse includes the following work components.

i) Geological Mapping of Powerhouse area

ii) 3D logging of exploratory drift

iii) Geological cross section across the powerhouse cavity

iv) Characterization of Rock Mass–RQD, RMR, Q and GSI

v) Stability analysis for unstable rock wedges on roof & sidewall

7.1. GEOLOGY OF POWERHOUSE AREA

Power house is located on the right bank of river Alaknanda. The powerhouse area is bounded on the northern side by Hat village and Jaisal nala on the southern side (Fig 7.1). The rocks exposed in the powerhouse area belong to Pipalkoti Formation of Garhwal Group. The rocks seen in the area mainly fall in two types- Black greyish thinly foliated slates and brownish grey colored well jointed dolomitic limestone. On the surface, the rocks are mostly covered by debris derived from the old landslides on the levels above the existing bridle path. The rocks are visible only close to the river bed and on the adjoining stream cut faces. In addition, river borne materials (RBM) spread extensively on the terrace present on the eastern side. The RBM is seen mainly on two major levels of terraces. The lower level terrace is seen close to river bed on which maximum clusters of houses are located. Agricultural terraces are mainly seen on the top level with a few houses. The top level terrace is a larger one having a length of more than 500m. While the slates are seen exposed close to the river bed and extend further upwards, the dolomitic limestones are exposed in the upper levels and on the hill slopes in higher levels. The contact between the two lithologies is concealed below the debris and river borne materials. The surface geological mapping of the proposed power house area upstream of suspension bridge has been carried out on 1:1,000 scale (Fig 7.2). Pyritiferous phyllitic slates dipping at 20° to 25° towards N310°-N 10° direction are exposed near the river level.

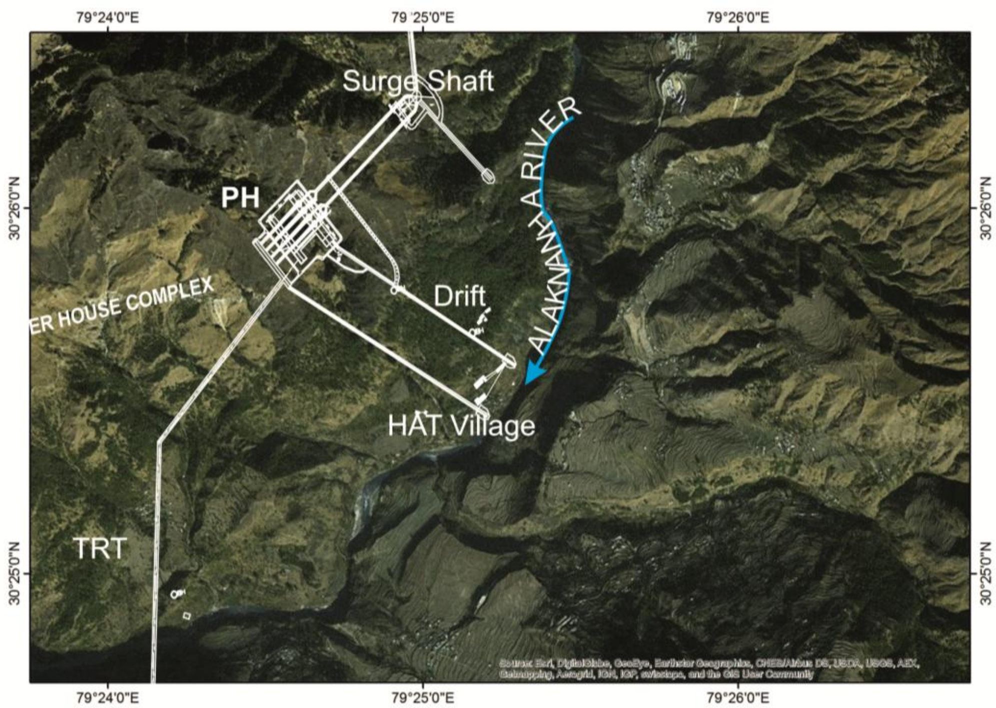

Fig 7.1 ArcGIS image of powerhouse area showing the layout of powerhouse

These are very tightly folded. Further above, the hill slope is mainly covered with debris and RBM with scanty outcrop of shale / slate. The massive to moderately jointed dolomitic limestones are exposed at higher levels and dip at 25° to 30° towards N320°W into the hill. The geological discontinuities observed in different rock units are presented in Table 7.1. An exploratory drift at EL 1057.63 m has been excavated in a general N50° W direction at the proposed location of the powerhouse for understanding the geology, rock mass parameters and for conducting in-situ field tests.

Table 7.1. The structural discontinuities obtained for PH from stereonet projection

Slates			
Type of discontinuity	**Dip Amount**	**Direction**	**Spacing (cm)**
Foliation (FJ)	25°-30°	N310°-N10°	15-30
Joint J1	55°-70°	N20°	2-30
Joint J2	30°-70°	N120°	5-10
Dolomitic limestones:			
Foliation (FJ)	60°	N120°	5-10
Joint J1	60°-65°	N215°	10-15
Joint J2	60°	N65°	5-10

Black greyish thinly foliated slates having strike N60°E with dip 25° towards N 150° direction are exposed at the river level from the suspension bridge of the Hat village to a Nala near the temple of Hat village (Fig 7.1). Near Hat village, the foliation planes of slates have a strike N35° to 60°E with an average dip of 30° towards NW to NNW direction that is into the hill. It also exhibits on the surface the impact of hot water movement in the geologic past within the rocks by presence of grey coloured very fine powdery substances. Here, two sets of joints are observed. They are given below:

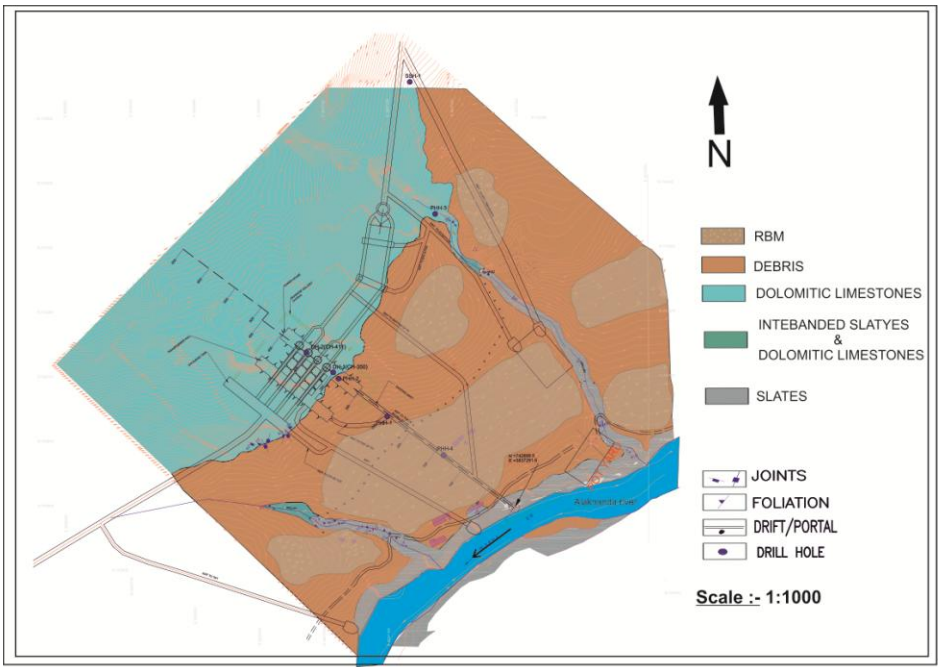

Fig 7.2 Geological map of powerhouse area

7.2. SUBSURFACE EXPLORATIONS

The subsurface exploration at the powerhouse site includes drill holes 4 nos. and a drift extending for 680m length. The drill holes are mainly intended to decipher the depth of debris over burden and to obtain data related to RQD of rocks and other rock characteristics. The drill holes namely PHH 1, PHH 2, PHH 3 and PHH 4 were logged and the drill log data is presented in Table 3.7. The lone exploratory drift excavated in N50ºW direction reaches up to the proposed power house location. The 3D log of the entire drift have been carried out (Fig 7.5a to 7.5d)

7.2.1 Drilling:

Four drill holes were drilled at different locations going up to a maximum depth of 150m. The drill logs are presented in Table 3.7. A perusal of the drill logs indicate the following

i) The thickness of debris varies from 9 to 17m above the proposed powerhouse location.

ii) Two drill holes namely PHH1 and PHH2 are located on the lower slate bed and hence penetrates single lithology, that is slates. Two more drill holes PHH3 and PHH4 are located on located on dolomitic limestones. These drill holes encounter slates at depth.

iii) The percent core recovery varies from 10% to 90%. However, the core recovery is more than 80% in most of reaches. The low core recovery zones are often seen in shallow depth or where the rocks are highly jointed.

iv) The rock quality designation (RQD) similarly varies from 10% to 81%. In segments, where slates are exposed the RQD is generally poor, less than 20% in many reaches. Wherever slates are massive the RQD shows improvement up to 40%. In the segments of dolomitic limestones the RQD shows slight improvement as compared to slates. Though the values range up to 40%, the core recovery poor intermittently at many places.

7.2.2 Drifting:

The drift was excavated up to a length of 680m for understanding the rock types, its nature, rock mechanics properties and to conduct in-situ field tests for design of the powerhouse. This drift is located on the right bank of river Alaknanda near Hat village. The drift is driven from El.1057.63m in a general N50ºW direction. The excavated dimension of the drift is 2m height between the crown and the floor as well as 1.8m width between the walls. In the interior stretch of the drift, water dripping is seen in large scale and the collected water flows out continuously with a measurable depth of about 30cm. The water inflow shows increase in tendency during rainy season. The entire stretch of exploration drift has been mapped 3 dimensionally showing lithological and structural variations.

The drift is unsupported in most of its length but in view of poor rock condition and possibility of rock fall, the drift has been supported between RD 60m and 65.5m as well as RD 130m and 140m. Pyritiferous phyllitic slates are exposed in the intial reaches of the drift and it continues up to RD 439m. The slates are fresh, dark grey colored, dense, occasionally iron stained, pyritiferous and calcareous in nature. The slatey cleavage/foliation are well developed and the joints show short continuity along the strike. The old traces of bedding plane seen in the slate are nearly parallel to the foliations. After RD 439m, phyllitic slates and dolomitic limestones are seen interbanded up to RD 460m. Later dolomitic limestones are exposed continuously till the end of the drift.

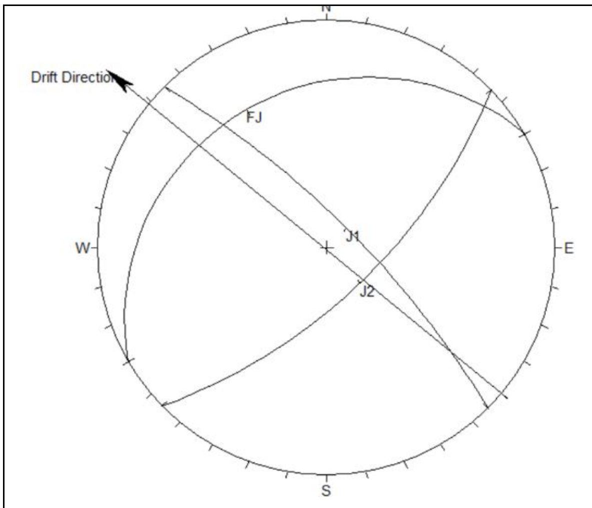	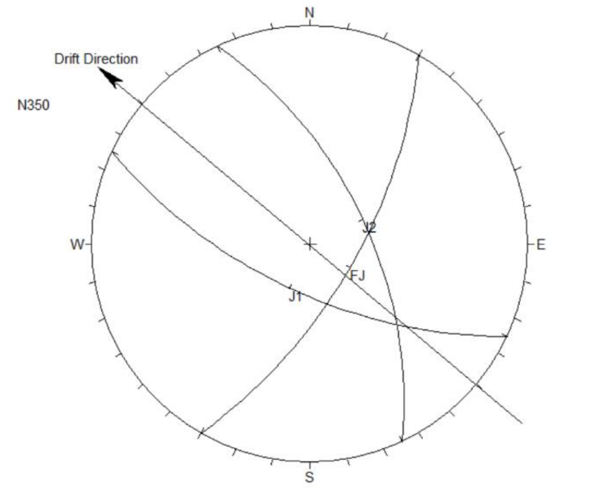
Fig 7.3 Stereoplot for left limb of syncline	**Fig 7.4 Stereoplot for right limb of syncline**

The foliation, being the major geological discontinuity dips at moderate angles of 25°-35° towards NNW. In addition, two sets of joints with close spacing are distinctly visible (Table.7.1). The rocks are acutely folded on small scale at places. The site observations and the 3D geological mapping at the exploration drifts indicate the following.

i) The dense and moderately foliated slates are present in the initial stretches of the drift up to about RD 480m. Later, dolomitic limestones are encountered till the end of the drift.

ii) The contact of slate / dolomitic limestone is gradational (RD 460m). The contact is marked by alternating bands of slates and dolomitic limestones over a distance of more than 20m. Later dolomitic limestones are continuously exposed.

iii) The foliation in general, dips at moderate angle of 25°-35° towards NNW in the initial portions of the drift and later it gets flattened to even 10°-20° from RD 500m onwards.

iv) The general foliation shows a reverse trend at about RD 580m with nearly similar shallow dips of 15°-25° towards NE to ENE directions. From this it can be deciphered that the reversal in dip direction is due to a major geological structure, that is, a syncline.

v) Since the beds dip towards each other, the water seeping through both the limbs gets collected at the hinge area. The collected water is appreciably of higher order that it flows continuously with a depth of 30cm.

vi) Two important sets of joints (J1 and J2) have been observed. While joint set J1 has greater continuity of more than 2–3 m, the joint set J2 has lesser continuity of about 1 m or even less. The geological discontinuities observed in the area are indicated in Table 7.2 based on stereonet analysis.

vii) Originally a powerhouse cavity was proposed with the centre line at RD 580m, incidentally coinciding with the hinge of the syncline. In view of excessive seepage at this location as explained above, this location is not a suitable one for the powerhouse cavity as continuous seepages within the cavity will cause instability and other related problems.

viii) Based on three 3D mapping of the powerhouse, the PH cavity had been shifted to RD 380m. Here rocks dip at moderate angles towards NNW. In the proposed location, slates are exposed in most parts of the powerhouse. Dolomitic limestones could be seen in certain portions in the roof region.

Table 7.2 Structural details of synclinal fold limbs obtained from 3D drift log

Type of Discontinuity	Left Limb of the syncline		Right Limb of the Syncline	
	Dip Amount	Dip Direction	Dip Amount	Dip Direction
Foliation	20°	N330°	10°	N120°
Joint J1	76°	N45°	65°	N205°
Joint J2	66°	N136°	60°	N65°

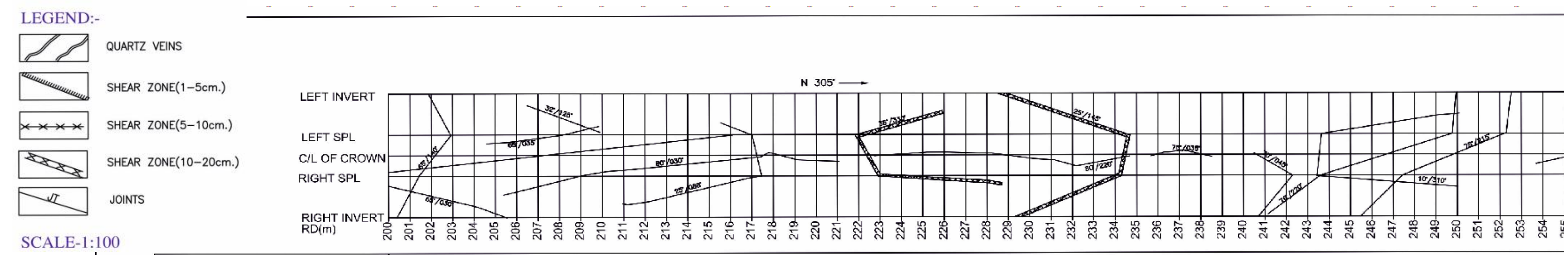

		ROCK TYPE	SLATE			SLATE		SLATE
		STRENGTH	R5			R4	R5	
		WEATHERING	Unweathered with grade W0					
		GROUND WATER		Dry		Dry		
Structural details	F/J1	AV. ORIENT	27°/040°	15°/45°	15°/45°	15°/45°	27°/310°	5°/310°
		SPACING mm.	15cm to 50cm	20cm to 50cm	10cm to 20cm	10cm to 20cm	10cm to 60cm	5cm to 10cm
		APERTURE	Tight	Tight	Tight	Tight	Tight	Tight
		CONDITION	Rough Undulating	Rough Undulating	Rough Undulating	Rough Undulating	Rough Undulating	Rough Undulating
	J2	AV. ORIENT	65°/030°	85°/030°	85°/030°	85°/030°	85°/215°	85°/215°
		SPACING mm.	5cm to 30cm	20cm to 30cm	20cm to 30cm	20cm to 30cm	20cm to 50cm	5cm to 15cm
		APERTURE	Tight	Tight	Tight	Tight	Tight	Tight
		CONDITION	Rough Undulating	Rough Undulating	Rough Undulating	Rough Undulating	Rough Undulating	Rough Undulating
	J3	AV. ORIENT	32°/120°	67°/120°	67°/120°	67°/120°	60°/85°	45°/135°
		SPACING mm.	10cm to 50cm	20cm to 40cm	20cm to 40cm	20cm to 40cm	10cm to 15cm	15cm to 25cm
		APERTURE	Tight	Tight	Tight	Tight	Tight	Tight
		CONDITION	Rough Undulating	Rough Undulating	Rough Undulating	Rough Undulating	Rough Undulating	Rough Undulating
		EQUAL AREA LOWER HEMISPHERE PROJECTION OF DEFECT SETS	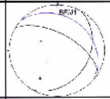				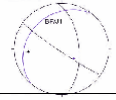	
		RMR/ROCK CLASS	67/Class II	68/Class II	66/Class II	63/Class II	67/Class II	64/Class II
		GSI	62	63	61	58	62	59
		Q-Value	22	20	23	20	22	18

200 201 202 203 204 205 206 207 208 209 210 211 212 213 214 215 216 217 218 219 220 221 222 223 224 225 226 227 228 229 230 231 232 233 234 235 236 237 238 239 240 241 242 243 244 245 246 247 248 249 250 251 252 253 254

Fig 7.5a 3D Geological log of powerhouse drift for RD 200m to 254m

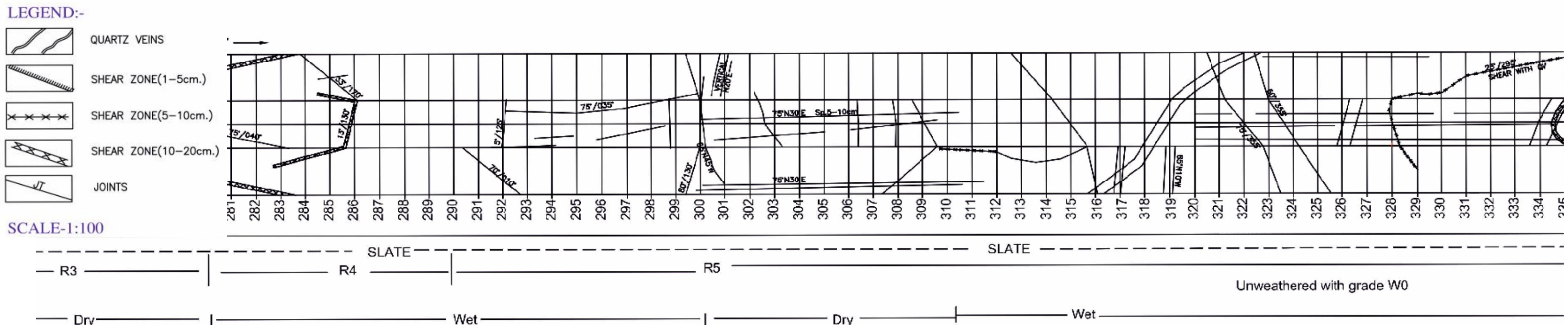

15°/30° 1cm to 5cm Tight Rough Undulating	7°/30° 6cm to 30cm Tight Smooth Undulating	7°/30° 6cm to 30cm Tight Smooth Undulating	7°/30° 6cm to 30cm Tight Smooth Undulating	7°/30° 6cm to 30cm Tight Smooth Undulating	10°/035° 20cm to 50cm Tight Smooth Undulating
75°/80° 6cm to 33cm Tight Rough Undulating	75°/30° 5cm to 33cm Tight Smooth Undulating	75°/30° 5cm to 33cm Tight Smooth Undulating	75°/30° 5cm to 33cm Tight Smooth Undulating	75°/30° 5cm to 25cm Tight Smooth Undulating	75°/030° 10cm to 30cm Tight Smooth Undulating
45°/135° 15cm to 25cm Tight Rough Undulating	70°/120° 20cm to 30cm Tight Rough Undulating	70°/120° 20cm to 30cm Tight Rough Undulating	70°/120° 20cm to 30cm Tight Rough Undulating	70°/120° 20cm to 30cm Tight Rough Undulating	20°/125° 20cm to 30cm Tight Rough Undulating
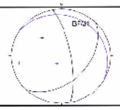		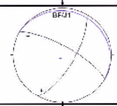			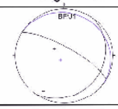
62/Class II 55 12	64/Class II 59 12	63/Class II 58 13	63/Class II 58 14	65/Class II 60 14	65/Class II 60 20

Fig 7.5b 3D Geological log of powerhouse drift for RD 275m to 334m

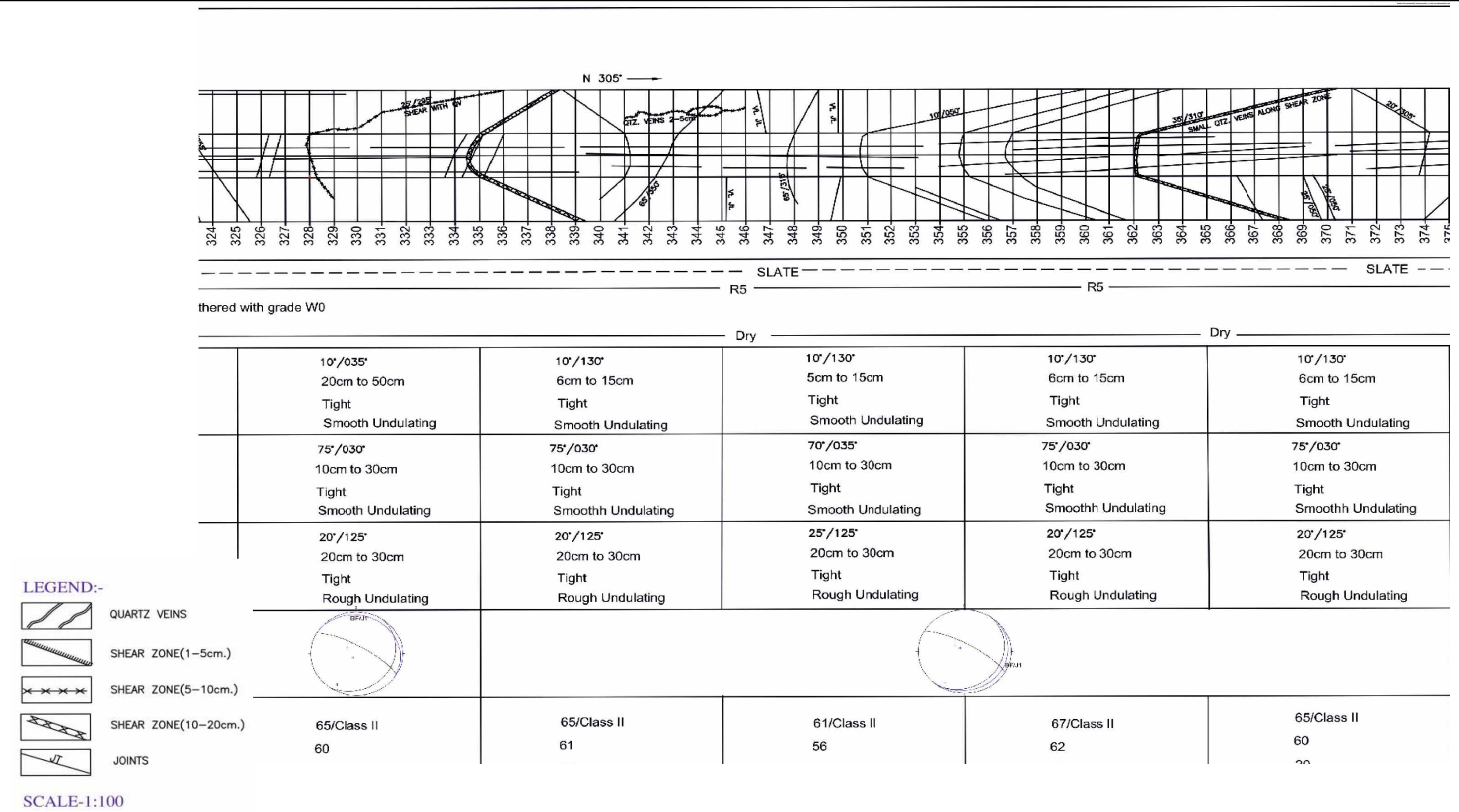

Fig 7.5c 3D Geological log of powerhouse drift for RD 325m to 374m

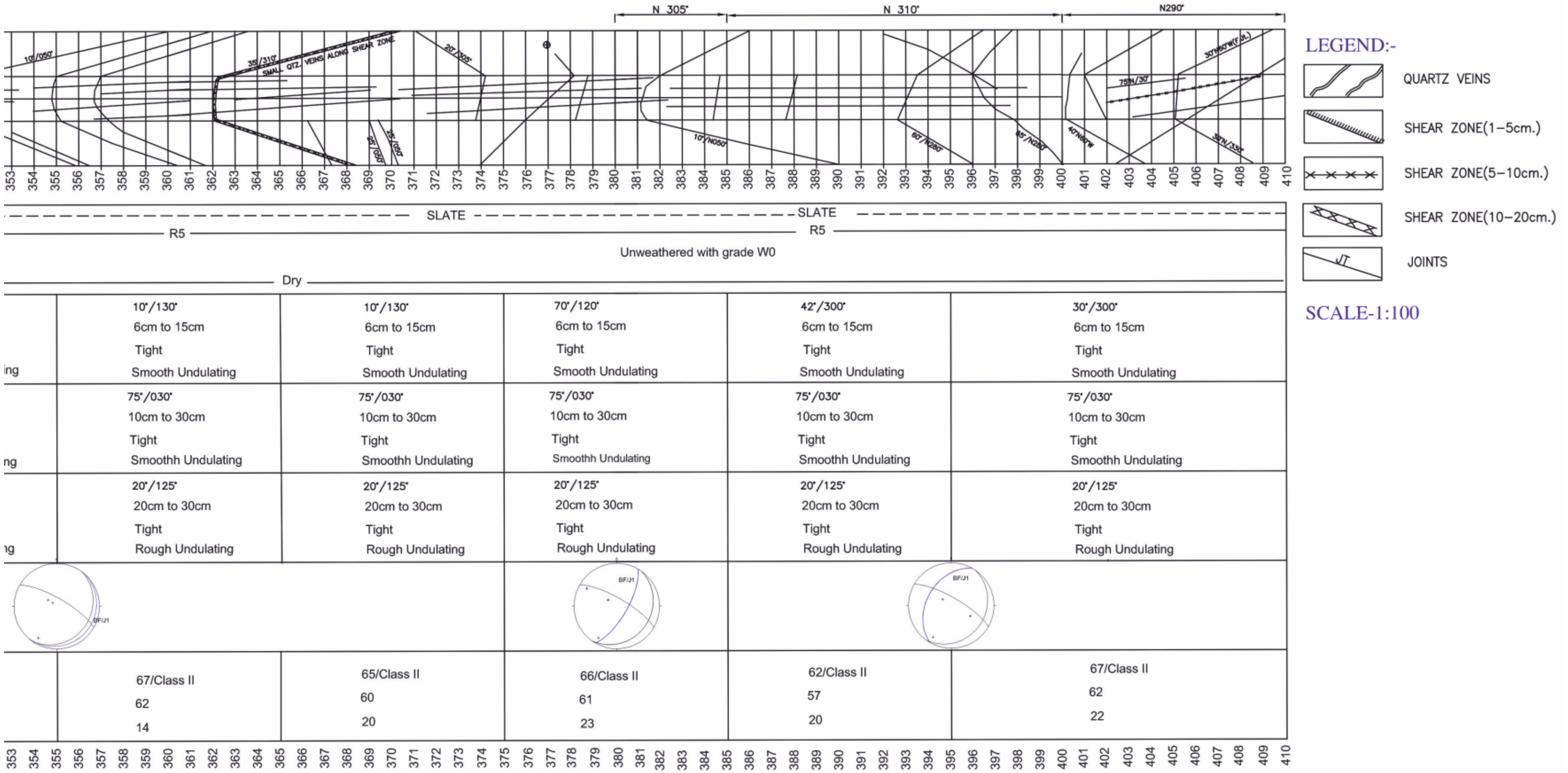

Fig 7.5d 3D Geological log of powerhouse drift for RD 353 m to 410m

The 3D drift logging indicates that foliations coinciding with the contact of dolomitic limestones/slates show a reverse trend inside the power house area indicating that the bedding has been folded into a broad, open and upright syncline.

If the location of the power house is introduced in the section (horizontally extending between Ch 530m and 630m and vertically extending from El. 1100m down to 980m), the fold axis will be located within the power house area (Fig 7.6).

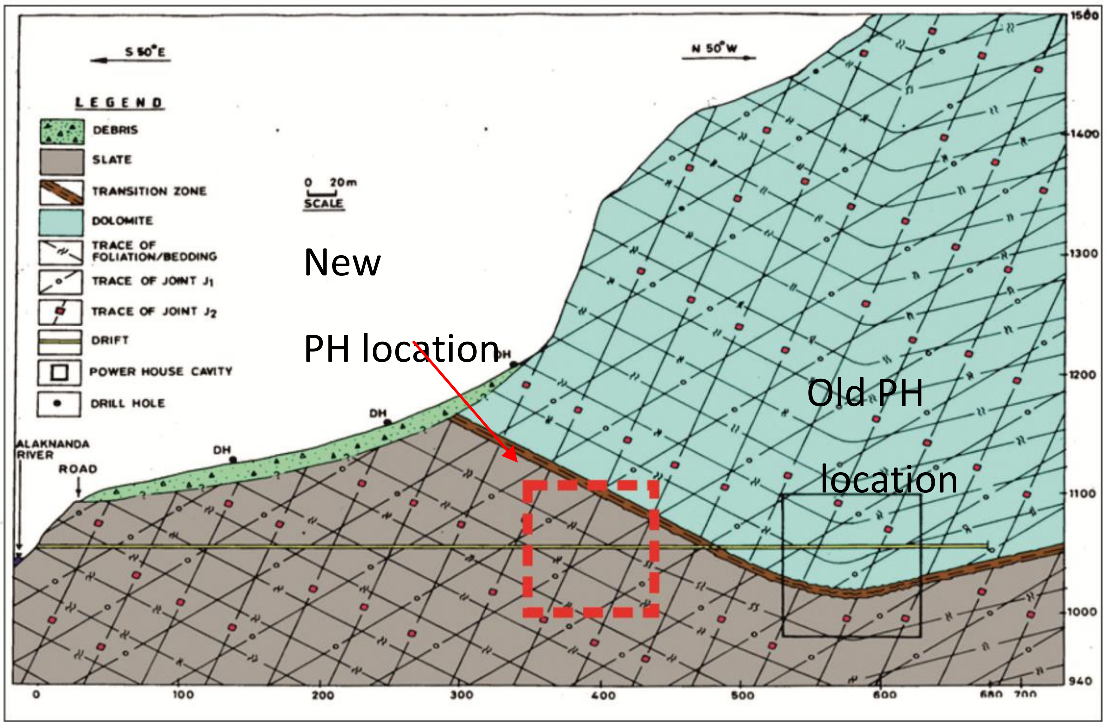

Fig 7.6 Geological cross section across powerhouse location with drift location and structural data obtained from 3-Ddrift log projected showing the synclinal fold axis.

In case of a syncline present within the power house cavity, both the limbs dip towards each other. The southeast limb dipping into hill from valley side present below the debris may cause seepage of subsurface water from debris toward the fold axis inside the power house. Similarly, the seepage from the northwest limb also will flow towards the fold axis causing excessive seepage inside the power house area. It is a major disadvantage in case of a syncline with fold axis present within the power house. It is suggested that power may be slightly shifted towards the valley side at RD 400 so that the powerhouse caver will be located within one limb of syncline (Fig 7.6). This helps in minimization of seepage. Wide zones of closely fractured slate have been encountered only beneath the Power House drift from about Ch 500m to the end. Excavations in the Power House Complex will encounter shears, faults, foliation partings and other geological defects which will combine to form unstable blocks and wedges in the walls of the excavations. The main cavern axes have a direction of 310° which is the same as the general dip direction of foliation in both slates and dolomitic limestones. This is a favourable direction to minimise the volume of kinematically admissible failures in the main caverns (Fig 7.3).

7.3 CHARACTERIZATION OF ROCK MASS- RMR, Q AND RQD

The rock mass parameters were calculated for slate and dolomitic limestones from the observed joint parameters in the drift (El. 1057.63m) the obtained results are presented in Table 7.3.

Table 7.3 Calculated RMR, GSI & Q between RD 200–410 in hat powerhouse drift

RD(m)	Average RMR	Class	Description	Average GSI	Q
200-205	67	II	Good	62	22
206-215	68	II	Good	63	20
216-225	66	II	Good	61	23
226-235	63	II	Good	58	20
236-245	67	II	Good	62	22
246-255	64	II	Good	59	18
256-265	72	II	Good	67	15
266-275	63	II	Good	58	12
276-285	62	II	Good	55	12
286-295	64	II	Good	59	12
296-305	63	II	Good	58	13
306-315	65	II	Good	58	14
316-325	65	II	Good	60	14
326-335	65	II	Good	60	23
336-345	65	II	Good	61	13
346-355	65	II	Good	56	14
356-365	61	II	Good	62	20
366-375	67	II	Good	60	23
376-385	65	II	Good	61	20
386-395	66	II	Good	57	22
396-410	67			62	22
410 Cross-Cut (0-10m)	64	II	Good	57	21
(10-20m)	65	II	Good	60	20
(20-30m)	65	II	Good	61	21

7.3.1 Field estimation of JRC and JCS

Determination of joint shear strength parameters are very essential for carrying out the stability analysis. As the analysis required joint shear strength parameters based on Barton and Bandis method the Joint roughness coefficient (JRC) and the joint wall compressive strength (JCS) are the two parameters are the governing factors for determination of factor of safety of the sliding wedge inside the tunnel soon after excavation.

The joint roughness coefficient JRC was estimated for slates in the power house area by following Barton and Choubey 1997 method. The JRC values estimated by comparing the appearance of discontinuity surface with standard chart were recorded and their representative values are presented in Table 7.4

The joint wall compressive strength JCS were estimated in field by adopting ISRM (1978) standard with the use of Schmidt hammer. The data were recorded in power house area and inside the exploratory drift. The obtained values were recorded and their representative values are present in Table 7.5. Necessary cautions were taken while estimating.

Table 7.4 The representative values of JRC and JCS for slates and dolomitic limestone (Barton and Choubey, 1977)

	Foliation		**J1**		**J2**	
Location	**JRC**	**JCS**	**JRC**	**JCS**	**JRC**	**JCS**
L1 (Near temple)	8	20	8	24	8	22
L2 (Nala)	12	27	6	22	8	22
L3 (Near Drift)	11	25	6	23	8	22
L4 (Close to river below drift)	14	20	6	22	7	22
L5(Drift RD 200-300m)	10	21	8	20	8	23
L6(Drift RD 300-400m)	12	20	6	20	8	22

The residual friction angle φ_r was estimated following Barton and Choubey (1977) model

$$\phi_r = (\phi_b - 20) + 20(r / R)$$

Where

φ r	=	Residual friction angle
φ b	=	basic friction obtained for laboratory tests
r	=	Schmidt rebound number wet and weathered fractured surface
R	=	Schmidt rebound number on dry and unweathered surface

The residual friction obtained for various

Table 7.5 The average (φ r) obtained for various discontinuities

Foliation Avg (φ r)	J1 Avg (φ r)	J2 Avg (φ r)
27°	30°	28°

7.4 STABILITY ANALYSIS FOR UNSTABLE ROCK WEDGES AT ROOF & SIDEWALL

Wedge Analysis of Underground Powerhouse (Unwedge)

Professor Hoke developed a software Unwedge software work based on Goodman and Shi's block theory. This has an ability to incorporate induced stress around the excavation and the effect on stability, new strength models such as Barton-Bandis and Power Curve, and the ability to improve the scaling and sizing of wedges.

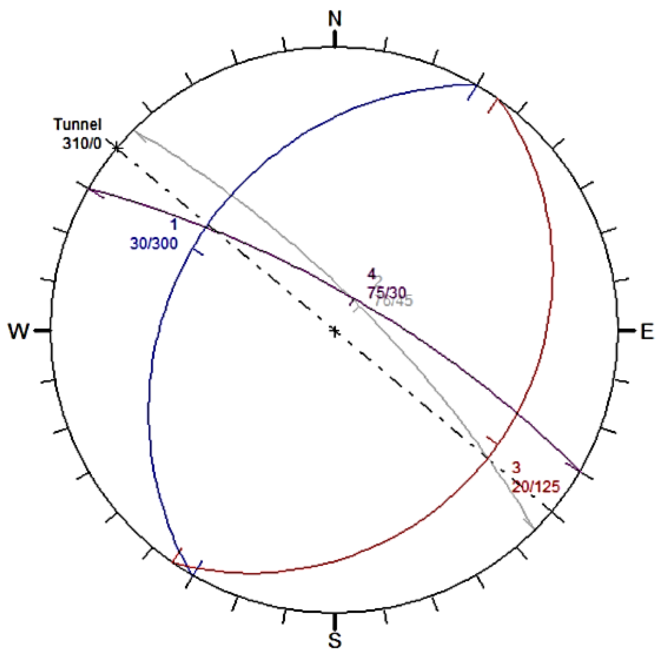

Fig 7.7 Stereoplot analysis showing the possible wedges along the PH alignment.

Vishnugad-Pipalkoti Hydroelectric project constitutes an underground powerhouse cavern with dimension 146 m x 20.3 m x 50 m

In the present analysis shear strength parameters suggested by Barton and Bandis were used. The discontinuity data set recorded between RD 350-450m were incorporated (Table 7.6).

For this analysis the essential shear strength input parameters are JRC, JCS and φ r

Table 7.6 Data set used in for wedge analysis recorded between Rd 350-450m

Sl.no	**Dip amount**	**Dip Direction**
Foliation/ Bedding FJ	30	300
J1	75	30
J2	20	125

The wedge analysis was carried out to identify the different types of wedges that are likely to be formed, their position, unit weight, volume and stability of wedges with low FOS <1. The analysis indicates that seven types of wedges are likely to be encountered between RD 350-450m (Fig 7.8).

Fig 7.8 The possible stable and unstable wedges formed along the PH alignment for RD 350-450m

The type of wedges formed by the combination of discontinuities are as follows.

Wedge Information

Floor wedge [1]
Factor of Safety: Stable
Wedge Weight:\0.026 MN

Upper Right wedge [4]
Factor of Safety: 2.725
Wedge Weight: 3.278 MN

Floor wedge [5]
Factor of Safety: 4.560
Wedge Weight: 14.481 MN

Roof wedge [7]
Factor of Safety: 0.872
Wedge Weight: 2.308 MN

Roof wedge [8]
Factor of Safety: 0.000
Wedge Weight: 0.230 MN

Near End wedge [9]
Factor of Safety: 3.310
Wedge Weight: 0.646 MN

Far End wedge [10]
Factor of Safety: 6.098
Wedge Weight: 0.646 MN

Total seven number of wedges are formed along the power house alignment. However only two wedges namely wedge no 7 and 8 are unstable with FOS<1.5. These wedges are located to the roof (Fig 7.9 & Fig 7.10) with FOS 0.87.

The wedge number7 is located on the up left roof corner and the wedge number 8 is posited on roof (Fig 7.10). The required support pressure was also estimated from the analysis indicate that the required support pressure for both wedges are 0.02MPa.

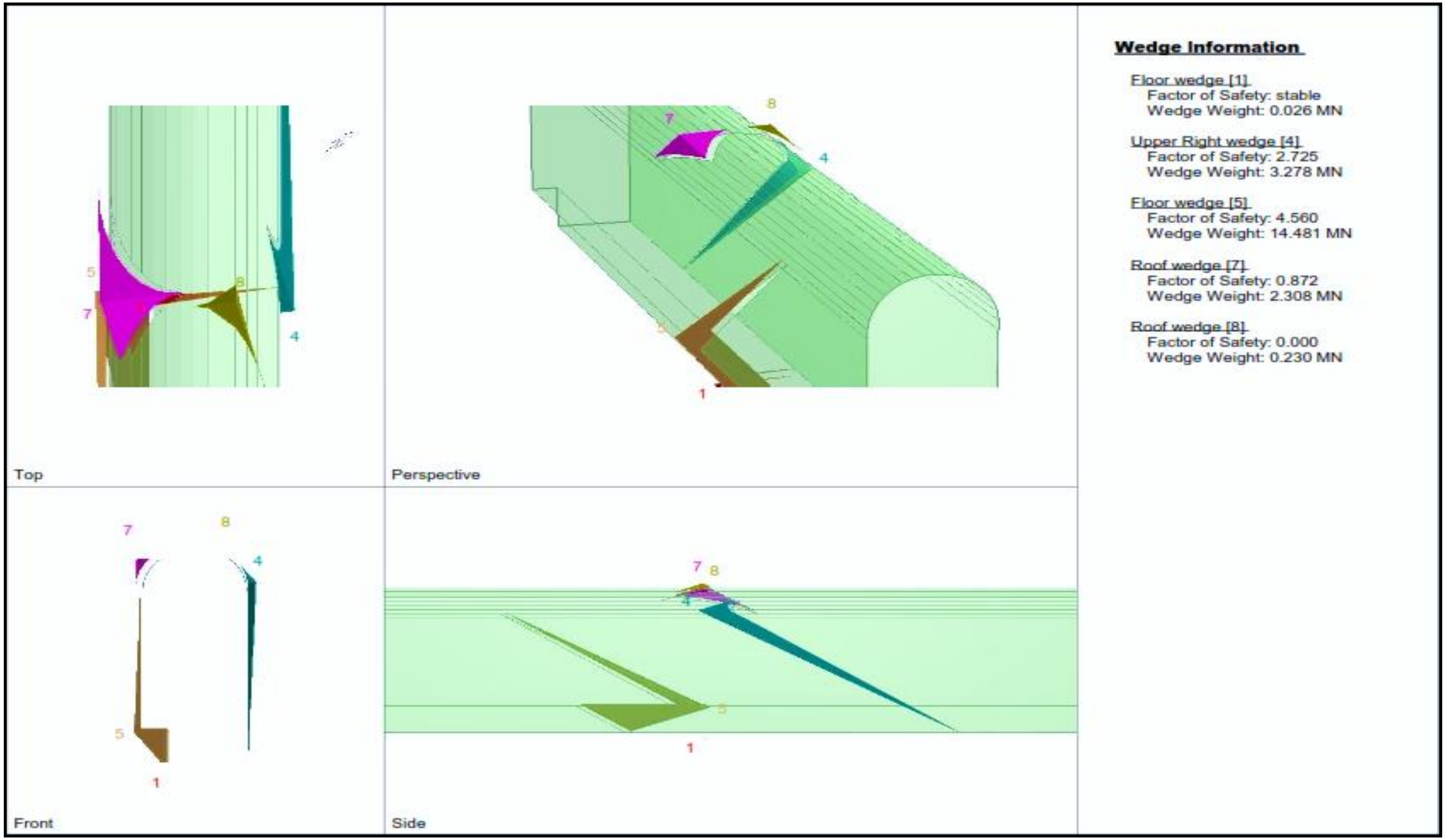

Fig 7.9 The Unstable wedges formed along the powerhouse alignment

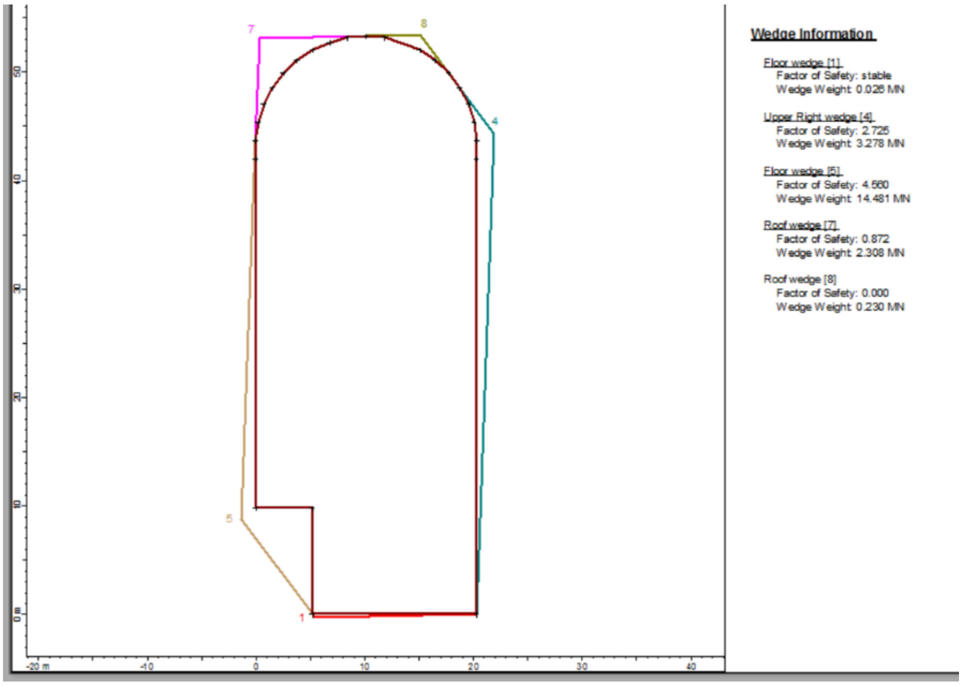

Fig 7.10 Wedge analysis showing possible major wedge on top right roof and side wall

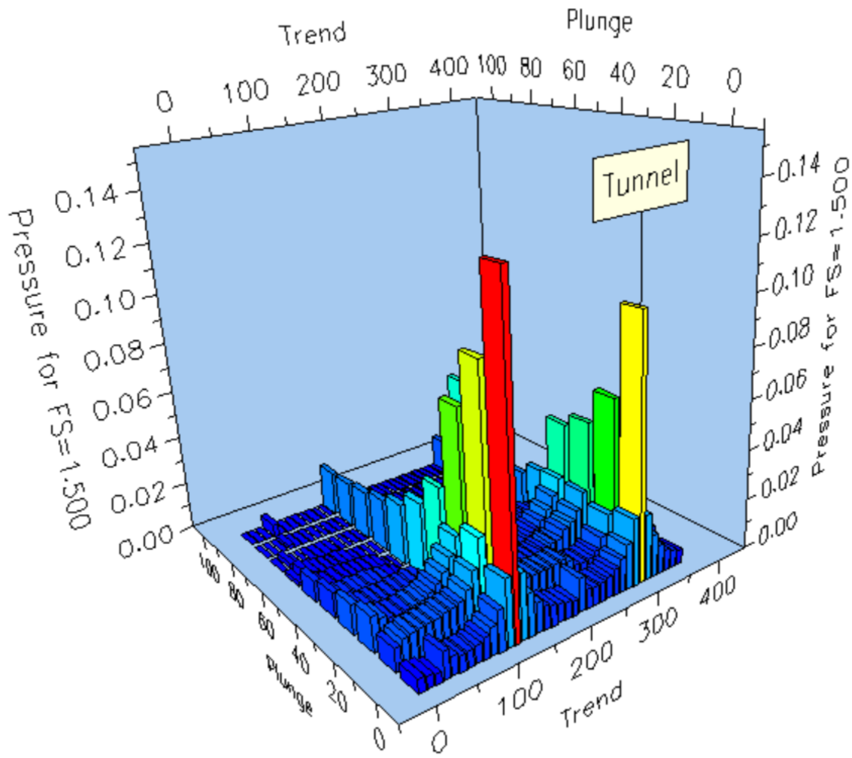

Fig 7.11 Power house orientation plot with respect to trend and plunge

An analysis was carried out for the best suitability of power house orientation for FOS 1.5 (Fig 7.11). The analysis reveals that for the present discontinuities trend with respect to power house orientation it requires a minimum support pressure of 0.02MPa to 0.10MPa to achieve a FOS 1.5. The best suitability seen for the chart is to orient the powerhouse cavern slightly towards north from 310° to 350°.

7.5 SUPPORT AND MEASURES

The underground powerhouse/Transformer caverns are being planned to be located in moderately jointed and compact dolomite. Suitable drainage galleries all around and these caverns shall have to be planned in advance for excavating the power house cavity as ingress of water while excavation cannot be ruled out and the same have to be retained during Operation & Maintenance of the project. Proper steel support system along with rock bolts, shotcrete etc. are to be planned in advance while excavating the power house cavity. As the slate intrbanded with dolomitic limestone which shall be encountered during excavation are expected to be moderately to highly jointed, and water charged. Control blasting with protective measures shall have to be adopted for safe excavation of these cavities.

Table 7.7:Support in Power House and Transformer Hall

	Power House	***Transformer Hall***
Crown	8m/6m 32**f** bolts at 1.5m c/c SFRS 150-250mm. thick lining	7m/5m 25**f** bolts at 1.5m c/c SFRS 125 mm. thick lining
Sidewalls	12m/10m 32**f** bolts at 1.5m c/c SFRS 150-250mm. thick lining	9m/7m 25**f** bolts at 1.5m c/c SFRS 125 mm. thick lining

The rockbolt pattern and thickness of shotcrete lining are consistent with precedent practice for large caverns. As well as pattern bolting, additional spot bolts will be required to support blocks and wedges defined by geological defects. 30m long prestressed cable anchors for stabilising large rock wedges are shown on the design drawings. These are conservative support measures for this size of cavern and maximum rockbolt lengths of 15m are more likely.

The cavern axis is more or less parallel with the general dip direction of the foliation. Wedge failures from the roof are likely where cross joints allow release along the foliation surfaces; there is also the potential for wedge failures in the sidewalls (e.g. from J2) The prevalence of vertical defects subparallel with the cavern walls will not be well defined by the present investigations.

Detailed design will require consideration of the stress concentrations around the excavation when data on the stress regime are available.

The crane beams in the caverns are supported on pillars which will obviate the problem of rock-anchored crane beams in blocky rock on the sidewalls.

Unwedge Analysis Information

Document Name

File Name: VPHEP PH.weg

Project Settings

Project Title: Stability Analysis of Wedges for VHEP Underground Excavations

Wedges Computed: Perimeter and End Wedges

Units: Metric, stress as MPa

General Input Data

Tunnel Axis Orientation:

Trend: 310°

Plunge: 0°

Design Factor of Safety: 1.500

Unit Weight of Rock: 0.026 MN/m3

Unit Weight of Water: 0.010 MN/m3

Seismic Forces

Not Used

Scale Wedges Settings

Not Used

Joint Orientations

Joint 1

Dip: 30°

Dip Direction: 300°

Joint 2

Dip: 20°

Dip Direction: 125°

Joint 3

Dip: 75°

Dip Direction: 030°

Joint Properties

Foliation

Water Pressure

Constant: 0 MPa

Waviness: 0°

Shear Strength Model: Barton-Bandis

JRC: 10

JCS: 22 MPa

Phi b: 30°

J1

Water Pressure

Constant: 0 MPa

Waviness: 0°

Shear Strength Model: Barton-Bandis

JRC: 10

JCS: 24 MPa

Phi b: 35°

J2

Water Pressure

Constant: 0 MPa

Waviness: 0°

Shear Strength Model: Barton-Bandis

JRC: 9

JCS: 20 MPa

Phi b: 28°

Wedge Information

Floor wedge [1]

Factor of Safety: stable

Wedge Weight: 0.026 MN

Upper Right wedge [4]

Factor of Safety: 2.725

Wedge Weight: 3.278 MN

Floor wedge [5]

Factor of Safety: 3.927

Wedge Weight: 14.481 MN

Roof wedge [7]

Factor of Safety: 0.864

Wedge Weight: 2.308 MN

Roof wedge [8]

Factor of Safety: 0.000

Wedge Weight: 0.230 MN

Near End wedge [9]

Factor of Safety: 3.364

Wedge Weight: 0.646 MN

Far End wedge [10]

Factor of Safety: 4.830

Wedge Weight: 0.646 MN

CHAPTER VIII

STABILITY OF HILL SLOPES IN RESERVOIR RIM AREA

The common types of problems encountered during the operation of the reservoir are the seepage and hill slope instability around the rim of reservoir. The reservoir area of Vishnugad–Pipalkoti project is essentially constituted of quartzites with bands of chlorite schist and gneissic rocks with MCT separating both the lithologies. The chlorite schist interbanded within quartzites is an incompetent rock and failures can be initiated along the foliation planes if these are unfavourably disposed. The foliation planes, which are the dominant discontinuity planes of these rocks, generally dip towards WNW to ENE, i.e. essentially towards the upstream side.

The maximum reservoir level (MRL) is approximately at El ±1267m and the dead storage level (DSL) is at El ±1252.5m. The 65m high dam will have a water spread that will extend to distance of about 2.5km on the upstream at the MRL of the reservoir. During drawdown conditions of the reservoir between MRL and DSL, the reservoir slopes may be subjected to alternate dry and water charged conditions, which may lead to instability of hill slopes around the rim of the reservoir. In the present case, close to MRL, thick piles of overburden can be seen on many places particularly on left bank. On right bank also, thin overburden material is often seen at the confluence of local streams with the main river. These overburden materials may absorb water, when the reservoir level is high. When the water level goes down, they remain fully saturated leading to reduction in shear strength and increase in weight, in addition to internal erosion of fine materials. This may result in hill slope instability. As a consequence of this, if the slopes close to NH-58 are affected, the strategically important Highway may face instability problems. Hence, the area has been mapped to delineate the debris zones and other lithological contacts. In order to study the slopes in detail, 12 geological cross sections of hill slopes, six each on either bank of the valley were prepared across slopes, which are potential for landslides. The topographical map, geological map and the geological cross sections provide important inputs to assess the instability potential of hill slopes bordering the reservoir. This is followed by detailed stability analysis of individual unstable slopes to understand the status of stability in terms of factor of safety. Accordingly, suitable control measures can be adopted to safeguard NH-58 and other human settlements located close to rim of the reservoir.

8.1 GEOLOGY OF RESERVOIR

The 65m high dam will have a water spread that will extend to about 2.5 km upstream of the dam. Quartzite rocks are exposed near the dam site and extend well in to the reservoir on the upstream side up to Main Central Thrust (MCT), which is present about a km upstream of the dam. Further upstream, Granitic gneisses are present till the end of the reservoir. Debris and RBM are seen as isolated pockets in many locations, which are seen frequently on the left bank (Fig.8.1). Structurally, foliation is major geological discontinuity, while two more sets of well developed joints, J1 and J2 are also seen in the area (Table 8.1 & 8.2). More structural details are given while discussing individual sites of stability studies

While preparing geological map of the area, potentially unstable slopes were identified for detailed studies on both the banks. They are discussed in detail below:

Table 8.1 General discontinuity attitude (Right Bank)

Sl. No.	Nature of discontinuity	Strike	Dip/Dip direction
1	Foliation	N300^{o}	40^{0}/N030^{0}
2	Joint J1	N010^{o}	75^{o}/N280^{o}
3	Joint J2	N310^{o}	60^{o}/220^{o}

Table 8.2 General discontinuity attitude (Left Bank)

Sl. No.	Nature of discontinuity	Strike	Dip/Dip direction
1	Foliation	N300^{o}	40^{0}/N030^{0}
2	Joint J1	N-80^{o}	65^{o}/N170^{o}
3	Joint J2	N320^{o}	65^{o}/230^{o}

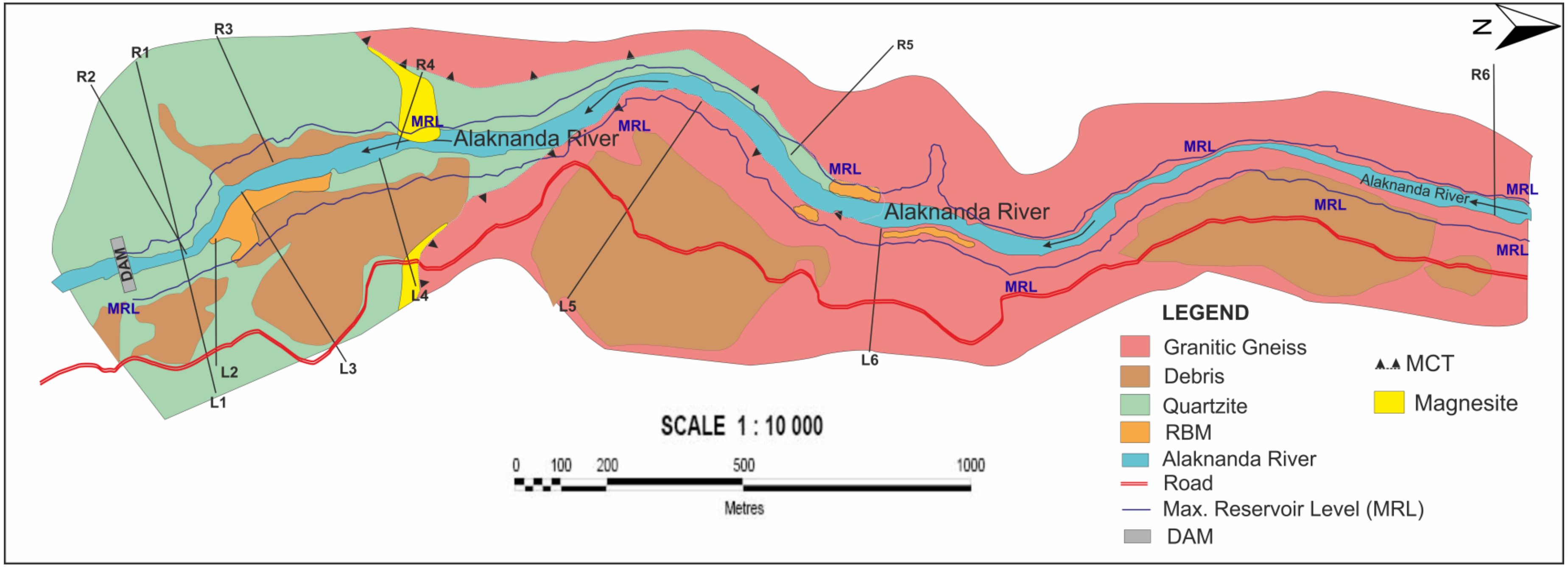

Fig 8.1 Geological map of Vishnugad–Pipalkoti reservoir area with section lines and MRL

In order carry out the stability analysis it was essential to delineate the rock slope and debris slope in the reservoir area.

Table 8.3 Summary of slope sections on right bank

Sl. No.	Section	Location and distance form dam axis	Type of slope
1	R1	Near dam axis, 00 m	Rock slope
2	R2	Near intake structure, 40m	Rock slope
3	R3	U/S of Nall, 270 m	Rock slope
4	R4	Opposite of LSH-2, 490 m	Rock slope
5	R5	Along Urgam bridge, 1330m	Rock slope
6	R6	Near Kalpaganga, 2860m	Rock slope

Table 8.4 Summary of slope sections on left bank

Sl. No.	Section	Location and distance form dam axis	Type of slope
1	L1	Near dam, axis	Mainly rock with some debris talus at higher level
2	L2	Along intake of diversion tunnel, 110m	Mainly rock with some debris at base and higher levels
3	L3	Near intake of diversion tunnel, 180m	Debris at lower level rock, slope at mid and again debris at higher level
4	L4	Near LSH-2, 450m	Debris slope
5	L5	Near D3, 1120m	Debris
6	L6	Near D5, 1610m	Debris and river borne material below road level and rock above road level

8.2 SLOPES ON THE RIGHT BANK

On the right bank six important slopes have been chosen for detailed stability studies. They are discussed below.

i) Section R1: This section is located just upstream of the dam site (N119°). In fact, it is just the continuation of section L1 (left bank) on the right bank. Quartzite rocks are present on the entire slope, which is fairly steep and extending for a height of 170m above the river bed

(Fig.8.2). The geological discontinuities were plotted in a stereonet and kinematic analysis carrier out (Fig. 8.3 and Table 8.6). The rock slope is found to be stable under static and dynamic conditions. No wedge/planar failure is expected under normal conditions. Theoretically no measures are required to stabilise the slope.

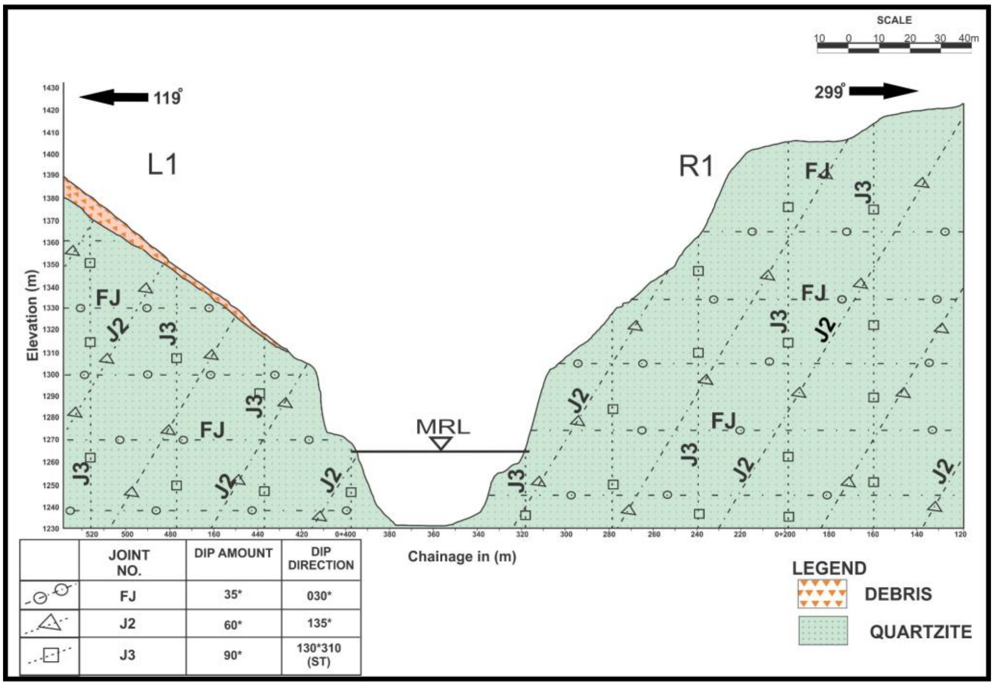

Fig 8.2 Geological cross section of R1 near dam axis

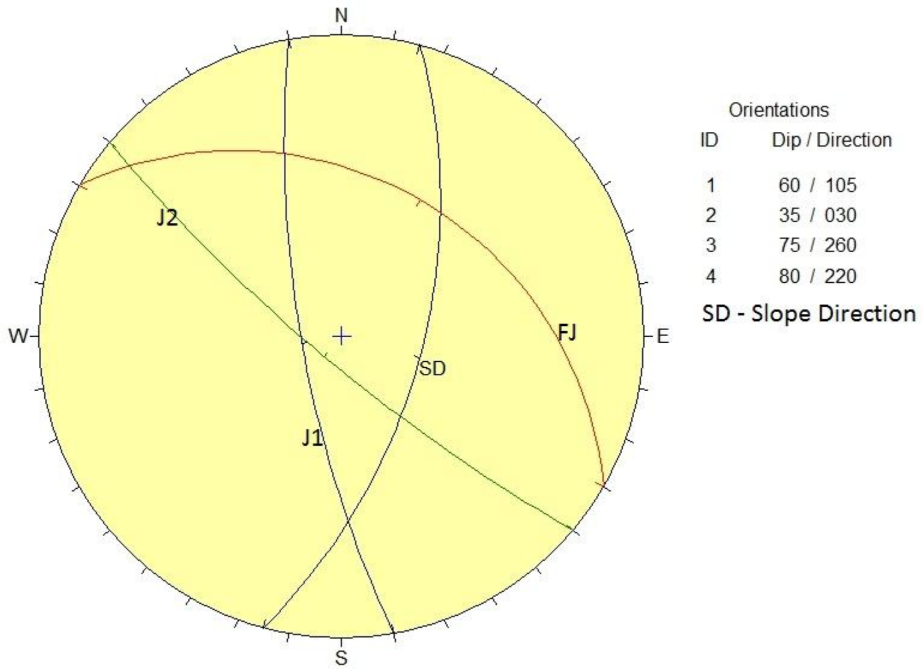

Fig 8.3 Stereonet analysis for Slope R1

However, since the slope is close to the dam axis, additional protection measures like flattening of slopes, installation of cable anchors, shotcreting, surface drainage, 10m deep sub-surface drainage holes at 10° inclined downward and towards valley at 10m c/c for a height of about 30m above MRL, are essential for slope protection. The protection measures will continue for least 100m on either side i.e. u/s and d/s of the dam axis.

ii) Section R2: In order to obtain further information about stability conditions of the area, the section R2 is considered in the nearly same location, but perpendicular to the slope (N105º). It is a rock slope with slope angles of more than 45º (Fig 8.4). The geological discontinuities were plotted in a stereonet and kinematic analysis carrier out (Fig. 8.5 and Table 8.6).

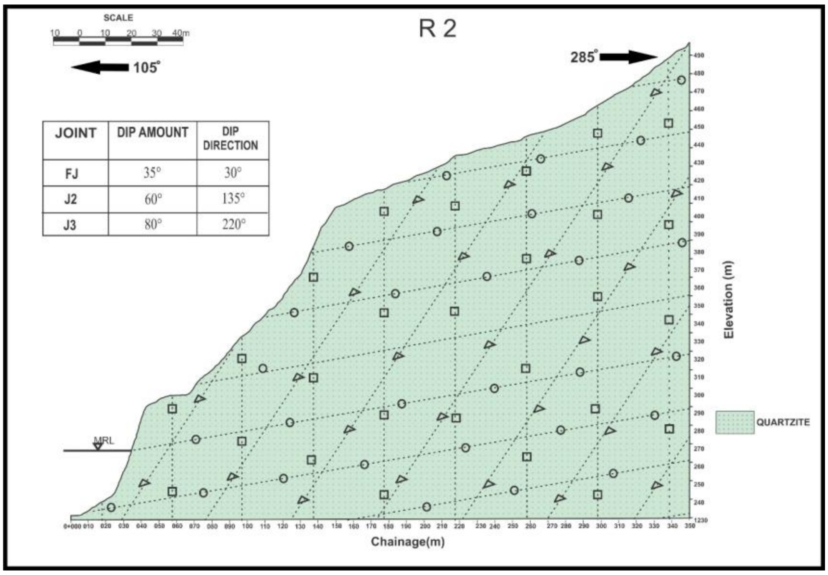

Fig 8.4 Geological cross section of R2 near dam axis Near intake structure, 40m

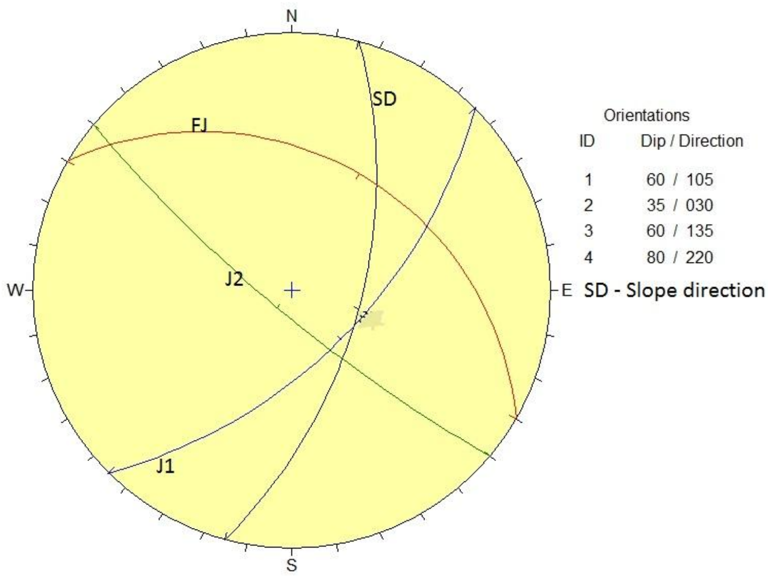

Fig 8.5 Stereonet kinematic analysis for Slope R2

It indicates that the planar failure is likely to occur even under dry static conditions. In view of that, protection measures as indicated for R1 section is justified in this area.

iii) Section R3: The section is located about 270m from the dam site. It is steep rock slope with slope angles of more than 55º (Fig 8.6). The geological discontinuities were plotted in a stereonet and kinematic analysis carrier out (Fig 8.7 and Table 8.6). The analysis indicates that no wedges, either plane or wedge, are formed and hence stable in nature.

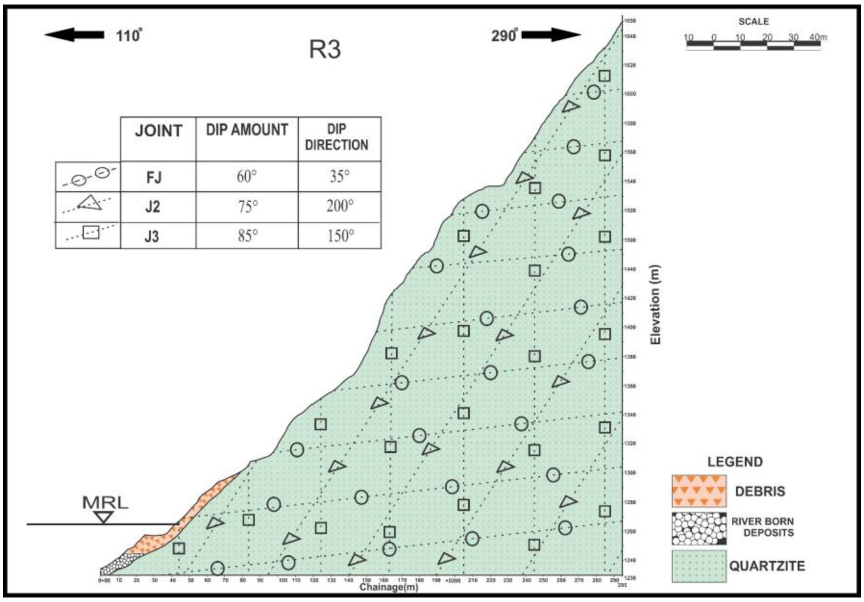

Fig 8.6 Geological cross section of R3 U/S of Nall, 270 m

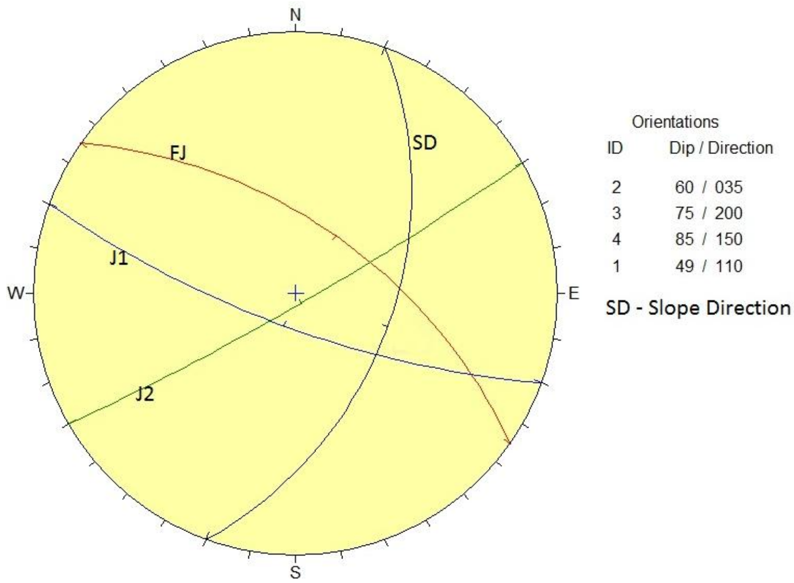

Fig 8.7 Stereonet kinematic analysis for Slope R3

iv) Section R4: This section is located on a steep rock slope about 490m upstream of dam axis. Dolomitic limestones intercalated with magnesite are exposed at the site (Fig 8.8). The observed geological discontinuities were plotted in a stereonet and kinematic analysis carrier out (Fig 8.9 and Table 8.6). Since the foliation dips into the hill and other joints are not favourably aligned, no adverse wedges are formed at this site. Hence, no measures are required at this site.

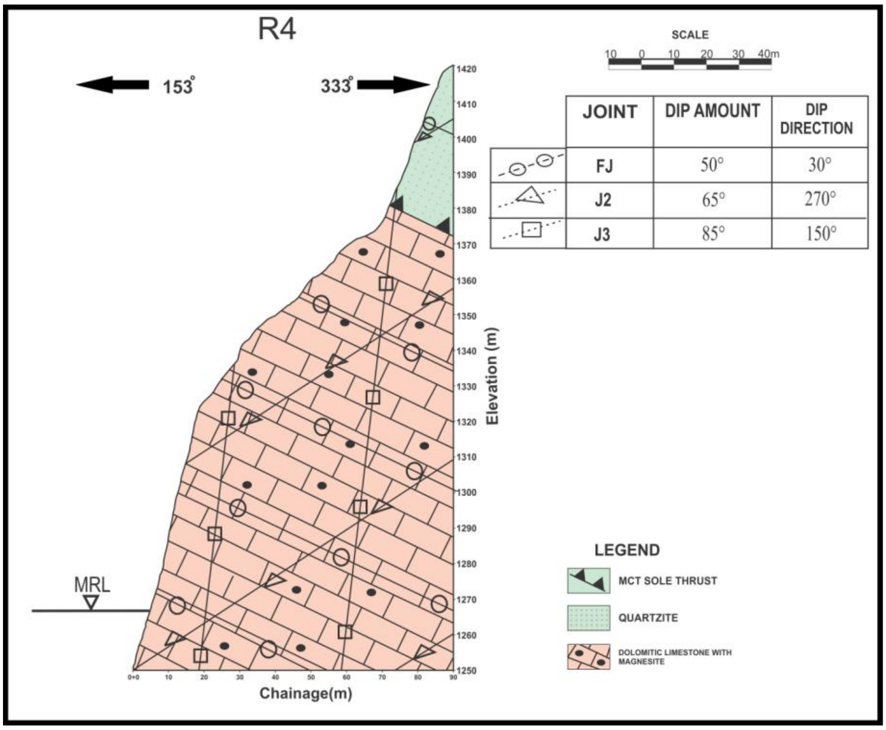

Fig 8.8 Geological cross section of R4 opposite of LSH-2, 490 m

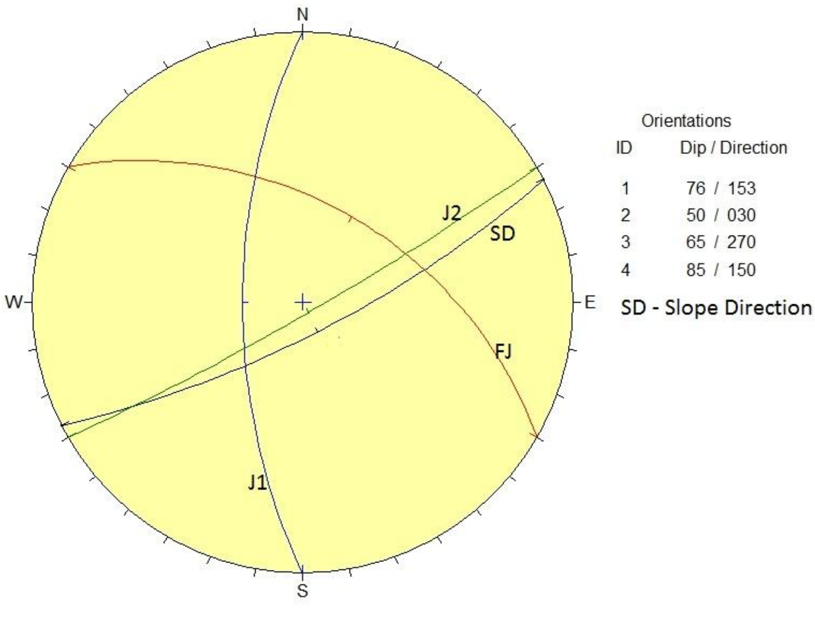

Fig 8.9 Stereonet and kinematic analysis for Slope R4

v) Section R5: This section is located just near the axis of the Urgam bridge on the right bank. It is located on a steep rock slope of more than 65º (Fig 8.10). Quartzites are exposed at the site. The observed geological discontinuities were plotted in a stereonet and kinematic analysis carrier out (Fig 8.11 and Table 8.6). The study indicated that unstable wedges were likely to form at this site. However, since the slope is at the tail reaches of the reservoir, no measures are actually required at the site as the water will be present very close to the river bed level and hence may hardly cause any impact on the stability of the slope.

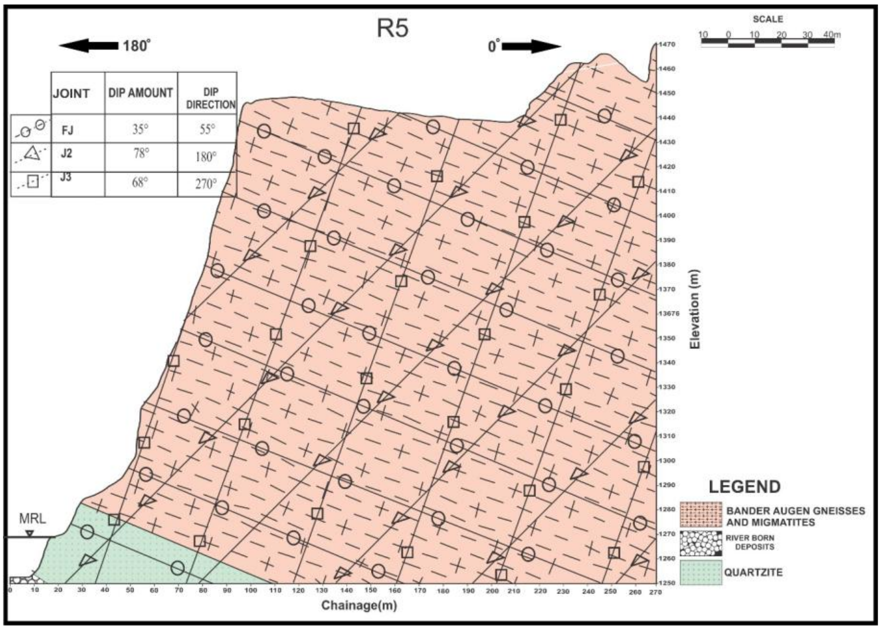

Fig 8.10 Geological cross section of R5 along Urgam bridge, 1330m

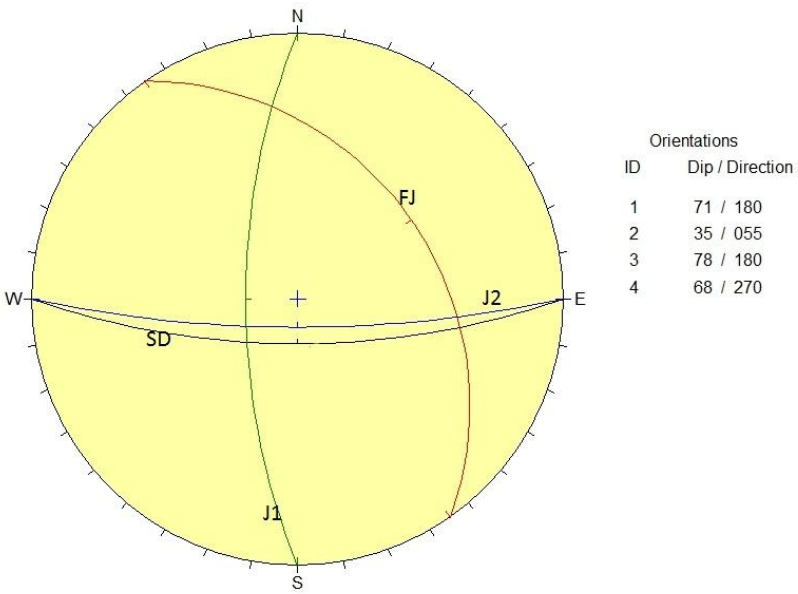

Fig 8.11 Stereonet and kinematic analysis for Slope R5

But, since the slope is located just adjoining the Urgam bridge, it is beneficial, if the slope is stabilized with the help of grouted anchors and shotcreting on polymer wire mesh in addition to providing an efficient drainage system.

vi) Section R6: This section is located Near Kalpaganga, 2860m upstream of dam axis (Fig 8.12). It is located on a steep rock slope of more than 75º. Gneiss rocks are exposed at the site. The observed geological discontinuities were plotted in a stereonet and kinematic analysis carrier out (Fig 8.13 and Table 8.6). The study indicates that unstable wedges were likely to form at this site. However, since the slope is at the tail reaches of the reservoir, no measures are actually required at the site as the water will be present very close to the river bed level and hence may hardly cause any impact on the stability of the slope.

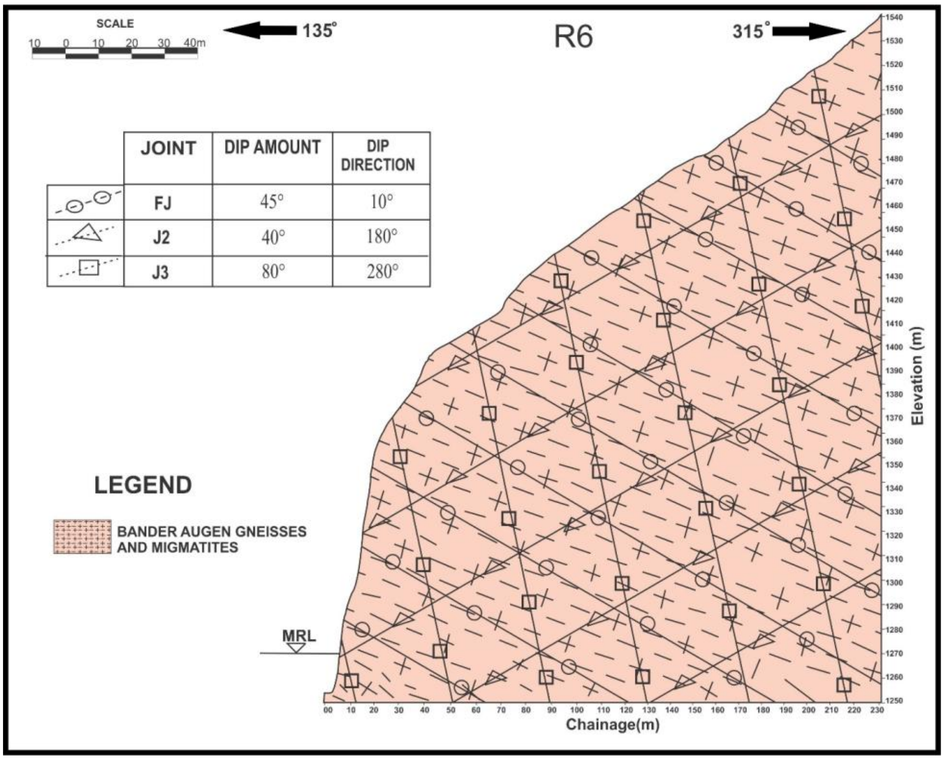

Fig 8.12 Geological cross section of R6 near Kalpaganga, 2860m

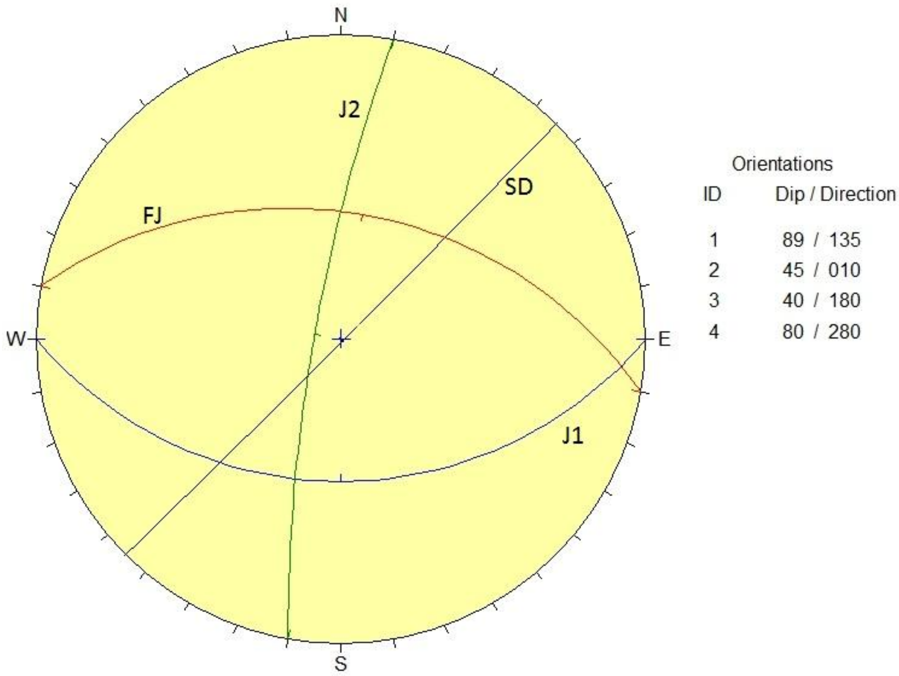

Fig 8.13 Stereonet and kinematic analysis for Slope R6.

8.3 SLOPES ON THE LEFT BANK

On the left bank six important slopes have been chosen for detailed stability studies. They are discussed below.

i) Section L1: It is located just upstream of the dam axis. It mainly consists of rock slope with thin debris cover above, which is seen above the reservoir level. The debris starts from EL± 1310m and further above, while the MRL is limited to EL± 1269m (Fig 8.14). The geological discontinuities were plotted in a stereonet and kinematic analysis carrier out (Fig 8.15 and Table 8.7). The rock slope is found to be stable under static and dynamic conditions with large factors of safety against wedge failure. However, under extreme conditions i.e. dynamic condition with tension crack filled with water, the failure is likely to occur due to over toppling. Here, it is essential to stabilise the slope by using protection measures as suggested for R1 section. The thin debris above the reservoir level may either be removed or proper retaining wall with adequate drainage should be provided at the toe of the debris. The protection measures should continue for 100m distance on either side of the dam axis.

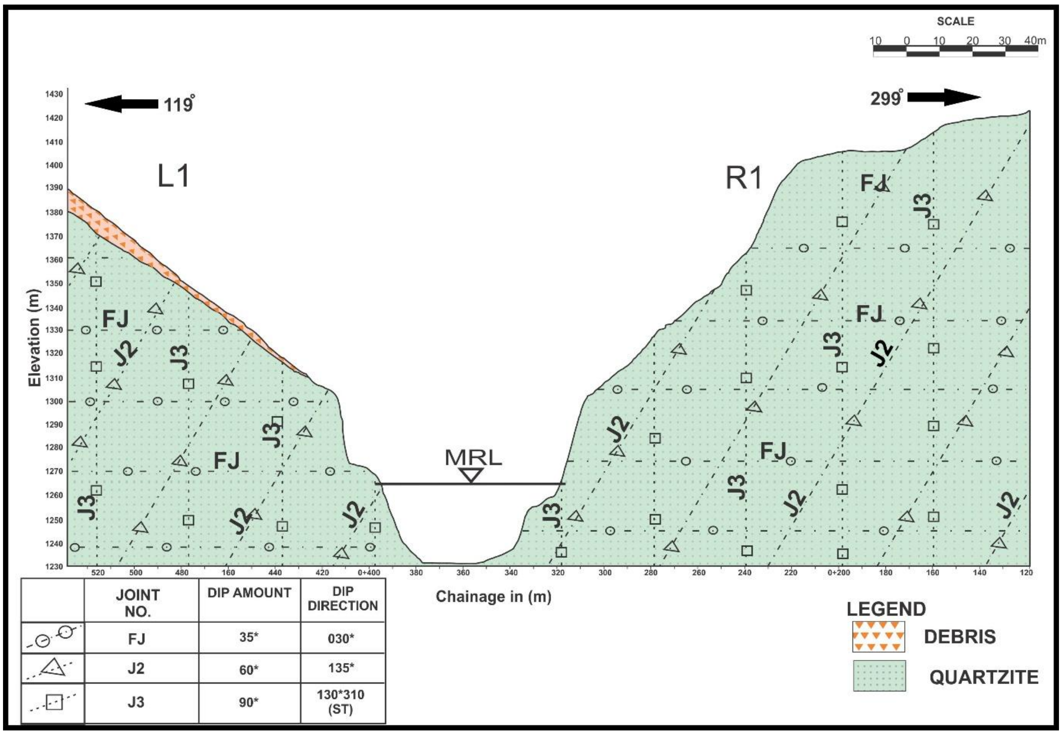

Fig 8.14 Geological cross section of L1. Near dam, axis opposite to L1

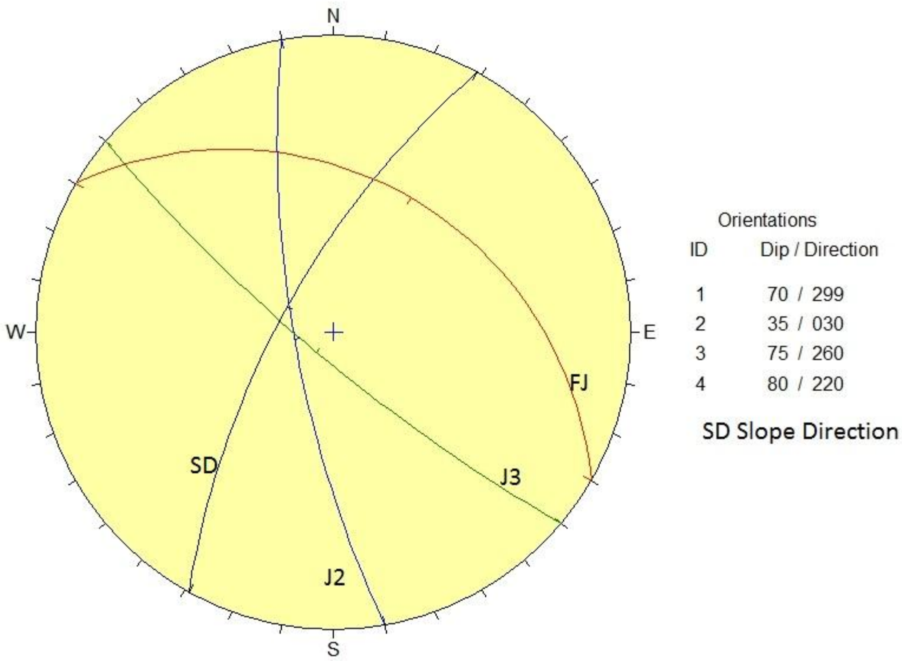

Fig 8.15 Stereonet and kinematic analysis for Slope L1.

ii) <u>Section L2</u>: The section basically shows a rock slope with thin debris cover seen between El ±1295m and El ±1356m (Fig 8.16). The geological discontinuities were plotted in a stereonet and kinematic analysis carrier out (Fig 8.17 and Table 8.7). The rock slope is found to be safe against wedge failure, though some overtopping may occur in extreme conditions.

However, the debris slope is not stable under the worst conditions. Due to close proximity of the section to the dam axis, slope protection work of rock and debris being adopted at section L1 should be extended to this section also.

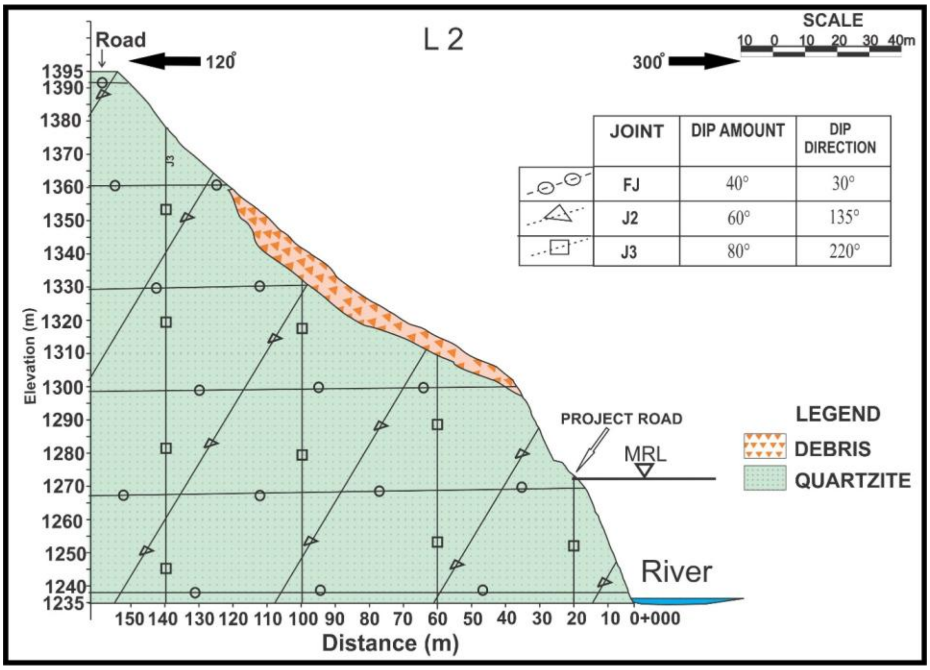

Fig 8.16 Geological cross-section of L2. Along intake of diversion tunnel, 110m

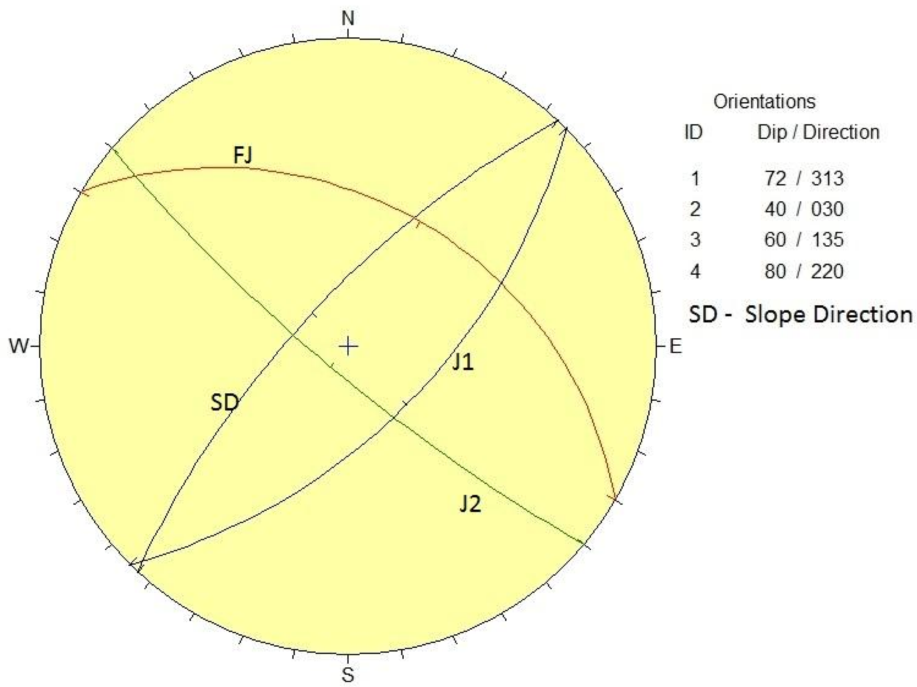

Fig 8.17 Stereonet and kinematic analysis for Slope L2

iii) Section L3: The section is located across the approach roads, which give access to the main dam from NH-58. The slopes are mainly characterised by thick debris extending from river bed to about El ± 1290m (Fig 8.18). The rock stability analysis indicates that they are stable (Fig 8.19 and Table 8.7). However, the debris slope may fail under dynamic and saturated conditions. The alternate draw-down conditions of water level may induce instability in the bottom portion of debris. Since most parts of the debris mass (about 80%) lie below MRL, the failure of the debris, may not adversely affect the overall reservoir capacity.

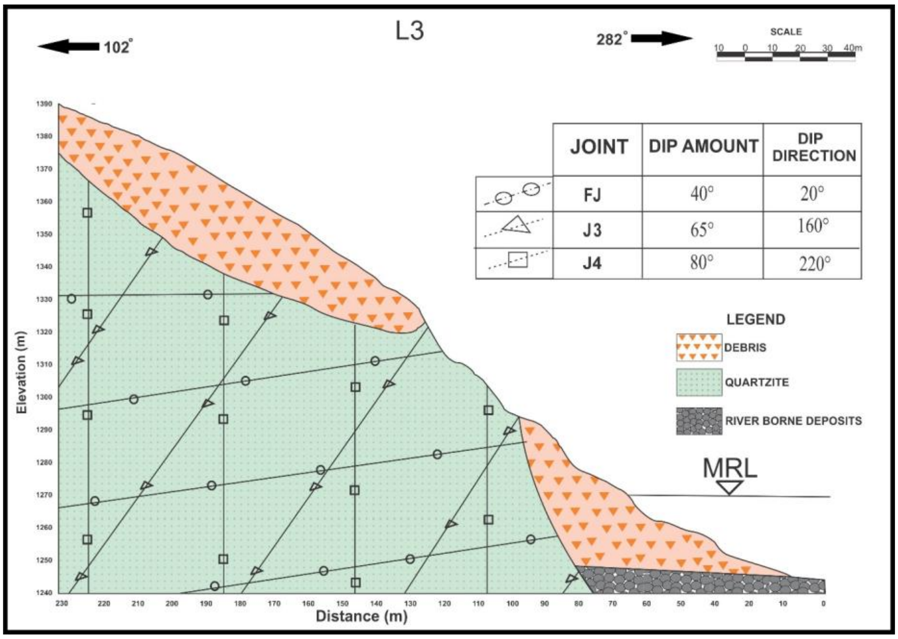

Fig 8.18 Geological cross section of L3 near intake of diversion tunnel, 180m

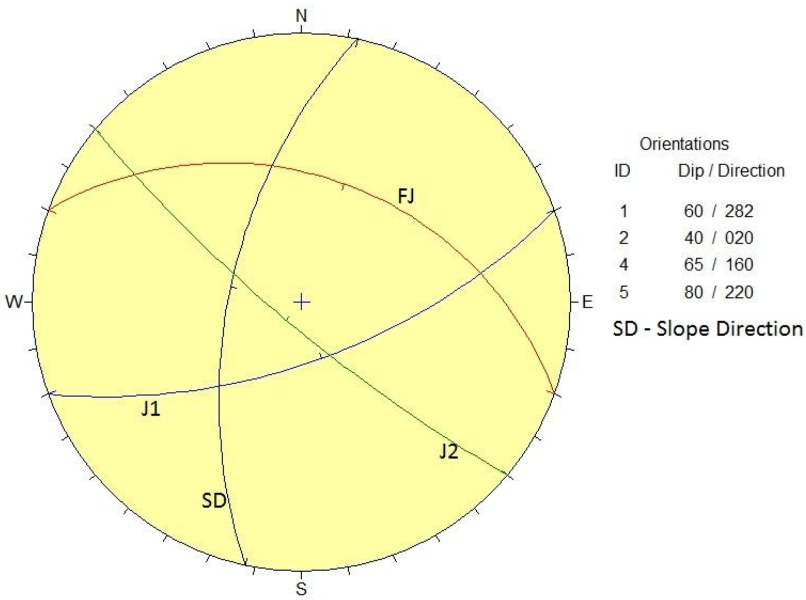

Fig 8.19 Stereonet and kinematic analysis for Slope L3

iv) Section L4: This section is located about 450m upstream of the dam axis. It is a rock slope with thick continuous debris occupying the entire slope above the river bed and extending up to El ± 1310m close to NH-58 (Fig 8.20). The maximum reservoir level (MRL) is located well in the middle of the debris slope. Though the underlying rock is likely to remain stable as indicated in the kinematic analysis (Fig 8.21 and Table 8.7), the debris slope may become unstable when saturated or subjected to dynamic conditions.

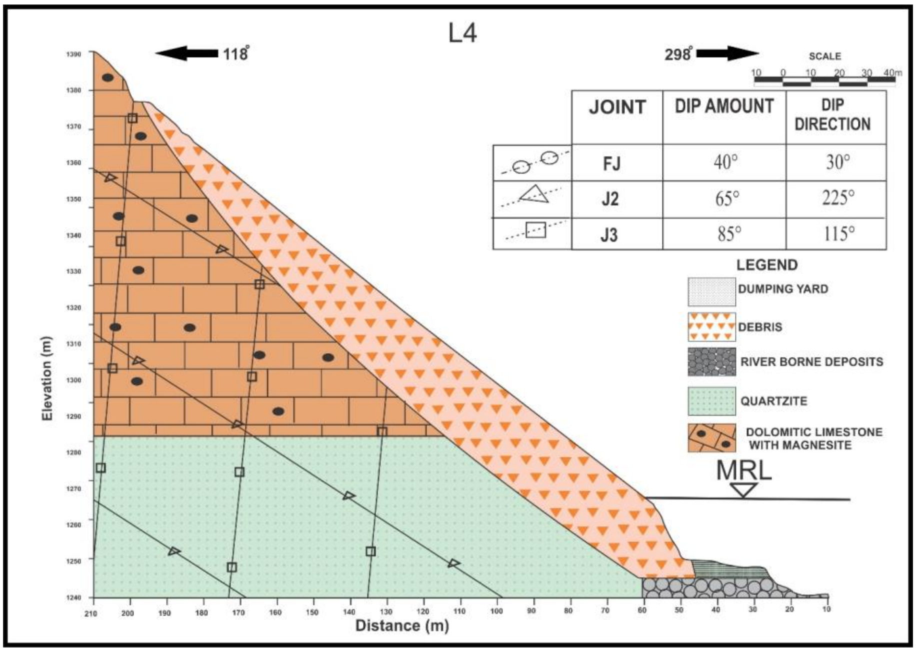

Fig 8.20 Geological cross section of L4. Near LSH-2, 450m

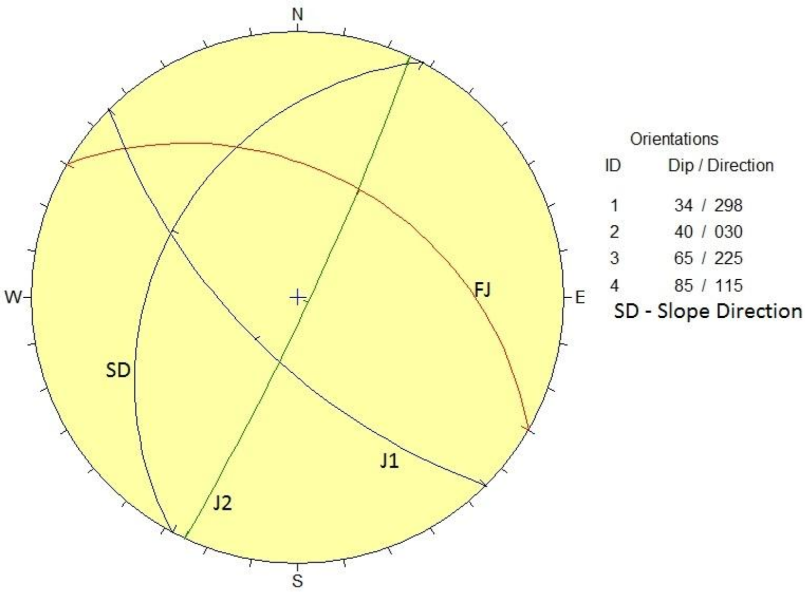

Fig 8.21 Stereonet and kinematic analysis for Slope L4

A near horizontal wide terrace is present at the toe of the slope. In case of any failure of the slope above due to draw-down conditions, the slide material may be easily accommodated within wide terrace so as to flatten the overall debris slope. However, since the failed materials will remain at the toe and will get compacted by the reservoir water, it is likely to get stabilized with time.

v) <u>Section L5</u>: This section is located downstream of Urgam bridge. The slope has an average angle of 25°-30° with moderately thick (8-10m) debris materials seen above the rock slope (Fig 8.22). The debris materials extend only up to El ±1320m in the lower lever and further down rock slopes are present. Since the MRL is at El ± 1269m, the top of water level will be located within the rocks and hence the debris slopes will not be affected due to reservoir water. The geological discontinuities were plotted in a stereonet and kinematic analysis carrier out (Fig 8.23 and Table 8.7). The analysis indicates that the slopes are stable as no unstable wedges are formed.

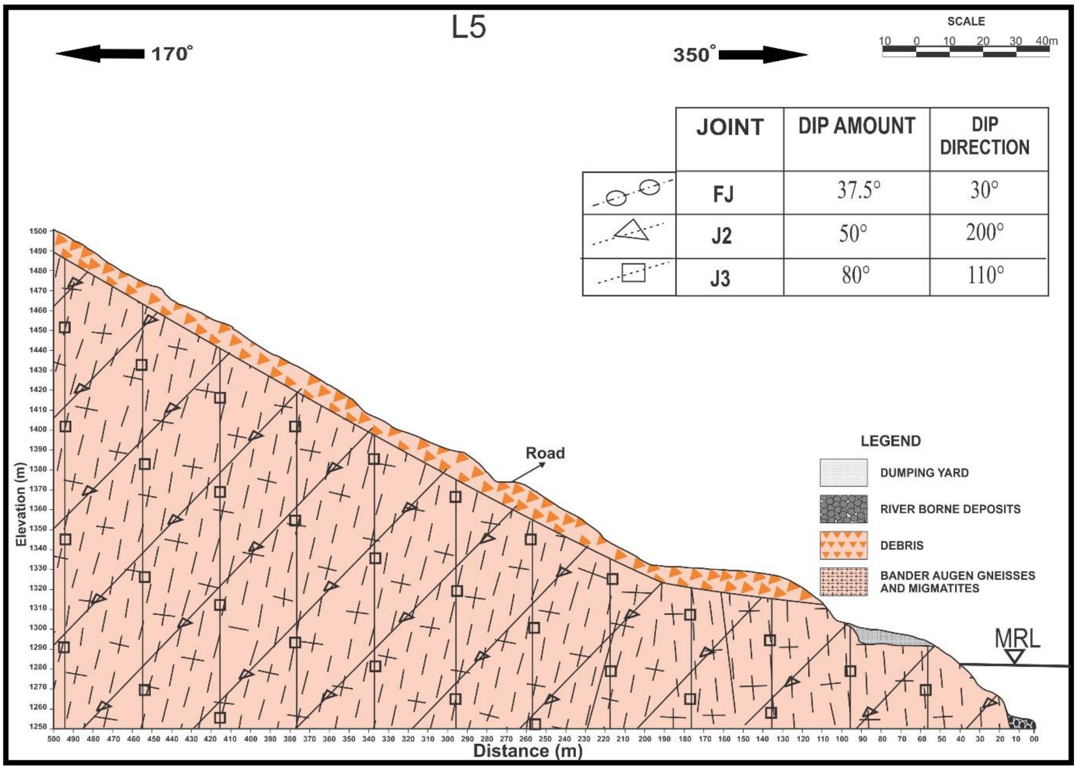

Fig 8.22 Geological cross section of L5 downstream of Urgam bridge, 1120m

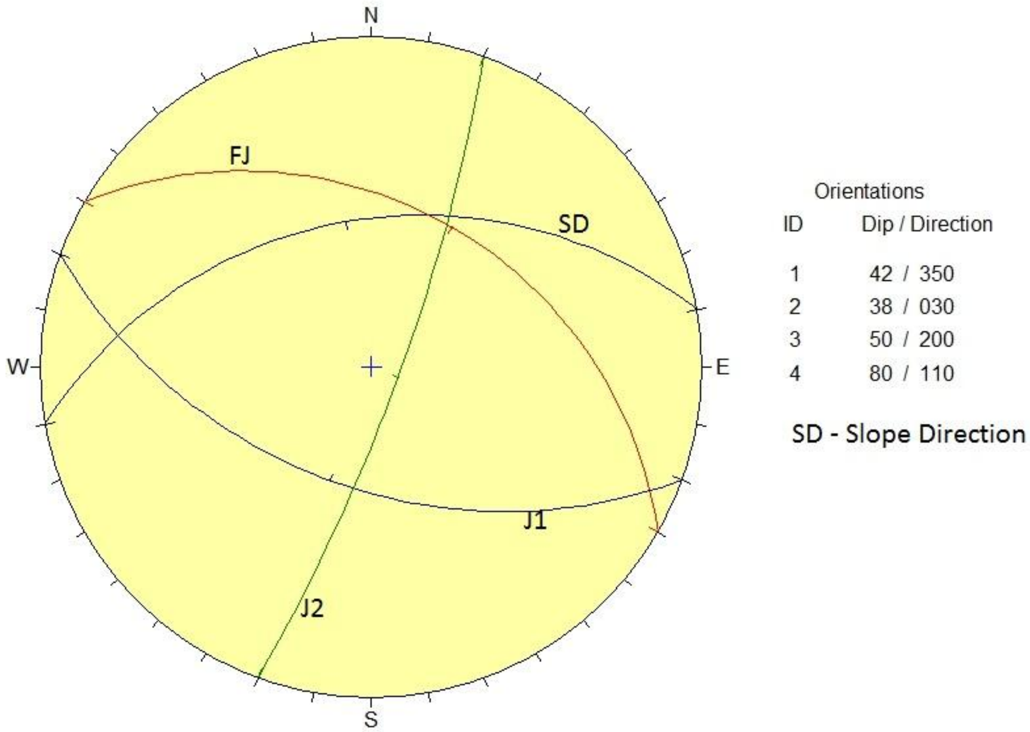

Fig 8.23 Stereonet and kinematic analysis for Slope L5

vi) Section L6: This section is located about 270m upstream of Urgam bridge. Though rocks are present in the upper reaches of the slope, a thick deposit of RBM is seen at the toe of the slope up to the river bed level (Fig 8.24). While RBM extends form river bed to El ±1310m, the MRL extends up to El ±1270m that is up to the middle of RBM deposit. During water draw-down conditions, the alternating saturation and dry conditions may induce instability of the RBM deposit causing minor instability and sliding leading flattening of the gradient. In view of the limited extension of RBM and the slided deposit will lie at the toe area and get compacted due to reservoir water, the flattened deposit will get stabilized in a short time frame. In fact, the thick layer of RBM at the toe of the rock slope provides support to rock slope above.

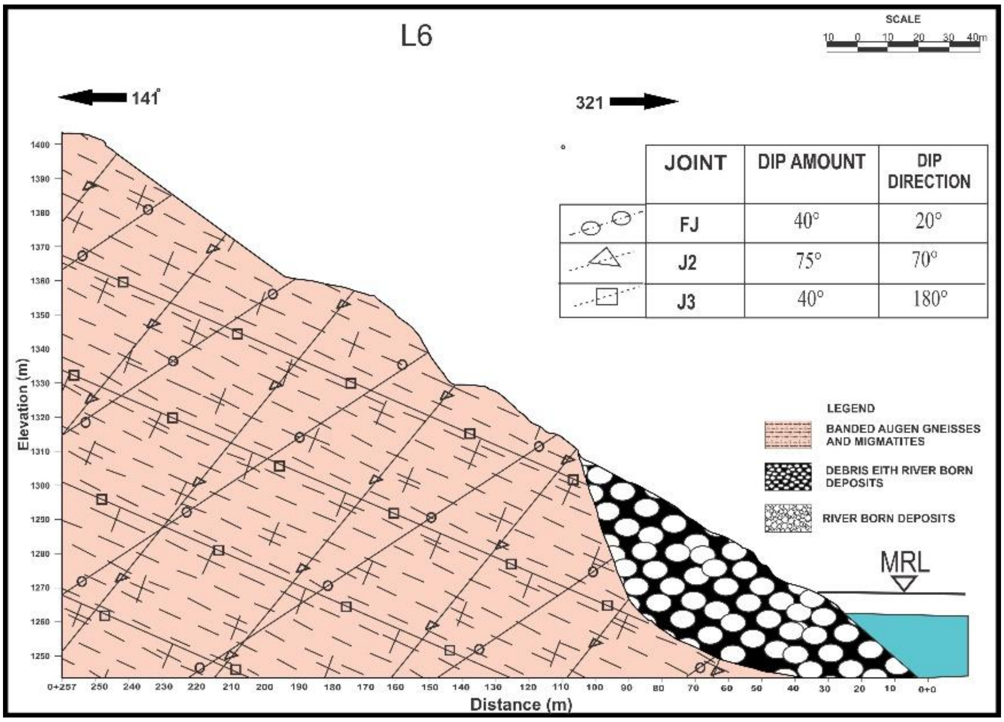

Fig 8.24 Geological cross section of L6, 1610m from dam axis

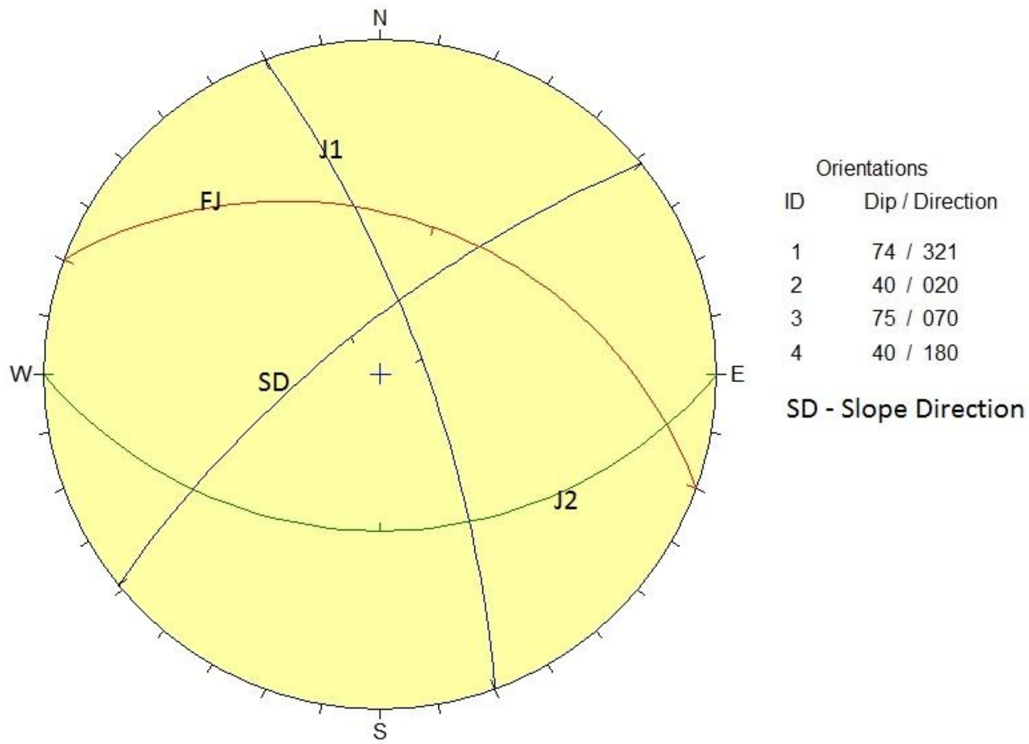

Fig 8.25 Stereonet and kinematic analysis for Slope L6

Table 8.5 Geological cross-section details for Right and Left Bank.

Slope Section	Height (m)	Reservoir water level (m)	Attitude of Slope Face (°)	Attitudes of Discontinuities (°) Dip/dip direction
R1	172	55	60/105	35/030, 75/260, 90/220
R2	273	55	60/105	35/030, 60/135, 90/220
R2	72	55	70/105	35/030, 60/135, 90/220
R3	217	50	49/110	60/035, 75/200, 85/150
R4	80	50	76/153	50/030, 65/270, 85/150
R5	197	30	71/180	35/055, 77.5/180, 67.5/270
R6	139	5	89/135	45/010, 40/180, 80/280
Slope Section	**Height (m)**	**Reservoir water level (m)**	**Attitude of Slope Face (°)**	**Attitudes of Discontinuities (°) Dip/dip direction**
L1	172	55	70/299	35/030, 75/260, 90/220
L2	65	55	72/313	40/030, 60/135, 90/220
L3	82	50	60/282	40/020, 75/280, 90/220
L4	140	50	34/298	40/030, 65/225, 85/115
L5	40	40	42/350	37.5/030, 50/200, 90/110
L6	112	20	74/321	40/020, 75/070, 40/180

Table 8.6 Kinematically possible failure modes in rocks: Right bank

Slope Section	Possibility of failure mode						
	Planar failure		Wedge failure		Toppling failure		Remark
	Yes/No	Along	Yes/No	Along	Yes/no	Along	
R1	-	-	-	-	-	-	
R2	Yes	J1	Yes	FJ& J1	-	-	
R3	-	-	Yes	FJ& J2	-	-	
R4	Yes	J2	-	-	Yes	J2	Face formed by J2
R5	Yes	J2	-	-	-	-	Face formed by J1
R6	-	-	Yes	J1& J2	-		

Fig. 8.26 Foliated stained granitic gneissic rocks exposed near Urgam bridge

Fig. 8.27 Debris and RBM material present upstream of Urgam bridge on Left bank

Fig 8.28 Contact of Granitic gneiss and Quartzites of Gulakoti in Reservoir area (NH-58)

Fig 8.29 Debris and RBM material present along section L6

Table 8.7 Kinematically possible failure modes in rocks: Left bank

Slope section	Possibility of failure mode					
	Planar failure		Wedge failure		Toppling failure	
	Yes/No	Along	Yes/No	Along	Yes/no	Along
L1	-	-	Yes	J1&J2	-	-
L2	-	-	Yes	J1& J2	Yes	J1
L3	Yes	J1	Yes	FJ& J1	-	-
L4	-	-	Yes	FJ& J2	Yes	J2
L5	-	-	Yes	FJ&J2		-
L6	-	-	Yes	FJ&J2	-	-

Table 8.8 Concluding remarks on stability and corrective measures required (Right Bank)

Sl. No.	Section	Slope Type	Stability Status	Corrective Measures
1	R1	Rock	No wedge/planer failure expected.	Due to proximity to dam axis, flattening, cable anchors, shotcreting, surface drainage, drainage holes should be provided. The protection measures should preferably continue 100m on either side i.e. u/s and d/s of the dam.
2	R2	Rock	Wedge instability when tension crack is filled with water. Planar failure is likely under dry static conditions.	Same as R1
3	R3		Probability of unsatisfactory performance ranging between 11.99 to 20.78% for circular failure of rock mass. Most likely values of FOS are	Surface drainage to be improved and weep holes to be provided. Steep slopes has to be stabilised with shotcrete and cable anchors upto 10m above FRL.

			also smaller than 1.5	
4	R4	Rock	Stable	No measures are required
5	R5	Rock	Unstable under normal condition.	Reinforcement is required to make slope stable. However, the slope is at the end of the reservoir rim, an efficient drainage system will reduce risk of failure to a great extent. The slope should be kept under watch.

Table 8.9 Concluding remarks on stability and corrective measures required (Left Bank)

Sl.No.	Section	Slope Type	Stability Status	Corrective Measures
1	L1	Rock slope with thin debris cover	Wedge instability under extreme conditions	Due to proximity to dam axis, protection measures suggested at R1 should be adopted. The thin debris may either be removed or proper retaining wall with adequate drainage should be provided at the toe of the debris. The protection measures should continue for 100m distance on either side of the dam axis.
2	L2	Rock slope with debris	Unstable debris under extreme conditions	Same as L1
3	L3	Deep Debris	Unstable debris under dynamic and saturated condition. Most of the debris mass lies below FRL. Failure of debris not likely to affect the overall reservoir capacity.	The debris may be allowed to slide down into the river. In the upper part gabion wall should be provided. The gabion should be supported (reinforced) with steel piles anchored into sound rock for adequate depth.
4	L4	Rock	The underlying rock is stable. The debris slope is just stable under normal conditions. In case of failure of slope above, the slide material may	Improve drainage through drainage holes. The slope needs to be carefully watched.

			be easily accommodated within terrace. It is not likely to create any harm to the reservoir.	
5	L5	Rock slope with debris		
6	L6	Thick debris slope	Unstable debris slope extends into the zone of water level fluctuations. Debris is likely to sink and slide down to get flattened to stable slope angle.	The slope should be kept under watch.

8.4 DISCUSSION

The 65m high dam will have a water spread that will extend to about 2.5km upstream of the dam. Quartzite rocks are exposed near the dam site and extend well in to the reservoir on the upstream side up to Main Central Thrust (MCT), which is present about 1km upstream of the dam. Granitic gneisses are exposed further upstream till the end of the reservoir. The small reservoir to be created due to dam construction will be mostly lying close to the river bed except in reaches close to the dam site.

During reservoir mapping and based on the potentiality of the slope for instability problems, twelve slopes, six on either bank were chosen for detailed study. On the left bank, the slopes having debris cover at MRL show minor instability problems due to draw down conditions (L3, L4 and L7). However, initial instability though may cause sliding of debris, they will be eroded out, but will get accumulated at the toe and the reservoir water will help to compact it. As a result, there will be reduction in the slope angle initially but in a few years time, it will tend to get stabilized. No major landslides are anticipated on the left bank. However, further stability measures may be adopted on the slopes just above the dam site on both the banks. These are only additional measures to stabilize the more important slopes above the dam. The right bank slopes are generally rock slopes which are generally stable and do not require any stability measures. The concluding remarks on the stability and the required corrective measures for both Right Bank and Left Bank are given in Tables 8.8 and 8.9 respectively.

CHAPTER IX

SUMMARY AND CONCLUSIONS

In view of fast development activities, the demand for energy increases day by day. For developing country like India the requirement of energy needs increases exponentially, which need to be balanced with additional power production and alternative energy sources. Himalaya holds enormous energy reserves, which are yet be harnessed to the full potential. The Engineering Geological challenges associated with harnessing of Hydropower potentials have to be evaluated thoroughly through systematic investigations.

Vishungad-Pipalkoti HEP located in Chamoli district, Uttarakhand envisages construction of 65m high diversion dam across River Alaknanda to carry water to an underground powerhouse to produce 444MW of power.

Dam site

The dam site is located in a narrow gorge where the quartzite rock of Gulabkoti Formation is exposed. The dam site has been mapped on detailed scale. Three major geological discontinuities namely foliation (FJ), joint (J1) and joint (J2) were identified on the basis of large number of structural observations at the site. The dam site has been explored with the help of drill holes and drifts. The surface mapping and subsurface explorations indicate that the stripping limit on the left bank will be of the order of 13m and on the right bank it will be about 6m. The water pressure test in the drill hole indicates that the depth of grouting will be at least one time the height (1H) dam. The slope stability analysis indicates that the slopes are stable under natural condition and after stripping.

Power Tunnel

The 8.8m diameter tunnel will have length of 13.4km and will pass through rugged mountainous terrain on the right bank. Initially quartzite rocks are exposed for 1km and later dense and grey colored slates are exposed till Maina River crossing. Further ahead, though alternative sequence of slates and dolomitic limestones are exposed, a thick band of dolomitic limestone is present in surge shaft and power house area. High geothermal gradients are expected in the initial reaches of tunnel excavation as indicated by the exploration drift.

The geological discontinuities observed along the tunnel alignment was plotted on a stereonet to identify the attitude of foliation and joints. The intersection of geological discontinuities forms rock wedges. In general it has been found that the unstable rock wedges are located on the roof. The ultimate roof support pressure (pv) based on Q system for quartzites is 0.0258MPa, for slates 0.0292 MPa and for dolomitic limestone 0.0264MPa. The ultimate wall support pressure for quartzite is 0.0152MPa, for slates 0.0172MPa and for dolomitic limestones 0.0157MPa. The corresponding support requirements for various rock types have also been calculated.

The tunnel orientation with respect to strike of foliation (FJ), the major geological discontinuity is more than 40º in most of the tunnel reaches. However, the tunnel orientation is nearly parallel in B-C segment of PT. In view of this, major over break conditions may be anticipated in this segment.

Maina River problem

The Maina river, which is an important tributary of Alaknanda, cross the tunnel alignment in C-D segment. In view of deep undercutting of the river, the cover above the tunnel is very less. From geological section it can be inferred that the maximum cover in the intersection Zone of Maina River with the tunnel, is of the order 20m (Rock) and 10m (fluvial). This possibly leaves fairly fresh to fresh rock cover of about 15m above the tunnel, which in anyway is less than the 3D cover (about 27m) above the tunnel roof. In view of inadequate rock cover the entire stretch should be excavated using fore polling methods, by which the roof will be supported while carrying out the excavation. In view of extensively sheared rocks with inadequate rock cover, the tunnel shall be supported with continuous steel ribs placed at close spacing as required at the site.

Blasting for Tunnel Excavation

The construction of various structural components of Vishnugad–Pipalkoti project will involve underground blasting on a larger scale. The blasting is likely to produce vibrations in the surrounding rock mass and on surface causing damages to land and properties. In unfavorable locations it can lead to major landslides also.

For the purpose of estimating the impacts of blasting geological cross sections were prepared for individual villages. On the basis of square root of the R (distance between the ground surface and the tunnel) the estimated vibrations were calculated. Taking into consideration the huts and other weak structures, the peak particle velocity (PPV) has been taken as 5 as per IS code, and the corresponding charge per delay for different locations has been calculated so that the blast vibrations will have no adverse impacts on the weak structures as well as on the land.

Powerhouse

The underground powerhouse is located to the south of Hat village on the right bank of Alaknanda River. Since thick debris overburden material are present on hill slopes, slate rock exposure are seen close to river bed and dolomitic limestones are seen on the hills on higher levels. The exploration drift proves slates up to RD 480m, the slate and dolomitic limestone interbanded zone upto RD 495m and dolomitic limestones beyond that up to the end of the drift (RD 680m).

In view of broad synclinal structure, the foliation dipping towards each other in the core area, excessive subsurface water gets collected in the drift and flows continuously for a depth of more than 30cm. The powerhouse location is chosen well within the slates where the foliations dip consistently towards north. Dolomitic limestones are exposed partly on the roof of the power house.

Support requirements.

Reservoir

The maximum reservoir level (MRL) is approximately at the elevation of 1267m and the dead storage level (DSL) is at elevation of 1252.5m. During drawdown condition of the reservoir between MRL and DSL, the reservoir slopes may be subjected to alternating dry and water charged conditions, which may lead to instability of hill slopes around the rim of the reservoir.

The general problems encountered during the operation of the reservoir are the seepage and hill slope instability around the rim. Quartzite rocks are exposed in the reservoir in the vicinity of the dam and further up stream up to Main Central Thrust (MCT). Further up stream granitic gneisses are exposed till the end of the reservoir. The thick debris over burden are seen at many places on the left bank. While rock slopes are mainly seen on the right bank. The reservoir water spread extends for 2.5km. The general height of water level in the reservoir is low as compared to the overall height of the hill slopes. More over the adjoining valleys are at higher level as compare to the reservoir valley, the seepage problems are negligible.

Twelve potentially unstable slopes were identified for stability studies, six on each bank. On the left bank only three sections shows the presence of debris at maximum reservoir level MRL. These slopes indicate the probability of failure of debris at the toe. However since the height of reservoir water is less at in these locations, the failed material will get accumulated at the toe and help to flatten the upslope. This will gradually help to stabilize the overall slope. The other sections don not indicate slope instability due to fluctuations on of reservoir water.

REFERENCES

1. Ahmad, T., Hanis, N., Bickel, M., Chapman, H., Bunbuoy, J. and Prince, C.. 2000. 'Isotopic constraints as the structural relationship between the Lesser Himalayan series and the High Himalayan Crystalline series, Garhwal Himalaya.' Geol. Soc. Am. Bull., 112, 467–477.
2. Ahmad, T., Tarney, J. 1991. 'Geochemistry and petrogenesis of Garhwal volcanics: implications for evolution of the N-Indian lithosphere.' Precambrian Res. 50, 69–88.
3. Ahmad, T. 2001. 'Geology of the Himalayan Mountain Range, with special reference to the western Himalaya.' GEOLOGI 63, 142-147.
4. Ahuja, D. and Tatsutani, M. 2009. 'Sustainable energies for developing countries.' S.A.P.I.EN.S [Online], 2.1.
5. Anbalagan, R. 1986. 'Geotechnical study and environmental appraisal of a water resource project in Kumaun Himalaya.' Kumaun University, Nainital, 126 Unpubl. Ph.D. thesis.
6. Anbalagan, R. 1992. 'Landslide hazard evaluation and zonation mapping in mountainous terrain.' Engineering geology, 32(4), 269-277.
7. Anbalagan, R., Chakraborty, D. and Kohli, A. 2008. 'Landslide hazard zonation (LHZ) mapping on meso-scale for systematic town planning in mountainous terrain.' J Sci Ind Res, 67, 486-497.
8. Anbalagan, R., Parida, S. and Lakshmanan, K. 2013. 'Geotechnical Evaluation of Lakhwar Underground Powerhouse, Uttrakhand Himalaya, India.' In On a Sustainable Future of the Earth's Natural Resources (pp. 239-249). Springer Berlin Heidelberg.
9. Anbalagan, R., and Singh, B. 1996. 'Landslide hazard and risk assessment mapping of mountainous terrains - a case study from Kumaun Himalaya, India.' Engineering Geology 43.4: 237-246.
10. Anbalagan, R. and Singh, Bhoop. 2003. `Landslide hazard zonation mapping – a need for sustainable development of Uttaranchal with special reference to route locations.' Jour. Engineering Geol., (ISEG) Vol. XXXII, 13-22.
11. Anbalagan, R. and Singh, B. 2006. 'Landslide hazard zonation mapping – a need for sustainable development of Uttranchal with special reference to route locations' Jour. Eng. Geol., (ISEG), 32, 13–22.
12. Anbalagan, R., Singh, B., Chakraborty, D. and Kohli, A. 2007. 'A field manual for landslide investigations.' A Publication of Department of Science and Technology Government of India, 64.

13. Asef, M.R., Reddish, D.J. and Lloyd, P.W. 2000. 'Rock–support interaction analysis based on numerical modelling.' Geotechnical & Geological Engineering, 18(1), 23-37.
14. Auden, J. B. 1935. 'Traverses in the Himalaya.' Rec. Geol. Surv. India 69.2: 123-167.
15. Aydan, Ö. and Dalgıç, S., 1998. 'Prediction of deformation behaviour of 3-lanes Bolu tunnels through squeezing rocks of North Anatolian Fault Zone (NAFZ).' Regional Symp. on Sedimentary Rock Engineering, Taipei, 228–233.
16. Sivakumar Babu, G.L., Reddy, K.R., Chouskey, S.K. and Kulkarni, H.S. 2009. 'Prediction of long-term municipal solid waste landfill settlement using constitutive model.' Practice periodical of hazardous, toxic, and radioactive waste management, 14(2), 139-150.
17. Barton, N., Bandis, S. 1990. 'Review of predictive capabilities of JRCJCS model in engineering practice.' Proc. Int. Symp. on Rock Joints, Loen, Norway,), 603–610.
18. Barton, N., By, T.L., Chryssanthakis, L., Tunbridge, L., Kristiansen, J., Løset, F., Bhasin, R.K., Westerdahl, H. and Vik, G. 1992. 'Comparison of prediction and performance for a 62 m span sports hall in jointed gneiss.' International Journal of Rock Mechanics and Mining Sciences & Geomechanics Abstracts. Vol. 31. No. 6. Pergamon.
19. Barton, N. and Choubey, V., 1977. 'The shear strength of rock joints in theory and practice.' Rock mechanics 10.1-2. 1-54.
20. Barton, N., Lien, R. and Lunde, J. 1974. 'Engineering classification of rock masses for the design of tunnel support.' Rock Mech., V.6, 189-236.
21. Barton, N., Løset, F., Lien, R. and Lunde, J. 1980. 'Application of the Q-system in design decisions.' In Subsurface space, (ed. M. Bergamon) 2 New York, 553-561.
22. Behrestaghi, M. H. N., Rao, K. S. and Ramamurthy, T. 1996. 'Engineering geological and geotechnical responses of schistose rocks from dam project areas in India.' Engineering Geology, 44(1), 183-201.
23. Bhasin, R. K., Barton, N., Grimstad, E., Chryssanthakis, P. 1995. 'Engineering geological characterization of low strength anisotropic rocks in the Himalayan region for assessment of tunnel support.' Engineering Geology 40.3: 169-193.
24. Bhasin, R. K., Barton, N., Grimstad, E., Chryssanthakis, P, Shende, F.P. 1996. 'Comparison of predicted and measured performance of a large cavern in the Himalayas.' International journal of rock mechanics and mining sciences & geomechanics abstracts. Vol. 33. No. 6. Pergamon.
25. Bhattacharya, A.K., Bhatnagar, G.S., Narayan Das, G.R., Gupta, J.N., Chabria, T. and Bhalla, N.S. 1982. 'Rb–Sr dating and geological interpretations of sheared granite-

gneisses of Brijranigad–Ingedinala, Bhilangana valley, Tehri District, U.P.' Himalayan Geol. 12, 212–224.

26. Bhawani Singh, Jethwa, J.L., Dube, A.K. and Singh, B. 1992: 'Correlation between support pressure and rock mass quality.' Tunn. and undg. Sp. Tech, V.7., 57-74.
27. Bieniawski, Z. T. 1973. 'Engineering classification of jointed rock masses.' Trans S. Afr.Inst. Civ. Engrs15, 335-344.
28. Bieniawski, Z. T. 1976. 'Rock mass classification in rock engineering.' In Expl. for rock engg. proc. of the symp., (ed. Z.T. Bieniawski) 1, CapeTown: Balkema, 97-106.
29. Bieniawski, Z. T. 1979. 'The geomechanics classification in rock engineering applications.' 4th ISRM Congress. International Society for Rock Mechanics.
30. Bieniawski, Z. T. 1984. 'Rock mechanics design in mining and tunnelling.' No. Monograph.
31. Bieniawski, Z. T. 1989. 'Engineering rock mass classifications.' New York: Wiley.
32. Bilgen, S., Keles, S., Kaygusuz, A., Sari, A. and Kaygusuz, K. 2008. 'Global warming and renewable energy sources for sustainable development: A case study in Turkey.' Science Direct, Renewable and Sustainable Energy Reviews 12. 372–396.
33. Burrard, S. G., and Hayden, H. H., revised by Heron, A. M. 1934. 'A Sketch of the Geography and Geology of the Himalayan Mountains and Tibet.' Govt. of India Press, Calcutta.
34. Central Electricity Authority (CEA) of India, 2014. Annual Report.
35. Craig, R. F. 2013. Soil mechanics. Springer.
36. Chowdhury, R. and Flentje, P., 2003. Role of slope reliability analysis in landslide risk management. Bulletin of Engineering Geology and the Environment, 62(1), 41-46.
37. Dahal, R. K., Bhandary, N. P., Timilsina, M., Yatabe, R. and Hasegawa, S. 2013. 'Earthquake-Induced Landslides in the Roadside Slopes of East Nepal after Recent September 18, 2011 Earthquake.' In Earthquake-induced landslides. Springer Berlin Heidelberg, 149-157.
38. Dahal, R. K., S. Hasegawa, A. Nonomura, M. Yamanaka, T. Masuda, and K. Nishino. 2008. 'GIS based weights-of-evidence modelling of rainfall-induced landslides in small catchments for landslide susceptibility mapping.' Environmental Geology. 54: 311–324.
39. Deere, D. U. 1963. 'Technical description of rock cores for Engineering purpose.' Rock Mechanics and Engineering Geology, Vol. 1, No. 1, 16-22.
40. Deere, D. U. 1988. 'The rock quality designation (RQD) index in practice.' Rock classification systems for engineering purposes. ASTM International.

41. Deere, D. U. and Miller, R. P., 1966. 'Engineering classification and index properties of rock.' Tech. Report Air Force Weapons Lab., New Mexico, 65-116.
42. Deere, D. U. and Patton, F. D. 1967. 'Effect of pore pressures on the stability of slopes.' In joint GSA-ASCE Symp., New Orleans.
43. Djordjevic, N, Brunton, I., Cepuritis, P., Chintombo, G., Heslop, G. 1999. 'Effect of blast vibration on slope stability.' EXPLO 99, 1-22.
44. Detailed Project Report (DPR). 2010. THDC, India, Ltd.
45. Duncan, J. M. 1999. 'Factors of safety and reliability in geotechnical engineering.' The seventh Spencer J. Buchanan Lecture, Texas A & M.
46. Fuchs, G. 1981. 'Outline of the geology of the Himalaya.' Mitt. östrr. geol. Ges., 101-127.
47. Fuchs, G. and Sinha, A. K. 1978. 'The Tectonics of the Garhwal-Kumaun Lesser Himalaya.' - Jb. geol. B.-A., 121 (2), 219-241, Wien.
48. Gansser, A. 1964. 'Geology of the Himalaya.' Wiley-Interscience, London, 289.
49. Ganesser, A., Heim, A. 1939. 'Central Himalaya: Geological Observations of the Swiss Expedition 1936.' Zürich, Memoires de la Société Helvetique des Sciences Naturelles, V. 73, No. 1, 245. [Reprinted in 1975 by Hindustan Publishing Corporation, Delhi., with an introduction by K.S. Valdiya.
50. Gaur Girish C. S., Dave V. K. S., Mithal R. S. 1977. 'Stratigraphy, structure and tectonics of the carbonate suite of Chamoli, Garhwal Himalaya.' Him. Geol. 7: 416-455.
51. Gaur Girish C. S., Dave V. K. S., Mithal R. S. 1977. 'Magnesite deposits of the calc zone of Chamoli, Garhwal Himalaya, Uttar Pradesh, India.' Him. Geol.ges 256-292.
52. Geological Survey of India. 1989. 'Geology and Tectonics of the Himalaya, Geological Survey of India.' Special Publication No. 26, 192.
53. Geological Survey of India. 2012. 'Mineral Resource of UP and Uttarakhand, India, Geological Survey of India.' Miscellaneous Report.
54. Geotechnical Baseline Report (GBR). 2010. THDC, India, Ltd.
55. Ghosh, A. and Jaak, J. K. Daemen. 1993. 'Fractal characteristics of rock discontinuities.' Engineering Geology 34.1: 1-9.
56. Goel, R. K. and Jethwa, J. L. 1991. 'Prediction of support pressure using RMR Classification.' Proceedings of an Indian Geotechnical Conference, Surat, India.
57. Goel, R. K., Jethwa, J. L. and Paithankar, A. G. 1995. 'An empirical approach for predicting ground condition for runnelling and its practical benefits.' In The 35th US Symposium on Rock Mechanics (USRMS). American Rock Mechanics Association.

58. Goodman R.E. 1976. 'Methods of Geological Engineering in Discontinuous Rocks. West Publishing, San Francisco.
59. Goodman, R. 1980. 'Introduction to Rock Mechanics.' First Edition. J. Wiley & Sons. New York, N.Y. 32-34.
60. Gopalakrishnan, M. 2015. 'Hydro Energy Sector in India: The Past, Present and Future Challenges.' In Proc Indian Natn Sci Acad. Vol. 81, No. 4, pp. 953-967.
61. Grimstad, E. and Barton, N. 1993. 'Updating of the Q-System for NMT.' Proc. Int. Symp. Modem Use of Wet Mix Sprayed Concrete for Underground Support, Fagernes 1993, Norway, 46–66.
62. Grothe, D. and Reinders, P. 2007. 'Advanced vibration management in quarries using a predictive blast vibration model.' European Federation of Explosives Engineers, ISBN 978-0-9550290-1-1, 93-190.
63. Gupta, P. and Anbalagan, R. 1995. 'A Landslide Hazard Zonation (LHZ) mapping of Tehri-Pratapnagar Area, Garhwal Himalaya.' Jour. Of Rock Mechanics and Tunneling Tech., 1, 41-58.
64. Gupta, P. and Anbalagan, R. 1997. 'Slope stability of Tehri Dam Reservoir Area, India, using landslide hazard zonation (LHZ) mapping.' Quarterly Journal of Engineering Geology and Hydrogeology, 30(1), 27-36.
65. Gupta, R.P., Saha, A.K., Arora, M.K. and Kumar, A. 1999. 'Landslide hazard zonation in a part of the Bhagirathi valley, Garhwal Himalayas, using integrated remote sensing-GIS.' Himalayan Geology, 20(2), 71-85.
66. Heuer, R. 1995. 'A quantitative, empirical and theoretical approach on water flow into tunnels.' Rapid Excavation and Tunneling Conference, San Francisco, CA, June 18–21.
67. Hoek, E. 1994. 'Strength of rock and rock masses.' ISRM News J2: 4–16.
68. Hoek, E. 2006. 'Practical Rock Engineering'. Rocscience Inc.
69. Hoek, E. and Bray, J.W. 1981. 'Rock slope Engineering.' 3rd ed., Insti. of Mining and Metallurgy, London., 358.
70. Hoek, E. and Brown, E. T. 1980. 'Underground Excavations in Rock'. London: Institution of Mining and Metallurgy.
71. Hoek, E. and Brown, E. T. 1982. 'Underground excavations in rock.' Inst. of Mining and Metallurgy, London, Rev. Ed., 527.
72. Hoek, E., and Brown, E. T. 1997. 'Practical estimates of rock mass strength.' International Journal of Rock Mechanics and Mining Sciences 34.8: 1165-1186.

73. Hoek, E. and Diederichs, M. S. 2006. 'Empirical estimation of rock mass modulus.' International journal of rock mechanics and mining sciences 43.2: 203-215.
74. Hoek, E., Kaiser, P. K., Bawden, W. F. 1995. 'Support of underground excavations in hard rock.' Balkema, Rotterdam.
75. Hoek, E. and Marinos, P. 2000. 'Predicting tunnel squeezing problems in weak heterogeneous rock masses.' Tunnels and tunnelling international, 32(11), 45-51.
76. Hoek, E., Marinos, P. and Benissi, M. 1998. 'Applicability of the Geological Strength Index (GSI) classification for very weak and sheared rock masses. The case of the Athens Schist Formation.' Bulletin of Engineering Geology and the Environment 57.2: 151-160.
77. Hoek, E., Wood, D. and Shah, S. 1992. 'A modified Hoek-Brown failure criterion for jointed rock masses.' Proc. Int. Conf. Eurock. Vol. 92.
78. Holland, T. H. 1908. 'On the occurrence of striated boulders in the Blaini Formation of Simla, with a discussion on the geological age of the rocks.' Rec. Geol. Surv. India, 37 (1908), 129–135.
79. Houlsby, A. C. 1976. 'Routine interpretation of the Lugeon water-test.' Querterly Journal of Engineering Geology, Vol. 9, 303-313.
80. ICOLD. 1973. 'Lessons from Dam Incidence.' Paris.
81. ICOLD 2000. 'Reservoir landslides: Guidelines for investigation and management.' Bulletin Draft 5a, 1-94.
82. ISRM. 1978. 'Commission on standardisation laboratory and field results. Suggested methods for determining hardness and abrasiveness of rocks.' Int. J. Rock Mech. Min. Geomech. Abstr. 15, 89–97.
83. ISRM. 1979. 'Suggested method for determining the uniaxial compressive strength and deformability of rock materials.' Int J Rock Mech Min Sci Geomech Abst 16(5):135–140.
84. Jain, A. K. 1971. 'Stratigraphy and tectonics of lesser Himalayan region of Uttarkashi, Garhwal Himalaya.' Him. Geol 1: 25-58.
85. Jayabalan, K., Bhattacharya, N.R., Gajbhiye, P.K., and Thinley Dukpa. 2010. 'Construction stage geotechnical evaluation of Powerhouse Cavern Punatsangchhu-1 HEP, Wandue Phodrang District, Bhutan.' Accelerated Devel. of Hydropower in Bhutan – Oppurtunities and Challenges, Thimphu, Bhutan.
86. Jayabalan, K., Bhattacharya, N.R., and Gajbhiye, P.K. 2010. 'Pre-construction stage geotechnical evaluation of alternate underground Powerhouse Complex of

Punatsangchhu-2 HEP.' Accelerated Devel. of Hydropower in Bhutan – Oppurtunities and Challenges, Thimphu, Bhutan.

87. Jommi, C. and Pandolfi, A. 2008. 'Vibrations induced by blasting in rock: a numerical approach.'
88.
89. Kaiser, P.K., MacKay, C. and Gale, A.D. 1986. 'Evaluation of rock classifications at BC Rail tumbler ridge tunnels.' Rock mechanics and rock engineering, 19(4), 205-234.
90. Kalamaras, G. S. and Bieniawski, Z. T. 1995. 'A rock mass strength concept for coal seams incorporating the effect of time.' 8th ISRM Congress. International Society for Rock Mechanics.
91. Kumar, G. 1971. 'Geology and sulphide mineralization in the Pokhri area, Chamoli district, Uttar Pradesh.' Geol. Surv. India Misc. Publ., 16, 92–98.
92. Kumar, G. 2005. Geology of Uttar Pradesh & Uttaranchal. *GSI Publications, 2* (1).
93. Kumar, G. and Agarwal, N. C. 1975. 'Geology of the Srinagar Nandprayag area (Alaknanda Valley) Chamoli Garhwal and Tehri Garhwal districts, Kumaun Himalaya, Uttar Pradesh.' Him. Geol., 5, 29–59.
94. Kumar, G., Mehdi, S. H., and Prakash, G. 1972. 'A review of stratigraphy of parts of Uttar Pradesh Tethys Himalaya.' Jour Pal. Soc. India 15: 86-98.
95. Le Fort, E. 1975. 'Himalyas: the collided range. Present knowledge of the continental arc.' Am. J. Sci., 275-A: 1-44.
96. Lugeon, M. 1933. Barrages et géologie.
97. Marinos, Paul, and Evert Hoek. 2000. 'GSI: a geologically friendly tool for rock mass strength estimation.' ISRM International Symposium. International Society for Rock Mechanics.
98. Marinos, P. and Hoek, E. 2001. 'Estimating the geotechnical properties of heterogeneous rock masses such as flysch.' Bulletin of engineering geology and the environment, 60(2), 85-92.
99. Marinos, V., Marinos, P. and Hoek, E. 2005. 'The geological strength index: applications and limitations.' Bulletin of Engineering Geology and the Environment, 64(1), 55-65.
100. Markland, J.T. 1972. 'A Useful Technique Fro Estimating the Stability of Rock Slopes when the Rigid Wedge Slide Type of Failure is Expected.' Imperial College of Science & Technology.
101. Mehdi, S. H., Kumar, G. and Prakash, G. 1972. 'Tectonic evolution of eastern Kumaun Himalaya: a new approach.' Himalayan Geol., 2 (1972), 481–501.

102.Mehrotra, V.K. 1992. 'Estimation of engineering parameters of rock mass.' (Doctoral dissertation, Ph. D. thesis. Department of Civil Engineering, University of Roorkee, Roorkee).

103.Mehta, P.N., Pradhan, S.R. 1972. 'Geological cases for mishaps and failures of engineering structures.' GSI record Vol. 104, Pt. 2.

104.Middlemiss, C. S. 1885. 'A fossiliferous series in Lower Himalayas.' Rec. Geol. Surv. Ind., 18, 73–77.

105.Misra, R. C. and Sharma, R. P. 1967. 'Geology of Devidhura Area, Almora, U.P.' Jour. Geol. Soc Ind, Vol 8.

106.Mohamed, M. T. 2010. 'Vibration Control.' MickaÃƒÂ«l Lallart (Ed.), ISBN: 978-953-307117-6, InTech, Available from: http://www.intechopen.com/books/vibration-control/vibration-control, 355-380.

107.Negi, M. and Singh, H.R. 1990. 'Substratum as determining factor for bottom fauna in the river Alaknanda.' In Proc. Indian Nat. Sci. Acad. B, Vol. 56, 417-423.

108.Oldham, T. 1882. 'A catalogue of Indian earthquakes from the earliest time to the end of A.D. 1869.' Memoir Geological Survey of India 19, 163–215.

109.Oldham, R. D. 1899. 'Report on the great earthquake of 12 June 1887.' Memoir Geological Survey of India 29, 1–309.

110.Oyedpo, S. O. 2012. 'Energy and sustainable development in Nigeria: the way forward.' Energy, Sustainability and Society 2012, 2:15.

111.Pal, S., Kaynia, A. M., Bhasin, R. K. and Paul, D. K. 2012. 'Earthquake stability analysis of rock slopes: a case study.' Rock Mechanics and Rock Engineering, 45(2), 205-215.

112.Palmstrom. A. 1982. 'The volumetric joint count—a useful and simple measure of the degree of rock mass jointing.' Proc. 4th Cong. Int. Assoc. Eng. Geol., New Delhi, vol. 2 (1982), 221–228.

113. Rai R, Shrivastva BK, Singh TN. 2005. 'Prediction of maximum safe charge per delay in surface mining.' Min Technol (Trans Inst Min Metall A) 114(4):A227–A231.

114.Ramanathan, K. and Abeygunawardena, P. 2007. 'Hydropower development in India.' Asian Development Bank.

115.Ramamurthy, T. 1993. 'Strength and modulus responses of anisotropic rocks.' Comprehensive Rock Engineering, 1 (13), 313–329.

116.Ramamurthy T. 2007. 'Engineering in Rocks for Slopes, Foundations and Tunnels.' Pub: PHI Learning Pvt. Ltd.

117.Ramamurthy T., Rao G. V. and Rao K. S. 1985. ‘Strength criterion for rocks.’ Proc, lndn. Geotech. Conf. Roorkee, Vol. I, pp. 59-64.

118.Ramamurthy T. 1986. ‘Stability of rock mass.’ 8th 1.G.S. Annual Lecture. lndn. Geotech. J. 16, 1-74.Rawat, P. V. S., and Gairola, B. M., 1999. ‘Report on Quaternary geological and geomorphological studies in Alaknanda/Ganga Basin, Chamoli, Pauri, Tehri, Haridwar and Dehradun districts, Uttar Pradesh.’ GSI, Unpublished report, F.S. 1992- 93, 93-94, 94-95 and 95-96.

119.Ramamurthy, T. ed. 2010. ‘Engineering in rocks for slopes, foundations and tunnels.’ PHI Learning Pvt. Ltd.

120. Reddy, K.R., Hettiarachchi, H., Parakalla, N.S., Gangathulasi, J. and Bogner, J.E. 2009. ‘Geotechnical properties of fresh municipal solid waste at Orchard Hills Landfill, USA.’ Waste Management, 29(2), 952-959.

121.Richards, A., Argels, T., Harris, N., Parrish, R., Ahmad, T., Darbyshire, F. and Dragantis, E. 2005. ‘Himalayan architecture constrained by isotopic tracers from clastic sediments.’ Earth & Planetary Science Letters, 236: 773–796.

122.Rupke, J. 1974. ‘Stratigraphic and structural evolution of Kumaon Lesser Himalaya.’ Sedimentary Geology 11.2 (1974): 81-265.

123.Sajinkumar, K.S. and Anbazhagan, S. 2015. ‘Geomorphic appraisal of landslides on the windward slope of Western Ghats, southern India.’ Natural Hazards, 75(1), 953-973.

124.Sarkar, S. and Kanungo, D.P. 2004. ‘An integrated approach for landslide susceptibility mapping using remote sensing and GIS.’ Photogrammetric Engineering & Remote Sensing, 70(5), 617-625.

125.Serafim, J. L. and Pereira, J. P. 1983. ‘Consider ation of the geomechanical classification of Bieniawski.’ Proc. Int. Symp. on Engineering Geology and Underground Construction, Lisbon, Volume 1 (1983), 33–44 (II).

126.Sheorey, P.R. 1997. ‘Empirical rock failure criteria.’ AA Balkema.

127.Silitonga, M.A.H.T.A.H.A.N. 1988. Prediction of ground vibration due to blasting.

128.Singh, B. and Goel, R. K. 1999. ‘Rock mass classification. A practical approach in civil engineering.’ Oxford, UK: Elsevier. 267.

129.Singh, B. and Goel, R.K., 2002. Software for engineering control of landslide and tunnelling hazards. CRC Press.

130.Singh, B., Jethwa, J. L., Dube, A. K. and Singh, B. 1992. ‘Correlation between observed support pressure and rock mass quality’. Tunnel. Underground Space Technol., 7 (1), 59–74.

131. Singh, M., Rao, K.S. and Ramamurthy, T. 2002. Strength and deformational behaviour of a jointed rock mass. Rock Mechanics and Rock Engineering, 35(1), 45-64.
132. Singh, M. and Rao, K. S. 2005. 'Empirical methods to estimate the strength of jointed rock masses.' Engineering Geology 77.1: 127-137.
133. Singh, T.N. 2013. 'Probabilistic and sensitivity investigation for the hill slopes in Uttarakhand, lesser Himalaya, India.' American Journal of Numerical Analysis, 1(1), .8-14.
134. Singh, T.N., Gulati, A., Dontha, L. and Bhardwaj, V., 2008. 'Evaluating cut slope failure by numerical analysis—a case study.' Natural Hazards, 47(2), 263-279.
135. Siskind, D. E., Stagg, M. S., Kopp, J. W. and Dowding C. H. 1983. 'Structure response and damage produced by ground vibration from surface mine blasting.' Report of investigations, Bureau of Mines; 8507, 1-74.
136. Sorkhabi, R. B. and Macfarlane, A. 1999. 'Himalaya and Tibet: Mountain roots to mountain tops.' Geological Society of America, Special Paper 328.
137. Srivastava, P. and Mitra, G. 1994. 'Thrust geometries and deep structure of the outer and lesser Himalaya, Kumaon and Garhwal (India): Implications for evolution of the Himalayan fold-and-thrust belt.' Tectonics13.1: 89-109.
138. Srivastava, R.N. and Ahmad, A. 1979. 'Geology and structure of the Alaknanda Valley, Garhwal Himalaya.' Himal. Geol., 9, 225–254.
139. Terzaghi, K. 1946. 'Rock defects and loads on tunnel supports.'
140. Terzaghi, K., Peck, R. and Mesri, G. 1996. 'Soil Mechanics in Engineering Practice.' Third Edition. J. Wiley & Sons. New York, N.Y. 72-73.
141. Thakur V. C. 1992. 'Geology of Western Himalaya.' Pergamon Press, Oxford, 363.
142. THDC India Limited. 2009. 'Environmental Studies for. Vishnugad Pipalkoti Hydro Electric Project.' Final Report. Consolidated Environmental Assessment (EA), Vol. 1, R4, 3-21.
143. Tomczak, J. 2006. 'Implications of fossil fuel dependence for the food system.' Tompkins Country Relocalization Project.
144. Trueman, R. 1988. 'An Evaluation of strata support techniques in dual life gateroads.' Ph D thesis, University of Wales, Cardiff.
145. Valdiya, K. S. 1978. 'Extension and analogues of the Chail Nappe in the Kumaun Himalaya.' Indian Jour. Earth Sciences, v. 5, 1-19.
146. Valdiya, K. S. 1980. 'Geology of Kumaun Lesser Himalaya.' Wadia Institute of Hima. Geol., Dehradun, 291.

147. Valdiya, K. S. 1995. 'Proterozoic sedimentation and Pan-African geodynamic development in the Himalaya.' Precambrian Research 74.1: 35-55.
148. Valdiya, K. S. 1998. 'Dynamic Himalaya.' University Press, Hyderabad, 178.
149. Valdiya K. S. 2014. 'Damming rivers in the tectonically resurgent Uttarakhand Himalaya.' Current Science 106: 1658-1668.
150. Vanmarcke, E.H. 1980. 'Probabilistic stability analysis of earth slopes.' Engineering Geology, 16(1), 29-50.
151. Vavro, M., Soucek, K., Staš, L., Waclawik, P., Vavro, L., Konicek, P. and Ptácek, J. 2015. 'Application of alternative methods for determination of rock quality designation (RQD) index: a case study from the Rozná I uranium mine, Strázek Moldanubicum, Bohemian Massif, Czech Republic.' NRC Research Press, Can. Geotech. J. 52: 1466–1476.
152. Verma, R. K. 1997: 'Paleomagnetism from parts of Tethys Himalaya, Indus Suture Zone, Ladakh and South Tibet: Implications for collision between Indian and Eurasian Plate.' Himalaya Geol., 18, 92-102.
153. Viladkar, M. N., Ranjan, G. and Sharma, R. P. 1993. 'Soil-structure interaction in the time domain.' Computers & structures, 46(3), 429-442.
154. Windley, B. E. 1983. 'Metamorphism and tectonics of the Himalaya.' J. Geol. Soc. London, 140: 849-865.
155. Windley, B. F. 1995. 'The evolving continents (3d ed.).' London, Wiley, 526.
156. Yan, Y., Zhang, Y. and Huang, C. 2014. 'Impact of blasting vibration on soil slope stability.' EJGE, Vol. 19, 6559-6568.
157. Yudhbir, Y., Lemanza, W. and Prinzl, F. 1983. 'An empirical failure criterion for rock masses.' 5th ISRM Congress. International Society for Rock Mechanics.
158. Zhang, L. 2010. 'Estimating the strength of jointed rock masses.' Rock mechanics and rock engineering 43.4: 391-402.

ANNEXURES

Annexure I

Power Tunnel Unwedge Analysis

Unwedge Analysis Information Segment AB

Document Name

File Name: VHEP PT Sg1 - - Copy (Recovered).weg

Project Settings

Project Title: VHEP PT
Wedges Computed: Perimeter and End Wedges
Units: Metric, stress as MPa

General Input Data

Tunnel Axis Orientation:
  Trend: 215°
  Plunge: 2°
Design Factor of Safety: 1.500
Unit Weight of Rock: 0.026 MN/m3
Unit Weight of Water: 0.010 MN/m3

Seismic Forces

Direction: Sliding
Seismic Coefficient: 0.12

Scale Wedges Settings

Not Used

Joint Orientations

<u>Joint 1</u>
  Dip: 38°
  Dip Direction: 010°
<u>Joint 2</u>
  Dip: 60°
  Dip Direction: 200°
<u>Joint 3</u>
  Dip: 80°
  Dip Direction: 285°

Joint Properties

<u>FJ</u>
  Water Pressure
    Constant: 0 MPa

Waviness: 10°
Shear Strength Model: Barton-Bandis
JRC: 9
JCS: 20 MPa
Phi b: 25°

J1
Water Pressure
Constant: 0 MPa
Waviness: 10°
Shear Strength Model: Barton-Bandis
JRC: 9
JCS: 10 MPa
Phi b: 27°

J2
Water Pressure
Constant: 0 MPa
Waviness: 10°
Shear Strength Model: Barton-Bandis
JRC: 9
JCS: 20 MPa
Phi b: 27°

Bolt Properties

Bolt Property 1
Bolt Type: Mechanically Anchored
Tensile Capacity: 0.1 MN
Plate Capacity: 0.1 MN
Anchor Capacity: 0.1 MN
Shear Strength: Used
Shear Strength: 0.02 MN
Bolt Orientation Efficiency: Used
Method: Unwedge 2.0

Shotcrete Properties

Shotcrete Property 1
Shear Strength: 2.00 MPa
Unit Weight: 0.026 MN/m3
Thickness: 1.00 cm

Support Summary

Summary of Perimeter Shotcrete
No Shotcrete on Perimeter

Summary of Perimeter Support Pressure
No Support Pressure on Perimeter

Summary of Perimeter Bolt Patterns
No Bolt Patterns on Perimeter

Summary of End Bolt Patterns
No Bolt Pattern on Ends

Summary of End Support Pressure
No Support Pressure on Ends

Summary of End Shotcrete
No Shotcrete on Ends

Wedge Information

Floor wedge [1]
Factor of Safety: 12.028
Wedge Weight: 0.001 MN

Lower Right wedge [2]
Factor of Safety: stable
Wedge Weight: 0.349 MN

Lower Left wedge [3]
Factor of Safety: 1.797
Wedge Weight: 0.007 MN

Upper Right wedge [6]
Factor of Safety: 1.009
Wedge Weight: 0.000 MN

Upper Left wedge [7]
Factor of Safety: 0.277
Wedge Weight: 0.149 MN

Upper Right wedge [8]
Factor of Safety: 0.000
Wedge Weight: 0.016 MN

Near End wedge [9]
Factor of Safety: 0.906
Wedge Weight: 0.587 MN

Far End wedge [10]
Factor of Safety: 1.480
Wedge Weight: 0.544 MN

Unwedge Analysis Information Segment BC

Document Name

File Name: VHEP PT Sg2.weg

Project Settings

Project Title: VHEP PT
Wedges Computed: Perimeter and End Wedges

Units: Metric, stress as MPa

General Input Data

Tunnel Axis Orientation:
  Trend: 240°
  Plunge: 2°
Design Factor of Safety: 1.500
Unit Weight of Rock: 0.027 MN/m3
Unit Weight of Water: 0.010 MN/m3

Seismic Forces

Direction: Sliding
Seismic Coefficient: 0.12

Scale Wedges Settings

Not Used

Joint Orientations

Joint 1
  Dip: 38°
  Dip Direction: 355°
Joint 2
  Dip: 70°
  Dip Direction: 210°
Joint 3
  Dip: 40°
  Dip Direction: 285°

Joint Properties

FJ
  Water Pressure
    Constant: 0 MPa
  Waviness: 10°
  Shear Strength Model: Barton-Bandis
    JRC: 8
    JCS: 24 MPa
    Phi b: 30°

J1
  Water Pressure
    Constant: 0 MPa
  Waviness: 10°
  Shear Strength Model: Barton-Bandis
    JRC: 6
    JCS: 22 MPa
    Phi b: 25°

J2
  Water Pressure

Constant: 0 MPa
Waviness: 10°
Shear Strength Model: Barton-Bandis
JRC: 10
JCS: 18 MPa
Phi b: 30°

Bolt Properties

Bolt Property 1
Bolt Type: Mechanically Anchored
Tensile Capacity: 0.1 MN
Plate Capacity: 0.1 MN
Anchor Capacity: 0.1 MN
Shear Strength: Unused
Bolt Orientation Efficiency: Used
Method: Cosine Tension/Shear

Shotcrete Properties

Shotcrete Property 1
Shear Strength: 2.00 MPa
Unit Weight: 0.026 MN/m3
Thickness: 10.00 cm

Support Summary

Summary of Perimeter Shotcrete
No Shotcrete on Perimeter

Summary of Perimeter Support Pressure
No Support Pressure on Perimeter

Summary of Perimeter Bolt Patterns
Number of Bolt Patterns on Perimeter: 5
Perimeter Bolt Pattern: 1
Property: Bolt Property 1
Strength type: Mechanically Anchored
Bolt Length: 5.00 m
Orientation: normal to boundary
Pattern Spacing - In Plane: 1.50 m
Pattern Spacing - Out of Plane: 2.50 m
Pattern Spacing - Out of Plane Offset: 0.00 m
Perimeter Bolt Pattern: 2
Property: Bolt Property 1
Strength type: Mechanically Anchored
Bolt Length: 8.00 m
Orientation: normal to boundary
Pattern Spacing - In Plane: 1.50 m
Pattern Spacing - Out of Plane: 2.50 m
Pattern Spacing - Out of Plane Offset: 0.00 m
Perimeter Bolt Pattern: 3
Property: Bolt Property 1

Strength type: Mechanically Anchored
Bolt Length: 8.00 m
Orientation: normal to boundary
Pattern Spacing - In Plane: 1.50 m
Pattern Spacing - Out of Plane: 2.50 m
Pattern Spacing - Out of Plane Offset: 0.00 m

Perimeter Bolt Pattern: 4

Property: Bolt Property 1
Strength type: Mechanically Anchored
Bolt Length: 8.00 m
Orientation: normal to boundary
Pattern Spacing - In Plane: 1.50 m
Pattern Spacing - Out of Plane: 2.50 m
Pattern Spacing - Out of Plane Offset: 0.00 m

Perimeter Bolt Pattern: 5

Property: Bolt Property 1
Strength type: Mechanically Anchored
Bolt Length: 1.50 m
Orientation: normal to boundary
Pattern Spacing - In Plane: 1.50 m
Pattern Spacing - Out of Plane: 2.50 m
Pattern Spacing - Out of Plane Offset: 0.00 m

Summary of End Bolt Patterns

No Bolt Pattern on Ends

Summary of End Support Pressure

No Support Pressure on Ends

Summary of End Shotcrete

No Shotcrete on Ends

Wedge Information

Lower Right wedge [2]

Factor of Safety: stable
Wedge Weight: 10.254 MN

Upper Right wedge [6]

Factor of Safety: 1067.952
Wedge Weight: 0.000 MN

Upper Left wedge [7]

Factor of Safety: 1.737
Wedge Weight: 7.037 MN

Roof wedge [8]

Factor of Safety: 0.000
Wedge Weight: 0.000 MN

Near End wedge [9]

Factor of Safety: 2.334
Wedge Weight: 0.055 MN

Far End wedge [10]

Factor of Safety: stable
Wedge Weight: 0.055 MN

Unwedge Analysis Information Segment CD

Document Name

File Name: VHEP PT Sg3.weg

Project Settings

Project Title: VHEP PT
Wedges Computed: Perimeter and End Wedges
Units: Metric, stress as MPa

General Input Data

Tunnel Axis Orientation:
  Trend: 205°
  Plunge: 0°
Design Factor of Safety: 1.500
Unit Weight of Rock: 0.026 MN/m3
Unit Weight of Water: 0.010 MN/m3

Seismic Forces

Direction: Sliding
Seismic Coefficient: 0.12

Scale Wedges Settings

Not Used

Joint Orientations

Joint 1
  Dip: 40°
  Dip Direction: 330°
Joint 2
  Dip: 65°
  Dip Direction: 030°
Joint 3
  Dip: 60°
  Dip Direction: 230°

Joint Properties

FJ
  Water Pressure
    Constant: 0 MPa
  Waviness: 10°
  Shear Strength Model: Barton-Bandis

JRC: 8
JCS: 18 MPa
Phi b: 25°

J1
Water Pressure
Constant: 0 MPa
Waviness: 10°
Shear Strength Model: Barton-Bandis
JRC: 9
JCS: 24 MPa
Phi b: 27°

J2
Water Pressure
Constant: 0 MPa
Waviness: 10°
Shear Strength Model: Barton-Bandis
JRC: 8
JCS: 25 MPa
Phi b: 28°

Bolt Properties

Bolt Property 1
Bolt Type: Split Set
Tensile Capacity: 0.1 MN
Bond Strength: 0.03 MN/m
Shear Strength: Unused
Bolt Orientation Efficiency: Used
Method: Cosine Tension/Shear

Shotcrete Properties

Shotcrete Property 1
Shear Strength: 2.00 MPa
Unit Weight: 0.026 MN/m3
Thickness: 10.00 cm

Support Summary

Summary of Perimeter Shotcrete
No Shotcrete on Perimeter

Summary of Perimeter Support Pressure
No Support Pressure on Perimeter

Summary of Perimeter Bolt Patterns
Number of Bolt Patterns on Perimeter: 3
Perimeter Bolt Pattern: 1
Property: Bolt Property 1
Strength type: Split Set
Bolt Length: 5.00 m

Orientation: normal to boundary
Pattern Spacing - In Plane: 1.50 m
Pattern Spacing - Out of Plane: 2.50 m
Pattern Spacing - Out of Plane Offset: 0.00 m

Perimeter Bolt Pattern: 2

Property: Bolt Property 1
Strength type: Split Set
Bolt Length: 5.00 m
Orientation: normal to boundary
Pattern Spacing - In Plane: 1.50 m
Pattern Spacing - Out of Plane: 2.50 m
Pattern Spacing - Out of Plane Offset: 0.00 m

Perimeter Bolt Pattern: 3

Property: Bolt Property 1
Strength type: Split Set
Bolt Length: 1.20 m
Orientation: normal to boundary
Pattern Spacing - In Plane: 1.00 m
Pattern Spacing - Out of Plane: 2.50 m
Pattern Spacing - Out of Plane Offset: 0.00 m

Summary of End Bolt Patterns

No Bolt Pattern on Ends

Summary of End Support Pressure

No Support Pressure on Ends

Summary of End Shotcrete

No Shotcrete on Ends

Wedge Information

Upper Left wedge [4]

Factor of Safety: 1.532
Wedge Weight: 5.613 MN

Lower Right wedge [5]

Factor of Safety: stable
Wedge Weight: 7.076 MN

Upper Right wedge [6]

Factor of Safety: 18.506
Wedge Weight: 0.000 MN

Roof wedge [8]

Factor of Safety: 16.851
Wedge Weight: 0.000 MN

Near End wedge [9]

Factor of Safety: stable
Wedge Weight: 0.002 MN

Far End wedge [10]

Factor of Safety: 2.056
Wedge Weight: 0.002 MN

Unwedge Analysis Information Segment DE

Document Name

File Name: VHEP PT Sg4.weg

Project Settings

Project Title: VHEP PT
Wedges Computed: Perimeter and End Wedges
Units: Metric, stress as MPa

General Input Data

Tunnel Axis Orientation:
  Trend: 170°
  Plunge: 0°
Design Factor of Safety: 1.500
Unit Weight of Rock: 0.026 MN/m3
Unit Weight of Water: 0.010 MN/m3

Seismic Forces

Direction: Sliding
Seismic Coefficient: 0.12

Scale Wedges Settings

Not Used

Joint Orientations

Joint 1
  Dip: 30°
  Dip Direction: 330°
Joint 2
  Dip: 65°
  Dip Direction: 030°
Joint 3
  Dip: 68°
  Dip Direction: 230°

Joint Properties

FJ
  Water Pressure
    Constant: 0 MPa
  Waviness: 10°
  Shear Strength Model: Barton-Bandis
    JRC: 8
    JCS: 22 MPa

Phi b: 25°

J1
Water Pressure
Constant: 0 MPa
Waviness: 10°
Shear Strength Model: Barton-Bandis
JRC: 6
JCS: 22 MPa
Phi b: 28°

J2
Water Pressure
Constant: 0 MPa
Waviness: 10°
Shear Strength Model: Barton-Bandis
JRC: 10
JCS: 18 MPa
Phi b: 30°

Bolt Properties

Bolt Property 1
Bolt Type: Mechanically Anchored
Tensile Capacity: 0.1 MN
Plate Capacity: 0.1 MN
Anchor Capacity: 0.1 MN
Shear Strength: Unused
Bolt Orientation Efficiency: Used
Method: Cosine Tension/Shear

Shotcrete Properties

Shotcrete Property 1
Shear Strength: 2.00 MPa
Unit Weight: 0.026 MN/m3
Thickness: 10.00 cm

Support Summary

Summary of Perimeter Shotcrete
No Shotcrete on Perimeter

Summary of Perimeter Support Pressure
No Support Pressure on Perimeter

Summary of Perimeter Bolt Patterns
No Bolt Patterns on Perimeter

Summary of End Bolt Patterns
No Bolt Pattern on Ends

Summary of End Support Pressure

No Support Pressure on Ends

Summary of End Shotcrete
No Shotcrete on Ends

Wedge Information

Upper Left wedge [4]
Factor of Safety: 2.165
Wedge Weight: 16.401 MN

Lower Right wedge [5]
Factor of Safety: stable
Wedge Weight: 19.363 MN

Upper Right wedge [8]
Factor of Safety: 0.000
Wedge Weight: 0.000 MN

Near End wedge [9]
Factor of Safety: stable
Wedge Weight: 13.266 MN

Far End wedge [10]
Factor of Safety: 2.204
Wedge Weight: 9.311 MN

Unwedge Analysis Information Segment EF

Document Name

File Name: VHEP PT Sg5.weg

Project Settings

Project Title: VHEP PT
Wedges Computed: Perimeter and End Wedges
Units: Metric, stress as MPa

General Input Data

Tunnel Axis Orientation:
Trend: 185°
Plunge: 2°
Design Factor of Safety: 1.500
Unit Weight of Rock: 0.026 MN/m3
Unit Weight of Water: 0.010 MN/m3

Seismic Forces

Direction: Sliding
Seismic Coefficient: 0.12

Scale Wedges Settings

Not Used

Joint Orientations

Joint 1
Dip: 30°
Dip Direction: 330°
Joint 2
Dip: 60°
Dip Direction: 030°
Joint 3
Dip: 68°
Dip Direction: 230°

Joint Properties

FJ
Water Pressure
Constant: 0 MPa
Waviness: 10°
Shear Strength Model: Barton-Bandis
JRC: 8
JCS: 22 MPa
Phi b: 25°

J1
Water Pressure
Constant: 0 MPa
Waviness: 10°
Shear Strength Model: Barton-Bandis
JRC: 8
JCS: 22 MPa
Phi b: 28°

J2
Water Pressure
Constant: 0 MPa
Waviness: 10°
Shear Strength Model: Barton-Bandis
JRC: 8
JCS: 25 MPa
Phi b: 30°

Bolt Properties

Bolt Property 1
Bolt Type: Mechanically Anchored
Tensile Capacity: 0.1 MN
Plate Capacity: 0.1 MN
Anchor Capacity: 0.1 MN
Shear Strength: Unused

Bolt Orientation Efficiency: Used
Method: Cosine Tension/Shear

Shotcrete Properties

Shotcrete Property 1
Shear Strength: 2.00 MPa
Unit Weight: 0.026 MN/m3
Thickness: 10.00 cm

Support Summary

Summary of Perimeter Shotcrete
No Shotcrete on Perimeter

Summary of Perimeter Support Pressure
No Support Pressure on Perimeter

Summary of Perimeter Bolt Patterns
Number of Bolt Patterns on Perimeter: 3
Perimeter Bolt Pattern: 1
Property: Bolt Property 1
Strength type: Mechanically Anchored
Bolt Length: 5.00 m
Orientation: normal to boundary
Pattern Spacing - In Plane: 1.50 m
Pattern Spacing - Out of Plane: 2.50 m
Pattern Spacing - Out of Plane Offset: 0.00 m
Perimeter Bolt Pattern: 2
Property: Bolt Property 1
Strength type: Mechanically Anchored
Bolt Length: 5.00 m
Orientation: angle to local x, Angle: 30.00 °
Pattern Spacing - In Plane: 1.50 m
Pattern Spacing - Out of Plane: 2.50 m
Pattern Spacing - Out of Plane Offset: 0.00 m
Perimeter Bolt Pattern: 3
Property: Bolt Property 1
Strength type: Mechanically Anchored
Bolt Length: 2.50 m
Orientation: normal to boundary
Pattern Spacing - In Plane: 1.50 m
Pattern Spacing - Out of Plane: 2.50 m
Pattern Spacing - Out of Plane Offset: 0.00 m

Summary of End Bolt Patterns
No Bolt Pattern on Ends

Summary of End Support Pressure
No Support Pressure on Ends

Summary of End Shotcrete
No Shotcrete on Ends

Wedge Information

Upper Left wedge [4]
Factor of Safety: 2.111
Wedge Weight: 12.374 MN

Lower Right wedge [5]
Factor of Safety: stable
Wedge Weight: 14.123 MN

Upper Right wedge [6]
Factor of Safety: 1.096
Wedge Weight: 0.000 MN

Roof wedge [8]
Factor of Safety: 0.000
Wedge Weight: 0.000 MN

Near End wedge [9]
Factor of Safety: stable
Wedge Weight: 3.461 MN

Far End wedge [10]
Factor of Safety: 2.194
Wedge Weight: 3.264 MN

Annexure II

Effect of Blasting on Slope

Stability analysis of Jharetha village,

****

UNITS USED -> TONNE - METER - DEGREE

INPUT FILE NAME ->isast.th7

OUTPUT FILE NAME ->osast.th7

****

CASE NUMBER = 1

~~~~~~~~~~~~~~~~~~

C = 8.000 PHI = 25.000 GAMA = 1.800 GAMAW = 1.000

Z = 38.000 ZW = 28.000 SIF = 28.000 AH = .100

AV = -.050 EQM = 7.000 Q = .000 FS = 1.200

~~~~~~

FACTOR OF SAFETY WITH DIFFERENT CONDITIONS****** CRITICAL DYNAMIC

ACCELERATION DISPLACEMENT(M)

FS1(No Surcharge & E.Q.,But Dry) =1.164

FS2(With Surcharge & W.T.,But No E.Q.) =1.097

FS3(No Surcharge & E.Q. , But W.T.) =1.097

FS4(No Surcharge , With E.Q. & Dry) = .949 .066 .04

FS5(No Surcharge , With E.Q. & W.T.[WORST]= .836 .013 .26

~~~~~~
~~~~~~

Stability analysis of Surenda village

```
******************************************************************************
    UNITS USED          -> TONNE - METER - DEGREE
    INPUT FILE NAME     ->isast.th6
    OUTPUT FILE NAME    ->osast.th6
******************************************************************************

CASE NUMBER =   1
~~~~~~~~~~~~~~~~~~
C    =    8.000   PHI  =   25.000   GAMA  =    1.800   GAMAW =   1.000
Z    =   35.000   ZW   =   25.000   SIF   =   32.000   AH    =   .100
AV   =    -.050   EQM  =    7.000   Q     =    .000    FS    =   1.200
~~~~~~~~~~~~~~~~~~~~~~~~~~~~~~~~~~~~~~~~~~~~~~~~~~~~~~~~~~~~~~~~~~~~~~~~~~~~~~~~
FACTOR OF SAFETY WITH DIFFERENT CONDITIONS******     CRITICAL     DYNAMIC
                                               ACCELERATION DISPLACEMENT(M)
FS1(No Surcharge & E.Q.,But Dry)        =1.139
FS2(With Surcharge & W.T.,But No E.Q.)  =1.070
FS3(No Surcharge & E.Q. , But W.T.)     =1.070
FS4(No Surcharge , With E.Q. & Dry)     = .927      .013          .25
FS5(No Surcharge , With E.Q. & W.T.[WORST]= .815    .000          10.57
~~~~~~~~~~~~~~~~~~~~~~~~~~~~~~~~~~~~~~~~~~~~~~~~~~~~~~~~~~~~~~~~~~~~~~~~~~~~~~~~
```

Stability analysis of Tirosi village

```
******************************************************************************
   UNITS USED          -> TONNE - METER - DEGREE
   INPUT FILE NAME      ->isast.th2
   OUTPUT FILE NAME     ->osast.th2
******************************************************************************

CASE NUMBER =    1
~~~~~~~~~~~~~~~~~~
C    =    8.000    PHI   =    25.000    GAMA  =     1.800    GAMAW =    1.000
Z    =    30.000    ZW    =    20.000    SIF   =    17.000    AH    =     .100
AV   =    -.050    EQM   =     7.000    Q     =      .000    FS    =    1.200
~~~~~~~~~~~~~~~~~~~~~~~~~~~~~~~~~~~~~~~~~~~~~~~~~~~~~~~~~~~~~~~~~~~~~~~~~~~~~~
FACTOR OF SAFETY WITH DIFFERENT CONDITIONS******     CRITICAL     DYNAMIC
                                                ACCELERATION DISPLACEMENT(M)
FS1(No Surcharge & E.Q.,But Dry)          =2.055
FS2(With Surcharge & W.T.,But No E.Q.)    =1.773
FS3(No Surcharge & E.Q. , But W.T.)       =1.773
FS4(No Surcharge , With E.Q. & Dry)       =1.513       .304          .00
FS5(No Surcharge , With E.Q. & W.T.[WORST]=1.292       .222          .00
~~~~~~~~~~~~~~~~~~~~~~~~~~~~~~~~~~~~~~~~~~~~~~~~~~~~~~~~~~~~~~~~~~~~~~~~~~~~~~
```

Stability analysis of Hyuna village

```
****************************************************************************
   UNITS USED         -> TONNE - METER - DEGREE
   INPUT FILE NAME     ->isast.th8
   OUTPUT FILE NAME    ->osast.th8
****************************************************************************

CASE NUMBER =   1
~~~~~~~~~~~~~~~~~~
C    =    8.000   PHI  =   25.000   GAMA  =    1.800   GAMAW =   1.000
Z    =   25.000   ZW   =   15.000   SIF   =   20.000   AH    =   .100
AV   =    -.050   EQM  =    7.000   Q     =     .000   FS    =   1.200
~~~~~~~~~~~~~~~~~~~~~~~~~~~~~~~~~~~~~~~~~~~~~~~~~~~~~~~~~~~~~~~~~~~~~~~~~~~~~~
FACTOR OF SAFETY WITH DIFFERENT CONDITIONS******     CRITICAL     DYNAMIC
                                      ACCELERATION DISPLACEMENT(M)
FS1(No Surcharge & E.Q.,But Dry)         =1.834
FS2(With Surcharge & W.T.,But No E.Q.)    =1.550
FS3(No Surcharge & E.Q. , But W.T.)       =1.550
FS4(No Surcharge , With E.Q. & Dry)       =1.407      .271           .00
FS5(No Surcharge , With E.Q. & W.T.[WORST]=1.175      .179           .00
~~~~~~~~~~~~~~~~~~~~~~~~~~~~~~~~~~~~~~~~~~~~~~~~~~~~~~~~~~~~~~~~~~~~~~~~~~~~~~
```

Stability analysis of Tapon village,

****

UNITS USED -> TONNE - METER - DEGREE

INPUT FILE NAME ->isast.th3

OUTPUT FILE NAME ->osast.th3

****

CASE NUMBER = 1

~~~~~~~~~~~~~~~~~~

C = 8.000 PHI = 25.000 GAMA = 1.800 GAMAW = 1.000

Z = 35.000 ZW = 20.000 SIF = 21.000 AH = .100

AV = -.050 EQM = 7.000 Q = .000 FS = 1.200

~~~~~~

FACTOR OF SAFETY WITH DIFFERENT CONDITIONS****** CRITICAL DYNAMIC

ACCELERATION DISPLACEMENT(M)

FS1(No Surcharge & E.Q.,But Dry) =1.594

FS2(With Surcharge & W.T.,But No E.Q.) =1.305

FS3(No Surcharge & E.Q. , But W.T.) =1.305

FS4(No Surcharge , With E.Q. & Dry) =1.228 .201 .00

FS5(No Surcharge , With E.Q. & W.T.[WORST]= .989 .103 .00

~~~~~~
~~~~~~

Stability analysis of Mat-Dadheta village

****

UNITS USED -> TONNE - METER - DEGREE

INPUT FILE NAME ->isast.th5

OUTPUT FILE NAME ->osast.th5

****

CASE NUMBER = 1

~~~~~~~~~~~~~~~~~~

C = 8.000 PHI = 25.000 GAMA = 1.800 GAMAW = 1.000

Z = 30.000 ZW = 20.000 SIF = 22.000 AH = .100

AV = -.050 EQM = 7.000 Q = .000 FS = 1.200

~~~~~~

FACTOR OF SAFETY WITH DIFFERENT CONDITIONS****** CRITICAL DYNAMIC

ACCELERATION DISPLACEMENT(M)

FS1(No Surcharge & E.Q.,But Dry) =1.581

FS2(With Surcharge & W.T.,But No E.Q.) =1.367

FS3(No Surcharge & E.Q. , But W.T.) =1.367

FS4(No Surcharge , With E.Q. & Dry) =1.233 .203 .00

FS5(No Surcharge , With E.Q. & W.T.[WORST]=1.054 .128 .00

~~~~~~
~~~~~~

Stability analysis of Pokhani village

****

UNITS USED -> TONNE - METER - DEGREE

INPUT FILE NAME ->isast.th9

OUTPUT FILE NAME ->osast.th9

****

CASE NUMBER = 1

~~~~~~~~~~~~~~~~~~~

C = 8.000 PHI = 25.000 GAMA = 1.800 GAMAW = 1.000

Z = 20.000 ZW = 15.000 SIF = 22.000 AH = .100

AV = -.050 EQM = 7.000 Q = .000 FS = 1.200

~~~~~~

FACTOR OF SAFETY WITH DIFFERENT CONDITIONS****** CRITICAL DYNAMIC

ACCELERATION DISPLACEMENT(M)

FS1(No Surcharge & E.Q.,But Dry) =1.794

FS2(With Surcharge & W.T.,But No E.Q.) =1.634

FS3(No Surcharge & E.Q. , But W.T.) =1.634

FS4(No Surcharge , With E.Q. & Dry) =1.411 .277 .00

FS5(No Surcharge , With E.Q. & W.T.[WORST]=1.277 .221 .00

~~~~~~
~~~~~~

Stability analysis of Lanji village

```
******************************************************************************
   UNITS USED          -> TONNE - METER - DEGREE
   INPUT FILE NAME     ->isast.th1
   OUTPUT FILE NAME    ->osast.th1
******************************************************************************

CASE NUMBER =    1
~~~~~~~~~~~~~~~~~~
C    =    8.000   PHI   =   25.000   GAMA  =    1.800   GAMAW =    1.000
Z    =   30.000   ZW    =   20.000   SIF   =   27.000   AH    =    .100
AV   =    -.050   EQM   =    7.000   Q     =     .000   FS    =   1.200
~~~~~~~~~~~~~~~~~~~~~~~~~~~~~~~~~~~~~~~~~~~~~~~~~~~~~~~~~~~~~~~~~~~~~~~~~~~~~~
FACTOR OF SAFETY WITH DIFFERENT CONDITIONS******     CRITICAL     DYNAMIC
                                          ACCELERATION DISPLACEMENT(M)
FS1(No Surcharge & E.Q.,But Dry)        =1.281
FS2(With Surcharge & W.T.,But No E.Q.)   =1.112
FS3(No Surcharge & E.Q. , But W.T.)      =1.112
FS4(No Surcharge , With E.Q. & Dry)      =1.037      .114           .00
FS5(No Surcharge , With E.Q. & W.T.[WORST]= .889      .045           .09
~~~~~~~~~~~~~~~~~~~~~~~~~~~~~~~~~~~~~~~~~~~~~~~~~~~~~~~~~~~~~~~~~~~~~~~~~~~~~~
```

Stability analysis of Dwing village

```
******************************************************************************
   UNITS USED          -> TONNE - METER - DEGREE
   INPUT FILE NAME      ->isast.thd
   OUTPUT FILE NAME     ->osast.thd
******************************************************************************

CASE NUMBER =    1
~~~~~~~~~~~~~~~~~~
C    =    8.000   PHI  =   25.000   GAMA  =    1.800   GAMAW =    1.000
Z    =   35.000   ZW   =   20.000   SIF   =   30.000   AH    =    .100
AV   =    -.050   EQM  =    7.000   Q     =     .000   FS    =    1.200
~~~~~~~~~~~~~~~~~~~~~~~~~~~~~~~~~~~~~~~~~~~~~~~~~~~~~~~~~~~~~~~~~~~~~~~~~~~~~~
FACTOR OF SAFETY WITH DIFFERENT CONDITIONS******     CRITICAL     DYNAMIC
                                        ACCELERATION DISPLACEMENT(M)
FS1(No Surcharge & E.Q.,But Dry)         =1.147
FS2(With Surcharge & W.T.,But No E.Q.)   =1.081
FS3(No Surcharge & E.Q. , But W.T.)      =1.081
FS4(No Surcharge , With E.Q. & Dry)      = .936       .044           .09
FS5(No Surcharge , With E.Q. & W.T.[WORST]= .820      .000          10.57
~~~~~~~~~~~~~~~~~~~~~~~~~~~~~~~~~~~~~~~~~~~~~~~~~~~~~~~~~~~~~~~~~~~~~~~~~~~~~~
```

Stability analysis of Jaisal village

```
******************************************************************************
   UNITS USED        -> TONNE - METER - DEGREE
   INPUT FILE NAME    ->isast.t10
   OUTPUT FILE NAME    ->osast.t10
******************************************************************************


CASE NUMBER =    1
~~~~~~~~~~~~~~~~~~
C    =    8.000   PHI  =   25.000   GAMA  =    1.800   GAMAW =   1.000
Z    =   20.000   ZW   =   10.000   SIF  =   16.000   AH   =    .100
AV   =    -.050   EQM  =    7.000   Q    =     .000   FS   =   1.200
~~~~~~~~~~~~~~~~~~~~~~~~~~~~~~~~~~~~~~~~~~~~~~~~~~~~~~~~~~~~~~~~~~~~~~~~~~~~~~~
FACTOR OF SAFETY WITH DIFFERENT CONDITIONS******    CRITICAL    DYNAMIC
                                 ACCELERATION DISPLACEMENT(M)
FS1(No Surcharge & E.Q.,But Dry)        =2.465
FS2(With Surcharge & W.T.,But No E.Q.)   =2.013
FS3(No Surcharge & E.Q. , But W.T.)      =2.013
FS4(No Surcharge , With E.Q. & Dry)      =1.799      .402          .00
FS5(No Surcharge , With E.Q. & W.T.[WORST]=1.452      .278          .00
~~~~~~~~~~~~~~~~~~~~~~~~~~~~~~~~~~~~~~~~~~~~~~~~~~~~~~~~~~~~~~~~~~~~~~~~~~~~~~~
```

Stability analysis of Dhari village

```
*****************************************************************************
    UNITS USED          -> TONNE - METER - DEGREE
    INPUT FILE NAME      ->isast.th4
    OUTPUT FILE NAME     ->osast.th4
*****************************************************************************

CASE NUMBER =    1
~~~~~~~~~~~~~~~~~~
C    =    8.000   PHI  =   25.000   GAMA  =    1.800   GAMAW =    1.000
Z    =   50.000   ZW   =   20.000   SIF   =   22.000   AH    =    .100
AV   =    -.050   EQM  =    7.000   Q     =    .000    FS    =   1.200
~~~~~~~~~~~~~~~~~~~~~~~~~~~~~~~~~~~~~~~~~~~~~~~~~~~~~~~~~~~~~~~~~~~~~~~~~~~~~~
FACTOR OF SAFETY WITH DIFFERENT CONDITIONS******     CRITICAL     DYNAMIC
                                            ACCELERATION DISPLACEMENT(M)
FS1(No Surcharge & E.Q.,But Dry)         =1.410
FS2(With Surcharge & W.T.,But No E.Q.)    =1.025
FS3(No Surcharge & E.Q. , But W.T.)      =1.025
FS4(No Surcharge , With E.Q. & Dry)      =1.090      .143           .00
FS5(No Surcharge , With E.Q. & W.T.[WORST]= .769      .009           .32
~~~~~~~~~~~~~~~~~~~~~~~~~~~~~~~~~~~~~~~~~~~~~~~~~~~~~~~~~~~~~~~~~~~~~~~~~~~~~~
```

Stability analysis of Hat village

```
********************************************************************************
   UNITS USED        -> TONNE - METER - DEGREE
   INPUT FILE NAME     ->isast.thd
   OUTPUT FILE NAME    ->osast.thd
********************************************************************************

CASE NUMBER =   1
~~~~~~~~~~~~~~~~~~
C    =   10.000   PHI   =   35.000   GAMA  =    2.100   GAMAW =   1.000
Z    =   25.000   ZW    =   15.000   SIF   =   18.000   AH    =    .100
AV   =    -.050   EQM   =    7.000   Q     =    2.000   FS    =   1.200
~~~~~~~~~~~~~~~~~~~~~~~~~~~~~~~~~~~~~~~~~~~~~~~~~~~~~~~~~~~~~~~~~~~~~~~~~~~~~~~~
FACTOR OF SAFETY WITH DIFFERENT CONDITIONS******   CRITICAL    DYNAMIC
                                        ACCELERATION DISPLACEMENT(M)
FS1(No Surcharge & E.Q.,But Dry)        =2.803
FS2(With Surcharge & W.T.,But No E.Q.)  =2.384
FS3(No Surcharge & E.Q. , But W.T.)     =2.393
FS4(No Surcharge , With E.Q. & Dry)     =2.087      .563         .00
FS5(No Surcharge , With E.Q. & W.T.[WORST]=1.761      .435         .00
~~~~~~~~~~~~~~~~~~~~~~~~~~~~~~~~~~~~~~~~~~~~~~~~~~~~~~~~~~~~~~~~~~~~~~~~~~~~~~~~
```

Annexure III

Unwedge Analysis Information for Powerhouse Cavern, Hat village

Document Name

File Name: VPHEP PH.weg

Project Settings

Project Title: Stability Analysis of Wedges for VHEP Underground Excavations
Wedges Computed: Perimeter and End Wedges
Units: Metric, stress as MPa

General Input Data

Tunnel Axis Orientation:
 Trend: 310°
 Plunge: 0°
Design Factor of Safety: 1.500
Unit Weight of Rock: 0.026 MN/m3
Unit Weight of Water: 0.010 MN/m3

Seismic Forces

Direction: Sliding
Seismic Coefficient: 0.12

Joint Orientations

Joint 1
 Dip: 30°
 Dip Direction: 300°
Joint 2
 Dip: 20°
 Dip Direction: 125°
Joint 3
 Dip: 75°
 Dip Direction: 030°

Joint Properties

Foliation
 Water Pressure
  Constant: 0 MPa
 Waviness: 0°
 Shear Strength Model: Barton-Bandis
  JRC: 10
  JCS: 22 MPa
  Phi b: 30°

J1
Water Pressure
Constant: 0 MPa
Waviness: 0°
Shear Strength Model: Barton-Bandis
JRC: 10
JCS: 24 MPa
Phi b: 35°

J2
Water Pressure
Constant: 0 MPa
Waviness: 0°
Shear Strength Model: Barton-Bandis
JRC: 9
JCS: 20 MPa
Phi b: 28°

Bolt Properties

Bolt Property 1
Bolt Type: Cable Bolt
Tensile Capacity: 0.2 MN
Plate Capacity: 0.1 MN
Bond Strength: 0.34 MN/m
Shear Strength: Unused
Bolt Orientation Efficiency: Used
Method: Cosine Tension/Shear

Shotcrete Properties

Shotcrete Property 1
Shear Strength: 2.00 MPa
Unit Weight: 0.026 MN/m3
Thickness: 10.00 cm

Support Summary

Summary of Perimeter Shotcrete
Number of Shotcrete Layers on Perimeter: 1
Perimeter Shotcrete Layer: 1
Shotcrete Property: Shotcrete Property 1

Summary of Perimeter Support Pressure
No Support Pressure on Perimeter

Summary of Perimeter Bolt Patterns
Number of Bolt Patterns on Perimeter: 2
Perimeter Bolt Pattern: 1
Property: Bolt Property 1
Strength type: Cable Bolt
Bolt Length: 5.00 m

Orientation: normal to boundary
Pattern Spacing - In Plane: 1.50 m
Pattern Spacing - Out of Plane: 2.50 m
Pattern Spacing - Out of Plane Offset: 0.00 m

Perimeter Bolt Pattern: 2

Property: Bolt Property 1
Strength type: Cable Bolt
Bolt Length: 5.00 m
Orientation: normal to boundary
Pattern Spacing - In Plane: 1.50 m
Pattern Spacing - Out of Plane: 2.50 m
Pattern Spacing - Out of Plane Offset: 0.00 m

Summary of End Bolt Patterns

No Bolt Pattern on Ends

Summary of End Support Pressure

No Support Pressure on Ends

Summary of End Shotcrete

No Shotcrete on Ends

Wedge Information

Floor wedge [1]

Factor of Safety: stable
Wedge Weight: 0.026 MN

Upper Right wedge [4]

Factor of Safety: 6.057
Wedge Weight: 3.278 MN

Floor wedge [5]

Factor of Safety: 7.857
Wedge Weight: 14.481 MN

Roof wedge [7]

Factor of Safety: 7.752
Wedge Weight: 2.308 MN

Roof wedge [8]

Factor of Safety: 22.674
Wedge Weight: 0.230 MN

Near End wedge [9]

Factor of Safety: 2.665
Wedge Weight: 0.646 MN

Far End wedge [10]

Factor of Safety: 4.514
Wedge Weight: 0.646 MN

LIST OF PUBLICATIONS

Publications in International Journals

i. Lakshmanan K, Anbalagan. R, Yadev A.K, Geotechnical evaluation of underground power house for Vishnugad-Pipalkoti Hydel Scheme, Garhwal Himalaya, India. *International Journal of Current Research. Vol. 7, Issue, 09, pp.20308-20314, September, 2015.*

ii. Lakshmanan K and Anbalagan R, *Impact of blasting on stability of hill slopes and villages located close to alignment of power tunnel and trail race tunnel Vishnugad – Pipalkoti hydroelectric project, Garhwal Himalaya*. (Manuscript no: GEGE-D-15-00198 under review: Journal of Geotechnical and Geological Engineering, Springer)

iii. Anbalagan, R., Rohan Kumar, Parida, S. and Lakshmanan, K. 'GIS Based Post Earthquake Landslide Hazard Zonation Mapping of Lachung Basin, Sikkim' *International Journal of Emerging Technology and Advanced Engineering, Vol. 4, Issue 1, Jan 2014,*431-441.

iv. R Anbalagan, Rohan Kumar, K Lakshmanan, Sujata Parida and S Neethu 'Landslide Hazard Zonation Mapping Using Frequency Ratio and Fuzzy Logic Approach, A Case Study of Lachung Valley, Sikkim' *Journal of Geoenvironmental Disasters 2015*

National Journal

i. S.K. Tripathi, K Lakshmanan *et al.,* A preliminary post-disaster assessment of the landslide-affected areas in Uttrarakhand –June 2013 disaster, *Indian Journal of Geosciences*, Volume 66, No.14 October December, 2012; pp193-202.

International Conferences:

i. Lakshmanan. K and Jina Mandal "Geological Impact Assessment of Kedarghati, A Mass Destruction during June 2013 Disaster, Rudraprayag District, Uttarkhand, India." International Conference on Engineering Geology in New Millennium, IIT, New Delhi, India: 27-29 October 2015. Indian Society of Engineering Geology.

ii. Jina Mandal and Lakshmanan. K “Post construction stage geotechnical investigation of Sidhata Medium Irrigation Project, Jawali, district Kangra, Himachal Pradesh” International Conference on Engineering Geology In New Millennium, IIT, New Delhi, India: 27-29 October 2015. Indian Society of Engineering Geology.

iii. Anbalagan, R., Parida, S. and Lakshmanan, K. ‘Geotechnical evaluation of Lakhwar Underground Powerhouse, Uttrakhand Himalaya, India.’ Humboldt Kolleg and International Conference, Sept, 2011, Salem.